PREDICTION OF DETONATION CHARACTERISTICS OF CONDENSED EXPLOSIVES

Morton H. Friedman
Propellant Research Laboratory
Minnesota Mining and Manufacturing Company
St. Paul 19, Minnesota

Abstract

To date, the only completely non-empirical method of predicting detonation parameters is that developed by Paterson and based on the virial equation of state. This method is more appealing now than in the past because of improved techniques for the estimation of virial coefficients, and because of interest in new explosive materials which cannot be expected to adhere to correlations based on familiar CHON explosives.

In the present work, the virial technique is updated and expanded to include explosives based on B,C, H, O, N and F. Predicted detonation pressures in CHON explosives agree with experimental values with an accuracy comparable to that exhibited by the Cook and Kistiakowsky-Wilson-Brinkley methods. A closed-form equation for detonation pressure is presented. The detonation parameters of several systems based on boron and fluorine are also predicted.

By applying suitable approximations to the solution for detonation pressure, an equation is derived which relates this parameter to the structure of the detonating molecule and the stoichiometry of the decomposition reaction. The detonation pressure rises nearly linearly with heat of explosion and very rapidly as the average number of atoms per product molecule decreases.

Introduction

A knowledge of the properties of stable detonations in explosive materials is necessary to an appreciation of the safety hazards encountered in handling these substances. The characteristics of detonations in conventional explosives have been deduced to a large extent from detonation velocity measurements, but such an approach cannot be applied to many compounds or mixtures which have been produced in small quantities, are impure, or indeed, may be hypothetical. When enough of a material of interest has been made to permit a shock sensitivity test, the final velocity of the acceptor shock can be compared with the predicted Chapman-Jouguet velocity to ascertain whether, in fact, a high-order detonation has been produced sympathetically. A scheme for predicting detonation characteristics might also be useful for predicting detonability and brisance, and for computing exothermicity and virial coefficients from experimental detonation measurements.

The prediction of Chapman-Jouguet (C-J) properties is made difficult by the lack of a simple equation of state for the hot, highly-compressed product gases. Those most commonly used have been the Abel and Kistiakowsky-Wilson (K-W) equations of state:

Abel: $P(V-\alpha)=NRT$ (1a)

Kistiakowsky-Wilson: $PV/NRT = 1 + x\exp(\beta x)$ (1b)

where P = pressure
V = specific volume
α = Abelian covolume
N = number of gaseous moles
R = gas constant
T = temperature

$x = \frac{Kk'}{V(T+\theta)^a}$

k' = KW covolume

and θ, a, β and K are empirically-determined constants.

When the Abel equation of state is used, the covolume is assumed to be a constant empirical property of the explosive or a generalized function of specific volume. Cook[1] found that a single curve of covolume versus C-J specific volume could be drawn through experimental points for two picrates, lead azide, mercury fulminate and a series of CHON explosives. The K-W equation has formed the basis of a computer code, RUBY[2], developed at the Lawrence Radiation Laboratory, which has been used widely to predict detonation parameters in CHON explosive systems. Here, the virial equation of state will be used.

Analysis

1. Mathematical Formulation in the Absence of Condensed Products

The general virial equation of state of a gas is

$$PV/NRT = 1 + b_o/V + a_2 (b_2/V)^2 + a_3 (b_3/V)^3 + \ldots \quad (2)$$

where b_i = virial coefficients
a_i = constants

Several particular virial equations have been proposed, differing only in minor aspects. They all predict nearly identical gas properties in the range of interest here. The simplest form, that due to Majumdar[3], was used

$$PV/NRT = 1 + b_o/V + .833 (b_o/V)^2 + .287 (b_o/V)^3 \equiv 1 + f (b_o/V) \quad (3a)$$

where b_o = high-temperature second virial coefficient.

In application to the problem at hand, Equation (3a) becomes

$$P_1V_1/nR'T_1 = 1 + f (b_o/V_1) = 1 + f \quad (3b)$$

where $\mathcal{A}_1$ = C-J condition
n = mols product gas/g
R' = 82.1 atm-cc/°K-mol
$b_o = \sum_{\text{all gaseous products}} n_i b_{oi}$, cc/g product gas mix
b_{oi} = virial coefficient of the i-th gaseous product, cc/mol
n_i = mols of the i-th gaseous products/g product mix

It is assumed below that only gaseous products are formed by detonation; the analysis applicable when condensed species are formed will be discussed later.

Paterson[4] has shown that

$$V_1 = \frac{k_1 V_o + \alpha_1}{k_1 + 1} \tag{4}$$

where α = in undetonated state
and k_1 is defined by

$$k_1 = 1 + nR/C_{v1} - d\alpha/dV\Big|_1 \tag{5}$$

where C_{v1} = heat capacity of product gases at the C-J point,

$$\text{cal/g} - {}^\circ\text{K} = \sum_{\substack{\text{all} \\ \text{products}}} n_i C_{vli}$$

$R = 1.987$ cal/mol - °K
C_v = molar heat capacity at constant volume

From Equations (1a) and (3a),

$$\alpha = \frac{V f}{1+f} \tag{6}$$

The heat capacity at constant volume of a virial gas is independent of pressure and, at low pressures,

$$C^\circ_{pi} - C^\circ_{vi} = R = C^\circ_{pi} - C_{vli} \tag{7}$$

where $^\circ$ = at zero pressure and C-J temperature.

Define γ_1 by

$$\gamma_1 = C^\circ_p / C^\circ_v = C^\circ_p / C^\circ_v \tag{8}$$

Multiplying Equation (7) by n_i and summing over all products; and using Equations (5) and (8),

$$k_1 = \gamma_1 - d\alpha/dV\Big|_1 \tag{9}$$

Then, performing the required differentiation in Equation (9) with the aid of (6), and substituting the result and (6) into (4),

$$V_o(g-f) = V_1(g+1) \tag{10}$$

where

$$g = \gamma_1(1+f)^2 - V_1 df/dV\Big|_1 - f^2$$

Equation (10) gives the C-J specific volume as a function of γ_1, b_o and V_o. When the heat of explosion and the mean heat capacity of the product gases between T_o and T_1 ($\bar{C}_v$) are known, the value of V_1 found from Equation (10) can be substituted into the Rankine-Hugoniot equation and (3b) to yield C-J pressure. The values of the remaining C-J variables are then easily determined with the aid of Equation (9).

The procedure indicated above involves cycling on both pressure and temperature if the product distribution is unknown; if, however, the products formed are stipulated, cycling on only temperature is required. As both γ_1 and $\bar{C}_v$ are weak functions of temperature, few iterations are needed.

Both γ_1 and $\bar{C}_v$ can be found from published thermochemical tables. V_o is known. Taylor[5] has tabulated the high temperature second virial coefficients of the most frequently observed products of detonation in CHON explosives, and the values of b_o for other species can be estimated or calculated from measured intermolecular force constants.

2. Corresponding Equations when Condensed Products are Formed

The results cited above are applicable only in the absence of condensed detonation products; however, explosives which produce solids can be treated if certain assumptions are made regarding the participation of the solid in the detonation process. It is assumed here that the solids produced are incompressible and in thermal and momentum equilibrium with the product gases. The first of these assumptions is not strictly true, but Cowan and Fickett[6] have shown that only a small error in predicted C-J properties is so introduced. Upon carrying out the earlier analysis in this case, Equation (10) is replaced by

$$V_o^{\dagger}(g^{\dagger}-f)=V_1(g^{\dagger}+1) \tag{11}$$

where $V_o^{\dagger} = \dfrac{V_o-\phi(1-m)}{m}$

$$g^{+} = \gamma_1^{+}(1+f)^2-V_1\,df/dV\Big|_1 - f^2$$

V_1 = specific volume of the gas at the C-J plane
ϕ = specific volume of the condensed phase
m = weight fraction of detonation products which are gaseous
$\gamma_1^{+} = 1 + nR/C_{v1}$
n = mols gas per gram total products
C_v = heat capacity at constant volume of total products, cal/g-°K

Equation (11) reduces to Equation (10) when m = 1.

Applications

1. Comparison with Experiment.

In a fashion analagous to that applicable in the absence of condensed products, all the detonation parameters of an explosive can be calculated once Equation (11) is solved for V_1. A computer program has been written to predict the detonation parameters of any exothermic material or mixture, requiring as input the loading density and heat of formation of the explosive, and the stoichiometric coefficients of each of 29 possible products, including any solid.

It is instructive to compare the present method of prediction with established techniques; the current study was initiated in an effort to obtain refined predictions of detonation pressure, so this parameter is used in the comparisons to follow. In Table I, results of the present analysis and that due to Cook are compared with experimental data on a number of high explosives. The two techniques predict the experimental detonation pressures with comparable accuracy. A similar comparison with the predictions of the RUBY code is included as Table II. When these predictive methods are applied to other classes of explosive compounds,

the virial coefficient approach, because of its more fundamental basis, is expected to predict detonation properties at least as accurately as the other approaches. The virial technique also offers the advantage of leading to explicit solutions for detonation parameters, as will be shown below.

Table I. Detonation Pressures Predicted from Generalized Covolumes (Cook) and from the Virial Equation of State

Compound	ρ_o, g/cc	Reference for product distribution	Detonation Pressure: Virial Equation	Cook	Experimental	Ref.
Nitroglycerin	1.6	5	217	247	253	b
TNT	1.0	5	60	67*	64	b
TNT	1.455	5	120	136*	165	b,c
RDX	1.20	a	133	136	141	a,b
RDX	1.40	a	181	181	213	b
RDX	1.59	a	242	223	287	b
RDX	1.755	a	305	276	366	b
Mean percent error			14	14**		

* Experimental results on TNT were used by Cook to generate the generalized plot of covolume versus C-J specific volume.

** Excluding TNT

a. M. A. Cook, "The Science of High Explosives", Reinhold, 1958.
b. A. N. Dremin et al, Eighth Symp. (Int'l.) on Combustion, Williams and Wilkins, 1960, p. 610.
c. W. B. Garn, J. Chem. Phys. 32, 653 (1960).

Table II. Detonation Pressures Predicted from the RUBY Code[2] and from the Virial Equation of State

Reference for product distributions: C. R. Mader, "Detonation Performance Calculations using the Kistiakowsky-Wilson Equation of State" Los Alamos Scientific Laboratory Report LA-2613, October 9, 1961.

Compound	ρ_o, g/cc	Detonation Pressure: Virial Equation	RUBY	Experimental	Ref.
NM	1.128	76	151	130	a
NM/TNM 1/.071 mol/mol	1.197	105	168	138	b
NM/TNM 1/.25 mol/mol	1.310	149	195	156	b
NM/TNM 1/.5 mol/mol	1.397	167	200	168	b
AN/TNM 1/1.25 mol/mol	1.380	196	191	156	b
EDB/TFDNE 1/7.5 mol/mol	1.467	189	185	206	c
Mean percent error		17	19		

Table II (Cont'd.)

NM = nitromethane
TNM = tetranitromethane
AN = acyrlonitrile
EDB = ethylderaborane
TFDNE = tetrafluorodinitroethane

a. W. C. Davis, Los Alamos Scientific Laboratory unpublished data
b. W. Garn, Los Alamos Scientific Laboratory unpublished data
c. W. Garn and C. L. Mader, Los Alamos Scientific Laboratory unpublished data

In gaseous detonations, $b_o << V_1$, and the virial equation reduces to the ideal equation of state. Therefore, the computer program described above can be used to determine the ratio between C-J pressure and initial pressure for gases sufficiently exothermic to justify the inequality $P_1 >> P_o$.

2. Detonations in High Energy Propellant Systems

A substantial amount of effort has been expended to determine and optimize high-impulse propellant systems. Many of these mixtures contain atoms different from those in solid secondary explosives. The computer program referred to above accepts product species containing fluorine and boron, and has been used to predict the detonation characteristics of several impulse-optimized bipropellants based on these elements. The results of the analysis are presented as Table III. Product distributions are from Dobbins[7], except where noted.

As none of the mixtures in Table III have been optimized as explosives, only qualitative conclusions can be drawn regarding this use of bipropellants. They exhibit the desirable high energy of perfectly or nearly balanced systems, but have too low a density and too high a volatility to be very promising.

Table III. Predicted Detonation Characteristics of High-Energy Bipropellants

Oxidizer	Fuel	Percent oxidizer	Basis	Loading Density, g/cc	Detonation Properties		
					Temperature, °K	Velocity, mps	Pressure, kb
N_2O_4	N_2H_4	33	Mol*	1.222	5170	6710	131
N_2F_4	N_2H_4	50	Mol**	1.438	8280	8250	224
F_2	N_2H_4	55	Weight	1.230	6250	9990	248
F_2	B_5H_9	20	Weight	1.172	7520	6790	137
NF_3	B_5H_9	87	Weight	1.288	7160	6800	141
OF_2	UDMH	72	Weight	1.209	6940	8340	187

* Stoichiometric to H_2O and N_2
** Stoichiometric to HF and N_2. This mixture is ordinarily hypergolic

3. Approximate Solution for Detonation Pressure

The procedure outlined above yields fair predictions of the detonation characteristics of systems of interest. If, however, some further assumptions are made in the analysis, equations can be derived which still predict detonation parameters with fair accuracy, yet can be used to make more rapid estimates of C-J properties of interest. In addition, these equations can indicate to what degree various properties of a detonating explosive and its products affect the conditions behind a C-J detonation.

It can be shown that, if heat capacity is independent of temperature, the C-J properties can be determined when the values of only four parameters are specified; these variables are b_o, V_o^+, γ^+, and Q, the standard change, in calories, of internal energy accompanying the reaction. Dimensionless or reduced detonation parameters can be defined as functions of only b_o, V_o^+ and γ^+, viz:

$$P' \equiv \frac{P_1 m}{Q+C_v T_o} = \left[\frac{C_v V_1}{nR'(1+f)} - 0.0121\ (V_o^+ - V_1)\right]^{-1} \quad \text{atmosphere-g/cal} \qquad (12)$$

V_1 is found from Equation (11). Cgs units are used except where indicated. The analysis to follow will be limited to the deviation of a simple method of predicting detonation pressure; similar approaches can be used to derive analogous equations for other detonation parameters.

A digital computer was used to prepare tables of reduced detonation parameters for a series of input values of V_o^+, b_o and γ_1^+. The range of independent variables covered was:

(1) γ_1^+: 1.01 to 1.30, in intervals of 0.01

(2) b_o: 0.6 to 1.4 cc/g, in intervals of 0.1 cc/g

(3) V_o^+: 0.5 to 1.0 cc/g, in intervals of 0.1 cc/g

Over the range of interest of these variables, plots of P' versus $\gamma^+ - 1$ are essentially linear and pass through the origin, with the degree of curvature rising as b_o and $\rho_o^+ = 1/V_o^+$ increase. However, even for the largest values of b_o and ρ_o^+, $P C_v/nR$ decreases only eleven percent between γ^+ values of 1.01 and 1.30. Therefore,

$$P' \doteq \frac{nR}{C_v}\ \mu(b_o, V_o^+) \qquad (13)$$

where μ = slope of plot of P' versus $\gamma^+ - 1$.

Usually, $Q \gg C_v T_o$, so

$$P \sim \frac{QnR}{mC_v}\ \mu(b_o, V_o^+) = \frac{QR}{M_p C_v}\ \mu \qquad (14)$$

where M_p = mean molecular weight of the gaseous products

Plots of $\mu(b_o, V_o^+)$ are given as Figure 1.

Equation (14) indicates some directions to be taken in tailoring molecules to produce high or low detonation pressures. It would appear to be rather difficult to effect large changes in the virial coefficient, although a study of this property might indicate which classes of compounds should detonate more or less strongly. The formation of solid detonation products is seen from Fig. 1 to reduce detonation pressure and the well-known effects of loading density and heat of detonation are confirmed. From a statistical mechanical interpretation of M_pC_v, a very important parameter determining detonation pressure is found to be the average number of atoms in the product gases. In the absence of condensed products, as this ratio is lowered from five to four to three to two, with no other changes, predicted detonation pressure rises from $P_1 \equiv P^*$ to $1.3P^*$ to $1.9P^*$ to $3.6P^*$! The effect of this parameter bears further study.

Conclusions

A method of predicting the Chapman-Jouguet detonation characteristics of a condensed explosive has been developed. The gaseous explosion products are assumed to obey the virial equation of state. The analysis involves no adjustable parameters and predicts detonation pressure as well as or better than solutions based on the Abel or Kistiakowsky-Wilson equations. The solution has been simplified to permit the explicit estimation of detonation pressure, which is seen to rise very rapidly as the average number of atoms per product molecule decrease.

Acknowledgment

The author would like to express his appreciation to Dr. G. B. Rathmann for suggesting this investigation and for his encouragement during its course.

Bibliography

1. M. A. Cook, J. Chem. Phys. 15, 518 (1947)

2. H. B. Levine and R. E. Sharples, Lawrence Radiation Laboratory Report UCRL-6815, March 20, 1962 "Operator's Manual for RUBY"

3. R. Majumdar, Bull. Calcutta Math. Soc. 21, 107 (1929)

4. S. Paterson, Research 1, 221 (1948)

5. J. Taylor, "Detonation in Condensed Explosives" Clarendon Press, Oxford, 1952

6. R. D. Cowan and W. Fickett, J. Chem. Phys. 24, 932 (1956)

7. T. O. Dobbins, "Thermodynamics of Rocket Propulsion and Theoretical Evaluation of Some Prototype Propellant Combinations" WADC TR-59-757, December 1959.

MHF:vw
5-17-63

FIG. 1

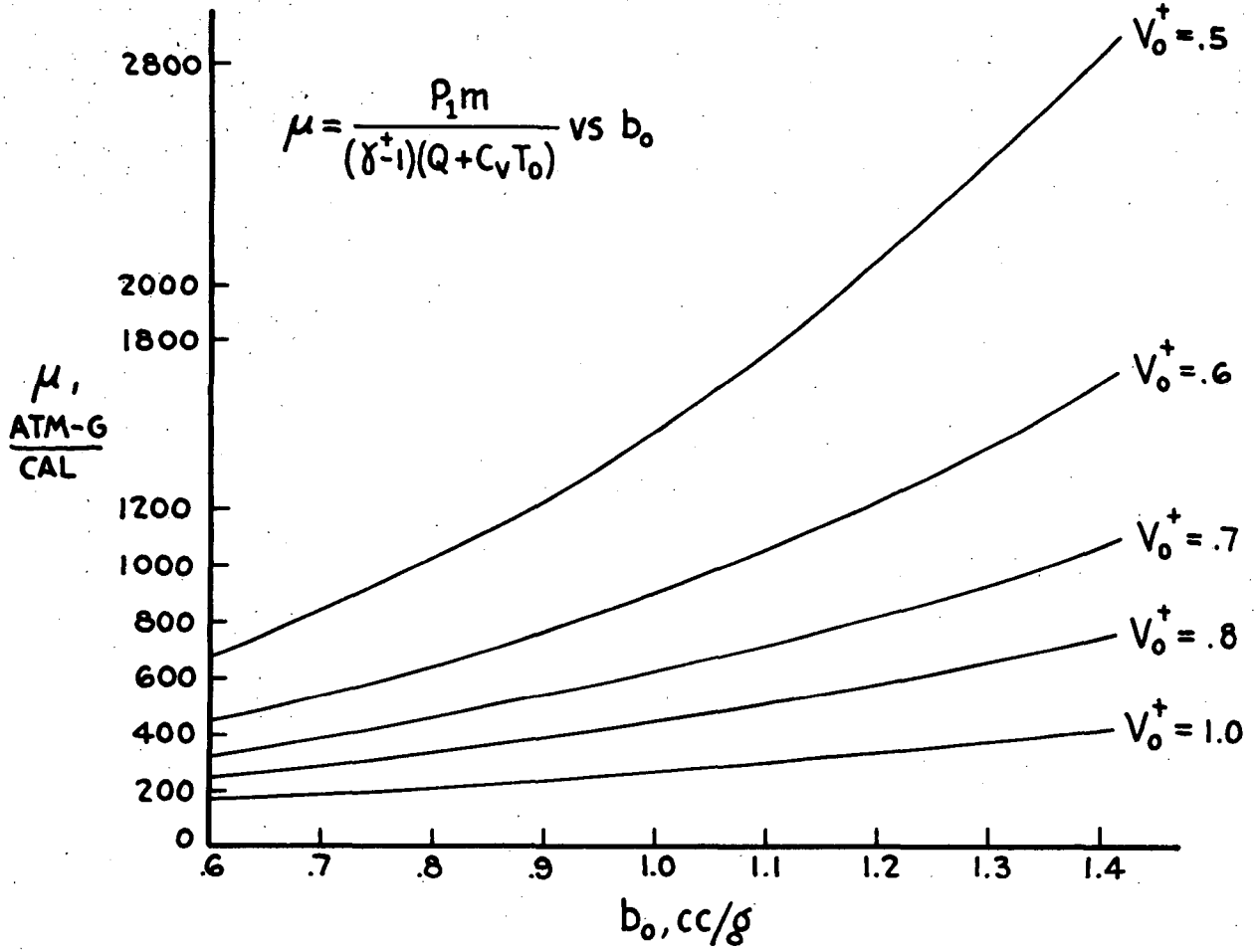

REDUCED DETONATION PRESSURE vs. HIGH TEMPERATURE SECOND VIRIAL COEFFICIENT

Effect of Gas Composition on Compression Sensitivity of Liquids(1)

G. A. Mead(2)

Air Reduction Company, Inc.
Murray Hill, N. J.

The ignition of liquid explosives and propellants by the rapid compression of gas bubbles has been studied extensively both because of scientific interest and because of immediate needs for devising safe operating procedures and for estimating the sensitivity of new materials (1,2,3,4,5)(3). Two explosions of tank cars of nitromethane that might have been initiated by this mechanism have occurred in recent years, as have a number of smaller accidental explosions in the testing of experimental propellants.

Nature of the Ignition Process

In the simplified model of the ignition of a liquid explosive by adiabatic compression of an entrapped gas bubble, the temperature is considered to increase during compression according to the relation:

$$\frac{T}{T_o} = \left(\frac{P}{P_o}\right)^{\frac{\gamma-1}{\gamma}} \qquad [1]$$

---

(1) This work was supported by the Rocket Research Laboratories, Space Systems Division, Edwards, California, Air Force Systems Command, USAF, under Contract AF33(616)-5732.

(2) Section Head, Combustion & Fuels Technology. Member ARS.

(3) Numbers in parentheses indicate references at end of paper.

When a sufficiently high temperature is reached in the gas, it is postulated that ignition of explosive vapor in the bubble occurs, further raising the temperature at an exponentially increasing rate. At this stage the process becomes self-sustaining through the evaporation and reaction of fresh material surrounding the heated region.

An exact analysis of the process cannot be made because of uncertainties about the exchange of heat and mass between the liquid and gas and the configuration of the liquid-gas interface during compression.

From the assumptions of adiabaticity and a characteristic minimum ignition temperature in the compressed bubble, it follows that the energy required for ignition is related to the initial conditions in the bubble by the expression for compressive work in an adiabatic non-flow process:

$$W_i = \frac{P_i V_i}{\gamma - 1} \left(1 - \frac{T_i}{T_o}\right) \qquad [2]$$

Changes in the gas specific heat ratio, γ, should therefore affect the minimum ignition energy in inverse ratio to $(\gamma - 1)$. Also, the minimum ignition energy should be proportional to the initial bubble volume.

Experimental Procedure

The equipment and operating procedure have been described in detail previously(2,5).

The sample, consisting of a bubble in contact with liquid, is compressed by a gas driven piston. The sample chamber is one-half inch in diameter, with a total volume of about 1.5 ml. It is sealed with either a steel or aluminum burst disc that can contain static pressures above 20,000 psi.

All combinations of liquid and gas were tested at least three bubble volumes, 0.2, 0.4, and 0.8 ml. A reversal procedure was used to estimate minimum ignition energy at each bubble volume, first determining an approximate range, in terms of driving pressure, and then proceeding to vary driving pressure in small even increments up or down, depending on whether the preceding result was positive or negative. Usually each reversal series included at least six tests.

The energy of the piston is calculated by a derived expression in terms of the physical properties of the equipment, corrected by an empirical factor obtained from direct measurements of piston velocity. The accuracy of the energy estimate is about ± 15%.

To put gases other than air in the chamber, the area around the open sample chamber was loosely covered with a clear plastic cone with the point cut off. Purge gas entered through the side of the cone. Liquid sample was put in through the open end. The burst disc was then dropped in place, the cone removed, and the disc retainer bolted down.

To load a sample consisting of liquid and its own vapor, the piston was retracted far enough so that the chamber volume was equal to the desired amount of liquid. The chamber was then sealed with a burst disc and the piston retracted fully, leaving a vapor space of known volume above the liquid.

Test Results

Minimum ignition energies were determined for nitromethane with bubbles of air, oxygen, nitrogen, argon and carbon dioxide. Samples could not be made to ignite in the presence of nitromethane vapor alone. Results are shown in Table 1 in terms of minimum ignition energy per unit bubble volume, in kg-cm/ml. This was found to be constant for each liquid-gas volume combination, within limits of experimental error, with two exceptions out of a total of seventeen test groups.

Assuming that the minimum ignition energy for argon truly corresponds to a minimum temperature for ignition in the compressed bubble, minimum ignition energies were calculated for the other bubble gases by Eq.(2), and are also shown in Table 1.

The agreement between the observed and calculated values for the inert gases is nearly within the limits of experimental accuracy.

The inability to ignite the sample with only nitromethane vapor in the bubble can be explained on the basis of rapid condensation of the vapor in the liquid during compression.

Oxygen has a strong sensitizing effect, as shown by results with air and pure oxygen. The effect apparently reaches a maximum at some concentration below that of atmospheric air. This result, together with the observed effect of specific heat ratio with the inert gases, strongly indicates that the ignition of nitromethane, and presumably other C-H-O-N compounds, can start in the vapor phase by reaction with gaseous oxygen.

A related effect of oxygen concentration on the sensitivity of solid double-base propellants to ignition by detonating gas mixtures was found by Cook(3), so the possibility of reaction of the condensed phase surface with the gaseous oxidizer has been amply demonstrated.

The ignition temperatures calculated on the basis of an adiabatic process appear somewhat high for the inert gases, but reasonable for air and oxygen.

To get comparable data on a material qualitatively different in physical and chemical properties from nitromethane, tests were made on a nitric acid composite very similar to a Sprengel-type explosive. The vapor above the liquid is non-explosive at ordinary temperatures, since the vapor pressure of the fuel component is negligible.

Gases used in the tests were air, nitrogen, argon, carbon dioxide, and nitric acid vapor. Results are shown in Table 2.

The most significant result is that ignition could be obtained consistently, and that the energy required was not particularly large.

No differences in energy input between argon and nitrogen or air were detected. Carbon dioxide affected sensitivity measurably, although to a lesser extent than predicted. Calculated adiabatic ignition temperatures do not appear unreasonably high compared to those for nitromethane, but they lack quantitative significance because of the necessity for heat transfer in the ignition process. The only available explanations for ignition under these conditions are that the liquid got hot enough to react or that fuel was transferred to the vapor phase by non-equilibrium evaporation.

Evans and Yuill(6) have observed similar ordering of calculated temperatures in the ignition of nitroglycerine and PETN by compression of oxygen, air, nitrogen and argon, with the difference that the sensitivity of PETN is increased markedly in the presence of pure oxygen. The same authors report also the ignition of a number of solid explosives that have negligible vapor pressure.

If the requirement for ignition is that a surface layer of liquid reach some minimum temperature, this would largely account for the observation that the energy input required is only slightly affected by the specific heat ratio of the gas.

The total energy input in most of the tests described here is enough to evaporate a few milligrams of explosive; the mass of gas in the bubble is about one milligram. Some evaporation of the sample is thus possible during compression, and this would further tend to diminish the effect of gas specific heat on minimum ignition energy.

Conclusions

Bubble gas composition has a pronounced effect on compression sensitivity, even of liquids having non-explosive vapor under ordinary conditions.

Oxygen, in atmospheric concentration and greater, has a strong sensitizing effect on nitromethane and therefore probably on other C-H-O-N propellants and explosives. This observation, and the observation that minimum ignition energy can be correlated with gas specific heat ratio, strongly indicate that ignition of nitromethane and other volatile materials starts in the vapor phase, by reaction with oxygen if it is present.

Since materials that under ordinary conditions have a non-explosive vapor can be ignited, heat transfer, possibly accompanied by mass transfer, can take place across the gas-liquid interface at a significant rate during compression.

At least three factors can contribute to ignition. These are reaction in the gas phase, reaction at the surface with the gas phase, and reaction at the surface of the condensed phase caused by heat transfer from the compressed gas phase. There is also the possibility of mass transfer from the condensed phase to the gas phase, followed by reaction in the gas phase, although this is not a prerequisite for ignition. The nature of both the gas and the condensed phase determine which effect or combination of effects will predominate in any given ignition process.

The hazard of accidental ignition of liquid explosives initiated by the mechanism of rapid compression can be reduced by control of the composition of gas in contact with the liquid. Desensitizers should have high vapor pressure and specific heat, should be miscible to some extent with the liquid, and should be chemically inert toward the liquid.

Nomenclature

T = temperature

P = pressure

γ = specific heat ratio

W = energy input to sample

V = bubble volume

Subscripts

i = minimum required for ignition

o = initial condition

References

(1) BOWDEN, F. P. and YOFFE, A. D.
"Initiation and Growth of Explosion in Liquids and Solids"
University Press, Cambridge (1952).

(2) "Liquid Propellant Test Methods Recommended by the JANAF Panel on Liquid Propellant Test Methods"
The Liquid Propellant Information Agency, Applied Physics Laboratory, The Johns Hopkins University.

(3) COOK, M. A.
"The Science of High Explosives"
Reinhold Publishing Corp., New York (1958).

(4) GRIFFIN, D. N.
"The Initiation of Liquid Propellants and Explosives by Impact"
ARS Paper No. 1706-61, presented at the ARS Propellants, Combustion and Liquid Rockets Conference (April 26-28, 1961).

(5) MEAD, G. A.
"Compression Sensitivity of Monopropellants"
ARS Journal, Vol. 29, No. 3, p. 192 (1959).

(6) EVANS, J. I. and YUILL, A. M.
"Initiation of Condensed Explosives by Compression of the Surrounding Gas"
Proceedings of the Royal Society of London, Series A, Vol. 246, p. 176 (July 1958).

Table 1. Effects of Gas Properties on the Compression Sensitivity of Nitromethane

Bubble gas	Specific heat ratio, γ *	Measured sensitivity, kg-cm/ml	Calculated sensitivity relative to argon **, kg-cm/ml.	Ignition temperature, °K, calculated on the basis of measured sensitivity
Oxygen	1.34	10.4 ± 1.1	45	730°
Air	1.37	10.9 ± 1.1	42	900°
Nitrogen	1.37	40 ± 6	42	4000°
Argon	1.67	23 ± 3	23	4200°
Carbon dioxide	1.20	105 ± 15	77	5800°
Nitromethane	1.09	> 120	9	>70,000°

* At 700°K, arbitrarily taken as an average value.
** On the basis that the value measured for argon represents the true minimum ignition temperature.

Table 2. Effects of Gas Properties on the Compression Sensitivity of a Composite Explosive

Bubble gas	Specific heat ratio, γ *	Measured sensitivity, kg-cm/ml	Calculated sensitivity relative to argon **, kg-cm/ml	Ignition temperature, °K, calculated on the basis of measured sensitivity
Air	1.34	21 ± 2	47	1770°
Nitrogen	1.37	26 ± 4	44	2500°
Argon	1.67	24 ± 3	24	4400°
Carbon dioxide	1.20	35 ± 5	80	1730°
Vapor	1.11	81 ± 12	10	> 39,000°

* At 700°K, arbitrarily taken as average value.
** On the basis that the value measured for argon represents the true minimum ignition temperature.

THE EFFECT OF SPECIFIC SURFACE ON THE EXPLOSION TIMES OF SHOCK INITIATED PETN*

by

Robert H. Dinegar, Richard H. Rochester, and Mike S. Millican**

University of California, Los Alamos Scientific Laboratory
Los Alamos, New Mexico

ABSTRACT

Shock initiation experiments on small pressed charges of PETN have demonstrated that the explosion times in underinitiated charges decrease with an increase in the specific surface of the explosive. This is in accord with the generally accepted proposal that the reaction in the build-up zone is heterogeneous and is governed by a surface burning law.

Initiation of the charges with shocks above a certain strength resulted in overdriven detonations. In these cases the explosion times were independent of the specific surface of the explosive.

INTRODUCTION

The specific surface of a granular explosive may under certain conditions play an important role in shock initiation. The controlling factor is the magnitude of the entering shock velocity relative to the steady-state detonation velocity in the acceptor.

If the entering shock has a velocity such that the total explosion time is equal to or less than the time required for a steady-state detonation to traverse the acceptor, it is an indication that the temperature and pressure in the shocked explosive are high enough to insure complete release of the chemical energy to the shock front. If the entering shock produces an explosion time less than the transit time for a steady-state detonation the system is overdriven. Overdrive is an unstable condition that cannot be supported by the chemical energy available in the explosive. The velocity should decay with time, due to energy losses from the system, until it reaches the steady state. The rate of this decay of overdrive might be expected to be controlled by the geometry of the system. Increasing the specific surface of the explosive to speed up the decomposition should have no effect, for once all the energy can be delivered in the required time interval, to deliver it faster will be to no avail.

On the other hand, if the shock which enters the acceptor produces an explosion time greater than that which corresponds to the steady-state detonation in the acceptor, this indicates that the temperature and pressure in the entering shock are not high enough to complete the chemical reaction at a given point before the shock has moved out of the range of influence of that point. However, if a certain degree of reaction takes place at each successive point in the charge, the temperature and pressure at the front of the wave will eventually increase to the point where the material can

*Work done under the auspices of the U. S. Atomic Energy Commission.

**Deceased.

react completely while within the range of influence, and a stable detonation will be achieved. The time required for the hydrodynamic disturbance to reach the steady state is called the build-up time. Under the assumption of a surface controlled reaction, the rate of the chemical reaction would be expected to be directly proportional to the magnitude of the surface undergoing reaction. The rate of change of the velocity of the hydrodynamic disturbance does not depend so simply on the chemical reaction rate. It is nevertheless clear that the build-up time would be expected to decrease with an increase in the specific surface of the reacting explosive.

EXPERIMENTAL

In this experiment the total explosion time was measured for a small-scale gap test acceptor charge. This total explosion time includes the time for build-up and the time required to traverse the rest of the charge at the steady-state velocity, if such is achieved. The build-up time in an explosive, especially in a small charge, is difficult to measure. It can, however, be inferred from the acceptor explosion time, if the steady-state velocity is reached within the charge and if this velocity is independent of the specific surface. In this experiment the steady-state detonation velocity for these acceptor charges was reached in less than one charge length and was independent of the specific surface.

The experimental arrangement is shown in Figure 1. The PETN acceptor charges were one-half inch in diameter and one-half inch long, loaded to densities of 0.75 to 0.95 g cm^{-3}, in molded plastic holders. Although only the data for the higher density are reported, the lower gave similar results. The initiating shock strength was varied by changing the thickness of the brass[1] attenuator from zero to 0.250 inch. This corresponded to a change of pressure in the brass from 350 to 90 kbar.[2] The donor charges were 0.206 inch long by 0.300 inch diameter plastic-bonded cyclotrimethylenetrinitramine (RDX) pellets of 1.6 g cm^{-3} density initiated by low density PETN which, in turn, was set off by an exploding wire.

The range of specific surfaces investigated was about 3,000-12,000 $cm^2\ g^{-1}$. Although the data for only two (3,900 and 11,650 $cm^2\ g^{-1}$) are reported here, a third (ca. 8,000 $cm^2\ g^{-1}$) gave proportional intermediate results. The different specific surfaces were obtained by varying the conditions under which the PETN was precipitated from acetone by the addition of water. Experiments run with ball-milled material gave the same results as the precipitated material when the specific surfaces were the same. Specific surfaces were determined by a permeameter, an instrument that measures surface per unit mass by permeability methods.[3]

Acceptor explosion times were determined in the following manner: (1) rotating mirror camera records of the light emitted from the end of the donor and from the end of the acceptor gave the average time required for the wave to travel through both the brass attenuator and the acceptor charge; and (2) electronic switch measurements on the donor charge and on the donor-charge/brass-attenuator combination gave the average time spent by the shock in the brass attenuator. The difference between measurements (1) and (2) is the time through the acceptor charge which we have called the explosion time (t_{exp}).

DISCUSSION OF RESULTS

(a) Explosion Times

The data are plotted in Figure 2. With no brass attenuator in the system the donor charge initiated PETN of either specific surface so that the detonation traversed the acceptor in a time shorter (by 5%-6%) than that calculated on the basis of the steady-state detonation velocity throughout the charge. No specific surface effect was observed.

As the thickness of the brass attenuator was increased to 0.030 inch (270 kbar pressure) the overdrive dropped to zero as evidenced by the fact that here the explosion times were 2.56 μsecs - a value numerically equal to the time calculated using the steady-state detonation velocity of 4,960 m sec^{-1} and the charge length of one-half inch.

For brass attenuator thicknesses greater than 0.100 inch a clear cut separation of the explosion times was observed on a specific surface basis. The PETN pressings with the larger specific surface had the shorter times, which is attributed to a greater rate of reaction in the build-up zone with the larger specific surface.

For brass attenuators near the 50% fire point, some acceptors failed to detonate and the explosion times of the two PETN samples could not be compared properly. The 50% brass thickness has been determined[4] as 0.270 inch (80 kbar pressure) for the larger specific surface material and 0.310 inch (65 kbar pressure) for the smaller specific surface sample.

(b) Detonation Velocities

Variations of the build-up times can be inferred from observed variations of the explosion time measurements if information is available on the steady-state detonation velocities in these particular pressings of PETN. Such steady-state velocities have been measured for the two samples of PETN used in these experiments and no change with specific surface has been found. The explosion times were determined as a function of charge length by observing the light signals from the ends of charges of various lengths with a rotating mirror camera. Apparently the steady-state detonation had developed before the end of the first one-half inch of charge. A least-squares fit was made to the time-distance data shown in Figure 3. The calculated values of the steady-state detonation velocities with their standard deviations are 4,929 ± 37 m sec^{-1} for the larger specific surface and 4,995 ± 57 m sec^{-1} for the smaller, which are the same within the limits of experimental error.

CONCLUSION

It has been demonstrated that the explosion times of underinitiated small pressed charges of PETN decrease with an increase in the specific surface of the explosive. This decrease is believed to occur in the unstable build-up zone that precedes steady-state detonation and is explainable in terms of a surface-burning reaction.

Overinitiation of the charges of PETN gave rise to explosion times that were shorter than those calculated using the steady-state detonation velocity. These explosion times were independent of the specific surface and might be expected to be controlled by the geometry of the system.

REFERENCES

1. Free-machining yellow brass - 66% Cu + 34% Zn.
2. J. O. Johnson, Private communication.
3. R. M. Lea and R. W. Nurse, J. Soc. Chem. Ind., 58, 277 (1939).
4. R. H. Dinegar, R. H. Rochester, and M. S. Millican, Effect of Specific Surface on Shock Sensitivity of Pressed Granular PETN this session.

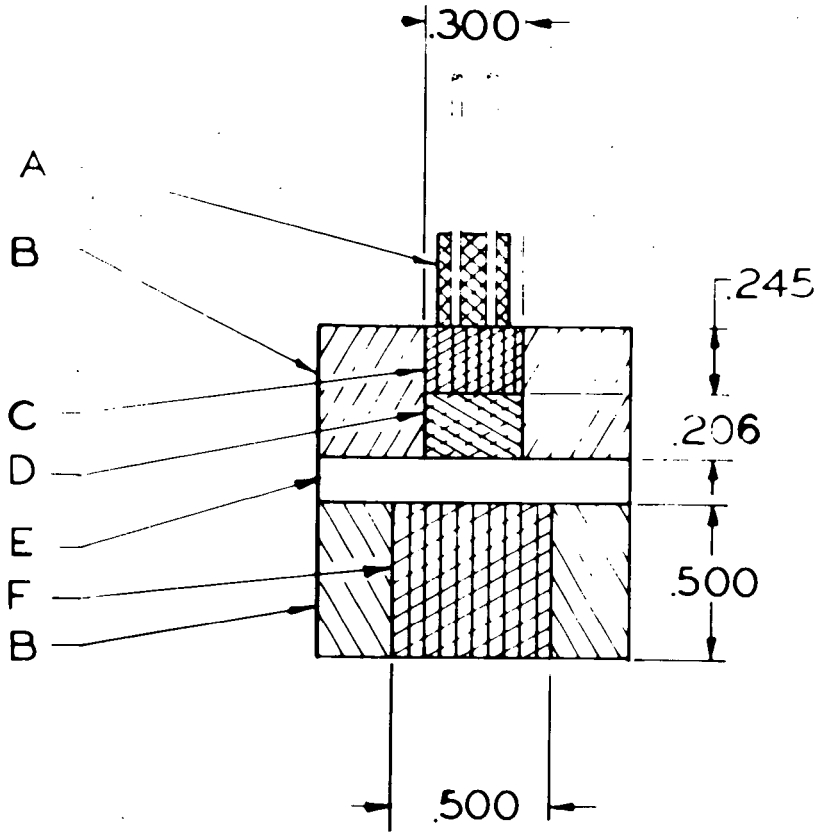

Figure 1

SMALL-SCALE GAP TEST ASSEMBLY

A = Exploding wire assembly; B = Plastic holders; C = PETN initiator; D = Plastic-bonded RDX donor; E = Brass attenuator; and F = PETN acceptor (test) charge.

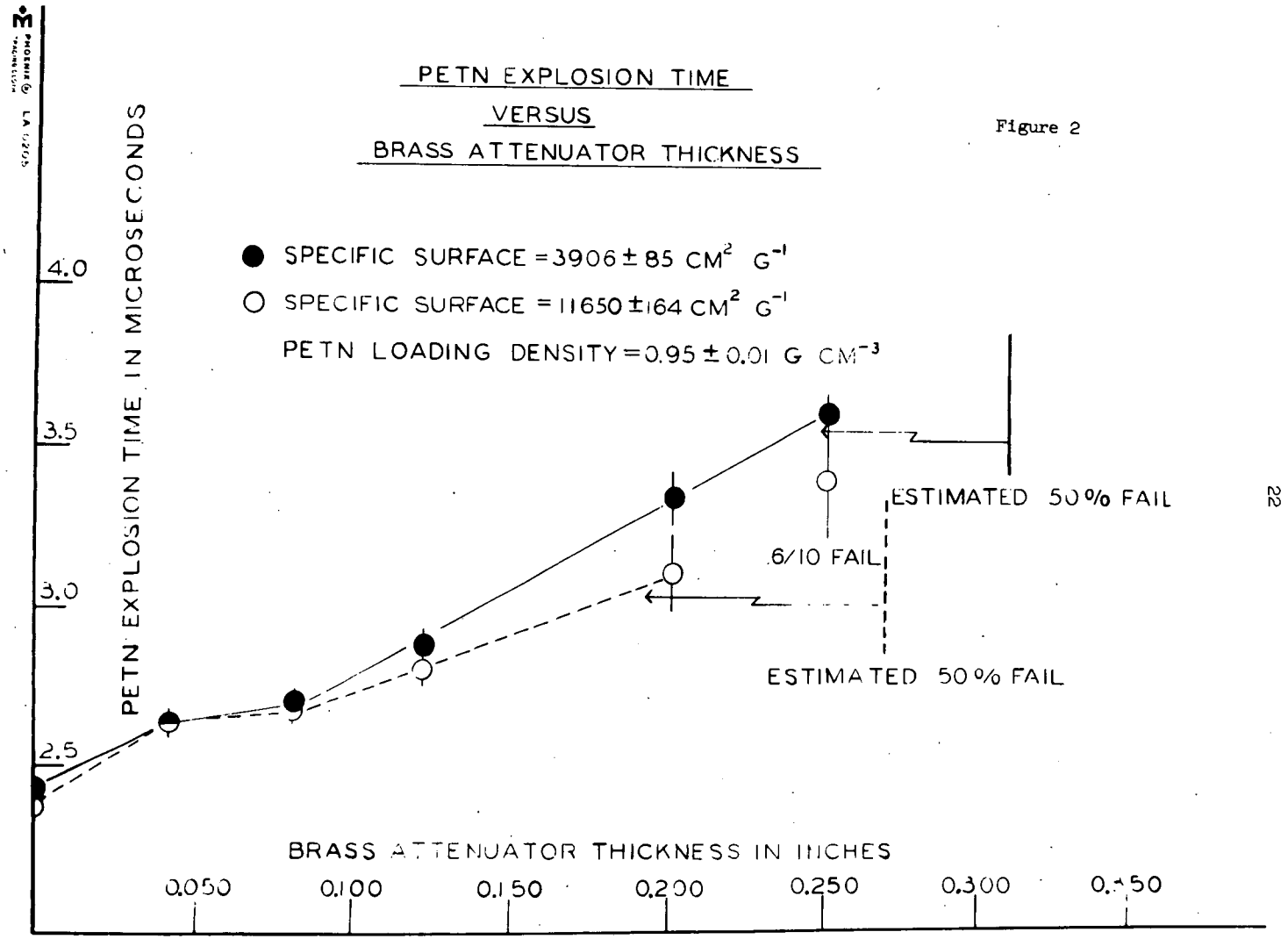
PETN EXPLOSION TIME
VERSUS
BRASS ATTENUATOR THICKNESS
SPECIFIC SURFACE = 3906 ± 85 CM² G⁻¹
SPECIFIC SURFACE = 11650 ± 164 CM² G⁻¹
PETN LOADING DENSITY = 0.95 ± 0.01 G CM⁻³
PETN EXPLOSION TIME IN MICROSECONDS
4.0
3.5
3.0
2.5
ESTIMATED 50% FAIL
6/10 FAIL
ESTIMATED 50% FAIL
BRASS ATTENUATOR THICKNESS IN INCHES
0.050
0.100
0.150
0.200
0.250
0.300
0.350

Figure 2

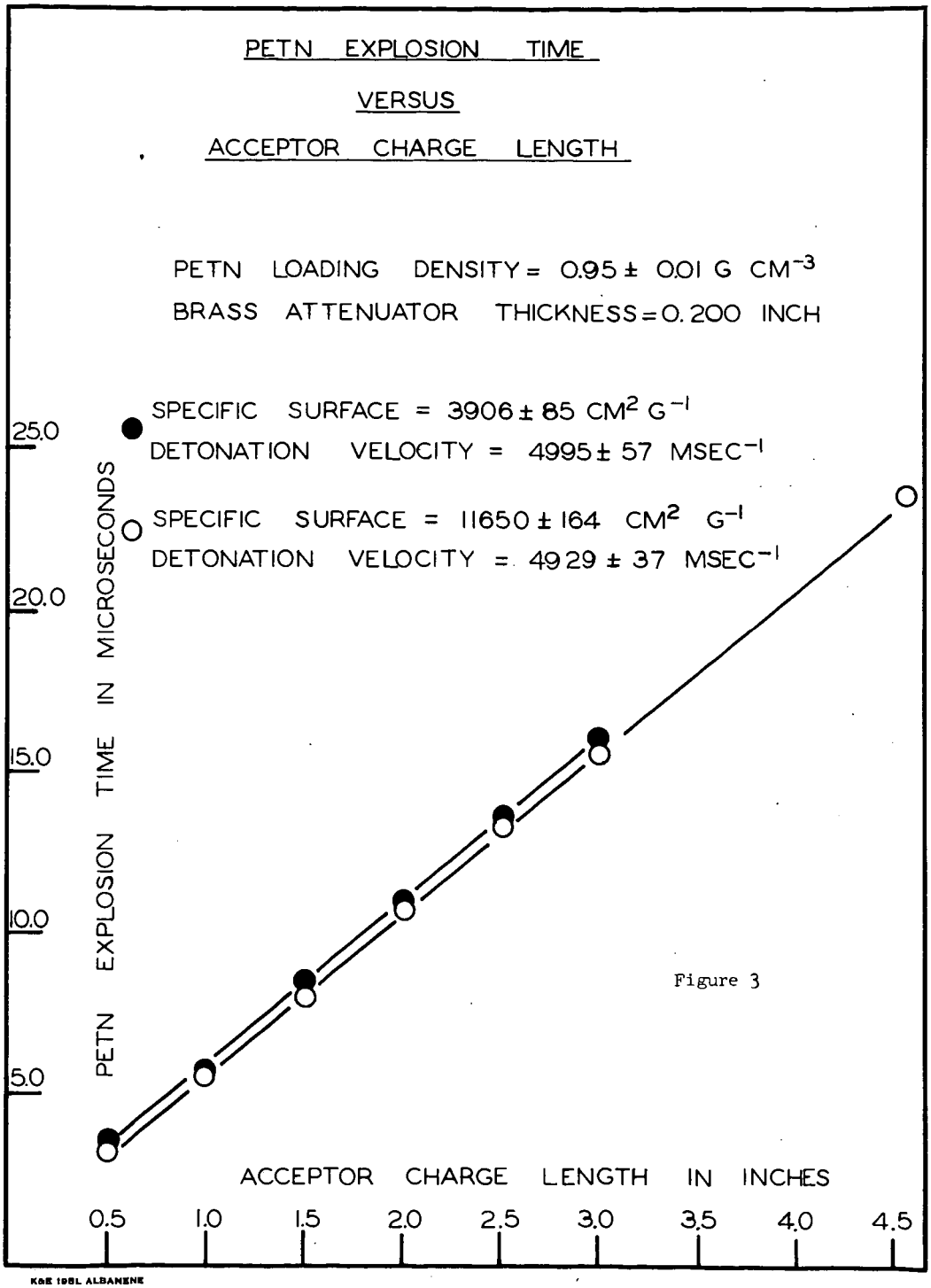
PETN EXPLOSION TIME
VERSUS
ACCEPTOR CHARGE LENGTH
PETN LOADING DENSITY = 0.95 ± 0.01 G CM⁻³
BRASS ATTENUATOR THICKNESS = 0.200 INCH
SPECIFIC SURFACE = 3906 ± 85 CM² G⁻¹
DETONATION VELOCITY = 4995 ± 57 MSEC⁻¹
SPECIFIC SURFACE = 11650 ± 164 CM² G⁻¹
DETONATION VELOCITY = 4929 ± 37 MSEC⁻¹
PETN EXPLOSION TIME IN MICROSECONDS
25.0
20.0
15.0
10.0
5.0
ACCEPTOR CHARGE LENGTH IN INCHES
0.5
1.0
1.5
2.0
2.5
3.0
3.5
4.0
4.5
KOE 1981 ALBANENE

Figure 3

Effect of Specific Surface on the Shock Sensitivity of Pressed Granular PETN*

by

Robert H. Dinegar
Richard H. Rochester
and
Mike S. Millican**

University of California, Los Alamos Scientific Laboratory
Los Alamos, New Mexico

One theory of the processes leading to detonation in pressed granular explosives postulates that the rate of the chemical reaction in the build-up zone determines the shock sensitivity. If this rate is described in terms of a surface burning reaction it follows that enhanced sensitivity should result when the size of the particles which compose the explosive pressing is decreased.[1-4] While this predicted increase in sensitivity with decreasing particle size has been experimentally studied and shown to exist in gap-test measurements on propellants,[5] we know of no similar investigation of this effect on high explosives although it is often considered to be in agreement with general experience.

We have recently performed a series of experiments in which the shock sensitivity of the explosive pentaerythritoltetranitrate (PETN) has been investigated as a function of its specific surface. The sensitivity test used was a small-scale gap test,[6] a diagram of which is shown in Fig. 1. The range of specific surfaces investigated was 2,000 - 18,000 $cm^2\ g^{-1}$. The specific surface was measured by a permeameter, an instrument that determines the surface per unit mass from air permeability measurements.[7]

Two different methods for obtaining the PETN with the desired specific surfaces were used. The first involved ball-milling the largest sized material for various periods of time to reduce the average size while the second consisted of precipitating the PETN from acetone by the addition of water under different conditions to obtain individual samples with the different specific surfaces.

*Work done under the auspices of the U. S. Atomic Energy Commission.
**Deceased

The PETN acceptor (test) charges were cylindrical, one-half inch long by one-half inch in diameter and pressed to a loading density of 0.95 g cm^{-3}. The donor charges were two-tenths inch long by three-tenths inch diameter plastic-bonded RDX pellets of 1.6 g cm^{-3} density initiated by low density PETN which in turn was set off by a length of primacord. The attenuator material was one-inch diameter brass[8] cylinders of various thicknesses.

The criterion of satisfactory initiation was the production of a dent in a one-half inch thick sheet of aluminum used as a "witness" plate. Twenty shots of each particle size were fired using the "up and down" or "step" method, with an interval of one-hundredth inch brass thickness. The reported thickness is that at which 50% of the samples detonated.[9] Preliminary investigation of the normality of the distribution of these points by the method of Davies[10] shows them to be normally distributed with a standard deviation of 0.023 inch.

The data we have collected are shown in Fig. 2. It is evident that the shock sensitivity of PETN, as measured by this method, does not increase with an increase in the specific surface of the material, but rather decreases slightly over a wide range of specific surface. Experiments run at two other PETN loading densities, 0.75 and 1.4 g cm^{-3}, show the same effect. These results indicate that some mechanism other than a surface burning reaction must determine the shock initiation to detonation in granular pressings of PETN.

References

1. A. Macek, Chem. Revs., 62, 41 (1962).
2. H. Eyring, et al., Chem. Revs., 45, 144 (1949).
3. F. P. Bowden and A. D. Yoffe, Initiation and Growth of Explosions in Liquids and Solids, Cambridge at the University Press, (1952) p.5.
4. G. B. Kistiakowsky, Third Symposium on Combustion and Flame and Explosion Phenomena, Williams & Wilkins Co., Baltimore, Md., (1949) pp. 560-565.
5. J. R. Hyndman, NAVORD Report 5746, XXX, 291
6. G. P. Cachia and E. G. Whitbread, Proc. Roy. Soc. (London), A246, 269 (1958).
7. F. M. Lea and R. W. Nurse, J. Soc. Chem. Ind., 58, 277 (1939)
8. Free-Machining Yellow Brass - 66% Cu + 34% Zn.
9. W. J. Dixon and A. M. Mood, J. Am. Stat. Assoc., 43, 109 (1948).
10. O. Davies, Statistical Methods in Research and Production, Oliver & Boyd Pub., London, 2nd Ed., (Rev. 1949) pp. 20-21.

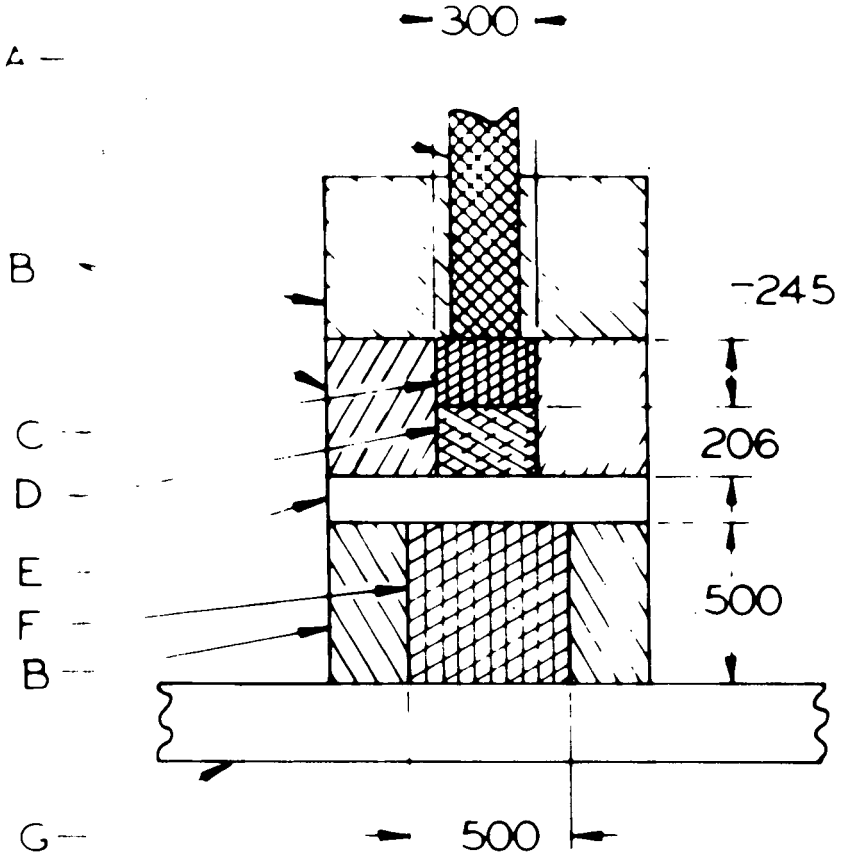

Figure 1

SMALL SCALE GAP TEST ASSEMBLY

A = Primacord; B = Plastic holders; C = PETN initiator; D = Plastic-bonded RDX donor; E = Brass attenuator; F = PETN acceptor (test) charge; and G = One-half inch aluminum "witness" plate.

SMALL SCALE GAP TEST SENSITIVITY OF PETN

Figure 2

Experimental data from small-scale gap sensitivity testing of pressed granular PETN. Brass attenuator thickness versus specific surface of the PETN. Decreasing brass attenuator thickness represents decreasing PETN sensitivity. Limit lines show the estimated 95% confidence levels.

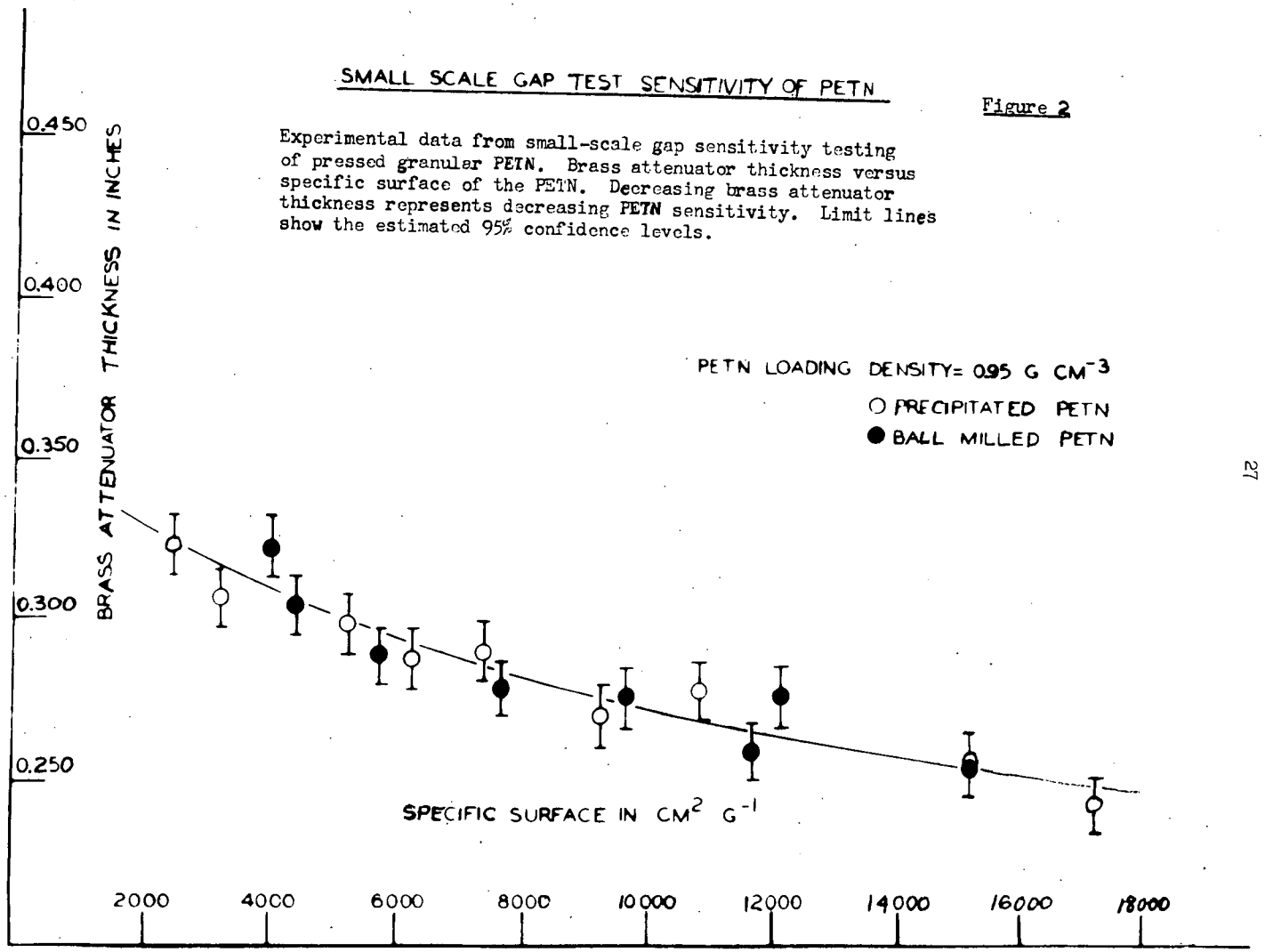

DETONABILITY OF THE SYSTEM NITROBENZENE, NITRIC ACID, AND WATER

C. M. Mason, R. W. Van Dolah, and J. Ribovich

Explosives Research Laboratory, Bureau of Mines,
U. S. Department of the Interior, Pittsburgh, Pa.

INTRODUCTION

It has been known for many years (2) that nitrobenzene and nitric acid form detonable mixtures. Cook (4) used a mixture of 24 percent nitrobenzene, 63 percent nitric acid, and 13 percent water to study the reaction thickness in detonation. As part of an investigation of liquid explosive mixtures based on nitric acid, Kurbangalina (7) studied the explosive properties of a mixture composed of 72 percent nitric acid and 28 percent nitrobenzene. It was observed that the critical charge diameter for this mixture was less than 0.6 mm in contrast to 2-2.5 mm for nitroglycerin under the same experimental conditions and that the stable detonation rate was 6,200-6,800 meters per second.

In considering the handling of liquid explosive systems some evaluation must be made of the ease of initiation of detonation by mechanical shock in addition to the compositional limits of detonable mixtures. In recent years the card-gap technique developed by Pape and Whitbread (8) has been used quite extensively (1, 3, 5, 6, 9) to evaluate the relative ease of initiation by an explosive shock, under very specific physical conditions of many explosive materials. This work has resulted in the accumulation of a fair amount of semiquantitative experimental data against which new results may be compared to give an evaluation of relative sensitivity to shock initiation (10).

In the present investigation the limits of detonability of the nitrobenzene-nitric acid-water system were determined by the card-gap technique at 25° and 80° C. Within these limits considerable data were obtained on the effect of composition on sensitivity, i.e., ease of initiation. Since part of the system forms two immiscible liquid phases, the solubility diagram of the three-component system was determined at 25° C in order to compare the area of detonability with the area in which two phases form. For comparison with the nitrobenzene system, limits of detonability were determined for the benzene-nitric acid system at 25° C.

EXPERIMENTAL DETAILS

The version of the card-gap technique employed in this investigation consists of the following elements:

A donor explosive charge, a variable gap of plastic cards, a container for the sample, and a steel witness plate to indicate whether or not initiation occurs in the acceptor cup. The donor is made up of two 25-gram cylindrical tetryl pellets (1 inch high by 1-5/8 inches in diameter) whose density is 1.57 ± 0.03 grams per cc. The shock-attenuating barrier or gap consists of an appropriate number of 0.010-inch-thick cards of cellulose acetate stock. Accurately-machined cylindrical blocks of polymethyl methacrylate are substituted for thick stacks of plastic cards when repetitive tests are made at large gap values; the finer gap variations are again attained by adding plastic cards. The container is a 3-inch length of 1-inch, Schedule 40, black steel pipe sealed off at the bottom with polyethylene film.

Evidence of initiation of the liquid is provided by a witness plate of cold-rolled mild steel, 4 by 4 inches by 1/4 inch. The tetryl booster rests on a cylindrical block of cork or soft wood 1.62 inches in diameter and 3/4 inch high, with a 0.280-inch hole along its cylindrical axis into which the detonator is inserted (fig. 1).

In use the components of the test are carefully aligned, the test liquid is added to the cup, and the witness plate is set in place on the top of the acceptor. After the shot a positive result is indicated by a clean hole cut through the witness plate. Any other condition of the plate was interpreted as a negative result.

RESULTS

The concentration limits of the detonable mixtures of nitrobenzene, nitric acid, and water at 25° C and 80° C were determined at zero gap. It was quickly apparent that mixtures yielding two phases were not detonable and that the limits of detonability coincided with the limits of miscibility over a wide portion of the compositional diagram. In confirmation the limits of miscibility were determined by titrating mixtures of nitrobenzene and nitric acid with water to a faint opalescence, indicative of the formation of a two-phase system. No attempt was made to determine miscibility limits in the region of low nitric acid concentrations. Figure 2 gives both the limits of detonability, under the conditions of the card-gap test, and the miscibility limits. The two limits are seen to be identical over a wide range of compositions.

The shock sensitivity of the binary nitrobenzene-nitric acid system as a function of composition was determined. Figure 3 shows the extreme ease with which mixtures near the stoichiometric composition can be shock-initiated. No attempt was made to determine card-gap values beyond 5 inches because of the decreasing significance of the results at these very large gaps. For comparison, a similar investigation was made of the sensitivity of the binary benzene-nitric acid system (fig. 4). In this case an apparent maximum sensitivity value at about 5 inches gap was obtained for the mixture containing 85 percent nitric acid. The comparable card gap value, i.e., the one allowing initiation of normal detonation in nitroglycerin, is about 0.4 inch. Although the real sensitivity of different materials cannot be directly equated to the magnitude of the gap values, the nitric acid systems must be considered quite sensitive. The region of maximum sensitivity of the two binary systems approximated the stoichiometric, or most energetic, mixture as anticipated.

To evaluate the relative sensitivity of various nitrobenzene-nitric acid-water mixtures, a series of trials were made on various mixtures at 1- and 2-inch card gaps. The results are shown in figure 5.

The card-gap technique, in common with most other empirical tests, yields results that are subject to variation if different test conditions, such as the size of the container or of the donor, are employed. Increasing the diameter of the container or increasing the strength of the booster could enlarge somewhat the area of detonable compositions in the single phase systems. The increase in apparent sensitivity from 25° to 80° C indicates that further temperature increase would also enlarge the range of detonable mixtures. The rather close agreement between the areas of detonability and miscibility in the ternary diagram indicates that the addition of another component to enlarge the range of miscibility in figure 2 could increase the detonable range as well.

The desensitization caused by low concentrations of water is quite marked. Thus in the region of stoichiometric compositions 8 percent water sufficed to reduce the card-gap sensitivity from >5 inches to about 2 inches; another 10 percent water reduced the sensitivity to about the 1-inch level. Such reduced sensitivity is quite out of line with a simple reduction of energy content.

To relate sensitivity and limits of detonability to the potential energy yields that could be expected on detonation from various compositions, the latter were roughly estimated from simple thermochemical considerations; precise computation of these energies did not seem warranted.

For the reaction $C_6H_5NO_2 + 5HNO_3$ (ℓ) = $6CO_2 + 5H_2O$ (ℓ) + $3N_2$, the liberated energy at 25° C is about 700 kilocalories per gram molecular weight of nitrobenzene. The stoichiometric mixture, 1 mole of nitrobenzene to 5 moles of nitric acid, thus can yield about 1,600 calories per gram of mixture, roughly equivalent to the energy yield from nitroglycerin. For nitric acid-rich mixtures, the liberated energy was estimated by assuming a complete consumption of the available nitrobenzene and correcting the final value for the total weight of the mixture. For fuel-rich mixtures, the liberated energy was estimated by assuming that the reaction proceeds in three steps. Oxidation of carbon to carbon monoxide, and of hydrogen to water are the two initial steps. These are followed by the final oxidation of the carbon monoxide to carbon dioxide. Water in the initial mixtures was treated as a simple diluent, i.e., not equilibrated with carbon in the fuel-rich compositions. On the basis of these assumptions, the available energy has been calculated for various mixtures of nitrobenzene, nitric acid, and water. The results are shown in terms of constant enthalpy contours superimposed on the region of detonable compositions (fig. 6).

The energy content of mixtures lying within the zone of detonability, as so estimated, is seen to be greater than 440 calories per gram of mixture, to a maximum of about 1,600 calories per gram for the anhydrous stoichiometric composition. That such low-energy liquid systems should be detonable in 1-inch diameter is indicative of quite facile reactivity. In contrast, liquid dinitrotoluene at 200° F cannot be initiated in 2-1/2-inch steel pipe with a 240-grain pentolite booster (the critical diameter is on the order of several inches), despite an approximate energy content of 560 calories per gram.

The addition of water, as shown in figure 6, has relatively little effect on the computed energy content, in contrast to its effect on sensitivity. This latter effect is most strikingly demonstrated by the abrupt change of high-energy detonable compositions (as high as 1,200 calories per gram) to nondetonable two-phase systems by small additions of water. Clearly, much of the two-phase system, if finely dispersed (emulsified) and in large diameter charges, should be detonable.

SUMMARY

The limits of detonability in 1-inch-diameter charges of the systems nitrobenzene-nitric acid-water at 25° C and 80° C and benzene-nitric acid at 25° C were determined. Relative shock sensitivities were estimated using the card-gap technique. In general, the limit of detonability of the nitrobenzene system was observed to coincide with the region of complete miscibility in the ternary diagrams, and water was found to markedly reduce the sensitivity. Thermochemical calculations showed the liberated energy of limit mixtures to fall as low as about 440 calories per gram, indicating rather high, intrinsic sensitivity to detonation.

ACKNOWLEDGMENT

This report is based in part upon work done under cooperative agreements with the Koppers Company, Inc., Pittsburgh, Pa., and with the Manufacturing Chemists' Association, Washington, D. C.

REFERENCES

1. Amster, A. B., Noonan, E. C., and Bryan, G. J., ARS J. 30, 960 (Oct. 1960).
2. Berthelot, M., Explosives and Their Power (translated by C. N. Hoke and W. Macnab), John Murray, London, 1892, p. 472.
3. Cachia, G. P., and Whitbread, E. G., Proc. Roy. Soc. (London) A246, 268 (1958).
4. Cook, M. A., The Science of High Explosives, Reinhold Publishing Corp., New York, 1958, pp. 138, 190-194.
5. Cook, M. A., and Udy, L. L., ARS J. 31, 52 (Jan. 1961).
6. Herickes, J. A., Ribovich, J., Damon, G. H., and Van Dolah, R. W., Communications of the 31st Internat. Cong. of Indus. Chem., Liège, Belgium, Sept. 7-20, 1958, pp. 121-126.
7. Kurbangalina, R. Kh., Zhur. Priklad. Khim. 32, 1467 (1959); Chem. Abs. 53, 19389 (1959).
8. Pape, R., and Whitbread, E. G., Sensitiveness of Solid and Liquid Explosives, Part 3: The Application of the Gap Test to Liquid Explosives. Explosives Research and Development Establishment, Tech. Memo. No. 21/M/52, March 1953.
9. Test No. 1, Card Gap Test for Shock Sensitivity of Liquid Monopropellants, Liquid Propellant Information Agency, The Johns Hopkins University, Silver Spring, Maryland, Dec. 1959.
10. Van Dolah, R. W., Ind. Eng. Chem 53, 59A (1961).

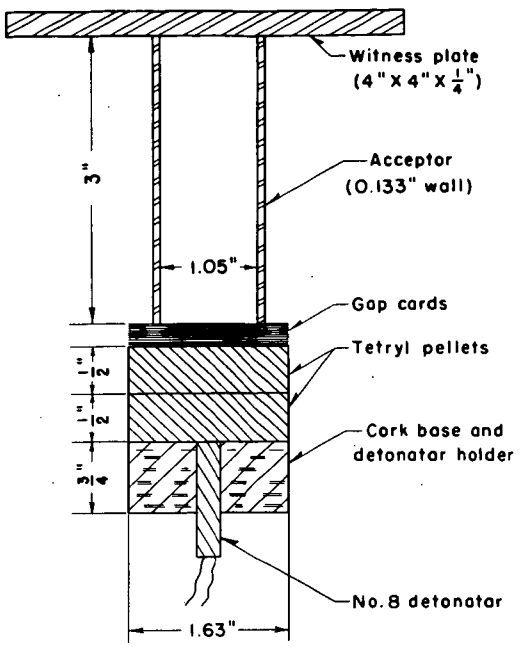

Figure 1.— Arrangement for cord gap experiments.

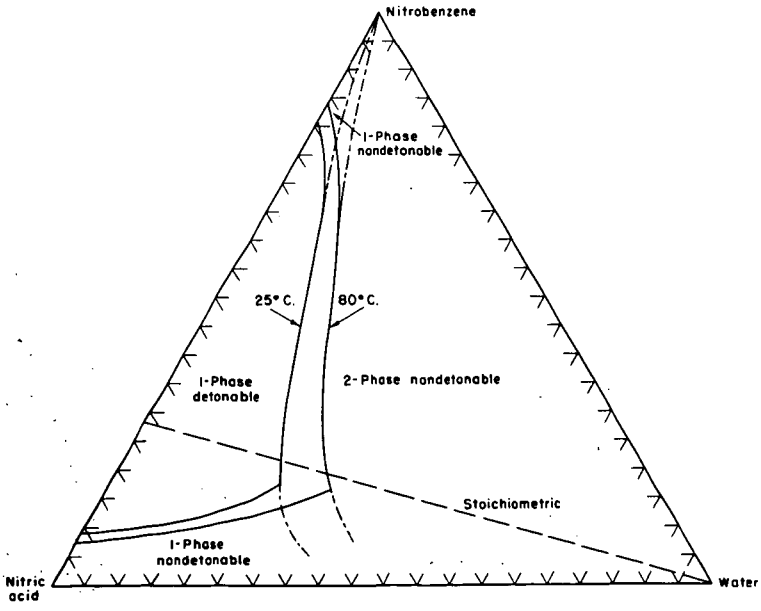

Figure 2.- Detonability and miscibility limits in the nitric acid–nitrobenzene–water system at 25°C. and 80°C. and zero gap. Detonable systems at given temperature are left of the solid lines, non-detonable to the right.

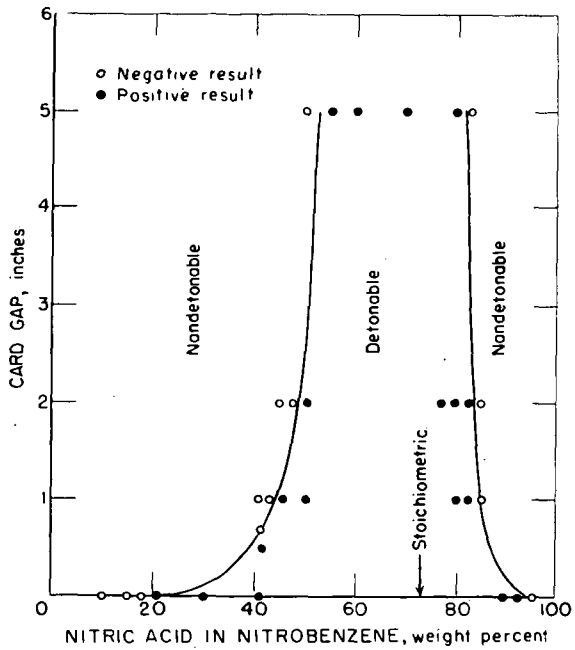

Figure 3.– Shock sensitivity studies of nitric acid–nitrobenzene system at 25°C.

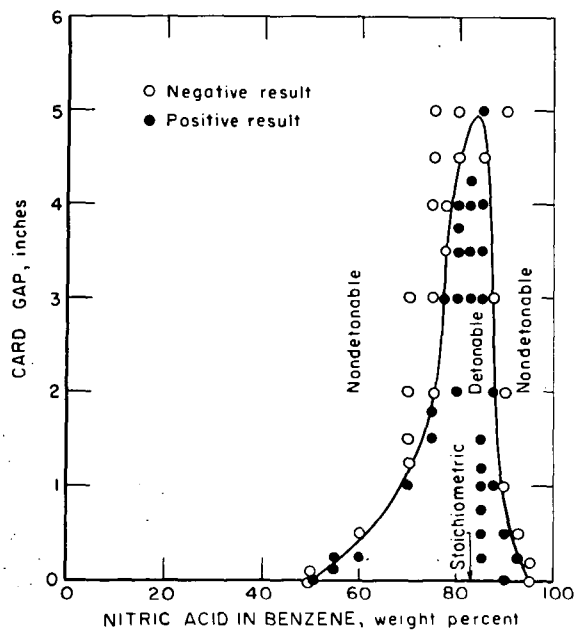

Figure 4.– Shock sensitivity studies of nitric acid–benzene system at 25°C.

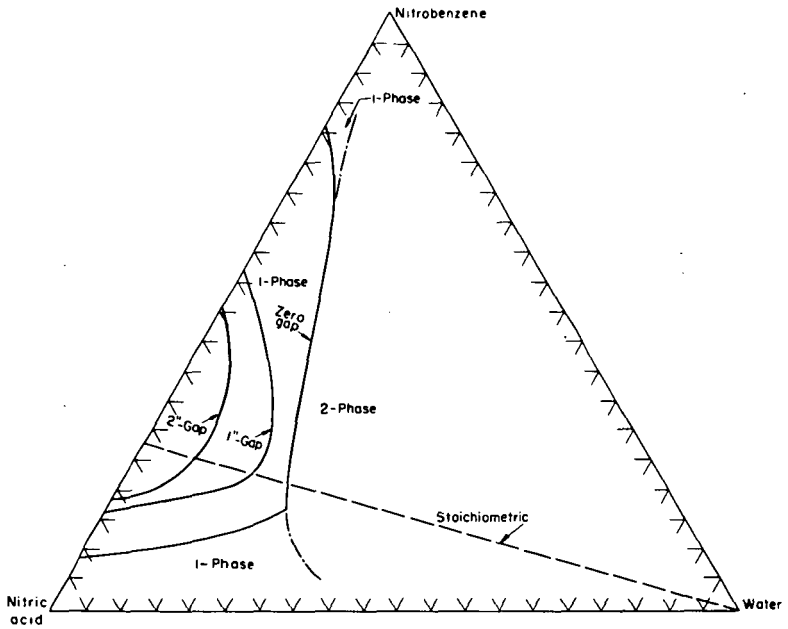

Figure 5.—Shock sensitivity of nitric acid–nitrobenzene–water system at 25°C. Detonable systems at given gaps are left of the solid lines, non-detonable to the right.

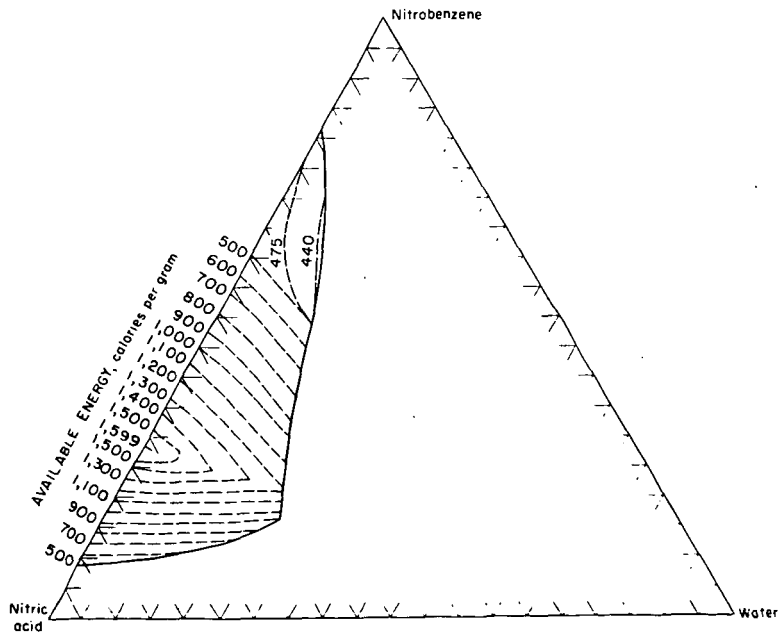

Figure 6.—Available energy in the system nitrobenzene, nitric acid and water at 25°C. Detonable mixtures are left of the solid curve.

Further Studies of the High Rate Decomposition of High Energy Materials

J. M. Rosen and J. R. Holden

U. S. Naval Ordnance Laboratory
White Oak, Silver Spring, Maryland

INTRODUCTION

Recent studies at the Naval Ordnance Laboratory have been carried out to gain additional information on the sensitivity of high energy materials. A unique thermal sensitivity method has been devised by Wenograd (1) in which small (3 to 4 mg) samples are very rapidly heated to temperatures in the range of 500 to 1000°C. The delay time to explosion is measured as a function of sample temperature.

This present report contains additional thermal sensitivity data on high energy liquid compositions using Wenograd's method. The work was performed primarily to demonstrate the capability of the thermal sensitivity method in following changes in the sensitivity of high energy systems.

In the thermal sensitivity determination a 2.1 microliter sample is enclosed in a $2\frac{1}{2}$ inch length of stainless steel hypodermic needle tubing. The tubing is then heated very rapidly by discharging a capacitor through it, and its resistance is measured as a function of time. The temperature to which the tubing has been raised by the capacitor discharge can be calculated from the ratio of its hot resistance to its room temperature resistance. When the sample within the tube explodes, it bursts the tube wall causing an abrupt change in the resistance of the tube. Therefore, both the temperature of the sample container and the delay time before the sample explodes can be determined by measuring the resistance of the hypodermic needle tube as a function of time. In the sensitivity apparatus, this is done by making the tube one arm of a Wheatstone bridge circuit and displaying the unbalance voltage of the bridge on an oscilloscope. The delay time is also measured with an electronic timer which is started by a signal from the capacitor discharge and stopped by a signal from a microphone located near the bursting sample tube.

EXPERIMENTAL

No basic change has been made in the original circuit designed by Wenograd (1). The fundamental part of the circuit is shown schematically in Figure 1. The high voltage pulser consists of a high voltage power supply, which charges a 2 μ F capacitor to voltages ranging to about 7 kV, and 5C22 thyratron for switching this charge. The capacitor discharges its energy through all three branches of the circuit, but because of the lower resistance of $R_1 + R_2$, the bulk of the current flows through this path. When the capacitor has finished discharging, the high-voltage pulser represents an open circuit and only the simple Wheatstone bridge powered by E_B through R_A remains.

The sample tubes are easily filled with a liquid by placing the open ends in the liquid as shown in Figure 2. Air is removed from the tubing by evacuation. When the atmosphere is readmitted, the liquid sample is forced into the tubing. About 0.1 cc of sample is required for a series of measurements.

It is possible to work with volatile liquids if the sample is cooled to reduce the vapor pressure. In this way the sample may be loaded by evacuation without permitting a significant loss of the sample.

A program for the IBM 7090 digital computer is used to treat the thermal sensitivity experimental data. In addition to computing temperatures from the unbalance voltages, the program yields a lease square fit of the data to the straight line defined by

$$\log_{10} \text{ delay time in milliseconds} = A + \frac{1000B}{T, \ ^\circ K} .$$

All of the data shown represent the results of the least square fit described above.

RESULTS AND DISCUSSION

The employment of improved experimental techniques has reduced the amount of scatter of the data compared to that previously reported (1). Figure 3 is representative of the measurements at the present time. The dashed lines represent the limits of one standard deviation of $\log_{10}$ delay time. Three replicate measurements of nitroglycerine made at intervals of about one month are shown in Table 1.

TABLE 1

THERMAL SENSITIVITY OF NITROGLYCERINE

Sample	Temp., °C at 250 microsec. delay	Slope, B /1	Stand. dev. of $\log_{10}$ delay time	No. of trials	Range, millisec.
1	395	7.7	0.21	17	0.03 to 8.27
2	392	8.3	0.22	13	0.02 to 6.03
3	397	8.1	0.19	20	0.04 to 27.50

/1 $\log_{10}$ delay time in milliseconds = $A + \frac{1000\ B}{T,\ °K}$

Most of the experimental error at the present time can be attributed to oscilloscope drift and uncertainty in the resistance measurements. It is not expected that a further improvement in the quality of data can be achieved with the apparatus in use.

Tetranitromethane (TNM) with two added fuels, toluene and nitromethane, was studied in an attempt to follow changes in sensitivity as a function of composition. The data obtained were extrapolated to the 10 microsecond delay times and the temperatures corresponding to these times were plotted as a function of composition, Figures 4 and 5. For purposes of comparison with booster sensitivity data, the 10 microsecond time seemed reasonable as that is the approximate time an explosive is heated to a high temperature by the shock wave in the booster type test.

A very sharp drop in temperature is obtained with the addition of 6% toluene, Figure 4, which is interpreted as a marked increase in sensitivity. The rise in temperature obtained with larger amounts of toluene is believed to represent a decrease in sensitivity.

The TNM-nitromethane system was briefly investigated, Figure 5. The temperature drop did not appear to be as sharp as that obtained with added toluene. Further measurements will be made to complete the TNM-nitromethane study.

Tschinkel and Morrison investigated the sensitivity of TNM with added benzene and nitromethane (2). They found the addition of 5% benzene increased the "card gap" value for TNM from 35 to greater than 300. TNM with 25% benzene also had a "card gap" value greater than 300. However, only a relatively small increase in sensitivity occurred with added nitromethane. The maximum "card gap" value was 80 at 70% TNM.

Tschinkel and Morrison point out the large difference between the shock sensitivities of TNM with added benzene and nitromethane. This large difference is not indicated by the thermal sensitivity method where the minimum temperatures required for thermal initiation differ by only about 100°C. The greatest sensitivity of TNM containing toluene occurs in the range of maximum energy as computed by Tschinkel and Morrison. In the TNM-hydrocarbon system, there is a general agreement between shock sensitivity and thermal sensitivity data as both show a marked increase in sensitivity with the addition of a small percentage of hydrocarbon.

It seemed worthwhile to examine the sensitivity of nitroglycerine with added dimethyl phthalate as this compound has been used as a desensitizer for nitroglycerine. Data obtained on a number of compositions are shown in Figure 6. Progressive increases in dimethyl phthalate content also increase the temperature required for thermal initiation. The decrease in sensitivity with the addition of 9.3% and 18.7% dimethyl phthalate appear to be rather small. It is believed this is a real effect although it could not be defended by a statistical proof. A very large difference is noted between 30% and 40% dimethyl phthalate, particularly at short delay times.

Although the hot-tube thermal sensitivity information is believed to provide a good characterization for high energy materials, it cannot be considered trustworthy in determining handling hazards. Certainly there are many properties that affect the sensitivity characteristics of a liquid such as vapor pressure, viscosity, and chemical reactivity.

Further studies of high energy systems will be carried out to gain insight into the parameters that affect the thermal sensitivity.

REFERENCES

(1) J. Wenograd, Trans. Faraday Soc., 57, 1612 (1961).

(2) J. G. Tschinkel and C. R. Morrison, J. of Chem. and Eng. Data, 3, 350 (1958).

$R_3 = R_4 = 25$ OHM NON-INDUCTIVE RESISTOR; $R_A = 10$ OHM NON-INDUCTIVE RESISTOR; R_2 = CONSTANTAN RESISTOR; R_1 = TUBE UNDER TEST; $E_B = 24$ V STORAGE BATTERY; E = OSCILLOSCOPE

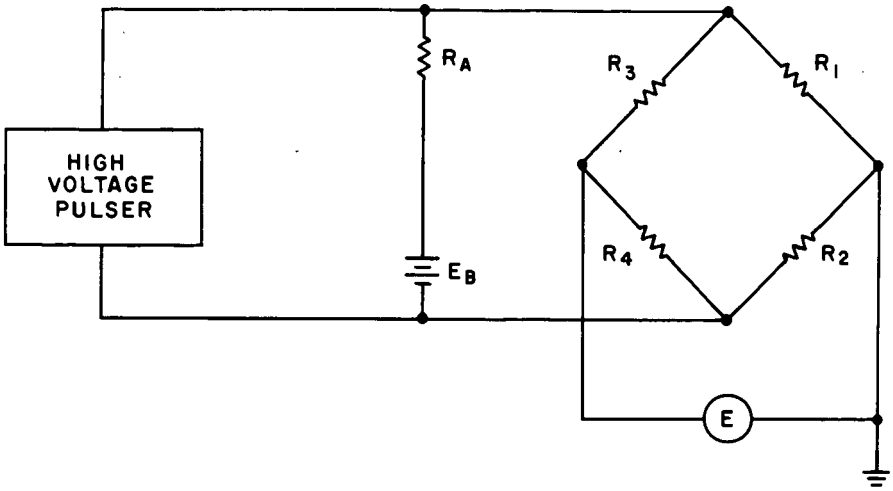

FIG. 1 CIRCUIT OF THERMAL SENSITIVITY APPARATUS

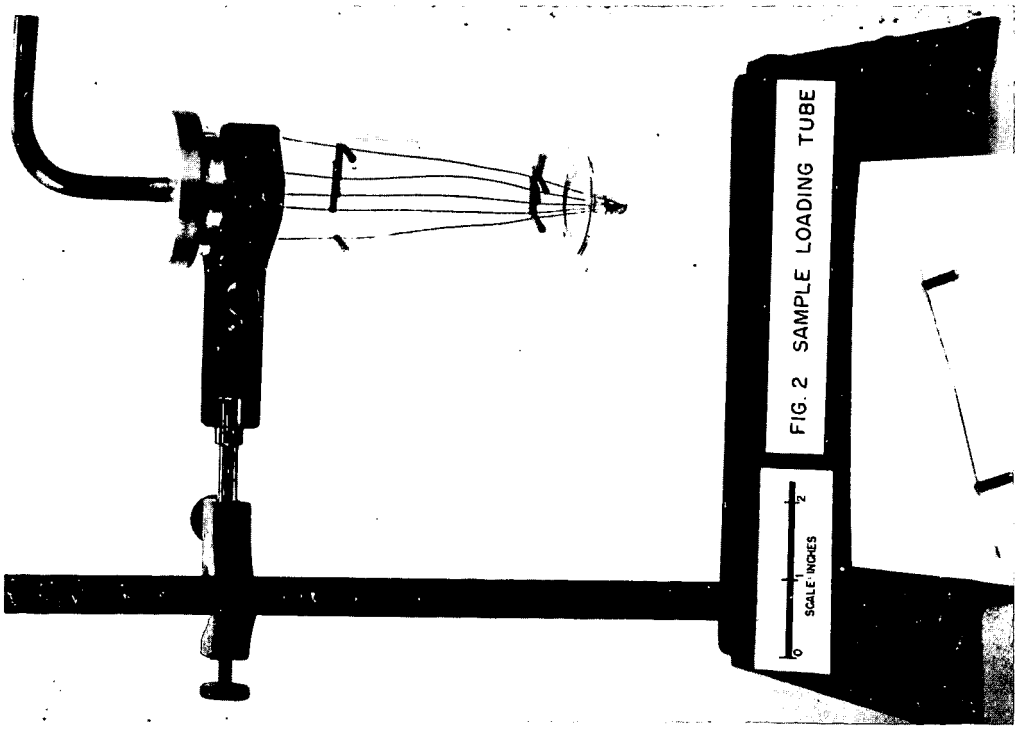

FIG. 2 SAMPLE LOADING TUBE

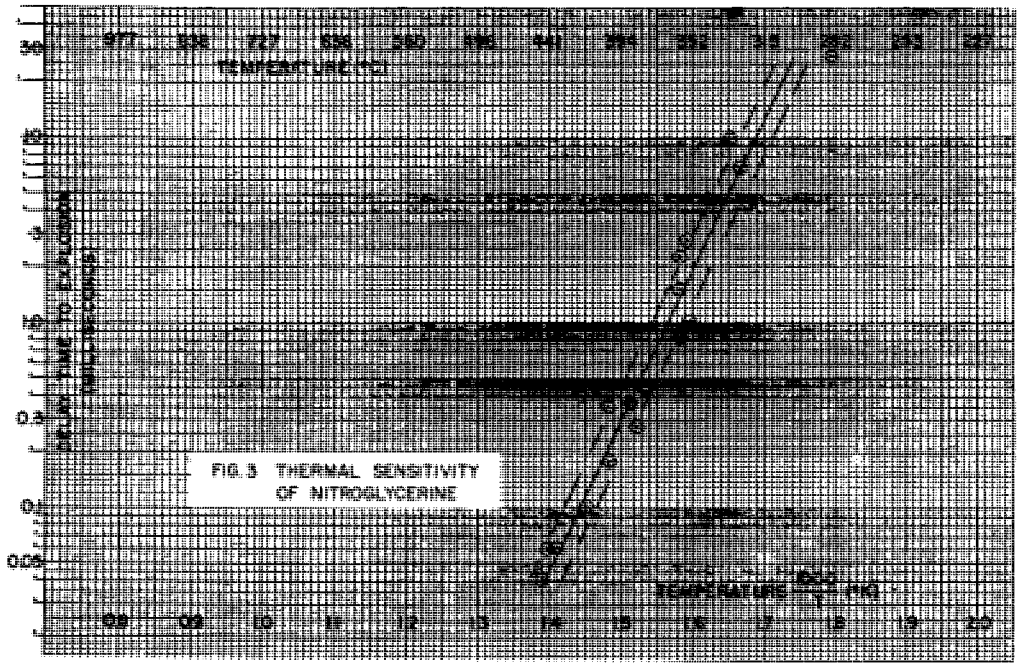

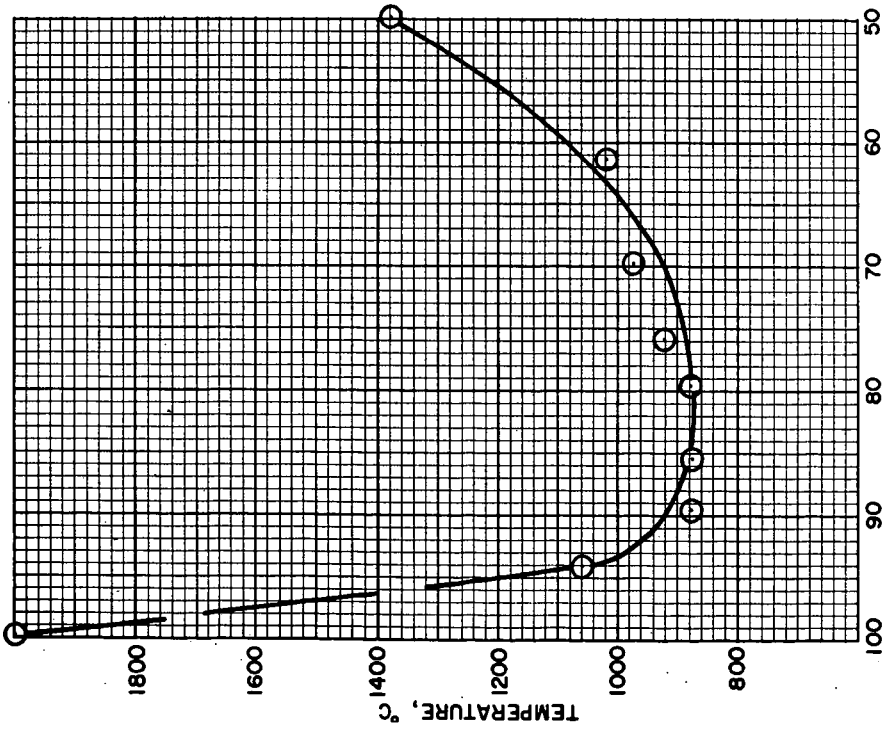

FIG. 4 TNM–TOLUENE COMPOSITIONS; TEMPERATURE AT THE 10 MICROSECOND DELAY TIME

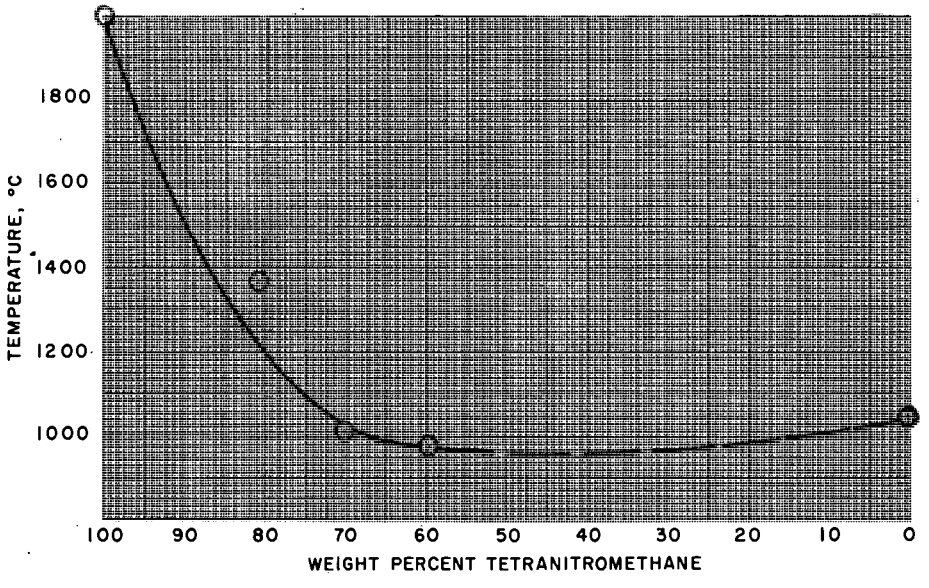

FIG. 5 TNM – NITROMETHANE COMPOSITIONS; TEMPERATURE AT THE 10 MICROSECOND DELAY TIME

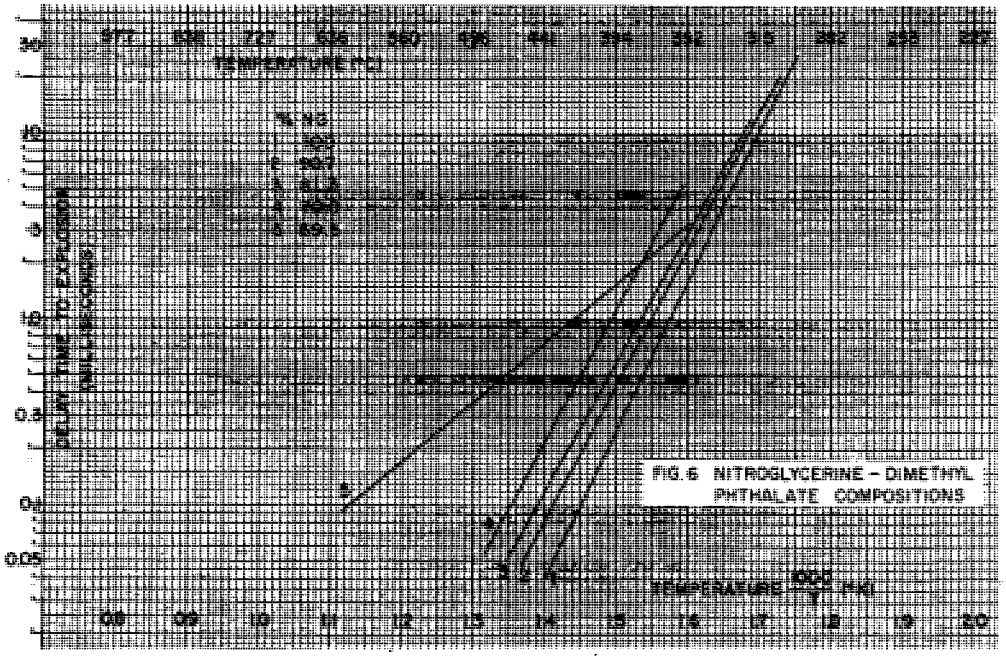

"PHOTOCONDUCTIVITY OF LEAD AZIDE"

M. A. Cook, R. T. Keyes, C. H. Pitt, and R. R. Rollins

Institute of Metals and Explosives Research
University of Utah
Salt Lake City, Utah

Introduction

Evans and Yoffe[1] reported lead azide to be a weak photoconductor with the maximum in its spectral distribution occurring at about 3650Å. McLaren[2] reported the absorption edge to be 4000Å and that absorption at frequencies below this was due to residual carriers and could be used as an indication of the purity of the sample. In the photoconductivity experiments of McLaren and Rogers[3] the photocurrent for lead azide was found to increase at first rapidly, (but at a rapidly decreasing rate) to reach a saturation value after about 30 seconds illumination, the initial rise being produced by photoelectrons migrating toward the anode. With continued illumination the photocurrent decreased by exponential decay typical of a space charge limitation of the flow of electrons, owing to the immobility of positive holes;[4] after prolonged illumination the primary photocurrent leveled off at about 0.2 of the maximum. A linear relationship was found between the primary photocurrent and the electric field strength indicating that most of the photoelectrons were trapped before reaching the anode. Saturation of the photocurrent by increasing the electric field strength did not occur.

Dumas[5] studied the rate of photolysis (photochemical decomposition) of amorphous lead azide as a function of the spectral quality of the incident light and found the rate to be proportional to the intensity of illumination with peaks occurring at 2800Å and 2400Å. Photocurrents were obtained in partially decomposed samples, although they were detected in freshly prepared samples. The peaks at 2800Å and 2400Å were ascribed to two exciton bands. An F center was assumed to be formed from an exciton by the trapping of an electron at an anion vacancy. The positive holes from the dissociation of the excitons then supposedly diffuse to the surface and combine in pairs to form nitrogen gas.

Rate-time and rate-intensity curves in the photolysis of sodium, mercurours, and lead azide were reported by Dodd.[6] For lead azide the experimental quantum yield was determined to be 0.056, a value considered by Dodd to be a lower limit. The diffusion constant for photolysis was given as $2 \cdot 10^{-17}$ cm^2/sec. Dodd considered that the rate controlling step in photolysis might be the diffusion of some large entity,[9] and that this diffusion entity was perhaps molecular nitrogen formed along grain boundaries. The rate of migration of these molecules to the surface was thus considered to be diffusion controlled.

The purpose of the present investigation was to determine some of the factors that affect the photoconductive behavior of lead azide thereby augmenting the rather limited information presently available, to study the defect structure and solid state properties of lead azide through photoconductivity, and finally to determine possible relationships between photoconductivity and explosive sensitivity.

Experimental Methods

Compressed pellets made either from especially-grown small single crystals or from commercial lead azide were used in this investigation. The single crystals were grown in the dark by a diffusion method which utilized the reaction of hydrazoic acid vapor on a lead nitrate solution.[7,8] Well-formed crystals approximately 5 mm long and 1 mm in diameter were grown by this method.

A special sample holder (Fig. 1) adapted to hold 1/4" and 1/8" pellets, held the pressed lead azide pellet under illumination. The sample holder was constructed of copper and mounted in a pyrex dewar flask to permit either cooling or warming the sample as well as evacuation to prevent oxidation of the sample surface. The lead azide pellet was mounted between silver electrodes electrically insulated from the copper block. Electrical connections were made by tungsten leads sealed through the pyrex dewar section. Quartz windows were used to permit transmission of ultra-violet light, the windows being placed on both sides of the assembly to permit light absorption measurements if desired. In experiments requiring monochromatic illumination the sample holder was mounted in a plastic block and placed in a Beckman DK-2 spectrophotometer. A Uvis Grating Monochromator obtained from the Farrand Optical Company with a range of 2200Å to 6500Å was also employed. Illumination was provided by an Osram HBO-200 high pressure mercury lamp Model 520-A. A Photovolt Corporation photometer was used to measure the intensity of the incident beam controlled by Kodak Wratten neutral density filters. The lead azide pellet was mounted in series with a decade shunt, which in combination with the electrometer formed a sensitive ammeter.

Under the influence of an electric field a small dark current was observed. This dark current was allowed to reach steady state, and the photocurrent was taken to be the increase in the current above this steady-state dark current when the sample was illuminated.

Experimental Results

Photoconductivity vs. time, temperature, field strength:

Figure 2 presents curves showing the variation of photocurrent at 36°C, -80°C, and -195°C with time of illumination, utilizing the full output of the lamp and an electrical field strength of about 160 volts/cm. At 36°C the photocurrent continued to rise even after 200 seconds illumination. For the lower temperatures the photocurrent rose to a maximum value then under continued illumination dropped to a fraction of the maximum.

The drop in photocurrent may be attributed to a build up of space charge resulting from the decreased mobility at low temperatures of the positive holes created when electrons are raised to the conduction band. This space charge was removed by permitting the sample to warm up to room temperature and remain over night with no applied field. At elevated temperatures, however, the space charge disappeared much more rapidly. The photocurrents in general decreased as the temperature was lowered. The fact that in the example here a higher photoconductivity was recorded at -195°C than at -80°C was evidently due to differences in the history of the samples. In runs (c) and (d) which were essentially the same, the maximum photocurrent was only about one half that of run (b) indicating that space charge was still present to limit the current. There are some peculiar flat sections in curve (b) which were found to be reproducible in subsequent experiments.

The effect of the electric field strength on the photoconductivity of lead azide illuminated at 4060Å was determined by varying the applied voltage. The result was a linear relationship between photocurrent and the applied voltage which indicated that most of the photoelectrons were trapped before reaching the anode, a fact which precluded determination of the quantum efficiency.

The effect of sample thickness for illumination at 4060Å was investigated using 1/8" diameter pellets containing 10, 15, 20, and 25 mg of colloidal lead azide. The dark current proved to increase with pellet thickness. This was the result of a greater number of electron donating centers present in the thicker pellets and the fact that the distance between electrodes remained constant at 1/8". The photocurrent, on the other hand, decreased with pellet thickness; the decrease was probably due to the fact that the number of electron traps increased with pellet volume (a bulk effect) but the region contributing photoelectrons remained constant since the photoelectrons were released in a thin surface layer on the illuminated side of the pellet. Because of this effect all runs (other than those involving the effect of sample thickness) were made using 20 mg pellets pressed to the same thickness.

Photocurrents vs. wave length of incident light and heat treatments: Typical curves of photocurrent against wave length for two pellets pressed from freshly dried, commercially prepared colloidal lead azide are shown in Fig. 3. The desired wavelength was set on the monochromator while the sample was shielded from the light. The pellet was then illuminated 10 seconds, which was sufficient time for the photocurrent to reach its maximum value, and the reading taken, the process being repeated in measurements at each wavelength. By far the most prominent peak fell at 4060Å, with smaller ones, somewhat difficult to resolve, located at 3650Å, 5400Å, and 5800Å. The major peak at 4060Å fell beyond the absorption edge located at 4000Å. Photolysis occurs at 3650Å which is within the absorption band of lead azide but according to Dodd, et. al.,[6] would not occur for longer wavelengths. Therefore, the peak at 4060Å was not due to photolysis.

Interesting conductivity effects were found in partially decomposed samples obtained by heat treating lead azide at 250°C for varying lengths of time,

250°C being well below the (usual) "explosion" temperature of lead azide. Initially the heat treatment was conducted by plunging a small aluminum capsule containing 50 mg of lead azide into a molten metal bath of the desired temperature. The spectral distribution of the photocurrents after 5, 10, and 15 minutes of such treatment is shown in Fig. 4a, and in Fig. 4b, plotted on a different scale, are the photocurrents after 20, 30, and 40 minutes heat treatment. The increased photoconductivity in the 4060Å band is striking, this increase becoming particularly large with 20 to 40 minutes heat treatment.

The effect of more extended "aging" at 250°C on the photoconductivity in the 4060Å band was studied in order to determine whether the photoconductivity continued to increase, reached a maximum and then leveled off, or attained a maximum and then decreased. Samples of colloidal lead azide heated in shallow metal trays in a drying oven at 250°C for times ranging from 5 minutes up to 260 minutes showed a marked increase in the dark conductivity with time. However, it was impossible to measure the photocurrents against this high-dark current background. In Fig. 5 are plotted the maximum dark currents as a function of the time of heat-treatment, these maxima occurring as a rule 2 to 3 minutes after application of the electrical field. The highest dark current occurred after about 15 minutes heat treatment. After 40 minutes heat-treatment the dark current had leveled off in time at a level considerably below this value. An electric field strength of 1575 v/cm was sufficient to destroy nearly all the available centers providing photocurrent electrons. This is suggested by the fact that the photocurrent was negligible compared to the dark current. Heat-treating the lead azide at 250°C in shallow trays in a drying oven evidently had a different effect than treatment in the small aluminum capsules in the molten metal bath. The samples were apparently more efficiently exposed to the heat owing to the smaller (50 mg) and more shallow samples. The thermal conductivity of lead azide at 45°C and a density of 3.62 g/cm^3 is only $4 \cdot 10^{-4}$ cal/cm^2 sec. C°/cm and thus the sample may not have heated efficiently in the former method.

Curve (b) of Fig. 5 was plotted from data obtained using the same pellets except that the dark current readings were taken after one minute exposure to the electrical field, at which time the maximum dark current had not as yet been reached, and curve (c) shows the results of a second run that was made in the same manner. The dark current was again a maximum after 10 to 20 minutes heat-treatment although in the re-runs the absolute magnitudes of current were lower. On the following day the pellet that had been heat-treated for 15 minutes was re-run. Before the dark current had leveled off it was illuminated at 4060Å and exhibited an increased current flow. When illumination was discontinued, a characteristic exponential decay of current was observed. The dark current, however, continued to increase. Upon re-illumination the electrometer pointer began to oscillate, and the sample suddenly detonated. Another pellet heat-treated 20 minutes was mounted in the holder and the electric field applied carefully. The dark current reading built up and went off scale on the 10^{-8} ampere range, at which time the potential was removed quickly to avoid another explosion.

Colloidal lead azide was treated in a similar manner at 100°C. In this case, photocurrents were measurable above the dark current background. The

photocurrent in the 4060Å band and the dark current are shown in Fig. 6 as a function of the time of heat treatment. Maximum values correponded again to treatment times in the 10 to 20 minute range.

Storage in different gases: The effects on photoconductivity in the 4060Å band of extended storage at 35°C in nitrogen, oxygen, air, carbon dioxide, and argon were investigated using samples prepared by Hong.[10] The colloidal lead azide was placed in pyrex test tubes wrapped with black tape so as to be light tight. The test tubes were mounted in a rack inside a box controlled at 35°C, and dried gases were passed at a constant rate of flow through the samples. Samples were removed at desired intervals and the lead azide content, sensitivity to light, ignition, and photoconductivity determined. The photoconductivities are shown in Fig. 7. Treatment times were continued to 80 days for nitrogen, air, oxygen, and argon and 28 days for carbon dioxide. Surprisingly, a large increase in photoconductivity was observed for samples stored in nitrogen. Storage in air and oxygen produced much smaller increases, while storage in argon appeared to lower the photoconductivity. The exposure in carbon dioxide was not sufficiently long to establish a definite trend. Measurements were usually made immediately after the samples had been removed from the treatment box. However, the points marked 1 and 2 are the values obtained for samples that had been treated in the nitrogen atmosphere for 65 and 80 days respectively, and then rerun for photoconductivity after having been stored in the dark in a sealed, hard rubber container at ambient conditions for about 6 weeks and 4 weeks respectively. The photocurrents were significantly diminished as a result of such storage in air indicating a decrease in the number of electron donating centers in the sample. In order to determine more definitely if the number of centers could be influenced in this way, new samples that had been treated 65 and 80 days in nitrogen at 35°C were placed in a vacuum oven at 100°C for 4 hours (with points 3 and 4 resulting) and for 16 hours (points 5 and 6). The photocurrents were thereby reduced to much lower values.

Discussion

By far the most important band in the spectral distribution of the photoconductivity of colloidal α-lead azide fell at 4060Å. Other bands located at 3650Å, 4300Å, 5400Å, 5800Å were much less prominent, but definitely real because they proved to be reproducible except for the band at 4300Å observed only in a sample that had been heat-treated for 15 minutes at 250°C (see Fig. 4a). These bands should correspond to the absorption spectrum of lead azide which, has not yet been measured because of technical difficulties. A recent development by Head[11] for producing extremely thin films and micro-crystals of lead azide may, however, permit such absorption measurements. The observed bands in the spectral distribution of α-lead azide are evidently due to the ionization of centers that can release electrons into the conduction band. These centers may be F, F', V_1, R, M, colloidal or exciton types.

The 3650Å band is believed to be due to the ionization of excitons formed in the photolytic decomposition of lead azide which may be represented as follows:

$$N_3^- + h\nu \rightarrow (N_3 + \epsilon^-)^*$$

$$(N_3 + e^-)^* + h\nu' \rightarrow N_3 + \epsilon^-$$

The result is the formation of a positive hole and a conduction electron, the former being immobile at low and mobile at high temperature.

The 4060Å band is by far the most prominent one in the photoconductivity spectrum of α-lead azide. It is not associated with photolysis because photolysis occurs only for wavelengths shorter than the absorption edge at 4000Å. The 4060Å band was strongly affected by heat treatment and by storage in nitrogen gas. For these reasons it is believed to be due to V_1 centers (interstitial nitrogen atoms). The enhanced photoconductivity resulting from the nitrogen environment indicates that the nitrogen molecules absorb on the lead azide surface, some of them dissociating into nitrogen atoms, eventually finding their way into interstitial positions in the lead azide lattice to promote photoconductivity. Since photoconductivity in lead azide may be largely a surface phenomenon, it is possible that the nitrogen atoms need not diffuse far into the lattice. The fact that the dark conductivity, which is a bulk effect, was also increased indicates, however, that considerably more than a thin surface layer may be involved. The size of nitrogen atoms and molecules and the lattice parameters of lead azide do not prohibit the possibility of diffusion into the lattice. The decomposition of lead azide with the evolution of nitrogen at surface and internal defects of the crystal should also contribute to the formation of the V_1 center. Indeed some of the enhancement in photoconductivity by heat-treatment may be due to this effect. These V_1 centers contribute to the photocurrent by the following mechanism:

$$N_3^- + N \rightarrow N_4^-$$

$$N_4^- \rightarrow 2N_2 + e^-$$

$$N_2 \rightarrow \text{surface}$$

Nitrogen molecules could dissociate and enter the lattice forming more V_1 centers or diffuse to the surface and escape. The latter would explain the diffusion constant reported by Dodd.[6] The presence of the N_4^- radical has been confirmed by Shuskus, et. al.,[12] in potassium azide; it was reported to be a linear configuration stable only at low temperatures. This configuration has been discussed also by King and Coworkers[13] in studies of sodium azide.

Of particular interest is the fact that a maximum in the dark conductivity against time curve occurred at about 10 to 15 minutes treatment at 250°C and at 100°C. It is surprising that the maximum for samples aged at 100°C occurred at

about the same time as samples aged at 250°C indicating that at least two opposing effects are involved or the effect is a zero enthalpy and finite entropy one.

The origin of the 4300Å band is as yet unknown. It appeared only in a sample aged at 250°C for 15 minutes (see Fig. 4a). The centers producing this band may have an important bearing upon sensitivity because this particular sample was the one that detonated in the photoconductivity apparatus.

The 5400Å band had approximately the same intensity as the F band and may thus be associated with it in one way or another. One possibility is a β-band produced by an excited electron on an anion near an F center. Another possibility is an R_1 center (two neighboring vacancies with an associated electron).

The 5800Å band is believed to be due to F centers, since this is the spectral region where F centers are usually located, and F centers were definitely present because the samples became colored under the effect of illumination. Electron micrographs of replicas of lead azide crystal surfaces[14] showed that lead azide decomposed by a semi-conductor mechanism, i.e., by a process involving the transfer of electrons. Decomposition is accompanied by the growth of lead nuclei on the crystal surfaces, primarily on the (010) face and electrons and/or excitons find their way to one of these nuclei which acts as an electron trap, charging the nucleus negatively whereupon the nucleus may then attract lead ions causing the continued growth of the nuclei during decomposition. Since the slow decomposition of lead azide occurs via an electron transfer processs, the concentrations and types of active centers might be expected to influence the slow decomposition of lead azide and the consequent formation of a "hot spot" in the case of initiation of detonation.

A miniature card gap test for the sensitiveness of primary explosives to shock initiation similar to the standard test adopted for liquid momopropellants was developed at this laboratory.[16] It was applied to colloidal lead azide heat-treated for various lengths of time at 250°C,[17] the lead azide being taken from the same batches as those used in the photoconductivity measurements, in order to make a direct comparison of the sensitivity and photoconductivity results. In these tests the lead azide exhibited a maximum sensitivity at a treatment time of 15 minutes. A test for measuring the sensitiveness to initiation by light similar to the one developed by Eggert[18] was also applied to heat-treated lead azide,[10] and a maximum in the sensitivity was found to occur after 5 minutes heat-treatment. It is interesting to note that the times to sensitivity maxima fell approximately in the same range of heat-treatment times that yielded the maximum dark conductivity for aging at 250°C and the maximum dark conductivity and photoconductivity in the 4060Å band for aging at 100°C. Originally it was thought that the increased sensitiveness from heat treatment was due to autocatalytic action of the lead specks, although the appearance of the maxima after such short heat-treatment times when very little decomposition and lead speck growth had occurred was difficult to explain. The dark conductivity and photoconductivity results indicated, however, active centers other than lead specks must be produced by the heat-treatments.

The colloidal lead azide samples that had undergone (dark) storage at 35°C in various dry atmospheres were also subjected to the light ignition

test for sensitivity[10] after 26, 65, and 80 days. In the case of the nitrogen, air, and oxygen treatments the sensitivity was not found to be significantly different, and it did not appear to vary with the length of treatment. After 26 days in argon, however, the lead azide was somewhat less sensitive than the standard and after 65 and 80 days the sensitivity proved to be lowered considerably more. In view of the photoconductivity results with the same material (Fig. 7) a possible explanation for these results is that during the previous history of the sample exposure to the air was sufficient for the diffusion of nitrogen and possibly oxygen into the lead azide lattice to produce active centers probably of the V_1 type. As far as these atoms were concerned the argon environment acted similar to a vacuum, reducing the partial pressure of nitrogen to zero and allowing the centers to diffuse from the crystal. In the case of lead azide stored in nitrogen, air, and oxygen additional active centers were formed as shown by the photoconductivity measurements; the increased number of centers, although easily detected by photoconductivity, were not sufficient to produce a significant change in sensitivity.

The above correlations suggest that one may eventually relate sensitivity to photoconductivity or possibly dark conductivity once the active centers are identified that exert the greatest effect upon sensitivity, and it is determined how these centers interact and how their concentrations alter the slow decomposition of lead azide.

REFERENCES

1. Evans, B. L. and Yoffe, A. D., Proc. Roy. Soc., (London), A250, 346 (1959).

2. McLaren, A. C., Ph.D. Thesis, Cambridge University, (1957).

3. McLaren, A. C. and Rogers, G. T., Proc. Roy. Soc., (London) A240, 484 (1957).

4. Mott, N. F. and Gurney, R. W., "Electronic Processes in Ionic Crystals", Oxford University Press.

5. Dumas, H. M., Jr., Technical Report, University of Arkansas, August 31, 1956.

6. Dodd, J. G., "Studies of the Decomposition Kinetics of Lead Azide", Proc. of the Ninth Annual Basic Research Contractors Conference and Symposium, Fort Belovir, Virginia, p 59, October 4-7, 1960.

7. Whitbread, E. G., Waltham Abbey, Essex, England, March 1960, private communication.

8. Head, N. L., "Growing of Alpha Lead Azide Crystals," Technical Report No. 3, Institute of Metals and Explosives Research, University of Utah, Sandia Corp., Purchase Order No. 15-6358-A, December 30, 1960.

9. Moss, T. S., "Photoconductivity in the Elements," Academic Press, Inc., New York, (1952).

10. Hong, J. J., "The Effect of Aging Treatments on the Sensitivity and Chemical Composition of Colloidal Lead Azide," Masters Thesis, Metallurgy Department, University of Utah, (1962).

11. Head, N. L., "Electron Micrographic Analysis of Lead Azide", Ph.D. Thesis, Department of Metallurgy, University of Utah, (1962).

12. Shuskus, A. J., Young, C. G., Gilliam, O. R., and Levy, P. W., J. Chem. Phys., 33, No. 2, p. 622 (1960).

13. King, G. J., Miller, B. S., Carlson, F. F., and McMillan, R. C., J. Chem. Phys., 35, No. 4, p. 1446 (1961).

14. Cook, M. A., Head, N. L., Keyes, R. T., and Rollins, R. R., "Photoconductivity, Electron Micrographs and the Mechanism of Thermal Decomposition of Lead Azide", Proc. of the Tenth Basic Research Group Contractors' Conference and Symposium, Fort Belovir, Virginia, p. 183, 24-26 October 1961.

15. American Rocket Society Committee Meeting on Monopropellant Test Methods, Recommended Test No. 1, Card-Gap Test for Shock Sensitivity of Liquid Monopropellants, American Rocket Society.

16. Shetty, Mangalore Nagappa, "A Modified Card-Gap Test for the Sensitiveness of Primary Explosives", Masters Thesis, Department of Metallurgy, University of Utah, (1960).

17. "Study of the Physical and Chemical Properties Controlling Reporductability in the Initiation of Detonation in Primary and Some Secondary Explosives", Summary Report Sandia Corp., Purchase Order No. 15-6358 and 15-6358-A, Institute of Metals and Explosives Research, University of Utah, August 1, 1961.

18. Eggert, J., "The Initiation of Explosion by Light", Proc. Roy. Soc., London, A246 (1950).

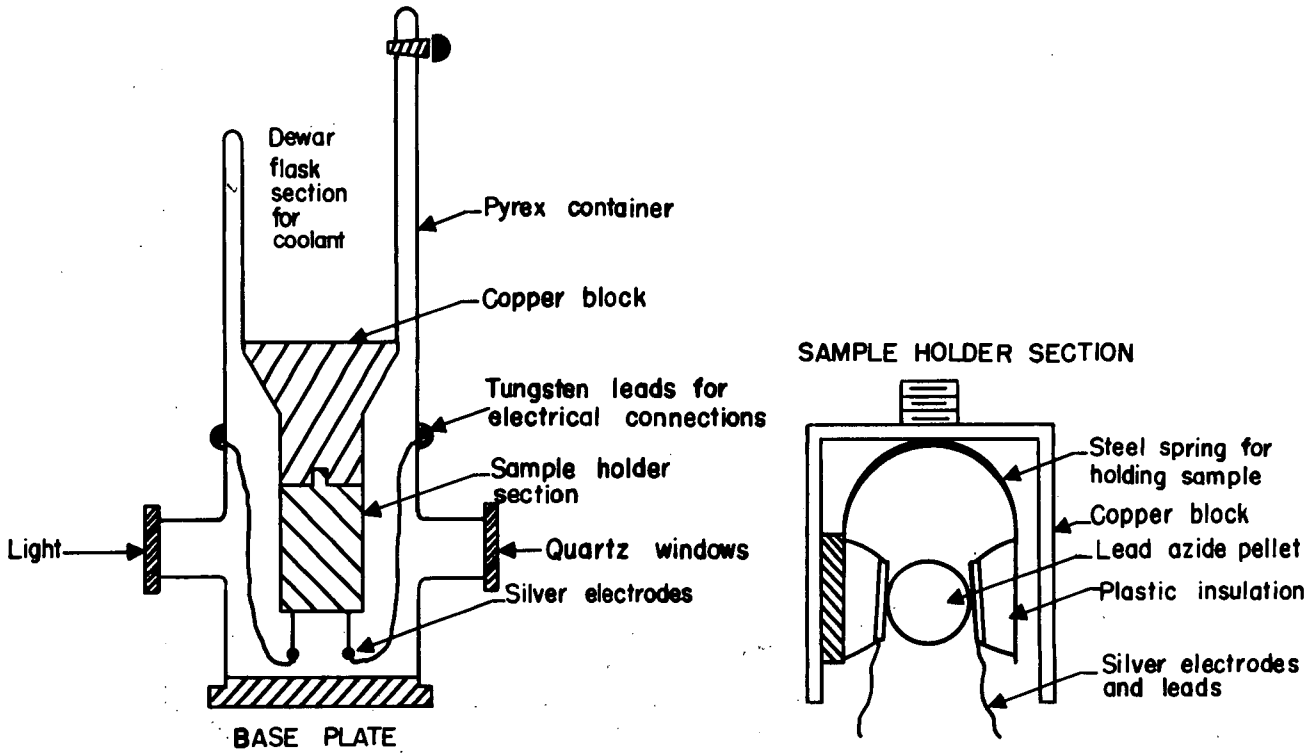

Figure 1. Sample holder used in the photoconductivity experiments.

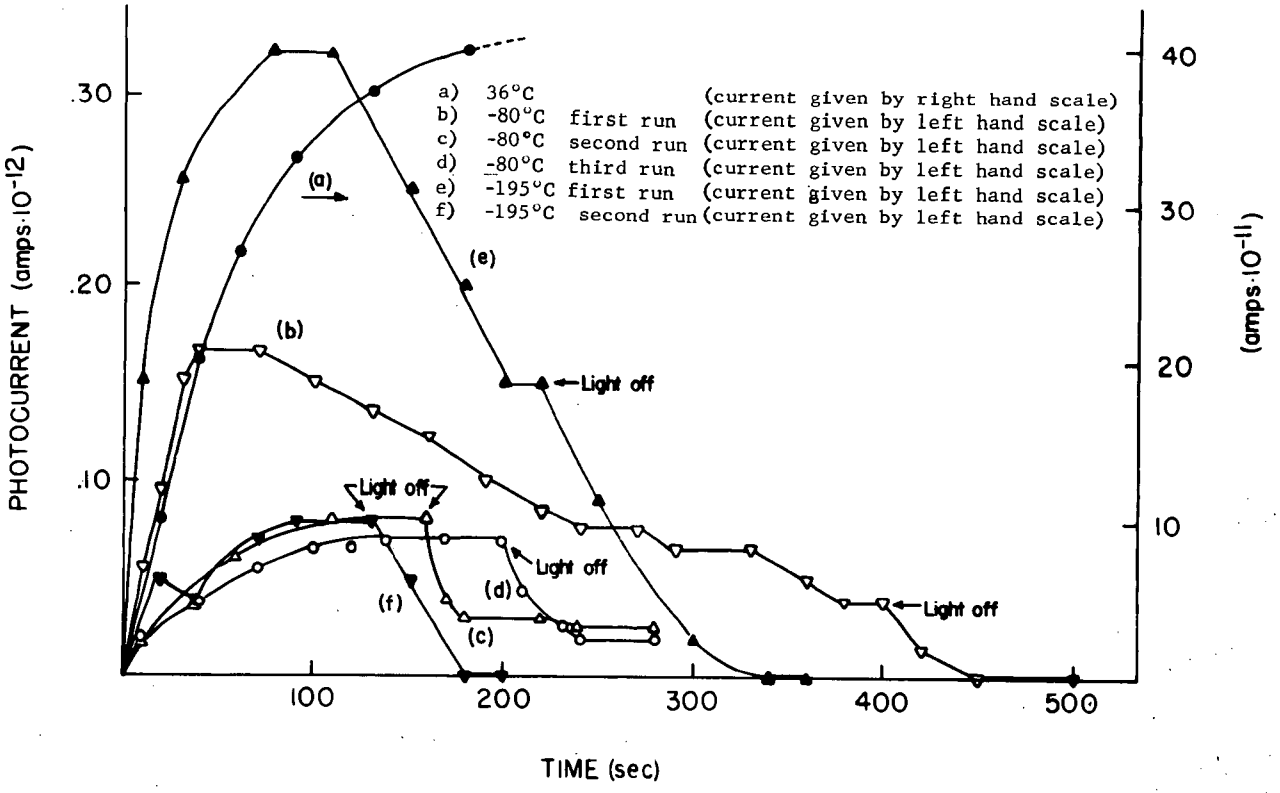

Figure 2. Photocurrent vs time for lead azide at various temperatures using the full output of the lamp and an electrical field strength of about 160 v/cm.

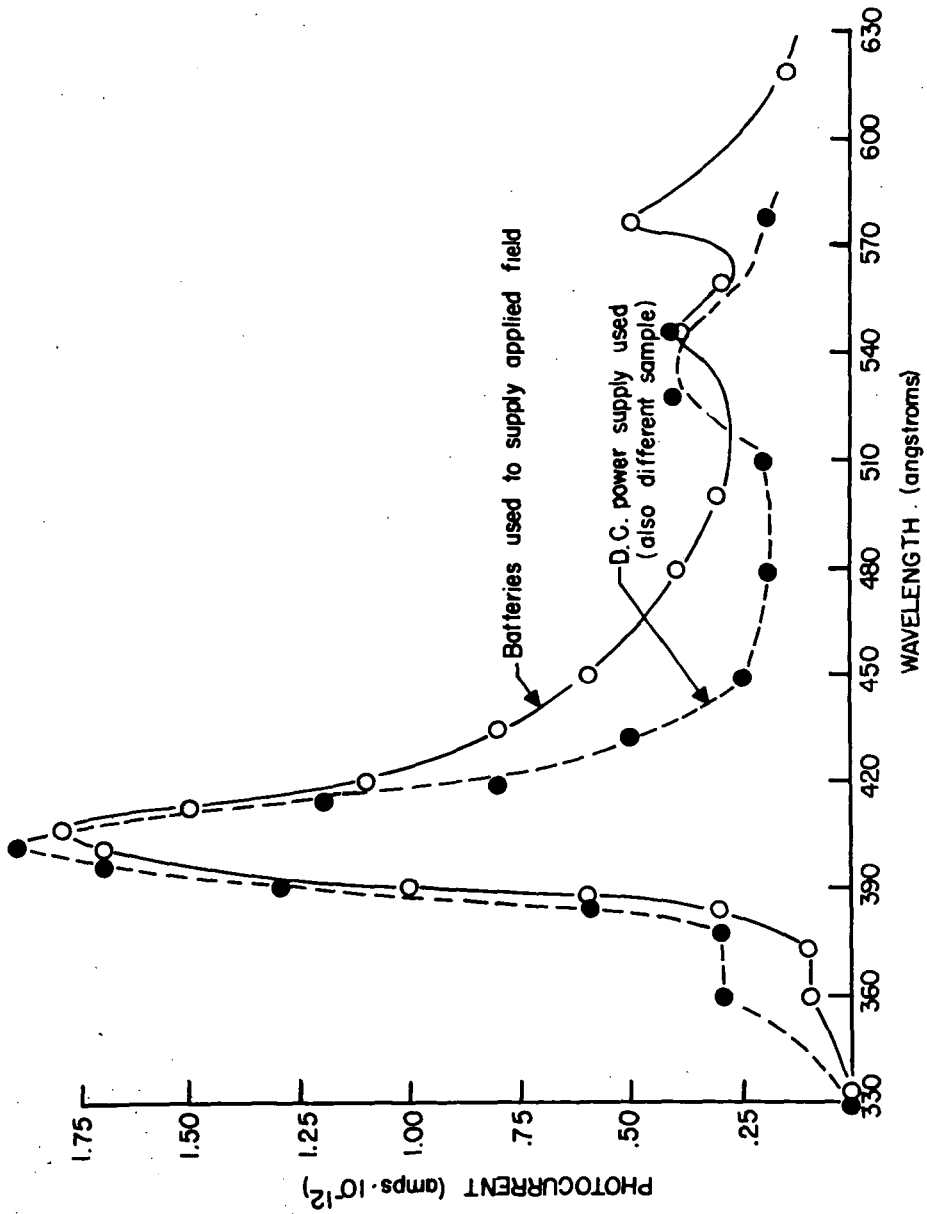

Figure 3. Photocurrent vs wave length for freshly dried colloidal lead azide.

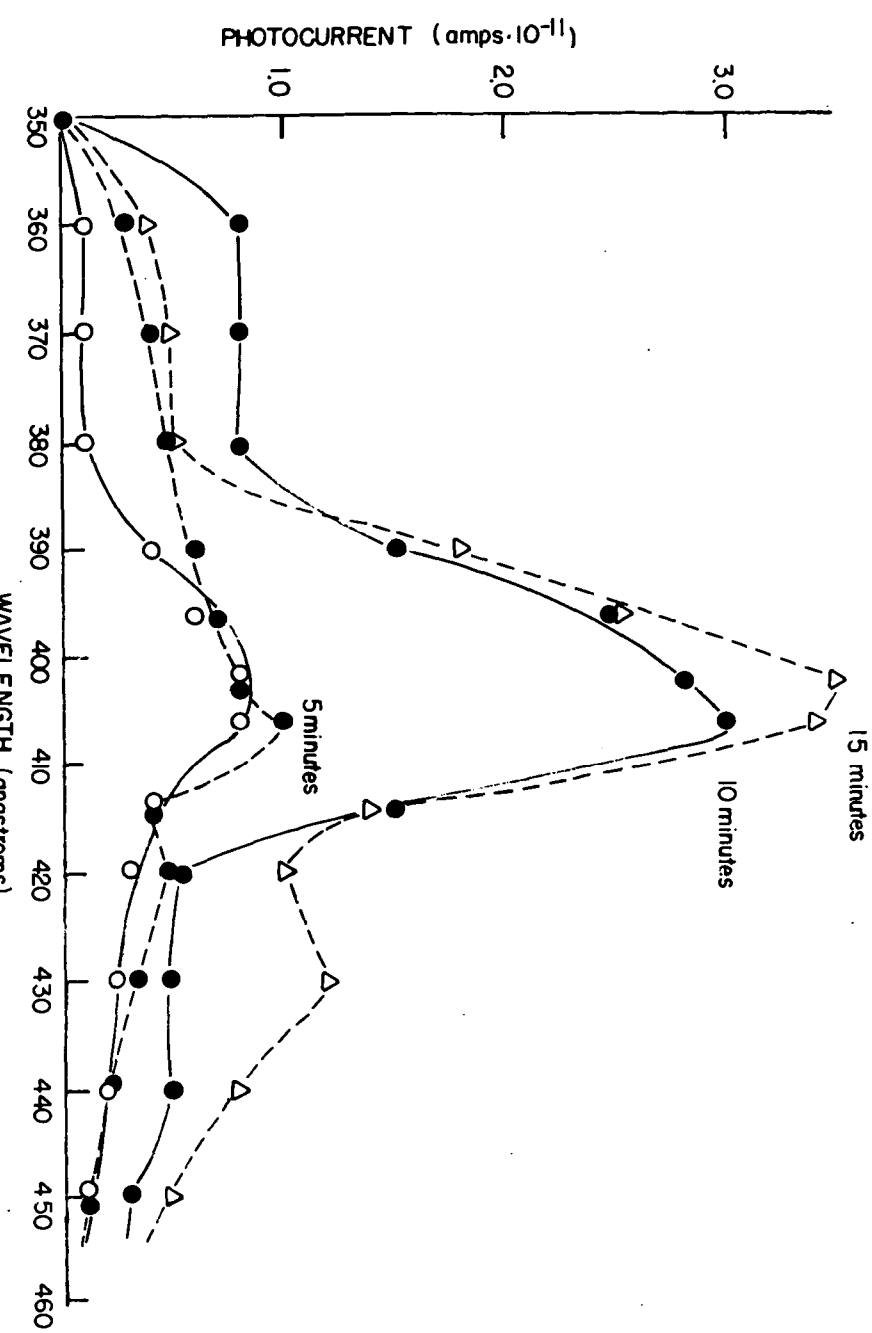

Figure 4a. Photocurrent vs wave length for colloidal lead azide heated to 250°C.

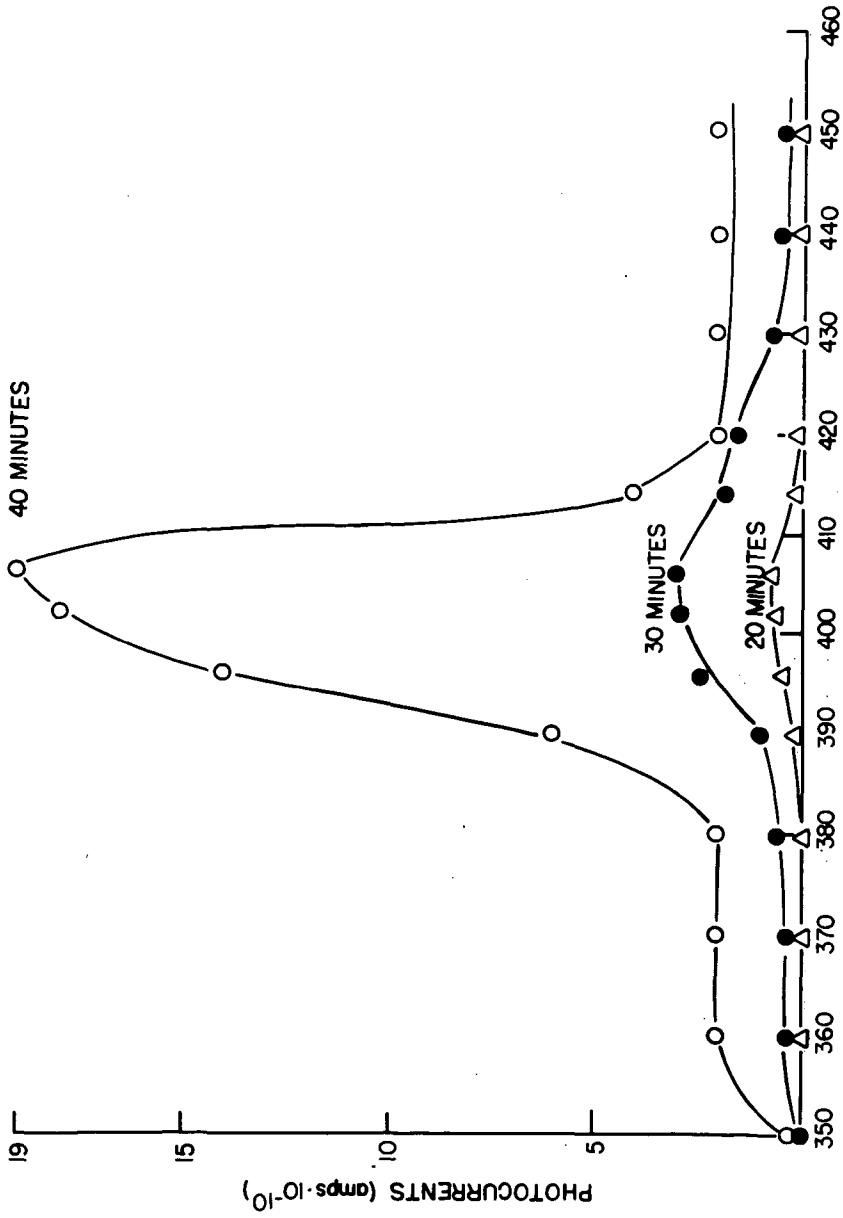

Figure 4b. Photocurrent vs wave length for colloidal lead azide heated to 250°C for extended periods:

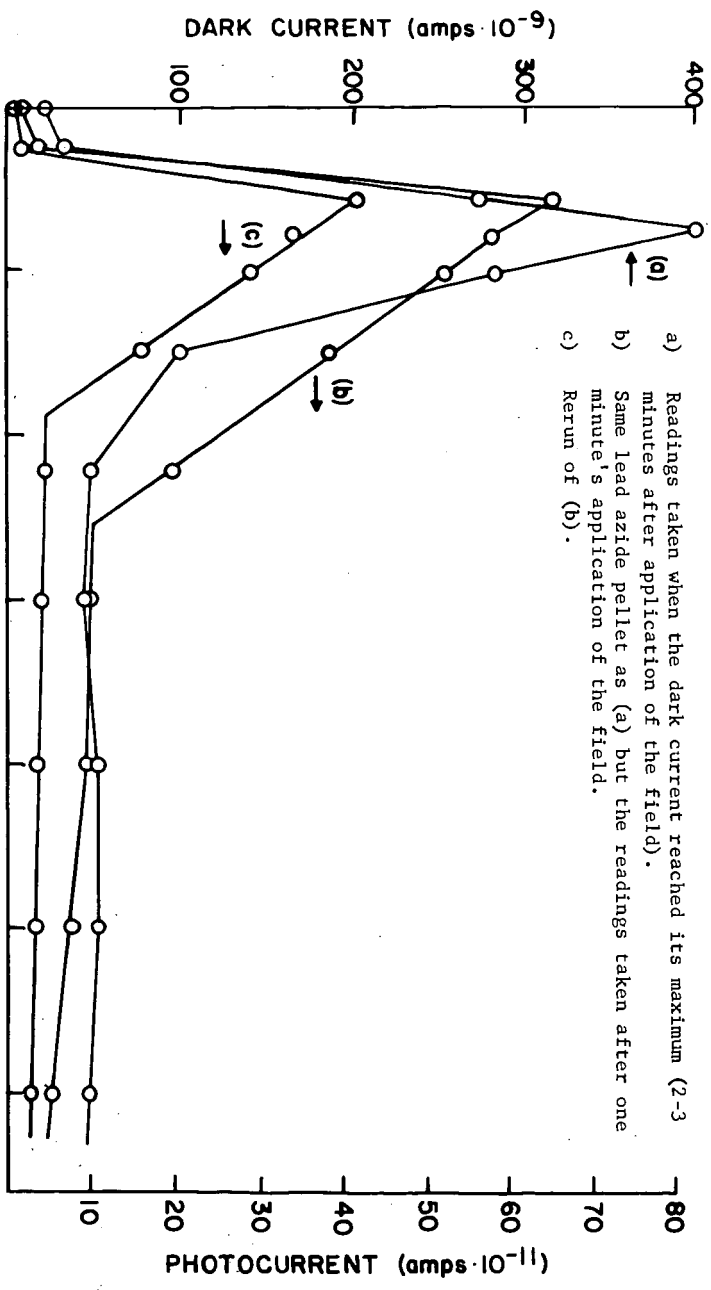

Figure 5. Dark current vs heat-treatment time at 250°C

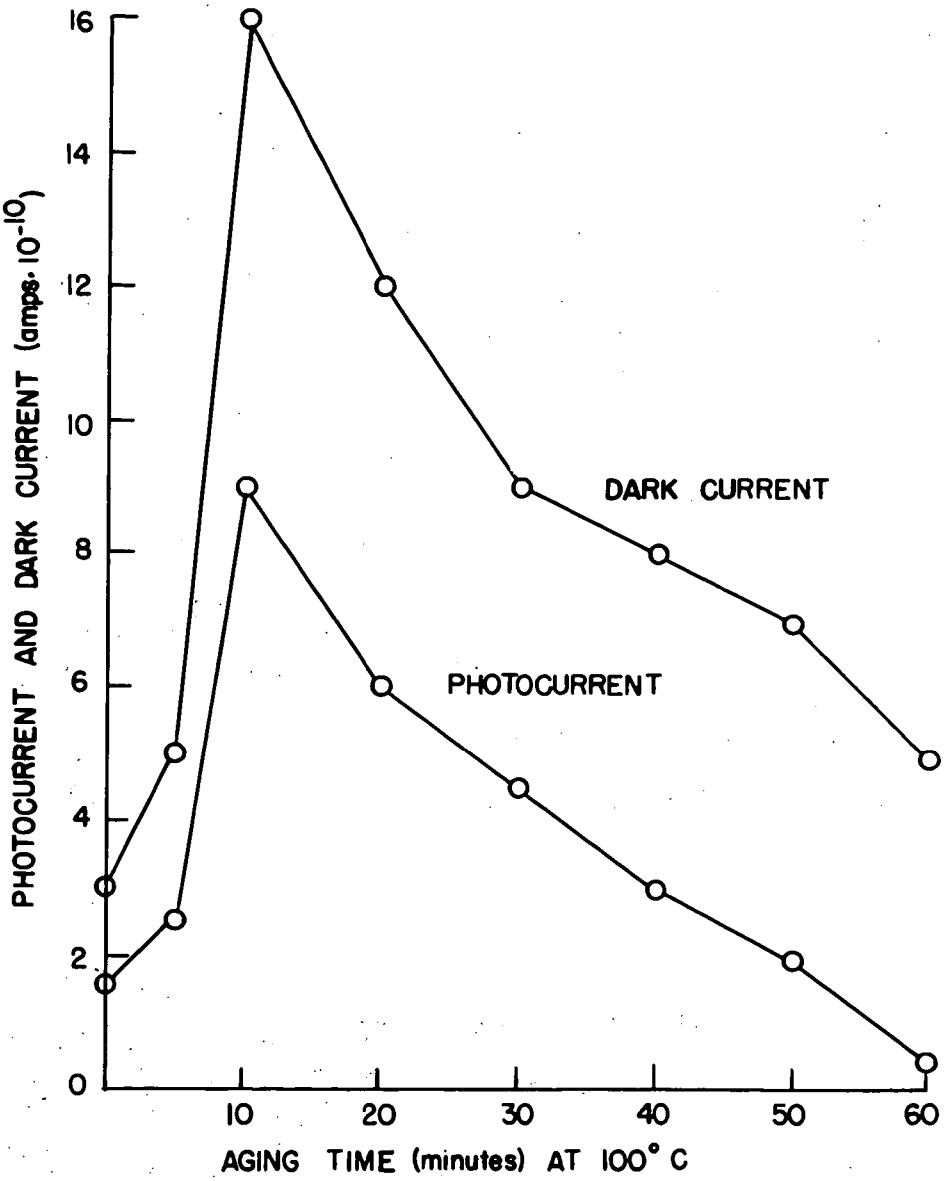

Figure 6. Photocurrent and dark current vs treatment time at 100°C.

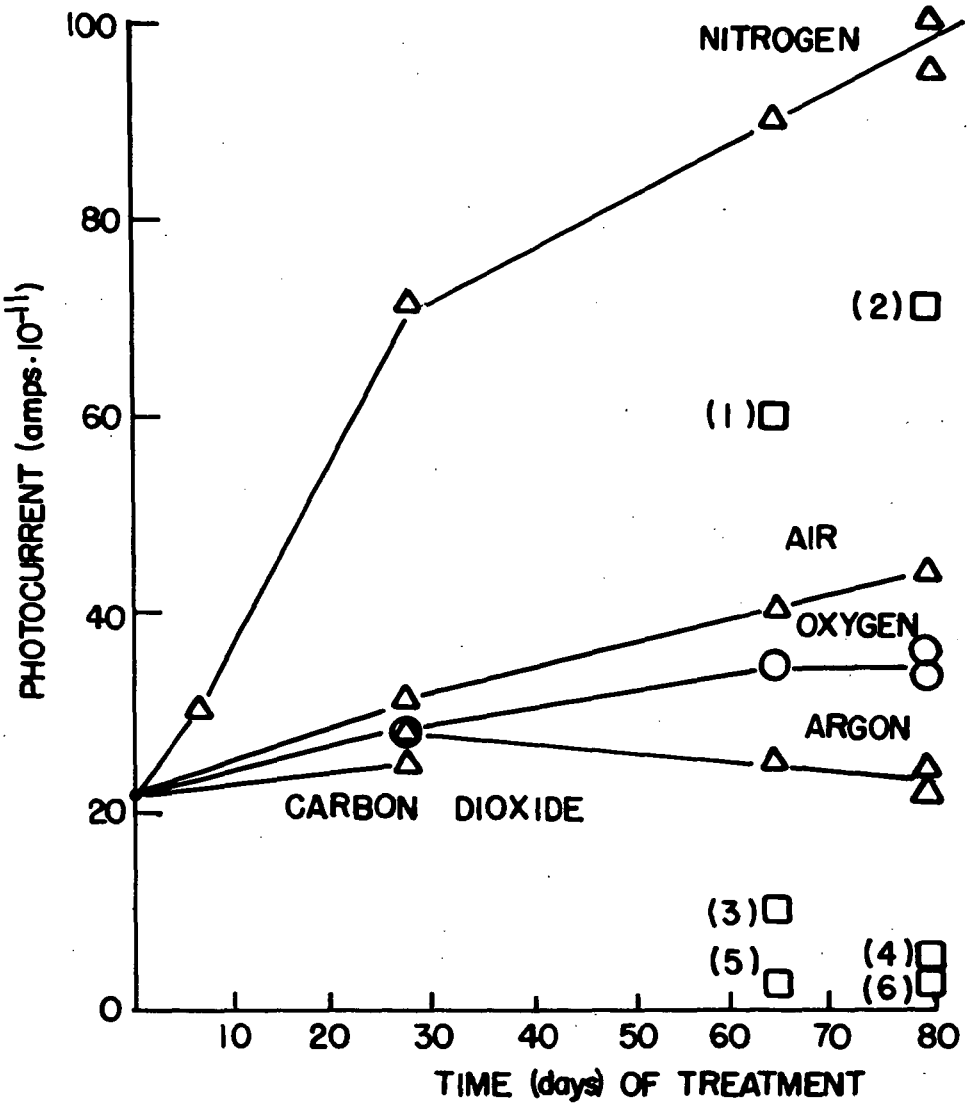

Figure 7. Photocurrent vs storage time in various gases at 35°C.

THEORY OF THE IGNITION ENERGY OF CONDENSED EXPLOSIVES

W.H. Andersen

Ordnance Division; Aerojet-General Corporation; Downey, California

Introduction

The one-dimensional ignition of an explosive from a pure thermal heat source is known from experiment to require a certain critical energy per unit area from the initiating source, below which ignition will not occur even though the explosive adjacent to the source may be induced to undergo some chemical reaction. Thus, a self-sustained combustion (i.e., ignition) can result only when the rate of heat production by the chemical reaction of a certain requisite quantity of the explosive is greater than the rate of heat loss to the surroundings. As to whether the ignition results in normal combustion, or a thermal explosion followed by detonation is a matter which is related to the kinetic nature of the decomposition of the explosive, the heat flux from the initiating source, and the physical conditions (e.g., packing density, charge diameter, etc.) of the explosive. This topic is generally beyond the scope of this paper.

Experimental values of the thermal energy required to ignite an explosive are very meagre. Morgan (1) investigated the ignition of highly flammable solids by means of short hot wires and found a linear relationship between the critical ignition energy and the initiating time. Jones (2) confirmed this finding using a variety of match-head compositions. Bryan and Noonan (3) determined the minimum energies delivered in a 3 millisec interval that were just sufficient to ignite a unit area of several explosives and found values which ranged from greater than 0.4 cal/cm^2 for TNT, to less than 0.1 cal/cm^2 for lead styphnate.

The theory of ignition of solid combustibles has received detailed treatment (4), although the results are not generally discussed directly in terms of the ignition energy. This paper discusses the thermal ignition energies of explosives from the viewpoint of the heat conduction and kinetic processes involved.

Ignition Energy

When a step function heat source is brought in contact with a unit area of an explosive, heat flows into the explosive raising its temperature. An essentially constant temperature T_s is

established at the interface between the heat source and the explosive in a time very short compared to the ignition delay time of the explosive; its magnitude depends on several factors, including the temperature and energy content of the heat source, the intimacy of contact between the source and the explosive, and certain physical and chemical properties of the explosive. The temperature T at a given distance x within the explosive is given as a function of time t by (5):

$$T = T_o + (T_s - T_o)\operatorname{erfc}\left[x/2(k_d t)^{\frac{1}{2}}\right] \qquad (1)$$

where T_o is the initial temperature of the explosive, and k_d is its thermal diffusivity $(K/\rho C_p)$, where K, ρ, C_p are the average coefficient of thermal conductivity, the density, and the average heat capacity, respectively. Chemical reaction is induced in the explosive at a rate consistent with the thermal decomposition kinetics and the local temperature of the explosive. For sufficiently low heat flux, ignition never occurs since heat conduction to the environment holds the temperature of the explosive low enough that self-heating does not occur. For higher heat flux, self-heating of the explosive does occur, and the time to explosion, which is calculable by the Frank-Kamanetski equation, depends on the size of the explosive. For sufficiently high heat flux, which is the case we consider in this paper, chemical reaction is initiated very rapidly due to the high surface temperature of the explosive. Self-sustained ignition occurs when the total conductive heat transfer from the source is sufficent to initiate a flame which will propagate with a velocity consistent with the ambient conditions for a requisite length that is determined by the thermal diffusivity and the burning velocity of the explosive. Under these conditions the reaction zone can further sustain itself from the explosive. For time periods less than that required to transfer the requisite energy, ignition will not occur even though local chemical reaction of the explosive takes place adjacent to the heat source. For time periods greater than that required to transfer the heat necessary to ignite the explosive the ignition energy becomes a function of the heating time.

The heat flux F through the surface of the explosive is obtained by multiplying the time derivative of Eq.(1), evaluated at $x = o$, by K. Substituting $E/t = F$ in the resulting expression gives:

$$E = (T_s - T_o)(K\rho C_p/\pi)^{\frac{1}{2}} t^{\frac{1}{2}} \qquad (2)$$

where E is the energy per unit area conducted into the explosive.

There are various criteria for defining ignition. The usually considered criteria for ignition are defined by the conditions necessary for a transition from a pseudo-steady heat transfer to a non-steady process of reaction (4). For the present case we may consider this to occur when the heat

flux in the surface of the explosive due to chemical reaction is equal to $1/e$ that due to heat transfer from the source, since under this condition thermal initiation is underway adiabatically and the heat source can have very little further influence on the ignition process. However, the computations are relatively insensitive to the factor used in relating the chemical heat flux to that from the heat source. The heat flux due to chemical reaction is ρqv, where q is the heat of chemical reaction and v is the linear burning velocity consistent with the surface temperature. Quite generally,

$$v = LZ\exp(-E/RT_s) \qquad (3)$$

$L = (M/\rho N)^{1/3}$ is the monolayer thickness of the explosive, where M is the molecular weight, and N is Avogadro's number; Z and E are the Arrhenius kinetic parameters for the rate controlling thermal surface decomposition reaction of the explosive, and R is the gas constant. Hence for ignition:

$$(T_s - T_o)(K\rho C_p/\pi e^2 t)^{\frac{1}{2}} = \rho qLZ\exp(-E/RT_s) \qquad (4)$$

The ignition energies calculated by Eqs. (2) and (4) of several secondary explosives which were studied experimentally by Bryan and Noonan (3) for a 3 millisec heating period are summarized in Table 1. The computed values of T_s are also given. Values of K and C_p of $5(10^{-4})$ cal/(cm-sec-°K) and 0.44 cal/gm-°K were employed; q was calculated assuming the oxygen in the explosive to first form CO, then H_2O, and finally CO_2. Values of 630, 814, 1220, and 1400 cal/gm were obtained for TNT, tetryl, RDX, and PETN, respectively. Crystallive densities were used, and the computations were performed using the available published decomposition kinetics.

Table 1. Comparison of Experimental and Theoretical Ignition Energies.

Explosive	Exptl E (cal/cm^2)	E'	Computed T_s (°K)	E, Eqs. (2), (4). E_2	T_s
TNT	>0.38	0.75	1571	0.66[2]	1426
Tetryl	0.33	0.48	1098	0.34[3]	861
RDX	0.33	—	—	0.39[4]	935
PETN	0.25	0.34	858	0.25[5]	705
		0.21	638		

[1]Kinetics from ref. 6; [2]ref. (7a); [3]ref. (7b); [4]ref. (7c); [5]ref. (7d).

The general agreement of the computed energies with the experimental values is very good; the perfect agreement in some cases is of course fortuitous since the estimated values of some of the parameters may be in error, and in any event the exact validity of the experimental data is not known. The factor $1/e$

which was used to relate the conduction and reaction flux changes (decreases) the computed energies by only about 10% from that of using a factor of unity. However, the factor $1/e$ is believed essentially correct since it roughly defines the inflection point on an adiabatic rise in reaction rate.

Three things may be especially noted from Eqs. (2) and (4). The ignition energy is a strong function of the temperature difference, (T_s-T_o). Hence a high initial ambient temperature will lower the energy required for ignition. This was previously noted by Hicks (4b) on ignition delay time. The value of T_s is very sensitive to the thermal decomposition kinetics for a fixed heating time; the faster the decomposition rate (at a given temperature) the lower the value of T_s. Thus initiating explosives usually require smaller initiating energies than do secondary explosives. Finally it is seen that the ignition energy varies as the square root of the heating time (for one-dimensional heating). This was also noted by Hicks, and has been discussed in detail by Yang (8). Yang also treated the line and point source cases, and showed that the ignition energy varies as t and $t^{3/2}$ respectively in these cases. These results are directly transposable to the present treatment. The influence of the heating time on the ignition energy given in Eq. (2), in Hick's paper, and in the paper of Yang is consistent with the experimental observations of Jones (2) on solid explosives, and Jones and Stout (9) on gaseous explosives.

The ignition time t_i for a fixed T_s is given by Eq. (4):

$$t_i = a(T_s-T_o)^2 \exp(2E/RT_s) \qquad (5a)$$

$$a = (KC_p/\pi e^2 \rho q^2 L^2 Z^2) \qquad (5b)$$

An estimate of T_s is required to use this equation.

Equations (2) and (4) give the energy required to ignite an explosive as a function of the heating time for high heat flux conditions. It was also mentioned, however, that some minimum energy is always required to initiate an explosive, below which energy ignition will not occur. This minimum energy may be estimated from a slight modification of concepts used in estimating the minimum ignition energy of gases, and will be discussed in a subsequent paper.

The quantitative approach employed in this paper is that ignition is a pure thermal reaction. However, it is known that certain subsidiary factors such as chemical effects from certain gases, such as oxygen, or catalytic effects from the heating source may influence the ignition process. The inclusion of

these factors is beyond the scope of this paper, but it may be mentioned that their general influence should decrease as the temperature of the source and its accompanying heat flux is increased.

Acknowledgment

The writer would like to extend his appreciation to Dr. O. R. Irwin for his stimulating discussions on this subject, and to his wife Jeanette, whose typing of the manuscript enabled this paper to be submitted.

References

(1) J. D. Morgan, Phil. Mag. 49, 323(1925).

(2) E. Jones, Proc. Roy. Soc. A198, 523(1949).

(3) G. T. Bryan and E. C. Noonan, Proc. Roy. Soc. 246, 167(1958).

(4) (a) Frank-Kamenetskii, Diffusion and Heat Exchange in Chemical Kinetics, Princeton University Press, Princeton, 1955, Chapt. VI; (b) B. L. Hicks, J. Chem. Phys. 22, 414(1954); (c) J. Zinn and R. N. Rogers, J. Phys. Chem. 66, 2646(1962)

(5) H. S. Carslaw and J. C. Jaeger, Conduction of Heat in Solids, Oxford University Press, London, 1947.

(6) M. A. Cook and E. T. Abegg, Ind. Eng. Chem. 48,1090(1956).

(7) (a) A. J. B. Robertson, Trans. Far. Soc. 44, 977(1948); (b) E. K. Rideal and A. J. B. Robertson, Proc. Roy. Soc. A195, 135(1948); (c) A. J. B. Robertson, Trans. Far. Soc. 45, 85(1949); (d) Ibid., J. Soc. Chem. Ind. 61, 221(1948).

(8) C. H. Yang, Combn. & Flame, 6, 215(1962).

(9) H. F. Stout and E. Jones, Third Symposium (International) on Combustion, Williams and Wilkins Press, Baltimore, 1949, p. 329.

Quantitative Analysis of Card-Gap Tests The Reflected Wave Technique

Paul K. Salzman
Aerojet-General Corporation
Downey, California

I. INTRODUCTION

One of the most useful methods of evaluating shock sensitivity of propellants and explosives is the card-gap shock attenuation test.[1-3] Because shock pressure is considered the most important parameter causing detonation in shock initiated explosives, conversion of gap thickness to shock pressure has been carried out at NOL[3] and Aerojet,[1,4] for various diameter card-gap tests using Plexiglas (or Lucite) as the attenuating medium.

It has been noted [1,5] that the shock pressure at the end of the attenuating gap is not the same as the shock pressure entering the test sample because of the "impedance-mismatch" at the interface between the Plexiglas attenuator and the test sample. The magnitude of this change depends on certain mechanical properties of the two media and is unknown since the data does not, in general, exist for most propellants and explosives. Without this knowledge card-gap test results remain qualitative.

An experimental-theoretical method, called the "Reflected Wave Technique" ("RWT") was developed[1] to determine transmitted shock pressures in card-gap test configurations without measurement or knowledge of the test-sample properties. The method uses the laws governing the modification of shock waves at the interface between the media and the experimental measurement of the velocities of the incident and reflected waves at the interface.

The main purpose of this investigation was to experimentally determine the accuracy of the "RWT". This was done by using the "RWT" to compute the shock pressure transmitted to water, carbon tetrachloride, 2024-T4 aluminum and C 1018 cold rolled steel using various diameter card-gap test configurations, and comparing the results with values of transmitted pressure obtained independently. The method was also applied to two other materials (simulated propellant[a] and #30 sand) for which the transmitted shock pressure could not be computed independently.

Since each application of the "RWT" requires the use of a streak camera, it was considered desirable to determine from the above results if an empirical correlation, independent of the test diameter, could be found between the incident and transmitted shock pressure for each Plexiglas-acceptor pair. Such a relation would save considerable time in allowing subsequent determination of transmitted pressure without further applications of the "RWT". In addition, application of the "RWT" provides pressure-particle velocity data for each material tested. Since this represents a new and relatively simple method of Hugoniot determination, the accuracy of the results were evaluated by comparison with values from the literature.

In this investigation, a series of framing camera studies were made in order to determine if a definite identification of the incident, reflected, and (for transparent acceptors) transmitted shock waves could be made. Also, observations were made to help determine to what extent the Plexiglas is altered by, or made opaque by, the prior passage of the incident shock.

[a] Polyurethane, aluminum and potassium chloride.

II. EXPERIMENTAL

Figure 1a is a schematic of the general experimental set-up used to determine the velocities of the incident and reflected waves. The relay lens was used to obtain an overall magnification of about 1 and was aligned with the streak camera lens by mounting it on an optical bench rigidly attached to the camera chassis. The distance between the lenses was about 48". The event, which was about 6' from the relay lens (approximately 33" from the armor glass at the end of the porthole), was mounted on a steel stand such that the Plexiglas-sample interface was near the optical axis. With this arrangement a field of view (on the vertical axis) of about 1", at the event, was obtained. Backlighting was provided by an argon bomb that consisted of a 3½" diameter by 7" long quart ice-cream container with a slab of composition C-4 high explosive at one end and a translucent covering of Saran wrap and vellum paper at the other end. The bomb was taped to a stand so that its axis was on the optical axis of the system and was placed from 13-15" behind the event. Figures 1b and 1c are details of the two types of events used in this program. The first shows the card-gap test configuration used for solid samples while the other shows the equivalent test set-up used for liquid samples (i.e. the "aquarium" method[4].) To eliminate the distortion of the light from the argon bomb by the curved surfaces of the Plexiglas column, narrow parallel flats were machined and polished along opposite sides of all the columns. In each test the length to diameter ratio of the tetryl donor was kept constant at a value of 2. The tetryl density varied from 1.5 - 1.6 g/cm^3. For the solid tests the acceptor diameter was kept equal to the column diameter while the sample height was always 2 inches.

A high-speed continuous writing streak camera was used for all shock pressure measurement tests. In order to make the set-up depicted in Figure 1a practical, a f/2.5 lens with a focal length of 7" was used in the camera. The relay lens, with an aperture of f/6, had a focal length of 24". The smallest available slit (0.004 in. wide) was used to make the shock front image as sharp as possible. In order to help minimize computation errors a turbine speed of approximately 2000 rps was used (writing rate = 2.9 mm/μsec) which gave a streak at an angle of about 45° to the film. For most of the acceptor materials, tests were conducted with columns of ½", 1", 1½", and 2" diameter and lengths of ½", 1", 1½", and 2". The slit of the streak camera restricts the field of view to the flattened portion of these columns.

The streak-camera film record produced for each test was reduced by reading the films with a Gaertner microcomparator. The data was then numerically differentiated[1] to give a velocity at the film plane. To obtain real values of shock velocity this data was multiplied by the ratio of the magnification and time factors for each test.

The event (test set-up), streak camera, film development procedure, microcomparator, and calculation methods may all be considered as sources of systematic and random error in the experimental determination of shock velocity. Where possible, procedural refinement and/or changes were adopted in an attempt to minimize error. The estimated overall error in velocity was about 3.5%. In addition, the error in the determination of shock pressure is always greater than in the determination of shock velocity because of the relationship between them. The average error in determining shock pressure was computed to be about 13%.

A high speed framing camera was used for the qualitative investigations of the program. The test set-up was similar to that depicted in Figures 1a - 1c except that no relay lens was used. A camera speed of about 4000 rps was used to obtain 25 frames at a framing rate of about 980,000 frames per second. At this speed the shock wave could be followed at about 1.05 μsec intervals.

III. THEORETICAL

The basic laws that govern the modification of a shock wave passing through the boundary between two media may be stated verbally as: "shock pressure and particle velocity must remain continuous across the boundary" [1,2, 6-8] or:

$$P_t = P_i \pm P_r \qquad \text{and:} \tag{1}$$

$$u_t = u_i \mp u_r \tag{2}$$

where P is shock pressure (kbar), u is particle velocity (mm/μsec) and the subscripts t, i and r refer to the transmitted, incident, and reflected waves respectively. The sign to be used in equation 1 is determined by the "impedance mismatch" between the media through which the incident and transmitted waves pass. If $\rho_t U_t > \rho_i U_i$ (ρ is the initial (unshocked) density (gm/cm^3) and U is shock velocity (mm/μsec)) the plus (+) sign applies and if $\rho_t U_t < \rho_i U_i$ the minus (-) sign applies. For a given case, the opposite sign is used in equation 2.

The shock pressure transmitted to a test sample can be computed by combining equation 1 with the well known hydrodynamic relation:[b]

$$P = 10\rho Uu \tag{3}$$

to give

$$P_t = 10\,\rho_i U_i u_i \pm 10\,\rho_r U_r u_r \tag{4}$$

In general, the incident wave passes through Plexiglas (i.e., the attenuator). If it is assumed that the incident wave does not greatly alter the Plexiglas,[c] the reflected wave may also be considered as passing through the same Plexiglas. In this case, (using subscript p to denote Plexiglas) $\rho_r = \rho_p$ and equation 4 becomes:

$$P_t = 10\,\rho_p(U_p u_p \pm U_r u_r) \tag{5}$$

The "Reflected Wave Technique" consists of an experimental measurement of U_p and U_r (from a streak camera record of the event),[d] computation of u_p and u_r from the previously measured equation of state of Plexiglas[1] (the reflected wave is assumed to be passing through unaltered Plexiglas) and application of equation 5 to give the shock pressure transmitted (P_t) to a test sample. It should be emphasized here that P_t is found without measurement or knowledge of the acceptor properties!

---

[b] Eq's 1-3 are strictly applicable only to one-dimensional (planar) shocks. Even though the shocks produced in these tests (see Figure 2) are non-planar and therefore at least two-dimensional, the slit of the streak camera used to obtain the data restricts the field of view to such a small portion of the wave that the curvature may be ignored and the waves considered planar.

[c] This assumption means, in this case, that the density and equation of state of the medium through which the reflected wave passes is unchanged (or only slightly different) from Plexiglas.

[d] Although the basic equation used to derive equation 5, (i.e., equation 1) is strictly valid only at the interface, the measurements of U_p and U_r were made at some small distance (< 1mm) from the actual interface. This was done because during reflection the incident and reflected waves overlap (for a time equal to the incident wave pulse width) causing distortions of the streak record. These distortions can be seen near the interfaces of the records shown in Figure 3. The error introduced by measurements near, rather than at, the interface is considered negligible since attenuation of the waves over such small distances is negligible.

Hugoniot data for the acceptor may be computed from this result (i.e., P_t) and equation 2 with $u_i = u_p$.

$$u_t = u_p \mp u_r \qquad (6)$$

Since both u_p and u_r were computed in applying the "RWT", u_t is found directly from equation 6. It is also possible to compute U_t from P_t and u_t by rearrangement of equation 3, if the density of the acceptor medium is known.

IV. RESULTS AND DISCUSSION

A. Framing Camera Studies

The results of 13 tests with a framing camera are summarized in Table I. A typical record is shown in Figure 2. Definite identification of the reflected wave was made in all but 3 of the tests. Further examination of the records showed that, except in one case, no visual damage (i.e., breakup or opacity) to the Plexiglas immediately behind the incident wave occurred. The two column diameters and various lengths provided a range of shock pressures (P_p) at the interface (7 to 70 Kbar) over which the above observation is valid. Although no definite conclusion can be made, these results help to support the assumption made in the development of the "RWT" that, "the incident wave does not greatly alter the Plexiglas."

The results in Table I show that the curvature of the waves for each diameter column was approximately constant. This indicates that curvature is a geometrical property independent of the total attenuation. The average, for $\frac{1}{2}$" diameter columns is 0.088 mm^{-1} while that for 2" diameter columns is 0.012 $mm.^{-1}$ In the worst case the maximum deviation from planarity for that portion of the shock wave viewed through the streak camera slit, is less than 0.001 mm. This result justifies the assumption made in the development of the "RWT" that the one-dimensional equations are applicable in this case.

No effects, pertinent to the results in Table I, of the acceptor material were noted. However, it was noted that for the liquid acceptors (water and CCl_4) the records were generally superior to the rest. This is probably due to the fact that the liquid surface (see Figure 1c) acts as a second blast shield and helps keep the gaseous detonation products which obscure the view, from following the incident wave too closely. In the dry shots, the lack of this added protection restricts the distance over which the reflected wave may be viewed since the gaseous products meet the reflected wave soon after reflection. This view is supported by the observation in Figures 3a-3d that the duration of the reflected wave is longer for the liquid acceptor (the scale of Figure 3a is $\sim$ half the others) than for the dry acceptors. Since actual card-gap tests are always dry the shorter duration over which the reflected wave may be measured is more realistic in terms of what is to be expected. However, this imposes no special restriction on the "RWT" since the velocity of the reflected wave can be determined even for very short durations when a microcomparator is used for the measurements.

A number of the framing camera tests gave some unusual results. Two are of some interest here. In one the shock wave appeared self-luminous and also the argon bomb apparently did not light. No immediate explanation can be given but if the conditions under which the result occurred could be repeated, it might be possible to carry out the "RWT" without backlighting, and subsequent simplification of the test. In another test the apparent shock wave thickness is $\sim$ 8.0 mm. This is unusually high (most shots average $\sim$ 2.5 mm) and indicates a low velocity shock wave. This would imply that variations in the tetryl donor quality may exist. This variation has been noted by Cook[2] and is of concern since the reliability of the card-gap test depends on the reproducibility of shock pressure at a given attenuator distance which in turn depends directly on the quality of the donor used.

B. Streak Camera Studies

1. Accuracy of "RWT"

In order to check the accuracy of the "RWT" for the two liquid and two solid acceptor materials, the transmitted pressure (P_t) was computed and compared to the transmitted pressure found independently (P_t^*). The acceptors were: water, $\rho = 1.00$ g/cm^3; carbon tetrachloride, $\rho = 1.59$ g/cm^3; 2024-T4 aluminum, $\rho = 2.77$ g/cm^3; and C 1018 cold rolled steel, $\rho = 7.86$ g/cm^3.

Two statistical measures were applied to the data. They are

$$|\overline{PE}| = \text{average absolute \% error} = \sum_1^N \left|\frac{P_t^* - P_t}{P_t^*}\right| \times 100/N$$

$$\overline{PE} = \text{average \% error} = \sum_1^N \left(\frac{P_t^* - P_t}{P_t^*}\right) \times 100/N$$

The first measure will always be positive and describes the overall percentage accuracy of the method and is the main one considered. The second measure may be positive or negative and describes the overall percentage bias (or direction) of the method and determines if any consistent trends exist.

For the transparent acceptors (i.e., H_2O and CCl_4) the shock transmitted appeared on the streak camera record (see Figure 3a) and u_t was measured directly, u_t computed from the equation of state reported in the literature,[9] and P_t^* (the independent measure) computed from equation 3. This was then compared to the value computed by the "RWT". Since the impedance of water and CCl_4 are known to be less than that for Plexiglas the negative (-) sign was used in equation 5 for the "RWT" calculation. Because of the health hazard involved at the test site only a small amount of similar data for CCl_4 was found.

For those acceptor materials that are opaque (i.e., steel and aluminum), the streak camera record did not show the transmitted wave (see Figures 3b-d). In this case the shock pressure transmitted (the independent measurement) may be found by a graphical method which uses the known Hugoniot's of the acceptor and Plexiglas.[5,6,8-10] These values (P_{th}) are then compared to the ones computed by the "RWT". For both of these materials, the impedance is known to be higher than that for Plexiglas and the plus (+) sign was used in equation 5. In order to check the accuracy of using this "reflected Hugoniot" method as an independent measure of transmitted pressure when applied to the opaque acceptors, it was first applied to the transparent acceptors mentioned above, so that a comparison with the measured results could be made (P_{th} vs P_t^*).

The "RWT" was also applied to two other acceptor materials which are opaque but for which the Hugoniots are unknown. The materials were simulated propellant, $\rho = 1.65$ g/cm^3 and #30 sand, $\rho = 1.36$ g/cm^3. The impedances of these materials are unknown but since simulated propellant is a coherent solid more dense than Plexiglas, the plus (+) sign was used in equation 5 while the minus (-) sign was used for sand since it is an incoherent material not much more dense than Plexiglas ($\rho \simeq 1.2$ g/cm^3).

a. Transparent Acceptors

Table II and Figure 4 show the results of P_t vs P_t^* for 12 tests with a water acceptor. The line drawn in Figure 4 represents equality of pressures (i.e., 45° line) and the distribution of the data about this line is a measure of the applicability of the method. For this data $|\overline{PE}| = 11.3\%$ which indicates that the "RWT" can predict transmitted pressure with an overall error of < 12% (which is less than the average error in determining shock pressure) for this acceptor. For the same data $\overline{PE} = +4.1\%$ which

indicates that, on the average, P_t falls slightly below P_t^*. Since $\overline{PE}$ is well within experimental error no bias of the data is indicated even though the three data points at high pressure are low. More data in this region is necessary to determine if any trends do exist and if the accuracy of the "RWT" falls off.

The "Hugoniot" method of determining shock pressure transmitted was applied to water and CCl_4 and provides data (P_{th}) also shown in Table II. This is used to evaluate the accuracy of the graphical method. The $|\overline{PE}|$ for this data (P_{th} vs P_t^*) is 37.1% and indicates that the "Hugoniot" technique predicts transmitted pressure with an overall error about 3 times as great as the "RWT" (and the experimental error). For the same data $\overline{PE}$ = 27.4% which indicates that P_{th}, on the average, is somewhat above P_t^*. This figure is also not within experimental error and thus indicates a bias. It may be concluded that the "Hugoniot" method gives values of transmitted pressure that are ~27% high.

Because of these differences, the reliability of using the "Hugoniot" method as an independent measure of transmitted pressure is in serious doubt. However, the bias in the data may be used to adjust the subsequent results for opaque materials to more realistic values.

b. Opaque Acceptors

The graphical method described was applied to the opaque acceptors, steel[11] and aluminum[11] and the results are shown in Table III (i.e., P_p vs P_{th}). Comparing the "RWT" method to this graphical method (P_t vs P_{th}) gives, $|\overline{PE}| = \overline{PE} = +21.8\%$. This poor agreement was at once resolved when the values of P_{th} were adjusted downward by the average bias (27.4%) computed above. These results (P_{tha}) are also shown in Table III, and the adjusted comparison (P_t vs P_{tha}) in Figure 5.

For this adjusted data, $|\overline{PE}| = 15.1\%$ which indicates that the "RWT" can predict transmitted pressure with an overall error of about 15% for these opaque acceptors. It should be noted that this value is somewhat conservative since the manipulation of the data necessary to establish realistic values of the independent transmitted pressure was done on an average basis. A more detailed analysis of the P_{th} vs P_t^* data might give a number of correction factors (instead of one) that would further improve the correlation seen in Figure 5. The $\overline{PE}$ for this data is +0.4% which is well within experimental error and indicates no bias.

From this discussion the results (P_t) of applying the "RWT" to simulated propellant and sand, shown in Table IV, may be considered to be accurate within 11-15%.

2. P_t vs P_p Correlation

From the data shown in Tables III and IV it is possible to determine if a simple relationship, independent of test diameter, exists between P_t and P_p for a given acceptor material. Figures 6-9 show the results of plotting P_p vs P_t for water and CCl_4, steel, aluminum, and simulated propellant and sand respectively. From the legend in each figure the diameter of the test used to find a particular point can be determined. The best-fit line drawn in each case was found by the least-squares method. They are:

water; $P_t = 0.837\ P_p - 4.387$ (7)

steel; $P_t = 1.083\ P_p + 6.18$ (8)

aluminum; $P_t = 1.221\ P_p + 1.36$ (9)

simulated propellant; $P_t = 1.050\ P_p + 1.81$ (10)

sand; $P_t = 0.9035\ P_p - 2.76$ (11)

Although in Figure 6 there is some spread of the water data in the low pressure region no trends with respect to test diameter are apparent. It may then be assumed that the spread is due to random deviations of the data. Comparing the data (less one very poor point) to equation 7 the $|\overline{PE}|$[e] is 23.2% which indicates the overall accuracy of using this relationship to predict P_t in water for a given P_p, independent of the diameter of the test, and without further streak camera records. Since there is only one data point for CCl_4 no correlation is possible.

The remaining correlations are somewhat better. For steel, aluminum, and simulated propellant the $|\overline{PE}|$ are 15.4%, 13.5%, and 7.7% respectively. Also no diameter trends are apparent. Since there are only two data points (at the same diameter) for sand, equation 11 passes through both and the accuracy of the correlation is unknown.

Although there is no specific reason to assume that the relationships in Figures 6-9 are linear (they could be quadratic, exponential, etc.) it is convenient to use the simplest form possible. The value of the $|\overline{PE}|$'s computed for the linear expressions indicate that this approach is warranted.

Since all the $|\overline{PE}|$'s except one are approximately within the average error in computing P_t ($\sim$13%) it may be concluded that a P_t vs P_p relationship does exist, and that it is independent of the diameter of the test. It is also interesting to note that the most accurate result ($|\overline{PE}|$ = 7.7%) was obtained with the material (simulated propellant) most closely resembling propellants and explosives.

3. Hugoniot Determination

As previously shown, equation 6 along with the result from the "RWT" can be used to compute one point on the Hugoniot of the acceptor. The results (P_t vs u_t) for water and CCl_4, steel, and aluminum appear in Table III and are plotted respectively in Figures 10-12 along with the Hugoniot curves from the literature.[6,9,11] It is evident that, except for CCl_4, the results are both inaccurate (considerable spread in the data) and biased (most points are below the line). It is difficult to explain these results but since the average error in computing P_t was shown to be $\sim$13% it is assumed that the scatter is due, at least in part, to errors in computing u_t. This was estimated to be from 13-40%, depending on the acceptor medium. In Figures 10-12 the computed errors in u_t are represented by the length of the horizontal lines through the points. Also, since the bias in computing P_t is only $\sim$+4% the bias in Figures 10-12 is assumed to be due mainly to a bias in computing u_t. It is not clear why this bias arises or what its magnitude would be.

From the foregoing results it may be concluded that further study and analysis, along with refinements in obtaining data, are needed before Hugoniot prediction by this method can be considered accurate and usable.

V. CONCLUSIONS

The major conclusions of this investigation are: (1) the "RWT" can be used to compute the shock pressure transmitted to a test specimen in card-gap test configurations with an accuracy of 11-15% without measurement or knowledge of the test sample properties; (2) the data from a few "RWT" tests may be used to determine a linear correlation for each acceptor material, between shock pressure transmitted and shock pressure in Plexiglas that is independent of the test diameter and; (3) Hugoniot prediction from the results of the "RWT" is not currently practical because of large errors in computing transmitted particle velocity.

[e] In this case: $|\overline{PE}| = \sum_1^N \left| \frac{P_{t\,equation} - P_t}{P_{t\,equation}} \right| \times 100 / N$

References

1. Salzman, P.K., "Analysis of Shock Attenuation for 0.5 and 2.0 In. Diameter Card-Gap Sensitivity Tests", presented at the ARS Solid Propellant Rocket Conference at Waco, Texas, January 1962.

2. Cook, M.A. and Udy, L.L., "Calibrations of the Card-Gap Test", ARS Journal, 31, 52-57 (1961).

3. Jaffe, I., Beauregard, R.L. and Amster, A.B., "The Attenuation of Shock in Lucite", presented at Third ONR Symposium, Princeton, September 1960; also NAVORD Rep. 6876, U.S. Naval Ordnance Laboratory, White Oak, Silver Spring, Md., May 27, 1960.

4. Pesante, R.E., unpublished work.

5. Price, D. and Jaffe, I., "Large Scale Gap-Test: Interpretation of Results for Propellants", ARS Journal, 595, May 1961.

6. Walsh, J.M. and Rice, M.H., "Dynamic Compression of Liquids from Measurements on Strong Shock Waves", J. Chem. Phys., 26, No. 4, 815 (1957)

7. Lubanov, A.I., "Reflection and Refraction of Shock Waves at the Interface Between Two Media", J. Tech. Phys. (USSR) 9, 2035 (1958)

8. Rice, M.H., McQueen, R.G. and Walsh, J.M., Compression of Solids by Strong Shock Waves, Solid State Physics, Volume 6, Seitz and Turnbull (Editors), Academic Press Inc., 1958

9. Rice, M.H. and Walsh, J.M., "Equation of State of Water to 250 Kilobars", J. Chem. Phys., 26, No. 4, 824 (1957)

10. Al'tshuler, L.V., Kropnikov, K.K. and Brazhnik, M.I., "Dynamic Compressibilities of Metals Under Pressures From 400,000 to 4,000,000 Atmospheres", Soviet Physics JETP, 34(7), No. 4, 614 (1958).

11. Katz, S., Doran, D.G. and Curran, D.R., "Hugoniot Equation of State of Aluminum and Steel from Oblique Shock Measurement", Jour. Applied Phys., 30, No. 4, 568 (1959).

TABLE I

Framing Camera Studies

Acceptor	Column Diameter	Column Length	$\sim P_p$ (Kbar)	Curvature[a]	Waves Visible[b]	Breakup Visible[c]	Opacity[c]	Comments
Water $\rho = 1.00$ g/cm^3	1/2"	1/2"	15	0.092	I,-,T	None	None	Incident wave not sharp
	1/2"	1"	10	0.098	I,-,T	None	None	Too much light
	1/2"	1-1/2"	7	0.074	I,-,-	None	None	Too much light
	2"	1/2"	70	0.012	I,R,T	None	None	Wave self-luminous!
	2"	1"	45	0.012	I,R,T	None	None	Wave ~8.0mm thick
	2"	1-1/2"	25	0.014	I,R,T	None	None	Excellent results
	2"	1-1/2"	25	0.016	I,R,T	None	None	Color film
Steel $\rho = 7.86$ g/cm^3	1/2"	1"	10	-	I,R	None	None	Incident wave not sharp
	2"	1"	45	0.010	I,R	None	None	-
	2"	1-1/2"	25	0.012	I,R	Slight	Slight	-
CCl_4 $\rho = 1.59$ g/cm^3	2"	1-1/2"	25	0.0096	I,R,T	None	None	-
Sand $\rho = 1.36$ g/cm^3	2"	1"	45	0.011	I,R	None	None	-
Air $\rho = 0.00129$ g/cm^3	2"	2.2"	15	0.0095	I,R,-	None	None	Too much light

[a] Curvature = 1/r, r = radius of curvature of incident wave (mm^{-1})

[b] I = Incident Wave, R = Reflected Wave, T = Transmitted Wave (applicable for Water, CCl_4 and Air only)

[c] Directly behind incident wave

TABLE II

Transparent Acceptors

Acceptor	Column Diameter	P_n (Kbar)	P_t^* (Kbar)	P_t[a] (Kbar)	P_{th}[b] (Kbar)	u_t (cm/μsec.)
water	1"	10.1	3.69	2.76	7.4	0.477
ρ= 1.00 g/cm^3	1"	15.8	5.38	4.80	11.6	0.683
	1/2"	7.35	6.46	5.70	5.4	0.760
	1"	10.4	6.98	7.57	7.5	0.867
	2"	18.1	8.32	9.94	13.5	0.963
	1-1/2"	15.6	8.73	10.1	11.8	0.951
	1/2"	20.4	10.0	9.31	15.1	0.774
	2"	24.0	10.0	17.5	22.2	0.929
	1-1/2"	32.3	20.6	20.7	24.9	0.982
	1"	41.3	34.6	31.9	32.0	1.07
	1-1/2"	49.8	47.8	44.2	38.6	1.09
	2"	62.6	54.9	44.2	47.9	1.51
CCl_4	2"	22.3	20.8	-	19.3	-
ρ= 1.59 g/cm^3	1-1/2"	10.3	-	9.89	8.5	0.286

[a] P_t vs. P_t^* : $|\overline{PE}|$ = 11.3%, $\overline{PE}$ = + 4.05%

[b] P_{th} vs. P_t^* : $|\overline{PE}|$ = 37.1%, $\overline{PE}$ = - 27.4%

TABLE III

Opaque Acceptors

Acceptor	Column Diameter	P_p (Kbar)	P_t (Kbar)	P_{th}[a] (Kbar)	P_{tha}[b] (Kbar)	u_t (mm./μsec.)
steel	1/2"	6.00	9.78	11.8	9.26	0.0589
$\rho = 7.86$ g/cm^3	1"	7.30	11.0	15.0	11.8	0.0948
	1/2"	7.67	12.7	15.4	12.1	0.0664
	1"	11.1	19.6	23.0	18.1	0.0820
	1-1/2"	12.5	22.9	25.4	19.9	0.0441
	1"	12.7	20.0	26.4	20.7	0.123
	1-1/2"	15.3	31.5	32.2	25.3	-
	1/2"	17.3	21.2	36.4	28.6	0.302
	1"	38.3	45.8	-	-	0.557
aluminum	1/2"	2.10	2.10	5.7	4.47	0.0658
$\rho = 2.77$ g/cm^3	1"	5.06	8.20	8.5	6.67	0.0526
	1/2"	7.57	11.4	12.7	9.97	0.0967
	1-1/2"	9.20	13.9	15.5	12.2	0.111
	1"	9.68	11.4	16.4	12.9	0.207
	1"	11.7	14.0	20.0	15.7	0.237
	1/2"	13.1	21.7	22.5	17.7	0.0972
	1-1/2"	18.1	20.6	30.6	24.0	0.357
	1-1/2"	29.7	38.8	51.6	40.5	0.387
	1"	33.2	41.0	58.0	45.5	0.476

[a] P_t vs. P_{th} : $|\overline{PE}| = 21.8\%$, $\overline{PE} = +21.8\%$,

[b] P_t vs. P_{tha}: $|\overline{PE}| = 15.1\%$, $\overline{PE} = +0.4\%$,

TABLE IV

Shock Pressure Transmitted

Opaque Accepters; Unknown Hugoniots

Accepter	Column Diameter	P_p (Kbar)	P_t (Kbar)
simulated	1"	10.9	10.9
propellant	1-1/2"	14.8	14.0
ρ= 1.648 g/cm^3	1"	12.6	15.5
	1-1/2"	14.6	20.8
	1-1/2"	23.8	27.4
	1"	43.6	45.2
	2"	56.8	58.9
	1-1/2"	110.5	119.6
sand	1"	6.60	3.20
ρ= 1.36 g/cm^3	1"	41.1	41.6

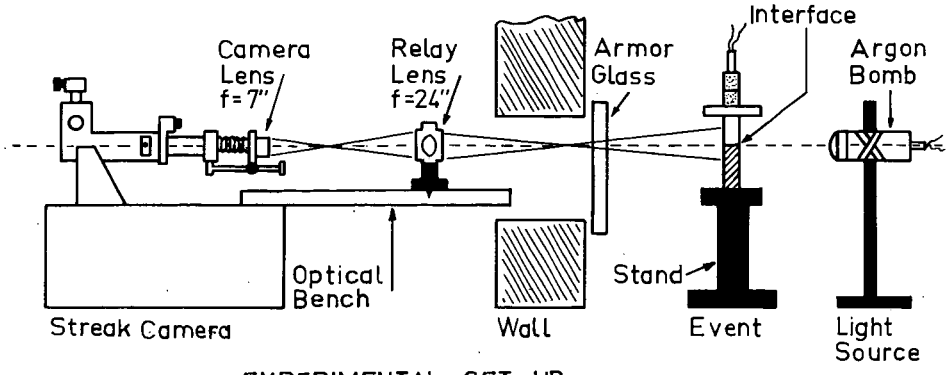

EXPERIMENTAL SET-UP
FIGURE 1a

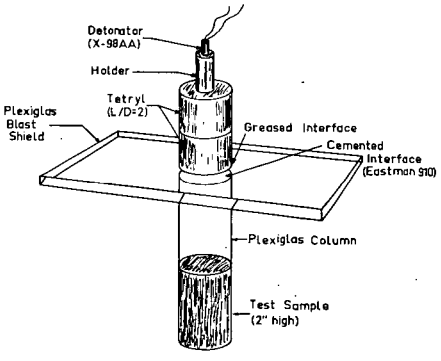

Gap Test (Solids)

FIGURE 1b

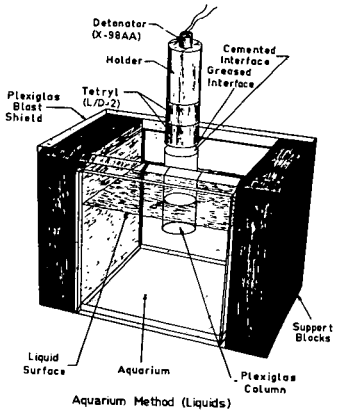

Aquarium Method (Liquids)

FIGURE 1c

Figure 2

FRAMING CAMERA STUDY

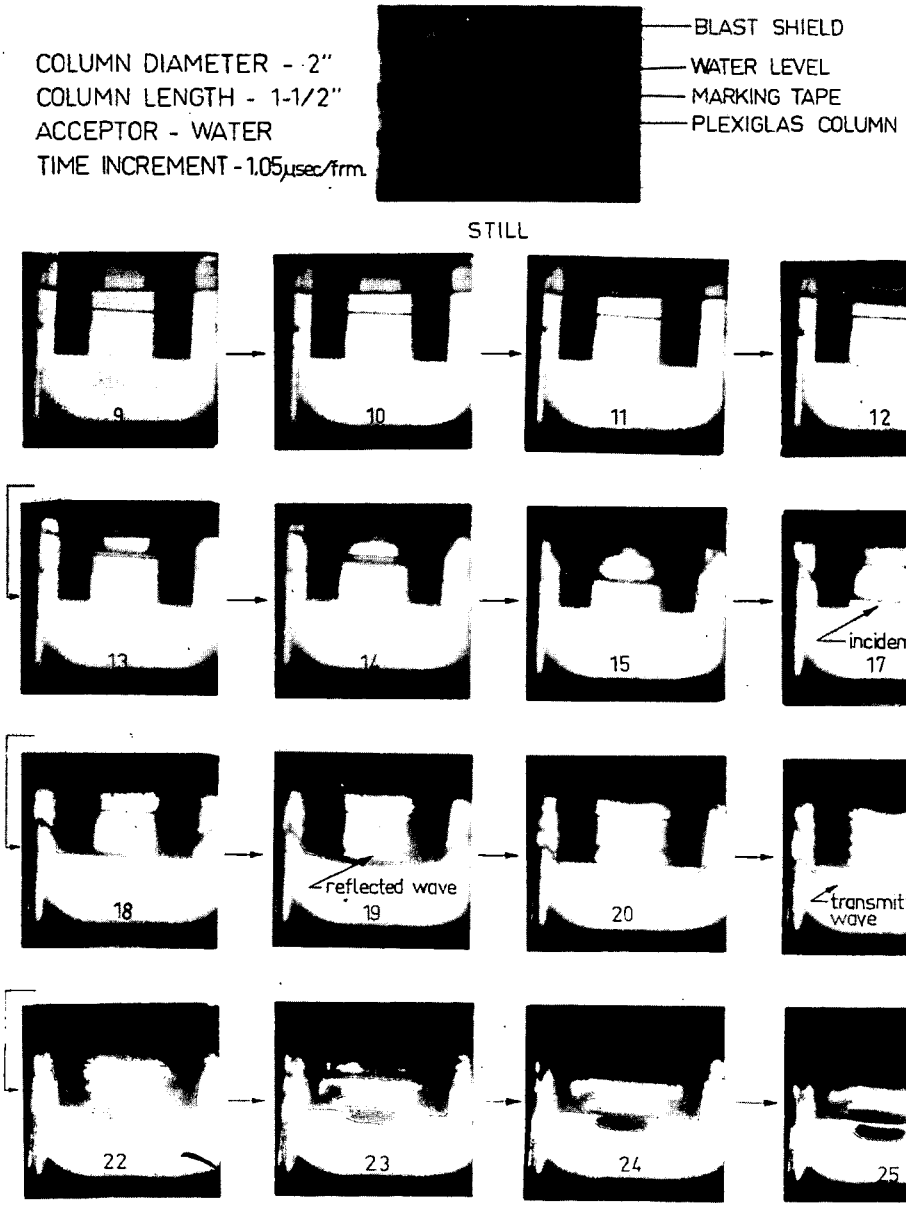

STREAK CAMERA STUDIES

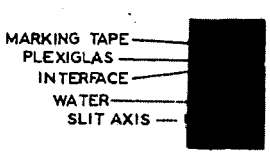

Still

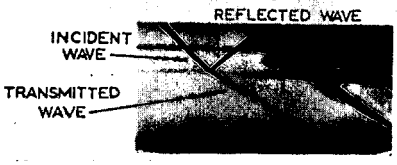

Streak

Column Diameter - 1"
Column Length - 1-1/2"
Acceptor - Water

Figure 3a

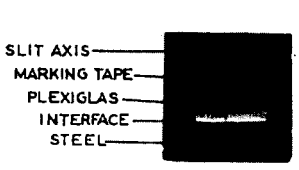

Still

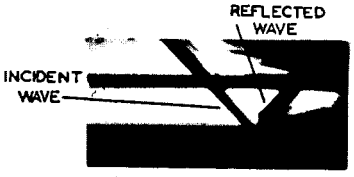

Streak

Column Diameter - 1-1/2"
Column Length - 2"
Acceptor - Steel

Figure 3b

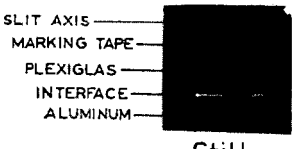

Still

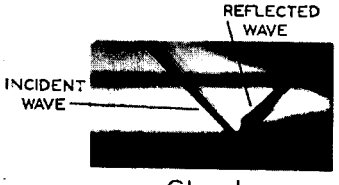

Streak

Column Diameter - 1-1/2"
Column Length - 2"
Acceptor - Aluminum

Figure 3c

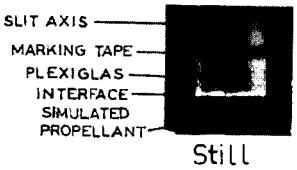

Still

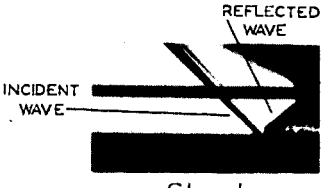

Streak

Column Diameter - 1"
Column Length - 1-1/2"
Acceptor - Simulated Propellant

Figure 3d

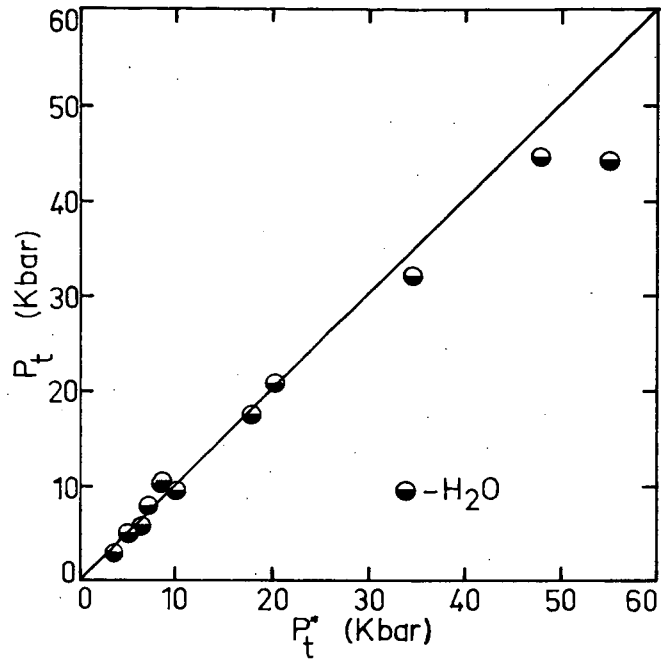

Figure 4 - Accuracy of "RWT", acceptor: water

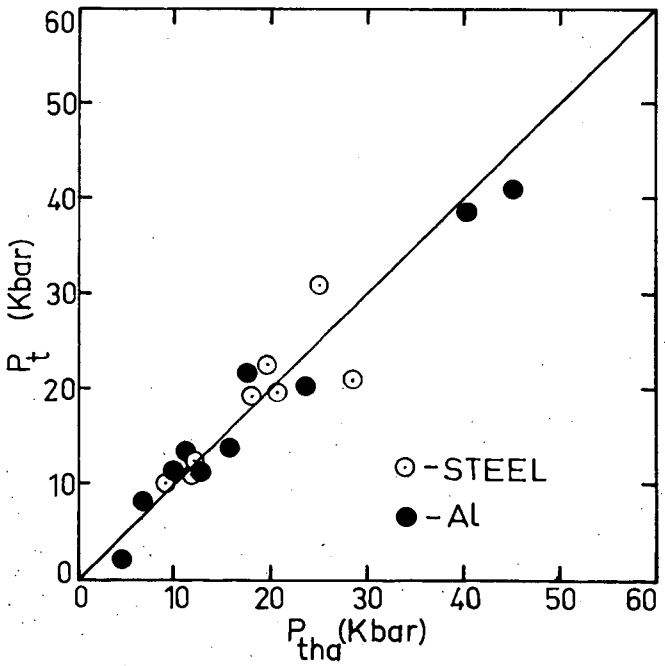

Figure 5 - Accuracy of "RWT", acceptors: steel, aluminum

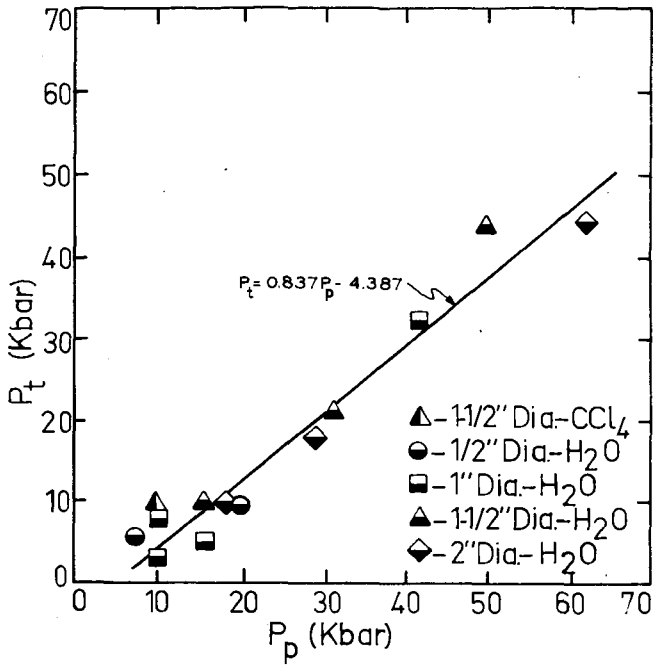

Figure 6 - P_t vs P_p Correlation, acceptors: water, CCl_4

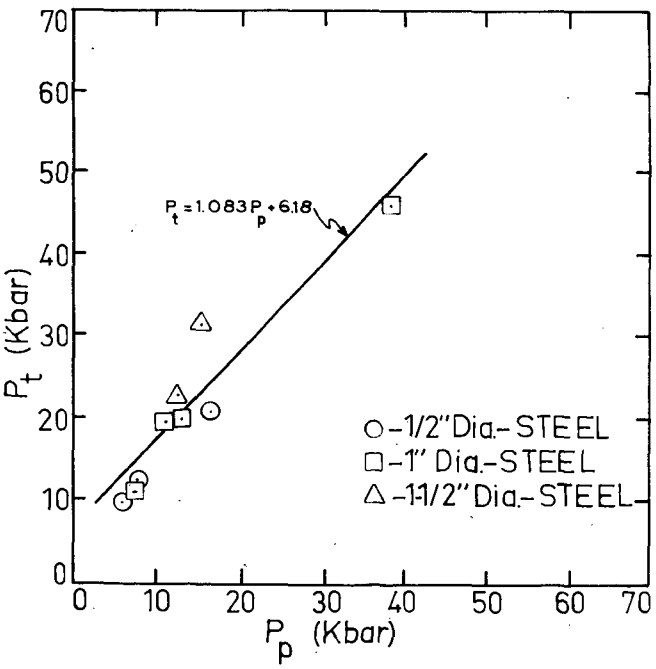

Figure 7 - P_t vs P_p Correlation, acceptor: steel

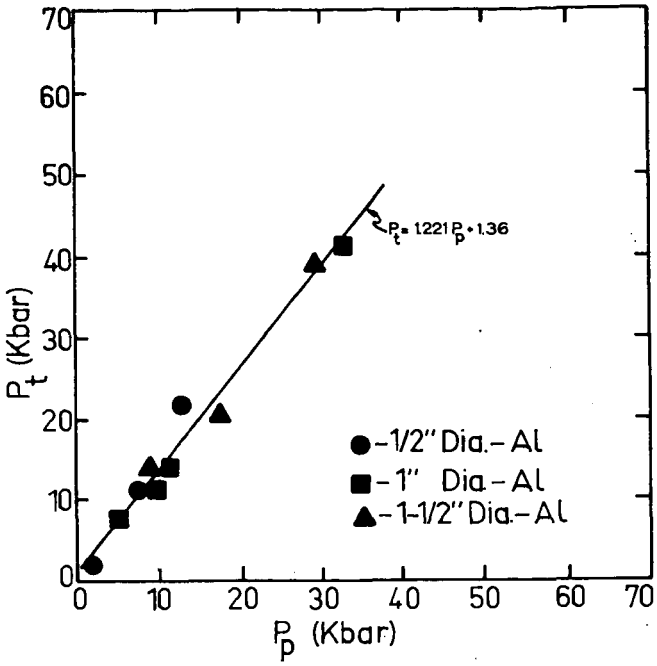

Figure 8 - P_t vs P_p Correlation, acceptor: aluminum

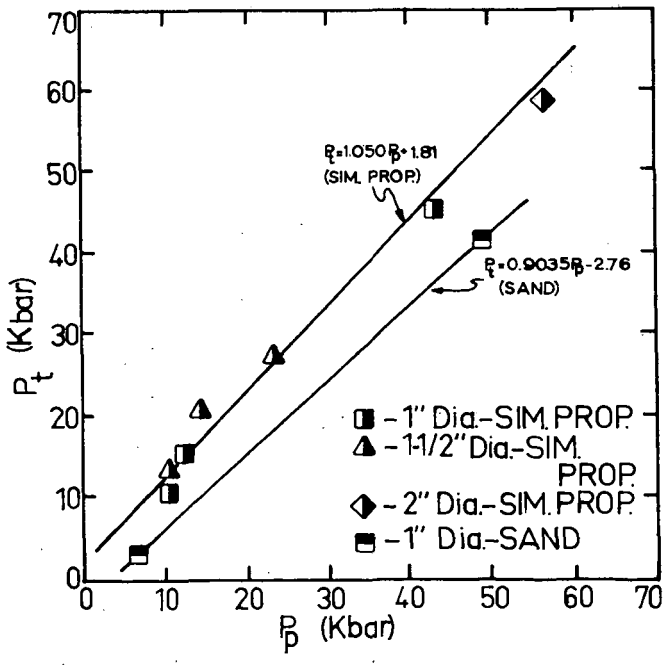

Figure 9 - P_t vs P_p Correlation, acceptors: simulated propellant, sand

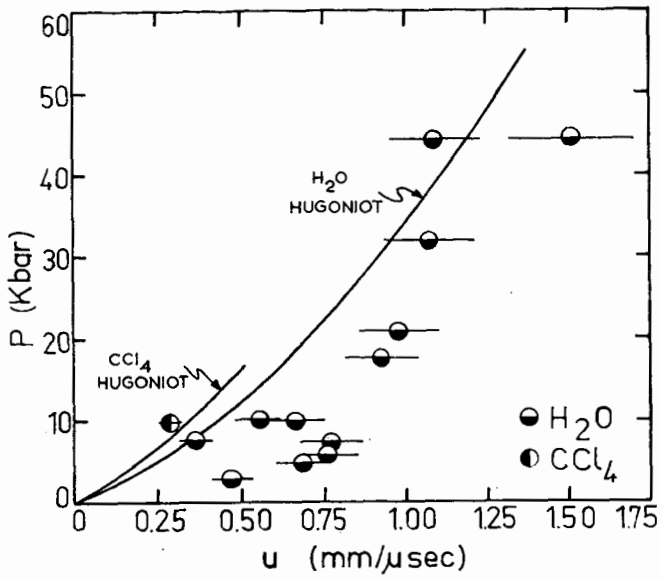

Figure 10 - Hugoniot Determination, water and CCl_4

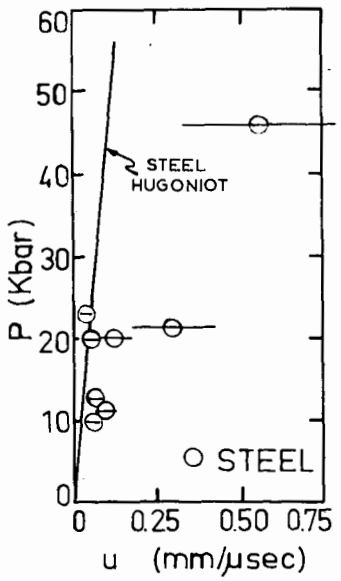

Figure 11
Hugoniot Determination, steel

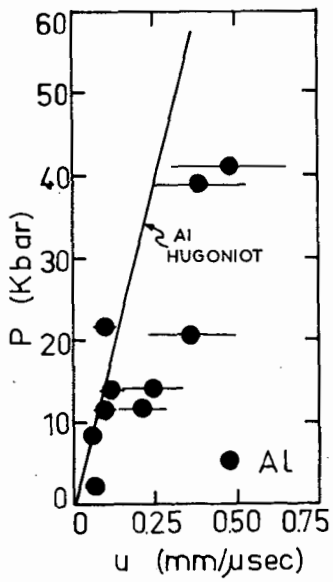

Figure 12
Hugoniot Determination, aluminum

Prediction of Detonation Hazard in Solid Propellants

by;
STANLEY WACHTELL
PICATINNY ARSENAL, DOVER, N.J.

Abstract

Classification of the detonation hazard after ignition of a large solid propellant rocket motor has in the past been based on sensitivity test methods which have little relationship to the actual conditions under which such an incident might occur. The development of a method by which prediction of such an occurence is possible is described in this paper.

Experimental work has shown that when a large mass of an explosive or propellant is burned in a closed system, a sharp change in slope of the burning rate/pressure curve occurs at a pressure which is specific for that material. This transition pressure is dependent on the initial temperature of the material. For explosives this transition pressure is in the range of 4-8000 psi and is related to the sensitivity of the explosive. For propellants, the transition pressure is somewhat higher and, this pressure as well as the slope of the transition curve appears to be related to the physical state and the energy level of the propellant.

From the transition pressure and the slope of the transition curve and from the physical configuration of a missile motor, the hazard of detonation may be determined.

To extend the range of measurements possible, a pressure vessel has been developed in which measurements of propellant burning rate at pressures as high as 250,000 psi can be made. This vessel has a unique design consisting of two concentric cylinders. Radial stresses are taken by the inner cylinder, which is replaceable if fracture should occur. Recording of pressure information precedes fracture of the inner vessel. The outer cylinder carries only axial stresses and is of sufficient strength to prevent fracture and retain fragments.

The development of this vessel has also made possible the examination of burning characteristics of cannon propellants for very high pressure applications. Results show that some standard cannon propellants have transition characteristics similar to those described for explosives and rocket propellants. This phenomenon explains some disastrous incidents resulting from very high pressure gun firings.

Introduction

In assessing the hazard involved in the use of a rocket motor there are a number of factors to be considered. First, the hazard of detonation while transporting the motor from its manufacturing site to place of launching in its shipping

container. Second, the hazard of detonation of the propellant if the warhead should explode. Third, the hazard of detonation of propellant if struck by a high explosive bomb. Fourth, the hazard of detonation of the propellant if struck by bomb fragments or projectiles. Fifth, the hazard of detonation after a normal ignition during launching.

Actually, numbers 1 and 5 are essentially the same hazard - that is transition from burning to detonation, while 2, 3 and 4 are essentially shock initiation.

Concern with these latter three problems of shock initiation are generally recognized and most propellants are well characterized as to shock sensitivity by various booster sensitivity or pipe tests. The information obtained tells little about transition from deflagration to detonation (DDT). This brings us to items 1 and 5.

A major hazard from missile transportation and handling is accidental ignition. In the confined condition, will this result in a pressure blow of the missile case or will it result in transition to high order detonation? The difference for a large motor containing tons of solid propellant could be a good fire or a major disaster. If the possibility (or non-possibility) of transition could be predicted, a much more realistic approach to storage and handling could be adopted.

The hazard of transition to detonation after normal ignition on a firing stand could result from unknown defects which exist in a motor resulting from manufacture, aging or handling.

This report describes work which has been done thus far in an effort to classify explosives with respect to the possibility of DDT under the conditions and geometry which may actually exist in a solid propellant motor.

Theory

Kistiakowsky (1) described a mechanism for the development of detonation in a large mass of granular or crystaline explosive ignited thermally at a localized region within the bulk. As the explosive burns, the gases formed cannot escape between crystals and a pressure gradient develops. This increase in gas pressure causes an increase in burning rate which in turn causes an increase in pressure with constantly increasing velocity. This condition results in the formation of shock waves which are reinforced by the energy released by the burning explosive and they eventually reach an intensity where the entire energy of the reaction is used for propagation of the shock wave and a stable detonation front is produced. A critical mass exists for each material above which this deflagration can pass over into detonation under proper conditions. Below this mass the burning will first increase and then decrease as the material is consumed.

The transition to detonation is considered largely a physical process in which the linear burning rate of the bed of material increases to several thousand meters per second although the individual particles are consumed at the rate of only a few meters per second.

The validity of this mechanism has been demonstrated experimentally for granular propellants by a number of workers (2) (3) (4).

In the experimental work described here, it was believed that very similar conditions could be established if a large mass of explosive or propellant were burned in a closed chamber. It has been shown (5) (6) that for composite propellants, the highly elastic binder material will undergo brittle fracture when stress is applied at very high strain rates. When propellants or explosives are burned in a closed chamber the rate of pressure build up accelerates sufficiently to develop surface strains in the large grain at rates which exceed those needed to produce brittle fracture. Combine this with the embrittlement accompanying the high pressures involved and the thermal shock produced by the hot gases of combustion on the cold grain and a condition equivalent to that existing for granular material could exist. A further verification of this mechanism is the increased tendency of propellants to detonate when cooled to low temperatures. This problem is well known to anyone working with solid propellants both for rockets or cannons.

Basis for Experimental Studies

If the mechanism suggested by Kistiakowsky for granular and crystaline explosives could apply to solid propellants by the mechanism suggested above, then it should be possible to demonstrate the increase in burning surface for such materials by burning large pieces in a closed chamber in which the burning of the material produced the higher pressures for accelerated burning. The first indication that such a reaction actually might occur was found when a series of cannon propellants, which had caused guns to blow up when fired at temperatures of -20°F and -40°F were tested in a closed chamber (7). When records were made of rate of change of pressure vs. pressure, it was found that a sharp increase in rate occurred at a pressure which was fairly specific for each lot of propellant tested. If such a mechanism did exist, then it should be demonstrable for high explosives as well. Since the normal burning rate laws are known to hold for both propellants and explosives when burned under static pressure conditions (as in a strand burning rate bomb) a comparison of these two methods of burning would demonstrate the existance of the mechanism. Calculation of the linear burning rate of a cylinder of material under constantly changing pressure from the measurement of dp/dt vs. pressure is given in references (8) and (9). In this calculation the assumption is made that the cylinder is ignited uniformly on all surfaces and always burns normal to that surface. Experience with interrupted burning of propellant grains of even complicated geometry verifies this. If, however, cracking or

crazing should occur, the calculated linear burning rate will be far in excess of the value expected and the increase in surface area can be calculated from this apparent increase in linear burning rate.

Experiments With Burning of High Explosives

Cylinders of TNT were prepared with diameters of 1" to 1¼" and lengths of 1" to 3". These cylinders were machined from solid blocks of TNT which had been carefully cast to prevent porosity or voids. All cylinders were machined from the same casting and were considered to have about the same crystaline structure. A series of these were fired at loading densities (weight of explosive, grams/volume of chamber, cc) of 0.11 to 0.387. In addition, in some tests the chamber was preloaded up to 10,000 psi by including some very fast burning mortar propellant which produced the preloading pressure before the TNT had a chance to burn appreciably. Figure 1 shows some of the typical oscillograms obtained. Strands were also cut from the block of TNT and were burned at pressures up to 20,000 psi in a Crawford strand burning rate bomb. Linear burning rate vs. pressure were calculated for all the results obtained and were plotted on a single log plot. Figure 2 shows the average curve obtained from this data. Note the change in slope that occurs for the closed bomb line at about 6,000 psi while the strand burner shows the normal burning rate/pressure relationship.

A calculation of increase in surface area with pressure is shown in Figure 3. This was done by substituting the burning rate obtained from the strand burner into the equation used for calculation of the closed bomb burning rate and solving for surface area at different values of pressure. Note that an increase in surface area of almost 20 times occurs. Figure 4 gives the ratio of calculated area/expected area for a typical cylinder of TNT.

Experiments of this same nature were made with Composition B which is a mixture of 60 percent of RDX with 40 percent of TNT with 1 percent of wax desensitizer added. Results similar to TNT were obtained although difficulty in obtaining uniform ignition required the use of preloading for all tests. Figures 5, 6, 7 and 8 show the data obtained for Composition B. This pretransition pressure appears to be somewhat lower than for TNT alone although detail in this area of the curve is lacking because of the preloading required.

Tests of Propellants

A number of experimental and high energy propellants were then tested using this same technique. These can only be described as composite and double base types because of security considerations. Results of these propellants are presented here, each one showing modifications of the same pretransition characteristics. The first propellant, a double base type with

solid oxidizer, when fired in the closed bomb showed a somewhat exaggerated pre-transition effect as shown in Figure 9. A series of these tests were calculated to linear burning rate vs. pressure as for TNT and Composition B. The results are shown in Figure 10. Note that the transition which occurs at about 15,000 psi is even sharper than for the explosives and the slope of the curve is steeper. This is believed due to the larger amount of energy resulting from combustion of this propellant as compared with the explosives. Strand burning rated data was not available for this propellant at high pressure. Therefore, the low pressure curve was extrapolated. Calculation of changes in surface area shows increases up to 25 times for this material. Other samples of similar composition were tested in which changes were made in the plasticizer; both in the material used and the percentage. These changes were found to shift the pre-transition pressure up or down. No effort was made at this time to relate this shift to differences in physical properties. All these samples of propellant were detonable with a #6 blasting cap.

A second propellant-designated ARP, a high energy double base type, gave the results shown in Figure 11. The straight line burning rate curve was obtained with points from strand burning rate tests and closed bomb tests at loading densities up to 0.4. However, when a preloading of 15,000 psi was used in one test, a pre-transition change in slope in the curve resulted at about 40,000 psi. The pressure rate was so high that a large part of the trace was lost. Extensive damage also resulted to the bomb and further testing of this composition was stopped at this time to await the development of more suitable high pressure equipment.

A third type of propellant tested was a composite double base - Type QZ manufactured by Rohm & Haas. This propellant type was known to have undergone DDT when fired in a large motor which contained some porous propellant. Tests at 70°F did not show any transition point. However, when cooled to -60°F a typical pre-transition curve resulted (Figure 12). In addition to these propellants, a number of lower energy and less sensitive materials were tested in the bomb both with and without preloading. No indications of pre-transition could be found within the pressure limitations of our test equipment.

Design of Ultra-High Pressure Equipment

Because of the limitations of our test equipment (80,000 psi) the design of a vessel that would contain much higher pressures, was undertaken. The basic design concept utilized was based on the fact that for sufficiently high rates of loading, the inertia of the vessel walls would resist failure sufficiently long to permit measurement of the pressure time history. To make a practical unit, two concentric cylinders were used. The inner replaceable cylinder contained the high pressure while the outer massive cylinder held

the end closures for the inner cylinder. A space between the cylinders was provided for expansion of the gases in case of failure of the inner cylinder. The outer cylinder also served as a confinement for fragments resulting from failure of the inner cylinder. All pressure on the end closures is transmitted axially to the outer cylinder which has sufficient strength to hold pressures in excess of 300,000 psi in the inner chamber. The seals between the inner cylinder and end caps were designed to expand as the outer cylinder stretched due to the pressure development. When the inner chamber did not break, it was found that the expansion of the seals maintained pressure on the end caps, making it impossible to open. Therefore, provision was made to recompress the seals with a hydraulic ram to release this pressure and permit opening of the bomb. After many difficulties with parts failures, a basic design shown in Figure 13 was evolved. An exploded view, of an early design, is given in Figure 14.

Actual detail of the final design of this vessel is not given here because it is still undergoing changes resulting from experience in its use. Suffice it to say, that when working with the dynamic pressures and high temperatures of the type encountered in this work, every conceivable type of failure has occurred. However, measurements of pressures as high as 250,000 psi have been made.

Measurement of pressures can be made in this vessel with any type of pressure transducer by suitably modifying the gage housing. In our initial testing, pressure/time measurements were made using a Kistler Gage Type 601 with a special hyperballistic probe. This gage is designed to measure pressures up to 300,000 psi. It is a piezoelectric type in which the charge that build up on a quartz crystal under compression is measured by means of a special electrometer circuit. The pressure is transmitted to the crystal through a small carefully ground piston which extends into the pressure chamber.

For interior ballistic work and for measurement of rate of change of pressure it is considered more desireable to obtain measurements of dp/dt vs. pressure rather than pressure time. However, at the time the work described below was done, such instrumentation was not available. Work being done at the present time is using such measurements.

Measurement of High Pressure Characteristics of Cannon Propellants

Following the reasoning and pre-transition characteristics described above for rocket propellants, it seemed reasonable to expect that a similar pre-transition mechanism might exist for cannon propellants.

Actually, over the past many years, numerous accidents in gun firings have occurred which have been difficult to explain in terms of anything other than propellant malfunction. Most frequently these have occurred in low temperature firing of propellants which function normally in average temperature conditions. Typical of this type of malfunction are low temperature mortar firings using

M9 propellant. High pressures developed under such conditions have, on some occasions, ruptured mortar tubes. M17 propellant has also been known to display erratic ballistic behavior at -40°F, and in 1958 a 76MM gun was blown up in such a malfunction.

It was during the investigation of this malfunction, that it was shown that certain lots of M17 propellant had the characteristic of developing a change in the burning rate/pressure curve (Reference 7). Under closed bomb tests it was possible to determine which lots of M17 propellant would actually develop this high pressure. Traces showing dp/dt vs. pressure of good and defective M17 propellants are given in Figure 15.

Up to this point, except for the low temperature tests, these transitions have only been noted in rocket propellants and explosives on an experimental basis. Cannon propellants have been used in these pressure ranges rather commonly with no such effects, except for occasionally unexplained malfunctions. One such malfunction occurred recently, when a gun designed for 86,000 psi max pressure was destroyed with T36 cannon propellant when an increase in charge weight of about 2 percent to increase pressure above 70,000 psi, caused an increase in max pressure of over 100 percent.

With the development of the ultra high pressure closed bomb, capable of testing propellants at much higher pressures than previously, it became possible to determine if the same type of behavior demonstrated for rocket propellants and explosives could be shown cannon propellants at high pressures. A M17 propellant of 0.045 web was loaded into this new bomb at a loading density of .40. A maximum pressure of 105,000 psi was anticipated. Figure 16 is the pressure/time trace obtained. Careful examination shows that at the end of this pressure rise (about 92,000 psi) there is a vertical rise of indefinite magnitude before the trace returns to low pressure. This is indicative of transition to detonation having taken place after 90 percent of the propellant has been burned. Other evidence of the detonation inside the bomb was the fracture of the inner cylinder which had been calculated to hold in excess of 150,000 psi, and a definite spalling condition existing in some of the fragments of the inner cylinder. The massive end plug of the bomb was also cracked all the way through.

After repairs were completed to the apparatus, tests were then made of T28 propellant using the same conditions. Figure 15 shows the pressure/time trace. While the burning time was much shorter, a maximum pressure of 105,000 psi was obtained with no unusual incident in the bomb to indicate a transition effect. T28 propellant has been fired at .40 loading density a number of times to verify this. At the time of these tests only pressure/time information was available. For future work it is expected that dp/dt vs. pressure will be available.

These results fit in very well with the mechanism stated previously. M17 propellant and T28 propellant are very similar in energy level. Their basic difference is in compressive strength and the difference in the homogeniety of their structure. M17 propellant is notoriously poor as far as compressive strength is concerned although with some modification in processing, improvement has been made as with T36 propellant.

It is interesting to note that in high pressure gun firings with M17 propellant, the transition effect of T36 which originally was demonstrated above 70,000 psi was found for M17 propellant to begin at 50,000 psi.

The very sketchy nature of the work presented here is the result of a very limited study of cannon propellant burning under very high pressure conditions. However, we believe it is significant enough to be reported at this time.

Conclusions

In the work presented herein, there is definite evidence that the process of transition from deflagration to detonation for explosives and propellants is a continuous reaction consisting of first - ignition; second - under confined conditions (such as might exist in a large mass of material or porous material) a pre-detonation reaction consisting of accelerated burning due to a physical breakdown of the surface resulting from the pressure, rate of change of pressure and temperature gradient; third - development of an accelerating shock front; fourth - detonation if sufficient mass of material is available.

It is believed that any material which can be detonated should exhibit this pre-detonation reaction. In the case of very sensitive primary explosives the level of controlling parameters required to start detonation is so low that they cannot be measured by present techniques. For "non-detonable" propellants the pressures required for the pre-detonation reaction to occur are so high that for all practical purposes, they cannot be attained.

It is considered practical that this technique can be used for the classification of the detonation hazard for a particular motor configuration if the pre-transition pressure and slope of the burning rate pressure curve of the propellant used is known. Thus, for example, if a defect or void should exist in a propellant, which might conceivably ignite on firing, by considering such an ignition as an interior ballistic system the pressure and rate of pressure rise can be calculated to determine if pre-detonation conditions could develop before tensile failure of the grain occurred. If such reaction can occur then the accelerated pressure rise could develop the shock front necessary for transition to detonation.

REFERENCES

1. Kistiakowsky, G. B., Initiation of Detonation in Explosives, Third Symposium on Combustion Flame and Explosion Phenomena Williams and Wilkins, 1949.

2. Hyndman, J. R., et al, Rohm and Hass Co. Ballistics Section Program Report #67, October 1957.

3. Mason, C. M. et al, (U. S. Dept. of Interior, Bureau of Mines) Final Summary Report #3734 Investigation of Susceptibility to Detonation of Propellants.

4. Macek, A. (Naval Ordnance Laboratory) NAVORD 6105, Sensitivity of Explosives VII. Transition from Slow Burning to Detonation: A Model for Shock Formation in a Deflagrating Solid, 3 February 1958.

5. Jones, J. W., Sagers, D. L., and Nolan, E. J., Fracture Mechanics of Solid Propellants, Progress Report No. ELab-A-19, 16 February 1959-15 February 1960, Eastern Laboratory, E. I. duPont de Nemours & Company (Confidential)

6. Jones, J. W., Prediction of Catastrophic Rocket Motor Explosion Conditions from Broad Spectrum Mechanical Property Analysis. Preprints of Sixteenth Meeting, JANAF Solid Propellant Group, Vol. 5.

7. Russell, K. H., Goldstein, H. M., Investigation & Screening of M17 Propellant Production for Lots Subject to Poor Low Temperature Ballistic Performance, Technical Report DB-TR 7-61 Ammunition Group, Picatinny Arsenal, Dover, N.J., June 1961

8. Pallingston, A. O., Weinstein, M., Method of Calculation of Interior Ballistic Properties of Propellants from Closed Bomb Data, Picatinny Arsenal Technical Report #2005, June 1954.

9. Wallace, W. F., New Formulas for Rapid Calculation of Linear Burning Rates of Solid Propellants. Picatinny Arsenal Technical Report #2488, April 1958.

10. Wachtell, S., McKnight, C. E., A Method for Determination of Detonability of Propellants & Explosives, Third Symposium on Detonation, ONR Symposium Report ACR-52, Also Picatinny Arsenal Technical Report DB-TR 3-61.

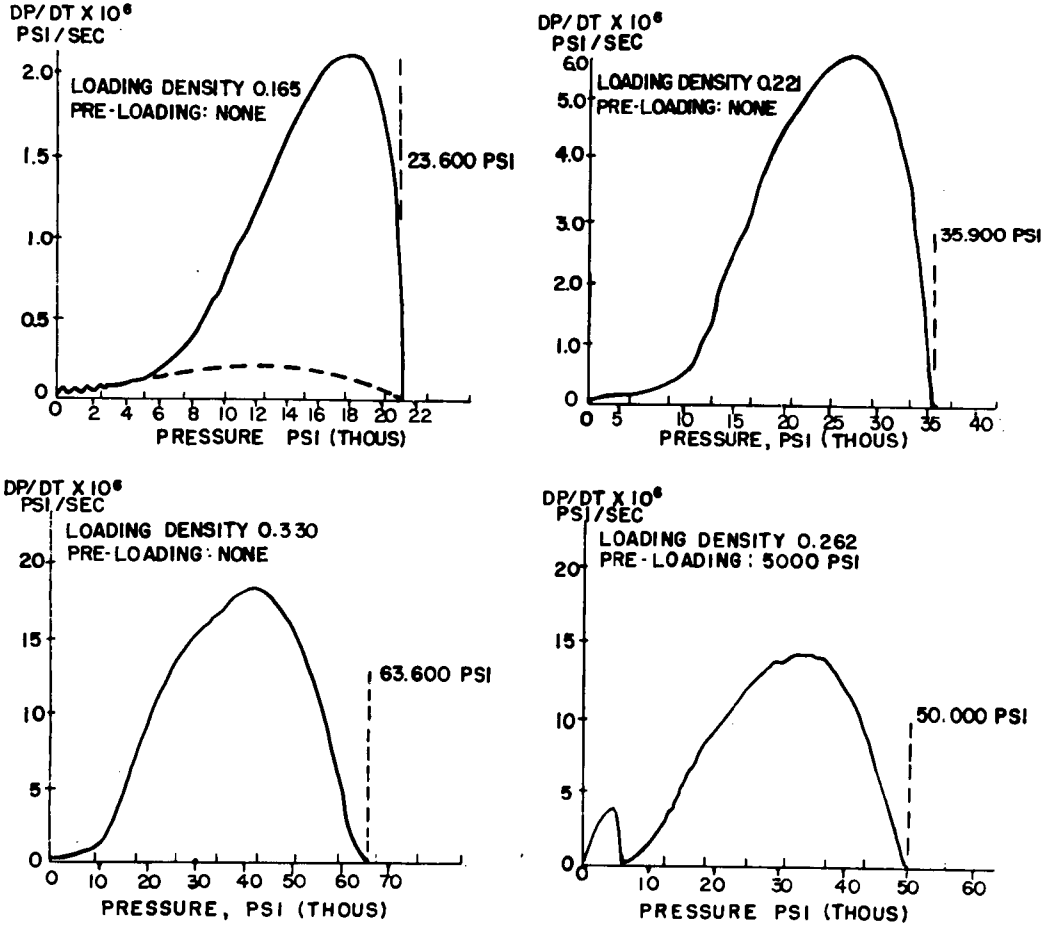

Figure 1. Closed Bomb Test TNT

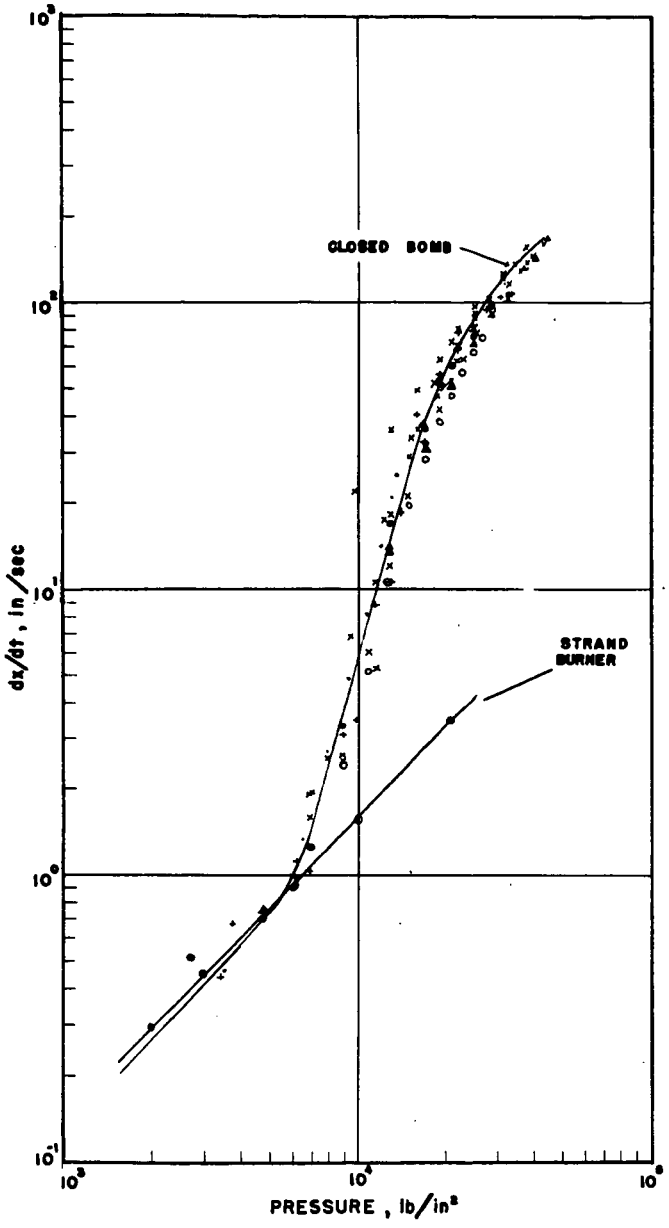

Figure 2. Linear Burning Rates of TNT Obtained with Closed Bomb and Strand Burner

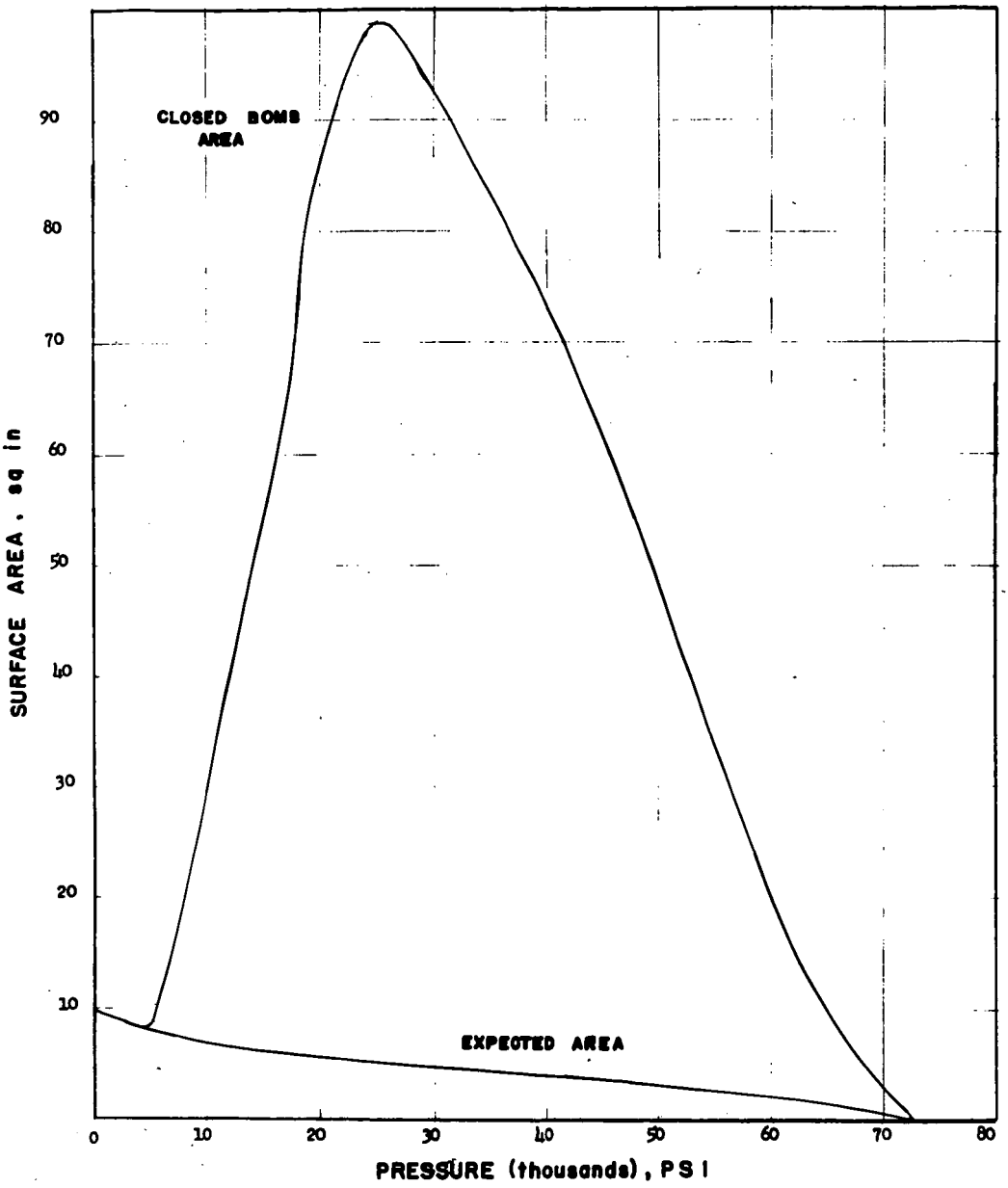

EXPECTED SURFACE AREA VS ACTUAL AREA OBTAINED FOR TNT CYLINDER BURNED IN CLOSED BOMB

FIGURE 3

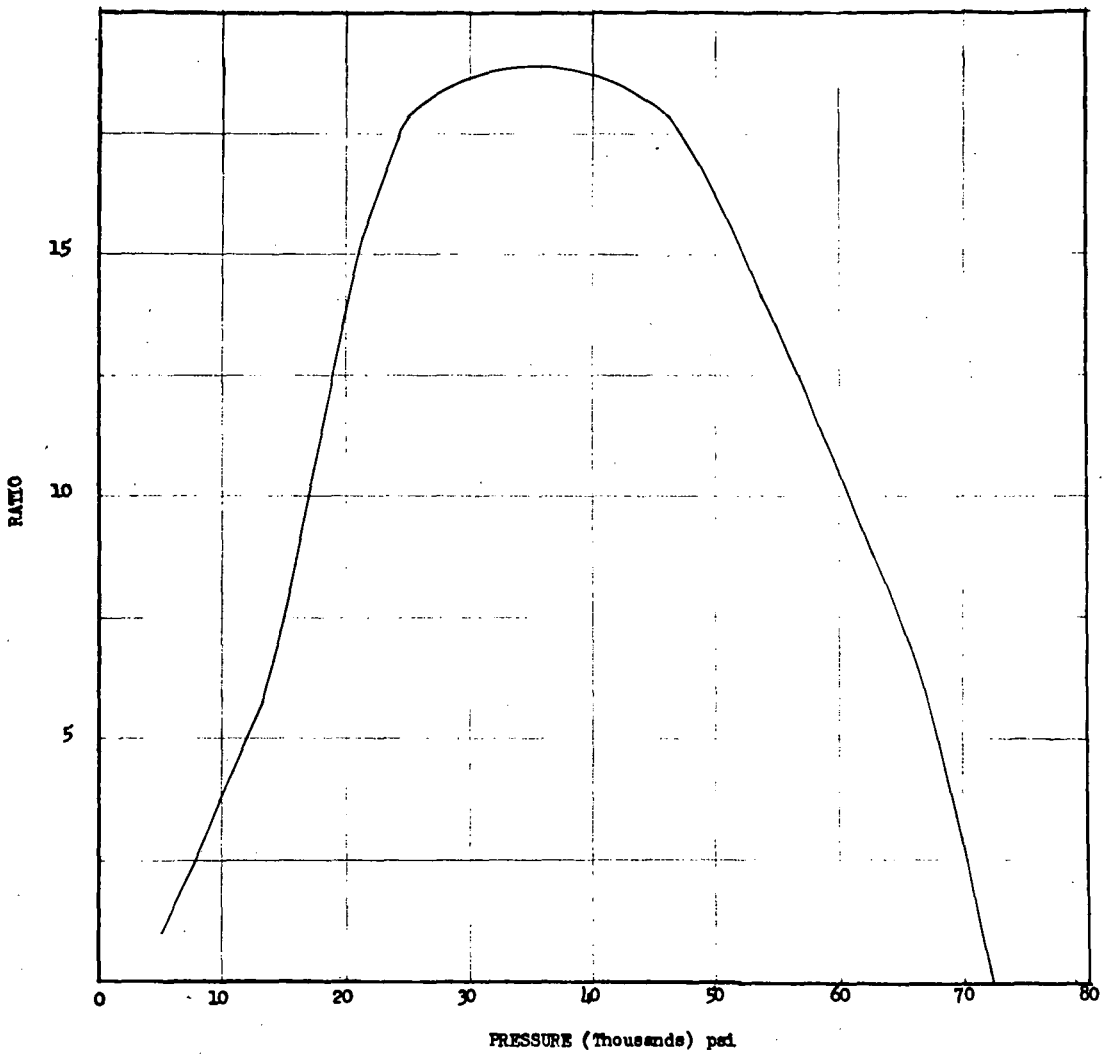

RATIO OF EXPECTED AREA TO ACTUAL AREA
FOUND FOR TNT CYLINDER

FIGURE 4

CLOSED BOMB TEST
COMPOSITION B

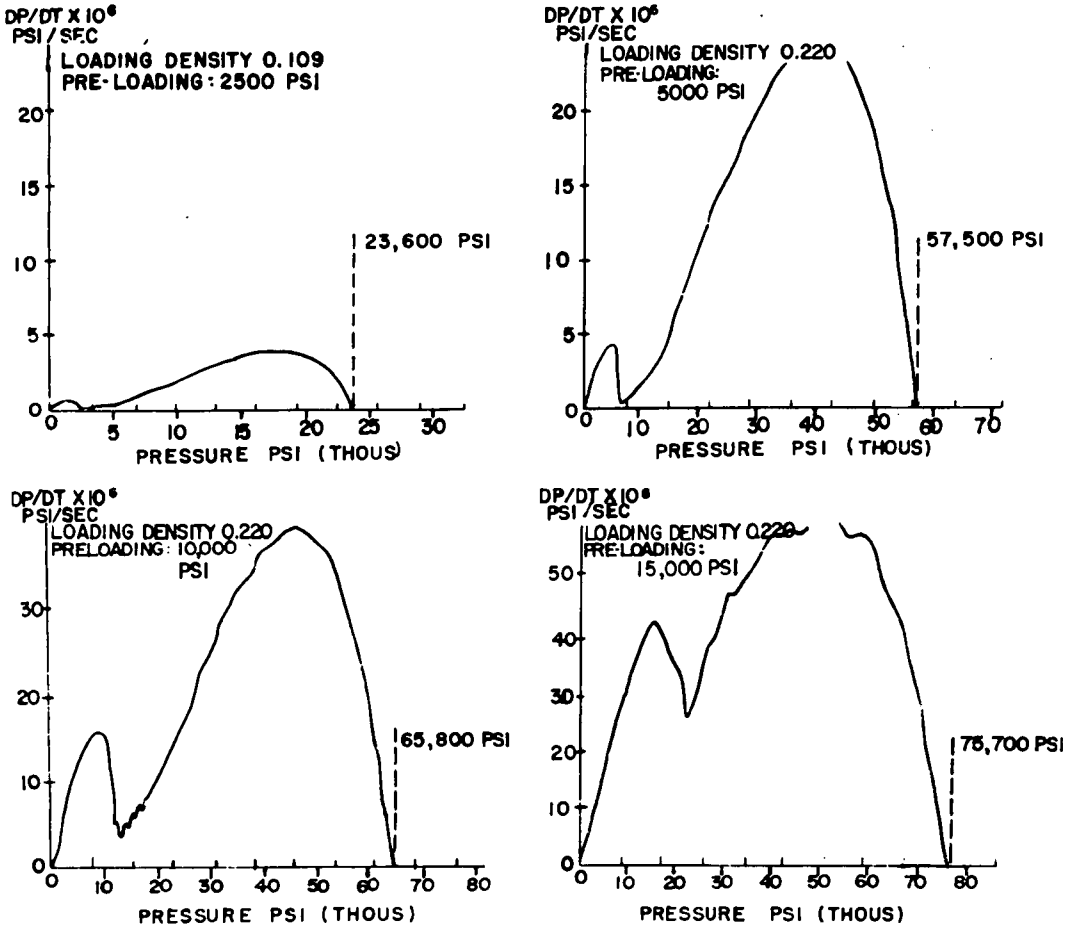

FIGURE 5

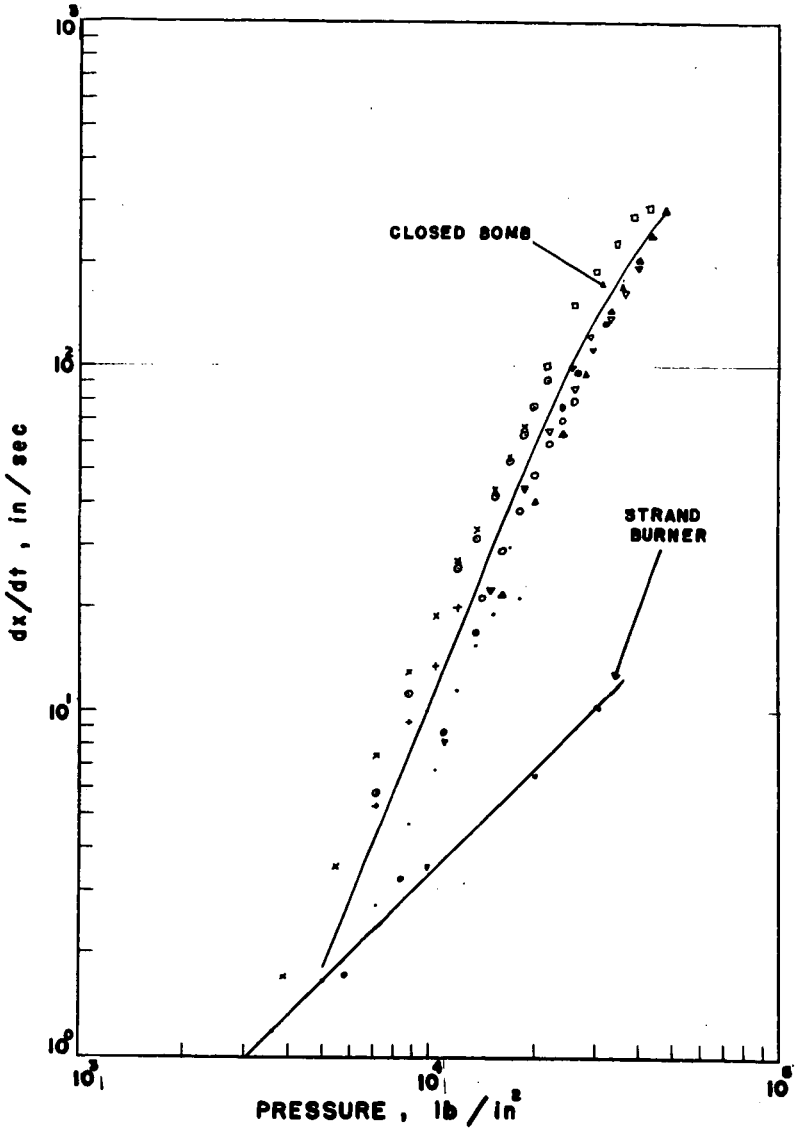

LINEAR BURNING RATES OF COMPOSITION B OBTAINED WITH CLOSED BOMB AND STRAND BURNER

FIGURE 6

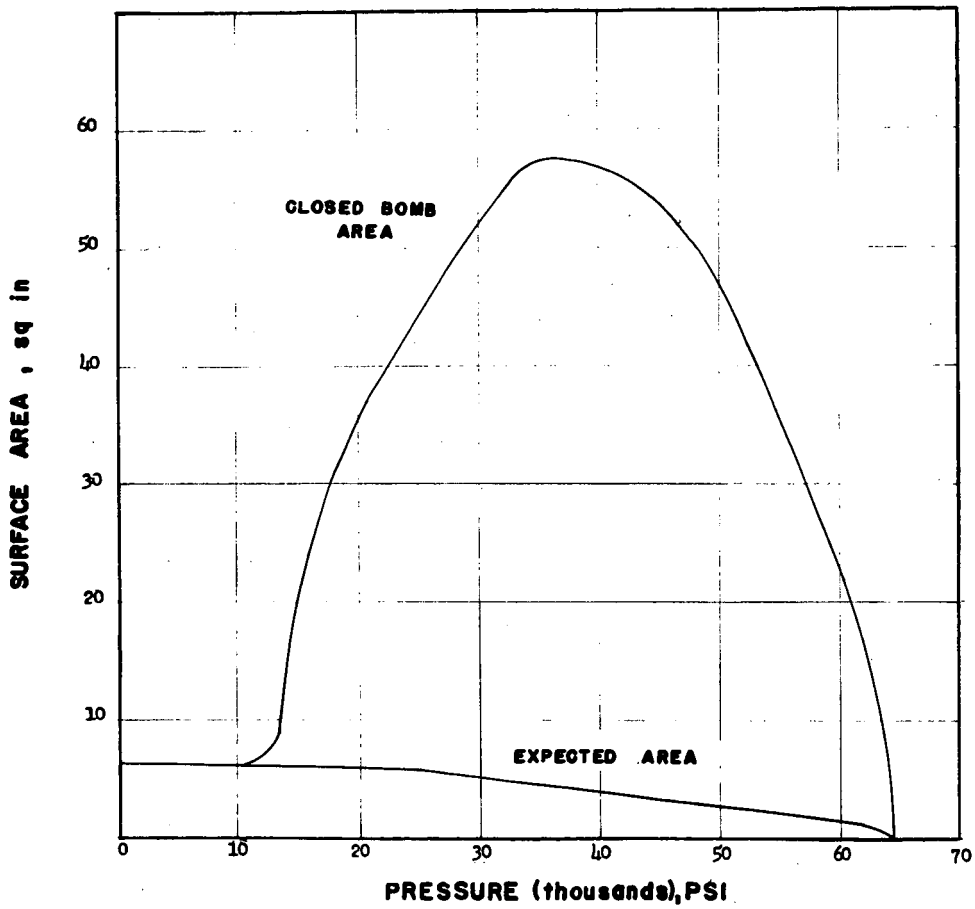

EXPECTED SURFACE AREA VS ACTUAL AREA OBTAINED FOR COMPOSITION B CYLINDER BURNED IN CLOSED BOMB

FIGURE 7

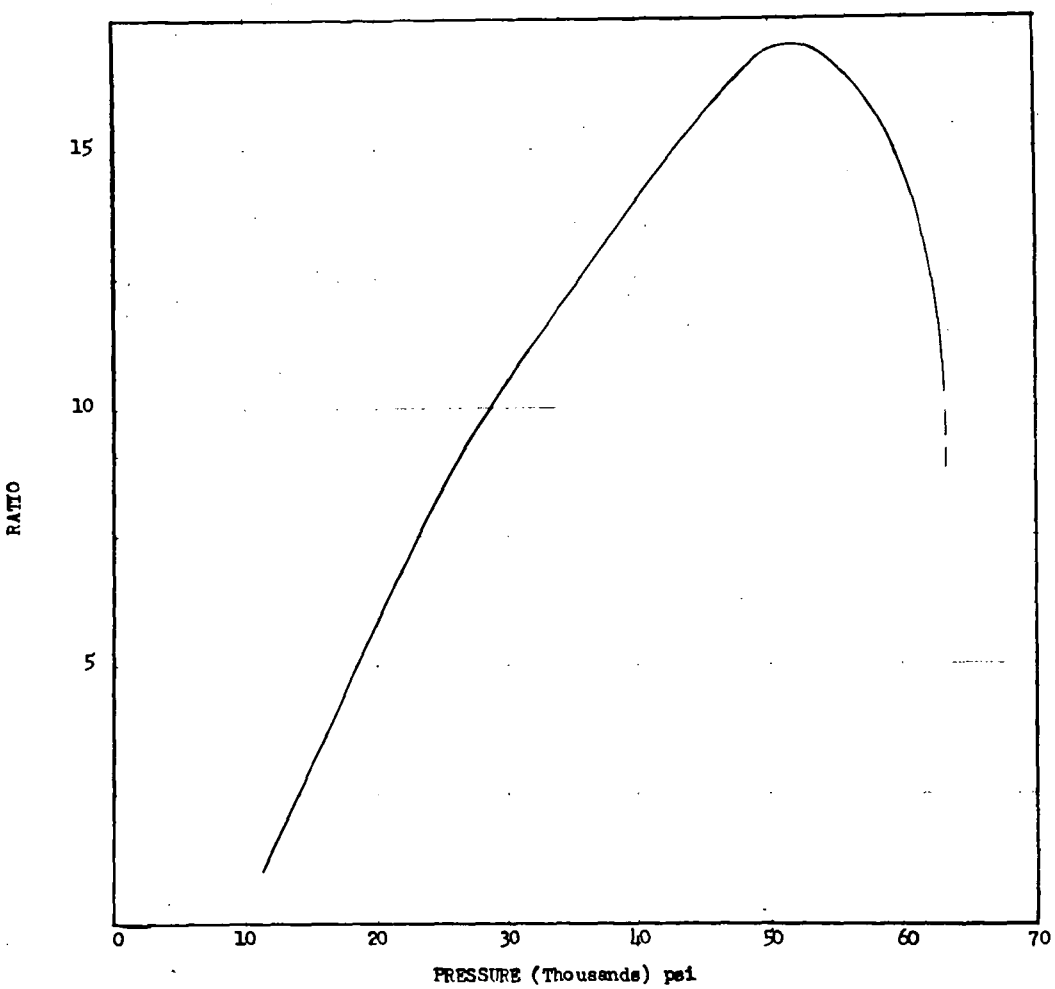

RATIO EXPECTED AREA TO ACTUAL AREA FOUND
FOR COMPOSITION B CYLINDER

FIGURE 8

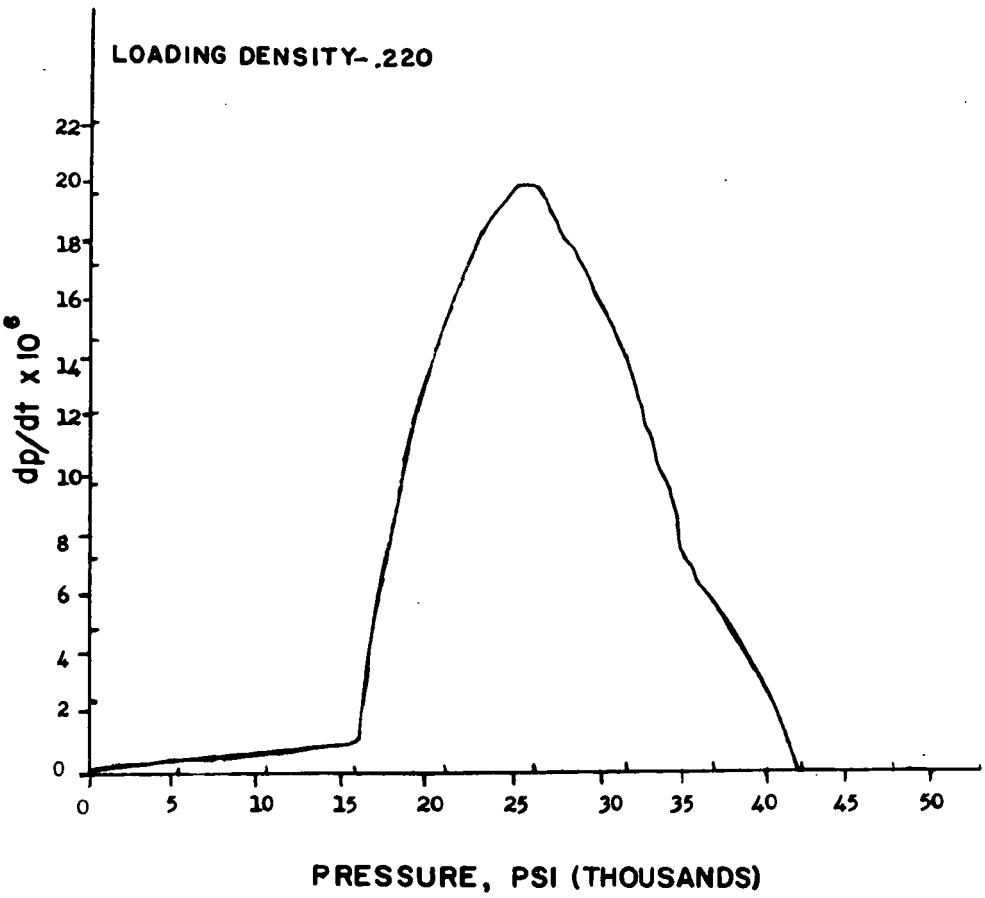

Figure 9. Closed Bomb Test Experimental Propellant

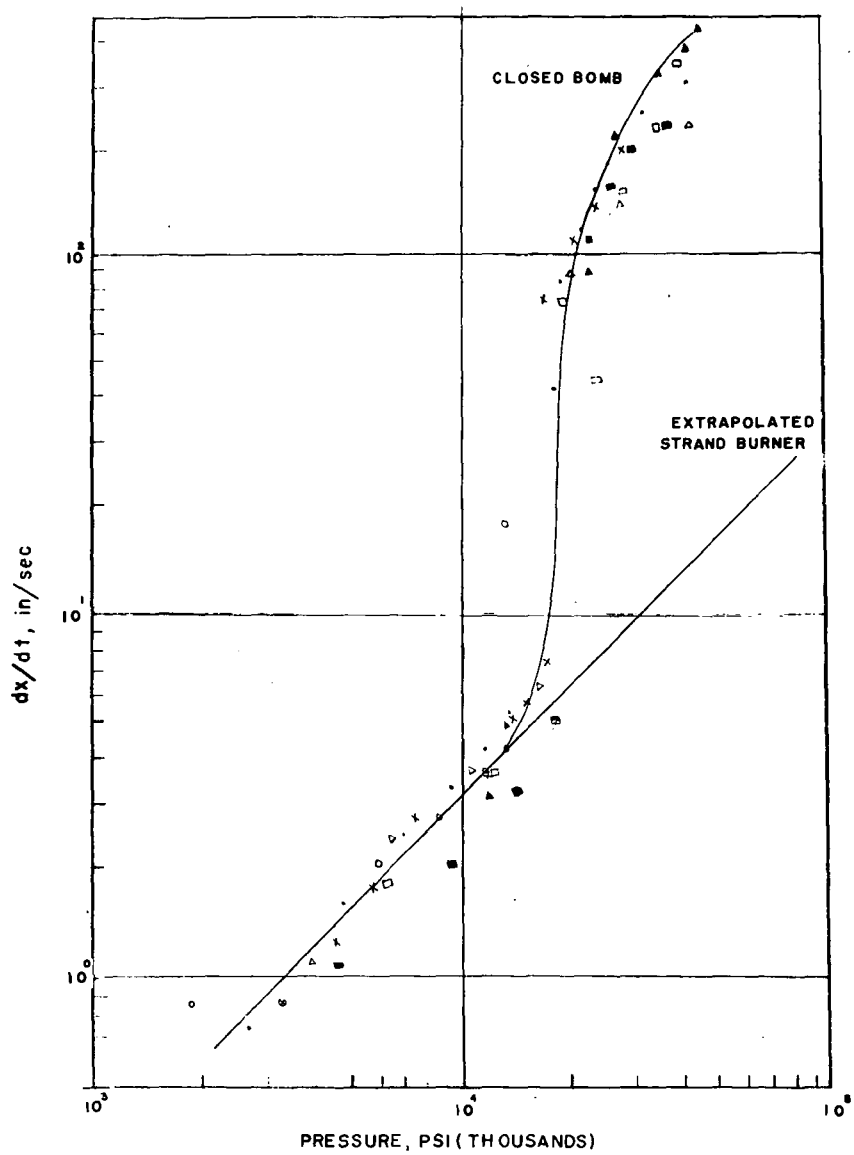

Figure 10 Linear Burning Rate of Experimental Propellant Obtained with Closed Bomb

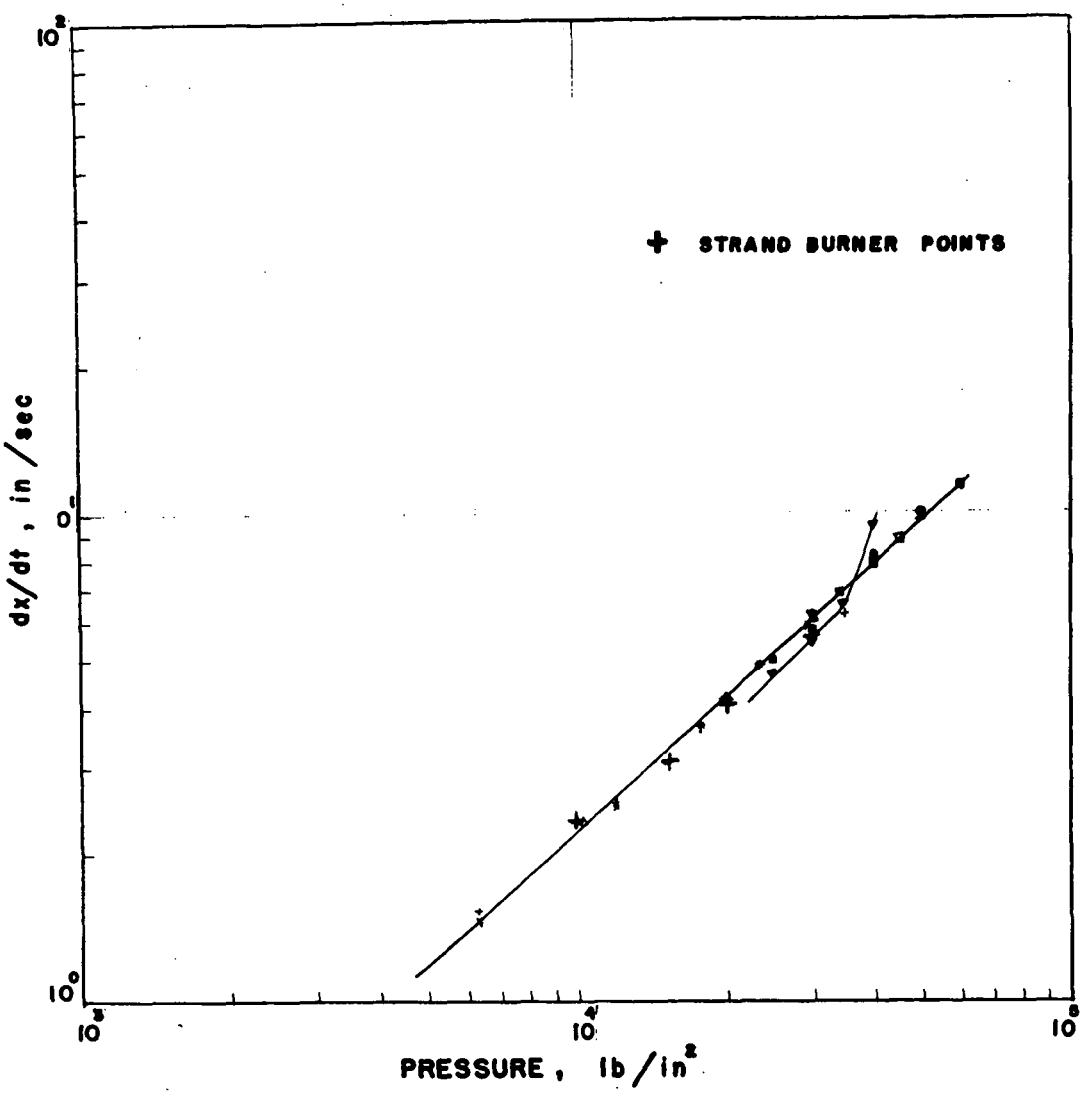

LINEAR BURNING RATES OF A R P PROPELLANT OBTAINED WITH CLOSED BOMB AND STRAND BURNER

FIGURE 11

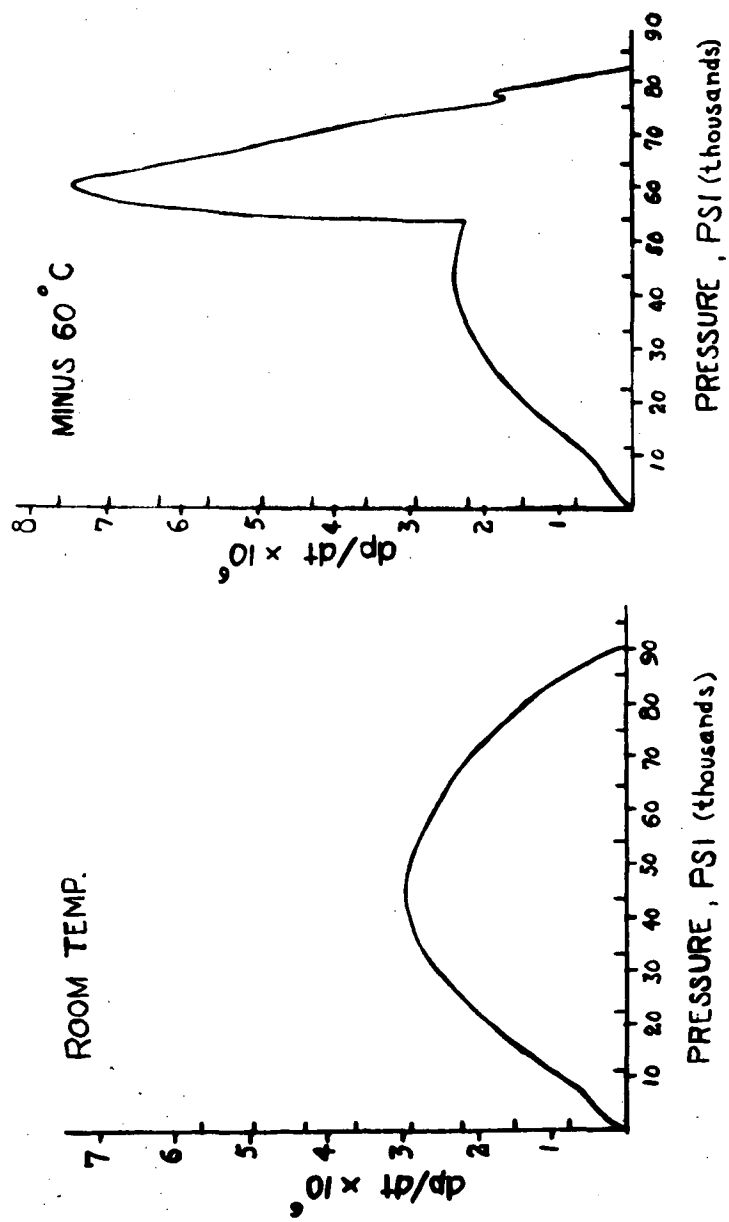

Figure 12 Closed Bomb Test Rohm and Haas Propellant Composition QZ

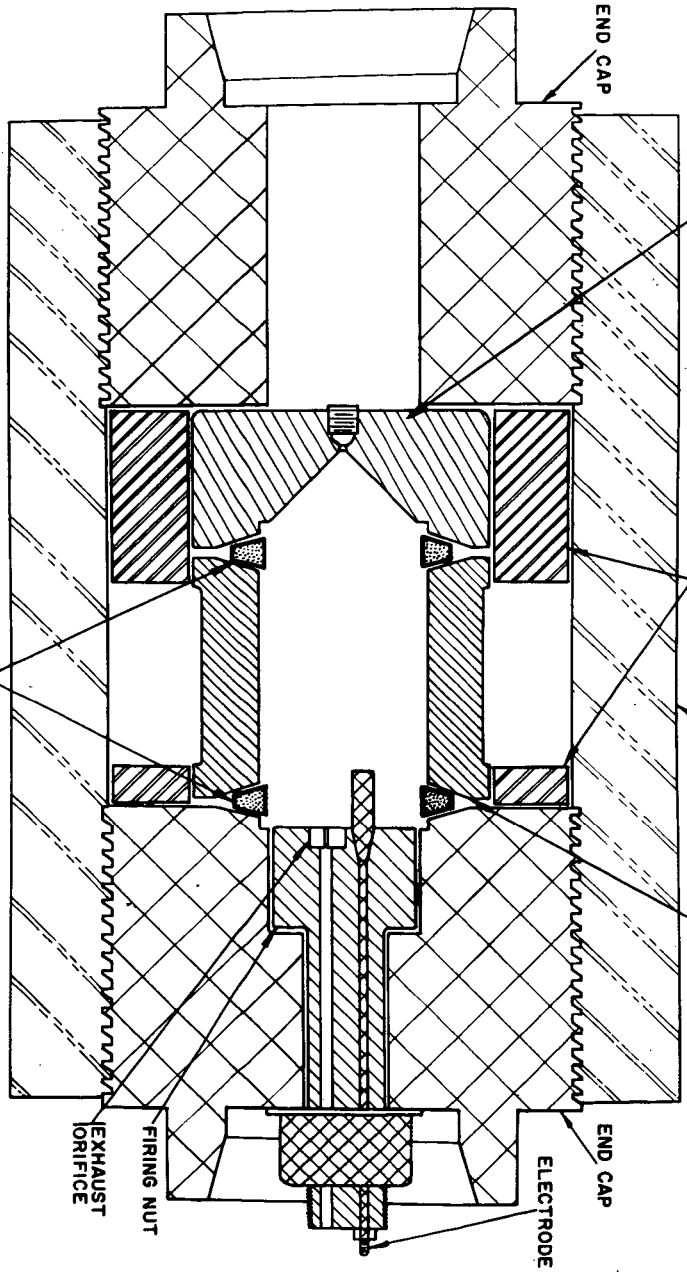

ULTRA-HIGH PRESSURE VESSEL FOR PROPELLANT TESTING

FIGURE 13

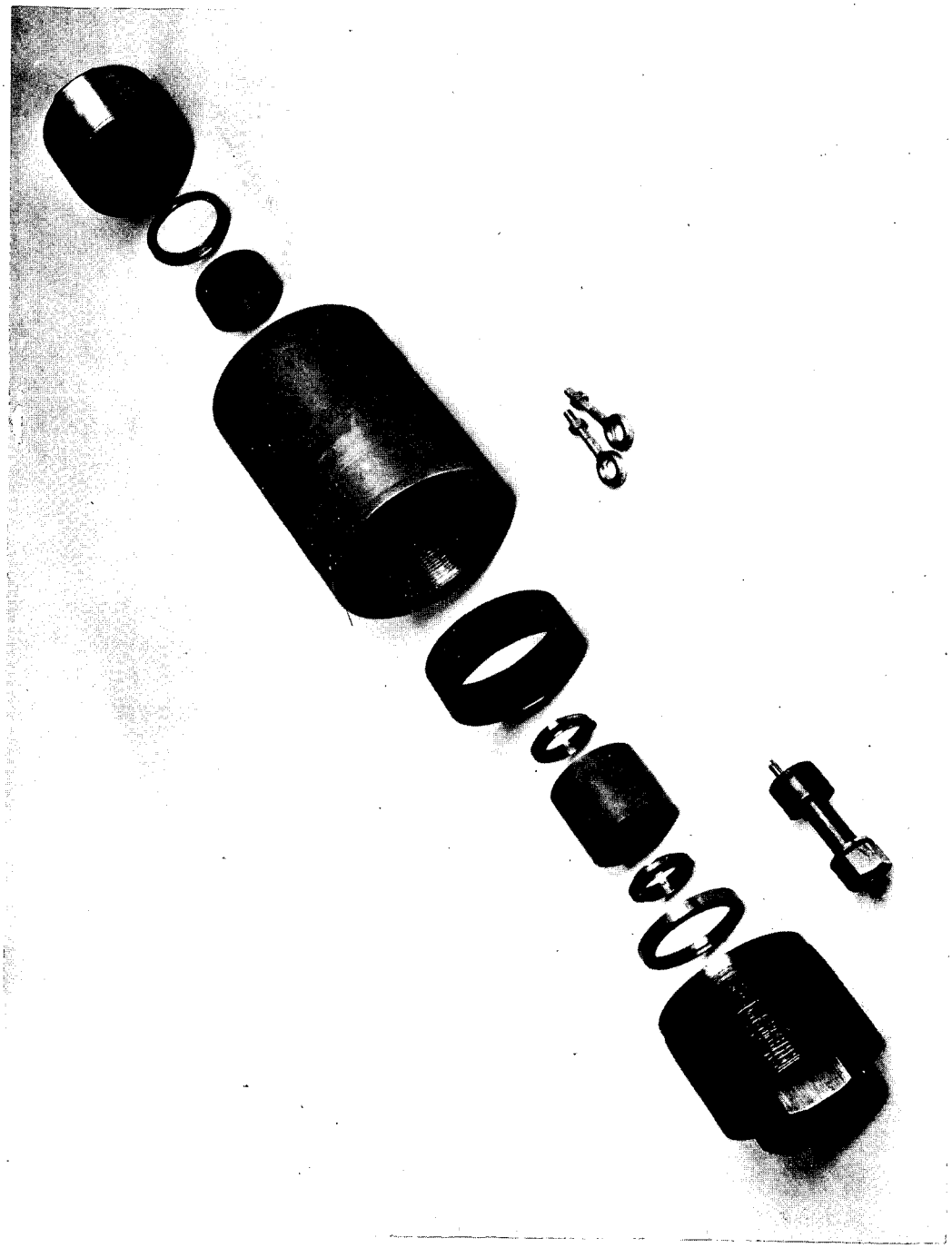

FIGURE 14 ULTRA-HIGH PRESSURE VESSEL, EXPLODED VIEW FROM FIRING END

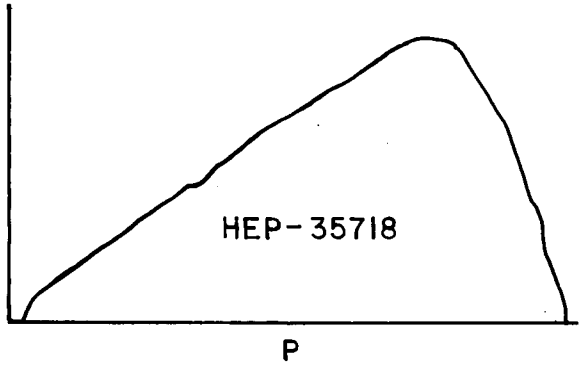

A sample trace classified as "OK", based on closed bomb firing at −40° F.

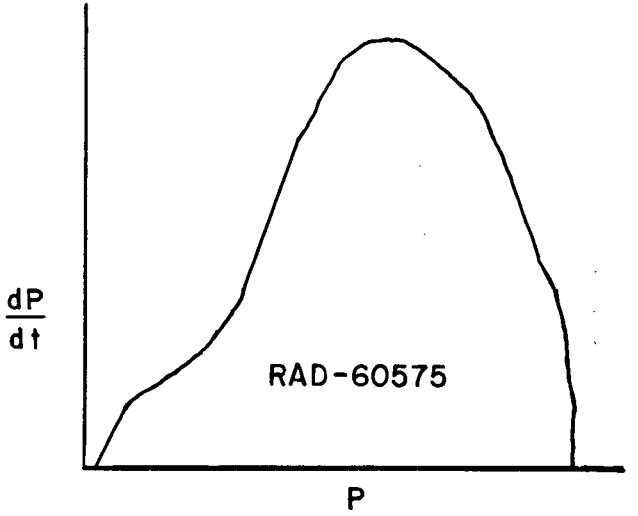

A sample trace classified as "bad", based on closed bomb firing at −40° F.

TESTS OF M17 PROPELLANTS SHOWING GOOD AND DEFECTIVE LOTS

FIGURE 15

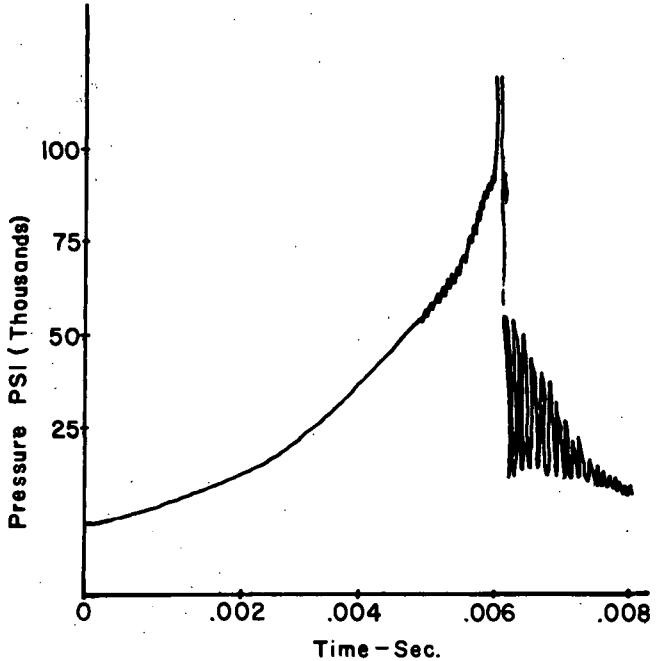

M17 PROPELLANT
Lot SUN-62815
0.4 Loading Density

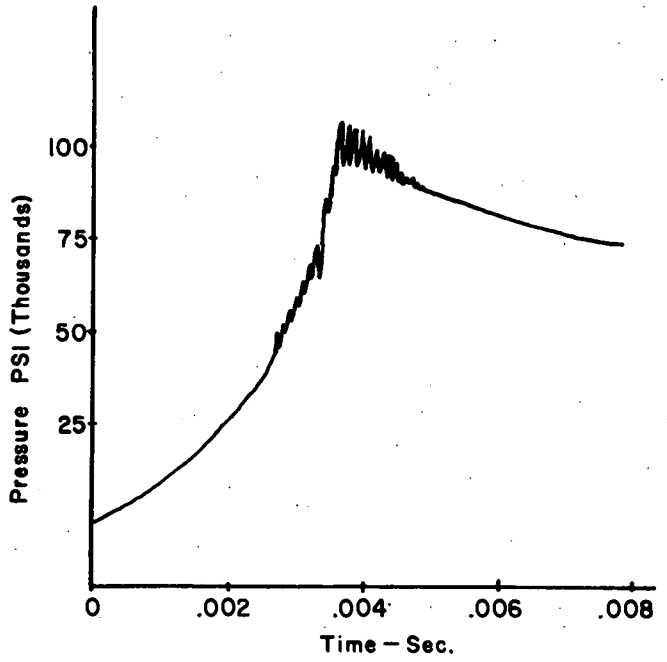

T28E1 PROPELLANT
0.4 Loading Density

HIGH PRESSURE CLOSED BOMB TESTS OF CANNON PROPELLANTS

Figure 16

Probability of Prevention of Explosive Propagation and Personnel Injury by Protective Walls

by:
C. E. McKNIGHT
PICATINNY ARSENAL, DOVER, N. J.

Abstract & Introduction

This paper deals with the details of calculating the probability of detonation occurrence in an explosive (acceptor) system or personnel injury resulting from detonation of an adjacent explosive system (donor) when the donor is separated from the acceptor or personnel by an intervening protective wall.

The capacity of a wall to confine explosions can be measured by the probability of occurrence of the secondary explosion or personnel injury at the opposite side of the wall. In all cases of flying fragments, either steel or concrete, both large and small, knowledge of the fragment size, velocity, acceptor distance-from-wall, acceptor size and acceptor sensitivity lead to a calculated probability of propagation.

The theory upon which the fragment probability rests is based on determining the mass-velocity distribution of the fragments and calculating how many could cause a detonation by virtue of their mass and velocity, if impact occurs. When the fragments are large, like spalls and chunks of a wall, the level of kinetic energy or momentum of the chunks is used to determine if they could cause detonation. Having determined the number of "potent" fragments, the number of them that can be expected to result in impact, the distances and acceptor sizes can be used to calculate a probability of detonation or damage to personnel due to fragments.

As a less important cause of damage, blast from the donor may reach the acceptor or personnel. Since blast is continuous, and not discrete, as in the case of fragments, the "explosion pressure" at the acceptor is a measure of the capacity of the walls for safety. If the donor explosive weight, wall height and distances from the wall are known, the "explosion pressure" at the acceptor or personnel area is calculable. The pressure being continuous, the probability is unity that the acceptor will "feel" the pressure. Therefore, from the pressure sensitivity of the acceptor, or the pressure tolerance of personnel, an assessment of "safe" or "unsafe" can be made.

The final assessment in all cases is "safe" or "unsafe" to the acceptor regardless of how much damage would occur to the wall. The degree of protection to be afforded the acceptor must be specified in each case. Having decided upon an acceptable level of safety, the design of protective walls can proceed with a great deal of insight into the question of whether the thickness, height or minimum permitted distances are realistic.

Probability of Detonation Propagation

In an explosive system failure to prevent detonation propagation may take place in various ways summarized for convenience in Table 1.

TABLE 1

Modes of Failure in Explosive System

Donor Effect	Mechanism	Input to Acceptor (Output from Mechanism)
1. Blast	A. Direct	Blast
	B. Walls	
	1. Leakage	Blast, reduced
	2. Shear (punching)	Secondary missiles
	3. Spalling	Secondary missiles
	4. Collapse	Secondary missiles
2. Primary Missiles	A. Direct	Primary missiles
	B. Walls	
	1. Perforation	Secondary missiles Slowed primary missiles
	2. Spalling	Secondary missiles
3. Miscellaneous		

The presence of unknown effects renders the situation typical for the use of probability as a means of comparing safety design calculations and of terminating or evaluating a safety design of structures to handle large amounts of explosive.

It is our basic assumption that a donor detonation has occurred. An interaction with the acceptor must occur by way of at least one of the mechanisms. Following impact, the acceptor sensitivity to missiles or blast must be such that the impact results in detonation. Thus if P_i and P_S are the probabilities of impact and sufficient impact respectively, these being independent events, the probability of detonation by way of any one mechanism alone is

$$P_{Dn} = (P_i \times P_S)_n$$

where n refers to the mode of failure in question. For all modes together, the probability is that of a mutually exclusive set of events. The overall probability of detonation is, P_o (see Nomenclature List)

$$P_o = \sum^{n} P_{Dn} \text{ - Interactions}$$

$$= (P_i\ P_S)_{B1} + (P_i\ P_S)_{B2} + (P_i\ P_S)_{B3} + (P_i\ P_S)_{B4}$$

$$(P_i\ P_S)_{M1} + (P_i\ P_S)_{M2}$$

$$\text{- interactions.}$$

The interactions are the corrections to be applied for the fact that since any one mode may cause detonation, the overall probability of detonation is less than the simple sum of probabilities of all possible events. It is sufficient to consider this term zero since its maximum for any pair of events cannot be greater than the greater of the two. A zero value is conservative.

The probability of impact due to blast is considered 1.0 in every case in which blast occurs as an input to the acceptor. This occurs only in two cases; blast without walls, and leakage around walls. The probability of detonation due to blast when impact is certain depends upon the blast sensitivity of the acceptor. This is determined by using various weight and distances between a donor explosive and many acceptors. The number of goes and no-goes at each distance-weight combination is recorded and a superficial probability of detonation is computed from the percentage of goes. This much of the procedure is subject to check by experimentation at a relatively reasonable cost.

To establish the probability region of interest to safety calculations the experimental, superficial probabilities are correlated simultaneously with distance and weight using a suitable multiple regression function. In this way the locus of probabilities in the region of 10^{-2} to 10^{-4}% are located in distance-weight coordinates. These values would be impossible to verify, except at great cost because of the large number of trials that would be required. Nevertheless they reflect actual sensitivity experience and represent an objective approach to safety determination. For the blast sensitivity of the example used in this paper, the standard normal probability function was used in log-log coordinates with a transformation of the distance parameter. The distance transformation was required to make the desired function reflect the experimental fact that the probabilities do not increase or decrease indefinitely with distance.

The case B2, shear failure resulting in punching, is a case of secondary missile damage. Analytical studies have shown the method if the weight and velocity of a punched-out piece of the donor and wall dimensions are known. As this piece leaves the wall it may go in any direction from the center, thus "searching" an area that can be calculated by assuming an 80° cone from the point of punching. The area of the base of this cone will be designated the search area, A_S. The probability for impact of any one punched-out piece is the ratio of the acceptor area to the search area. The piece is visualized as breaking into halves, thirds, quarters, etc. each in turn. Large pieces can cause detonation by a glancing hit, this is allowed for by increasing the acceptor area to include itself and the space occupied by the punched-out piece on all sides around the acceptor.

The probable number of effective hits is then

$$N = N_X \frac{A_{AL}}{A_S} = \frac{N_X (2\,dm + da)^2}{(1.67\,d)^2}$$

The probability of at least one hit is then the probability of missile impact,

$$P_{iB2} = 1 - e^{-N}$$

The sensitivity of acceptors to large missile like chunks of concrete can be based on kinetic energy or on a related function in an approximate but satisfactory manner. As with blast sensitivity one plots the kinetic energy at which various weights and velocities have caused detonations, fits a suitable regression curve to the go-no-go data and extrapolates to the region of low probability. A function that has been used is:

$$\log \log P_{SB2}/100 = \log \frac{1}{K.E.} + \text{const.}$$

For each of the above described pieces the probability based on sensitivity is found. Since the weight of halves is half that of the original piece, the sensitivity becomes less dangerous, but the number of missiles becomes greater, causing an increase in P_{iB2}. The maximum $(P_i \times P_S)_{B2}$ is taken as the value for probability of detonation due to failure mode B2.

Likewise for spalling and collapse, analytical methods permit the prediction of the kind of secondary missiles that are generated due to blast from the donor. A probability of impact in each case and the probability of detonation based on sensitivity are then found and their products taken. In this way all the probabilities of detonation, either by missile or blast, associated with blast impact to the wall are found.

If the donor is cased it can produce primary missiles striking against the wall. A wall may be perforated by the largest missiles. If so, the velocity versus size distribution is found by calculating the residual velocity of the missile for a selection of perforating weights. From fragment collection studies on the donor one finds the number of missiles having weights equal to or greater than the smallest perforating piece.

Experimental data from firing fragments of various sizes at various velocities into acceptors gives a missile sensitivity curve that is conveniently taken as representing a detonating probability of 1.0 (of course, if the data are known to be the 50% points widely used in vulnerability studies a probability of 0.50 could be used instead of 1.0). When using a fixed value for the sensitivity probability, only those missiles having the required weight or velocity are considered in getting the impact probability. Since detonation, if impact occurs, may be considered certain in safety calculations for these selected missiles,

$$P_{iM1} = 1.0$$

The number of missiles of any given weight which proceed from the donor is found from fragment collection experiments to be predictable if the dimensions of

the donor are known. The missiles are somewhat more direction than an even spherical distribution; the probability of any one impacting the acceptor is the presented area of the acceptor per unit spherical surface area of sphere around the donor, corrected for directional effect. The result is that the probable number of missiles impacting the acceptor is,

$$N = 0.1N_x \frac{A_A}{d^2}$$

where the factor 0.1 is to correct for directional effects, N_x is the number of missiles which could cause detonation if impact takes place, A_A is acceptor presented area and d is distance from acceptor to donor.

To find N_x, the residual velocity from the wall and weight of the perforating missiles is compared to the sensitivity curves. Their intersection defines the smallest "effective" missile. The fragment velocity studies then permit calculating N_x, the number of missiles having weight equal to or greater than that of the minimum effective missile. N is the expected number of impacts. The chance of only one impact is, as before, (see Figure 1).

$$P_{iM1} = 1-e^{-N}$$

Spalling due to missiles is handled like spalling due to blast. Thus all probabilities of impact and of detonation due to sensitivity are found. A set of possible values is shown in Table 2, the table of combined and overall probability.

TABLE 2

Overall Probability

Missiles	Impact Prob.		Sensit. Prob.		Combined (product)	
Perforation	P_{iM1}	.005	P_{SM1}	1.0	$(P_iP_S)_{M1}$	0.005
Spalling	P_{iM2}	-	P_{SM2}	0	$(P_iP_S)_{M2}$	0
Blast						
Leakage	P_{iB1}	1.0	P_{SB1}	.03	$(P_iP_S)_{M1}$	.03
Punching	P_{iB2}	.02	P_{SB2}	.50	$(P_iP_S)_{M2}$	.10
Spalling	P_{iB3}	.002	P_{SB3}	.30	$(P_iP_S)_{M3}$	.0006
Collapse	P_{iB4}	.30	P_{SB4}	.40	$(P_iP_S)_{M4}$	.120
					P_o =	0.2556

The overall probability of detonation, with probability interaction conservatively taken as zero, is 25%. This would be considered unsafe. The designer must now pick on the high probabilities and redesign so as to increase the safety of the explosive system, or declare its impossibility. In the later case he has ample proof for his position.

This analysis points out that not only must every mode of failure be safe, but all must be safe enough with a margin to allow for additivity.

Typical figures in Table 2 indicate that spalling is unimportant. This is believed to be the situation in many cases, but it should be considered at the start of every new problem.

It should be pointed out that the attempt at safety calculations involving propellants and explosives in a state of development may be defeated by the lack of sensitivity data, i.e. by a state of complete ignorance as to whether a new high energy composition might be detonable. A method has been devised to test small samples for the ability to detonate if burning starts. In this procedure a transition pressure is found for any propellant which correlates with the detonability of conventional high explosives. Propellants and explosives can thus be classified as mass-detonating or not using the procedure in one of the references.

The probability calculation represents a balance between the following parameters and any parameters which may be subsidiary to these:

Acceptor:	Wall:	Donor:
Area	Thickness	Distance
Distance	Height	Case
Case		Material
Material and Wt.		Explosive output
Sensitivity		Blast
Blast		Missile
Missile		Velocity
Chunks		

Depending upon the relative magnitude of these parameters, the various modes of failure assume greater or less importance. Thus the effect of some fifteen or twenty factors is evaluated objectively in one figure, the overall probability of detonation, P_o.

A major advantage of reducing the tangible effects to an objective figure is that the tangible considerations can be handled as a matter of routine, leaving the intangible factors to be reduced by judgement of those who are most experienced in the industry. An additional advantage is that when large uncertainties are shown to exist due to lack of data, a proper justification and allocation of funds for large programs can be prepared.

Personnel protection follows the principle given here with the additional restriction that the probabilities should be reduced to the equivalent of zero by designing so that the calculated number of missiles, punchings, and spalls are less than one (i.e. effectively zero); and designing blast resistant shelters to protect against blast and leakage.

NOMENCLATURE

A_A = presented area of acceptor, sq. ft.

A_{AL} = lethal area of acceptor, sq. ft.

A_S = area searched by missiles after punching, sq. ft.

d = distance from source of missile to acceptor, ft.

d_m = diameter of missile due to punching, ft.

d_r = diameter of round acceptor, ft.

e = base of natural logarithms.

K.E. = kinetic energy of large missile at acceptor, ft.-lbs.

N = probable number of impacts

N_x = number of missiles having weight and velocity suitable for causing detonation if an impact occurs.

P = probability of impact or detonability or both associated with a given mechanism of transfer or mode of wall failure.

Subscripts to P:

i = impact; S = sensitivity (detonability); M = missile donor effect;

B = blast donor effect; n = 1,2, etc. acceptor effect tabulated below;

D = detonation.

	Probability of Impact	Sensitivity Probability (Detonability)	Combined
General case	P_{in}	P_{Sn}	$(P_iP_S)_n$
Specified mechanisms			
Missiles: perforation	P_{iM1}	P_{SM1}	$(P_iP_S)_{M1}$
spalling	P_{iM2}	P_{SM2}	$(P_iP_S)_{M2}$
Blast: leakage	P_{iB1}	P_{SB1}	$(P_iP_S)_{B1}$
punching	P_{iB2}	P_{SB2}	$(P_iP_S)_{B2}$
spalling	P_{iB3}	P_{SB3}	$(P_iP_S)_{B3}$
collapse	P_{iB4}	P_{SB4}	$(P_iP_S)_{B4}$

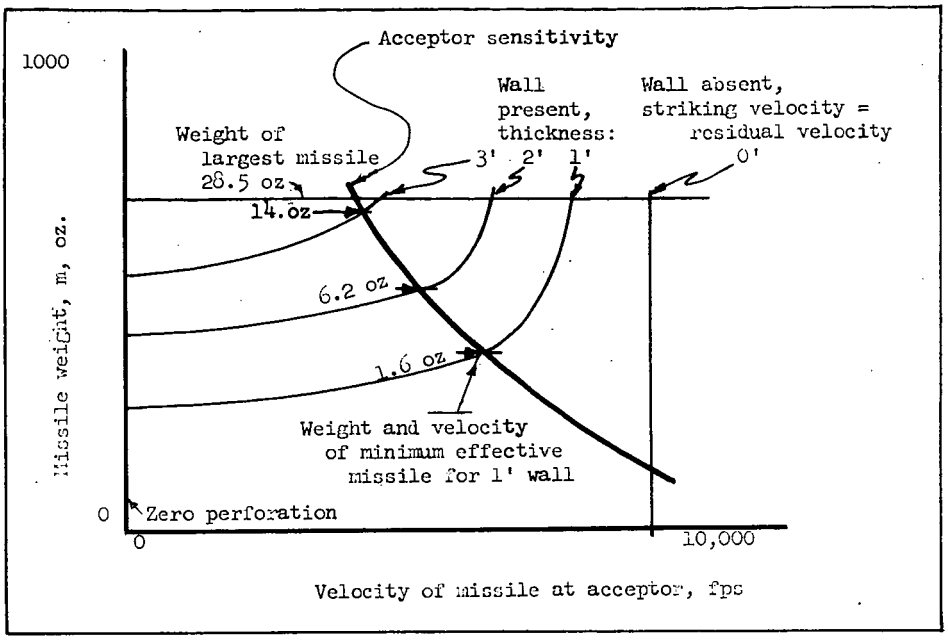

Illustrative Numerical Quantities *

Missile weight m ounces	Number of effective missiles, N_x, heavier than m	Probable number of hits for each wall, N	Probability of detonation for each wall, P_{iM2}
28.5	1	0.0058	0.005
14.0	15	0.0861	0.57
6.2	184	1.06	0.65
1.6	1,800	10.4	1
0.0	26,500	-	-

* Actual quantities depend on all parameters in the explosive system.

Figure 1. Nomenclature and relationships for perforation of wall by missiles from donor explosive.

REFERENCES

1. Rindner, R. M. and Wachtell, S. Establishment of Safety Design Criteria for Use in Engineering of Explosive Facilities and Operations. Report No. 3: Safe Distances and Shielding for Prevention of Propagation of Detonation by Fragment Impact. Picatinny Arsenal Technical Report DB-TR: 6-60, December 1960 (Classified)

2. Ammann and Whitney, Consulting Engineers. Industrial Engineering Study to Establish Safety Design Criteria for Use in Engineering of Explosive Facilities and Operations: Wall Responses. Prepared for Picatinny Arsenal under Contract No. DA-28-017-ORD-3889, April 1963

3. McKnight, C. E., Shulman, L., and Wachtell, S. Establishment of Improved Standards for Classification of Explosives and Propellants, Report No. 1: A Method for Determination of Susceptability of Propellants and Explosives to Undergo Transition from Deflagration to Detonation. Picatinny Arsenal Technical Report DB-TR: 3-61, June 1961. Also available in ONR Symposium Report ACR-52, Vol. 2, p. 635, Third Symposium on Detonation, James Forrestal Research Center, Princeton University, September 1960 under sponsorship of Naval Ordnance Laboratory (White Oak) and Office of Naval Research.

Safety Design Criteria for Explosives Manufacturing and Storage Facilities

by;
L. W. SAFFIAN AND R. M. RINDNER
PICATINNY ARSENAL, DOVER, N. J.

Abstract

The Picatinny Arsenal Safety Design Criteria Program is aimed at establishment of quantitative, realistic criteria for optimum design of protective structures to prevent propagation of explosion, injury to personnel, and damage of materiel.

The overall program consists of three phases. Phase I deals with prevention of propagation and personnel injury due to pure blast effects. Phase II deals with the effects of primary fragment impacts resulting from rupture of the donor explosive casing in causing explosion propagation. Phase III deals with the development of design criteria for barricades and substantial dividing walls for prevention of explosion propagation and personnel injury.

Phases I and II of this study cover establishment of quantitative design criteria for explosives facilities relating to prevention of explosion propagation by blast and fragment impact effects. The methods presented are based on prediction of large-scale behavior of these materials employing relationships which require data from small scale tests only. Relationships have also been developed which permit the calculation of safe distances for prevention of propagation of detonation due to fragment impact between adjacent potentially mass detonating explosive systems, for any assumed degree of risk and degree of steel casing. These relationships permit prediction of probability of propagation in an existing situation as well as calculation of necessary changes in acceptor shielding and/or separation distances for any other tolerable degree of risk.

Phase III of the program, deals with quantitative methods for realistic design of protective walls or combinations of walls (manufacturing bay or storage cubicle). Consideration is given to such factors as donor effects, wall responses, and acceptor (personnel, equipment or another explosive charge) sensitivity to the effects of donor detonation. Special emphasis is placed on close-in effects of donor detonation where non-uniformity of wall loading makes the application of the plane wave theory not valid. The donor charge which determines the blast loads and primary fragments is discussed in terms of various parameters of donor characteristics. Wall responses (to the blast loads resulting from the donor explosion) are discussed in terms of various modes of wall failure which may impair structural integrity of the wall. These are: (1) spalling (causing formation of secondary fragments) (2) punching (local shear failure causing formation of secondary fragments) (3) flexural failure (caused by overall flexing action of the wall which brings the wall to the point of incipient breakup) (4) total destruction of the wall

(causing complete breakup into secondary fragments) (5) penetration of the wall by primary missiles (resulting in either perforation of the wall or spalling). Also discussed are various degrees of wall support as well as different types of wall construction including sandwich-type walls.

The acceptor sensitivity is discussed in terms of either total protection level (for personnel and equipment) where essentially no damage to a protective wall can be tolerated, or lesser degrees of protection to protect against propagation of explosion.

Introduction

The lack of quantitative design techniques for safe explosives storage and manufacturing facilities has been a continuing problem. Although present safety regulations have been effective in preventing explosion propagation over the past years, this has been largely due to the high degree of overdesign incorporated in these regulations. Moreover it has become increasingly apparent in recent years, particularly with the advent of high energy propellants, that the present safety regulations are seriously inadequate in that they do not provide systematic techniques for optimum design of protective structures required in explosive and propellant manufacturing plants and storage areas. The aim of the Picatinny program is to establish such quantitative realistic design criteria which can be used with confidence in engineering protective structures to prevent propagation of explosions, injury to personnel, and damage to materiel.

The various phases of the program are shown schematically on Figure 1 which shows phases completed and those in progress at the present time. Phase I of the overall program deals with propagation of detonation due to pure blast effects (sympathetic detonation). Phase II deals with the effects of primary fragment impact (resulting from rupture of the donor explosive casing) in causing explosion propagation. Phase III deals with the development of design criteria for protective structures for prevention of explosion propagation and personnel injury.

The analytical portions of the overall program have been essentially completed. Detailed results of these studies are contained in References 1, 2, 3, and 4.

At present a model scale test program is in progress which is designed to confirm the design relationships developed, and/or to indicate areas where these relationships should be modified or supplemented.

Phase I - Sympathetic Detonation

This phase of the program deals with establishment of realistic quantity-distance relationships for prevention of sympathetic detonation. The general equation proposed is shown in Figure 2 and is based on correlation of available

data and relationships reported by various investigators. It has been found to hold fairly well for donor charges of various explosives ranging from 1-250,000 pounds of weight. This equation accounts for various factors in addition to weight (i.e. degree of confinement, ground reflection, explosive composition, and shape) which affect the peak pressure blast output of a donor charge. This is accomplished by means of the various coefficients indicated which refer the actual donor charge weights to a set of standard conditions. The factor K, therefore, is a constant for each explosive depending only on its sensitivity to blast (i.e. considering the explosive in the role of acceptor charge). Each K value corresponds to a particular peak pressure which is the minimum blast pressure required to cause sympathetic detonation. It should be noted at this point that the cube root law correlation and the method of donor weight adjustment employed are consistent with the assumption of peak pressure as the criterion of explosive blast output. The factor K for a particular material can be determined by a series of small scale tests in which different weights (e.g. 1-100 pounds) of bare spherical TNT charges held sufficiently high above the ground so that ground reflections may be considered negligible (i.e. F_c, F_s, F_e, and F_r each equal 1) are detonated at varying distances from an acceptor charge of the material in question. A logarithmic plot of the maximum distance at which sympathetic detonation occurs versus corresponding donor weight should give a straight line of 1/3 slope, the intercept of which on the distance axis is equal to K. Concerning the donor weight adjustment factors, a considerable amount of information relative to these factors is available in the literature (References 5 and 6). In cases where coefficients must be determined this can be accomplished by appropriate small scale tests. For example, the composition coefficient F_e, for a new mass-detonating explosive could be determined by the method outlined on Figure 3.

Figure 4 is a simplified illustration of what can be done with the proposed quantity-distance relationship for sympathetic detonation. First, it shows a logarithmic plot of the available test data relative to occurrence of sympathetic detonation. The effective donor weights ranging from 3-450,000 pounds were calculated by adjusting the actual donor weights (1-250,000 pounds) by the method previously described. The plotted distance corresponding to any indicated charge weight approaches the maximum distance at which sympathetic detonation would occur with that charge; or conversely the plotted donor charge weight corresponding to any indicated distance approaches the minimum weight necessary to produce sympathetic detonation at that distance. As would be expected, the plot shows a region in the weight-distance plane where sympathetic detonation did not occur. A straight line drawn to separate the region of non-occurrence of sympathetic detonation from the region where sympathetic detonation did occur, has a slope of approximately 1/3 and corresponds to the equation $d_m = 3.1W_e^{1/3}$ and a peak pressure of 100 psi. This is a gross separation based on the most sensitive explosive considered, i.e. dynamite. Of course, the methods previously described could be used to establish a family of such lines, one for each mass detonating explosive depending on its sensitivity. For many explosive materials of current military interest, such lines will lie considerably below the gross boundary shown on Figure 4. (i.e. they will be less sensitive). Indeed, for TNT-base explosives, threshold peak pressures

required for sympathetic detonation are of the order of several thousand psi. The line shown immediately above the sympathetic detonation boundary corresponds to a pressure of 30 psi and has the equation $d_s = 5W_e^{1/3}$ which constitutes the application of safety factor of 1.6. It is apparent that present intraline and magazine quantity-distances for mass-detonating explosives (broken lines on Figure 4) are overly conservative for prevention of propagation due to pure blast effects. It should be noted that, although a literal interpretation of these regulations is that they are for prevention of pure blast effects only, they are intended to provide some degree of protection against propagation by fragment impact, since a real situation where only blast effects are significant is unlikely. The extent of this protection against fragment effects, however, is not quantitatively defined. As will be discussed later in this paper, Phase II of the Picatinny program is concerned with a quantitative approach to quantity-distances for fragment effects.

The significance of factors affecting the output of a donor charge is shown in Figure 5 which is a summary of calculations made by the method previously described to arrive at effective weights of a 10,000 pound donor charge detonated under a wide range of conditions, and corresponding safe distances obtained from the $d_s = 5W_e^{1/3}$ quantity-distance relationship. We have assumed a cylindrical shape for the charge, corresponding to a shape correction factor (F_s) of 1.25. As indicated at the left of the table various explosive compositions were considered, corresponding to composition correction factors (F_e) ranging from 1.0 for TNT to 1.27 for explosive Z. Across the top of the table are assumed correction factors (F_r) ranging from 1.5 to 2.0 for various degrees of ground reflection, and for each of these reflection conditions, correction factors (F_c) ranging from 0.6 to 1.17 for various degrees of confinement are indicated. The calculated values of effective donor charge weights range from 12,500 pounds to 40,000 pounds with corresponding safe distances of 116 feet and 172 feet, respectively. According to present intraline regulations, the explosive weight would be taken as 10,000 pounds and the corresponding safe distance as 400 feet, regardless of the widely varying conditions indicated.

Phase II - Propagation by Primary Fragments

This phase deals with the effects of fragment impact in causing high order detonation in an explosive charge, and related safety design criteria. This work has resulted in the establishment of (1) a method of predicting the vulnerability to high order detonation of an explosive system (or vulnerability to mass detonation of adjacent explosive systems) in terms of geometry of the system (e.g. explosive weight/casing rate, casing thickness and diameter) and explosive properties (e.g. output and sensitivity), and (2) a method for calculating safe distances for any assumed degree of risk. The methods are based on correlation of various relationships developed by British and U. S. investigators as a result of theoretical studies, confirmatory tests, and actual experience. The general relationships are presented schematically on Figure 6. These equations permit prediction of the gross

mass-detonability characteristics of explosive systems. Shown are the factors which must be considered for any explosive system in either a donor or acceptor role. As indicated by equation (1) an output constant (E') must be established for the donor charge. Values for several standard explosives are available in the literature, Reference 7. For other explosives or propellants, E' could be established experimentally by conducting small scale tests in which cased samples of various E/C ratios are detonated and corresponding fragment velocities measured. The output constant is readily obtainable from a plot of (V_o) vs (E/C) in accordance with equation (1). Equation (2) is for calculation of the number of fragments in any particular weight range produced by detonation of a cased charge. A special case of equation (2) can be used to calculate the mass of the largest fragment (m_{max}) produced in the detonation according to equation (2a).

Considering, now, an explosive system in the role of an acceptor, equation (3) indicates that an explosive sensitivity constant (K_f) must be established for the acceptor explosive. As in cases of the other constants previously discussed, values of this constant are available for some of the well known explosives such as TNT and RDX/TNT mixtures (Reference 8). For other explosives and mass-detonating propellants the (K_f) value could be established by a plot of V_b vs $f(t_a)(m)$ in accordance with equation (3). A simple method of obtaining the necessary data would be to fire individual fragments of known mass against explosive charges with various degrees of casing, and determining, for each charge, the minimum velocity of a given fragment required to produce high order detonation.

Once the various explosive constants have been established, and knowing the overall geometry and dimensions of an explosive system, it can be seen from Figure 6 that a reasonably reliable prediction as to its vulnerability to high order detonation by fragment impact (or its potential ability to contribute to propagation of an explosion, when considered in relation to any specific environment of adjacent explosive systems) can be made by a straightforward series of calculations. Thus, for a particular donor-acceptor situation (V_o) and (m_{max}) are first calculated. Since the equations are based on the assumption of cylindrical cased charges (i.e. constant cross-section) this will often require consideration of the donor in sections in such a way that equivalent cylinders can be constructed, having average wall thickness, average charge diameter, and the same (E/C) ratio as the actual section. After calculating (V_o) and (m_{max}) for each section the corresponding value of (V_{bmin}), is calculated, assuming impact at the thinnest portion of the acceptor casing (i.e. the most severe conditions). It is also assumed that the acceptor is in very close proximity to the donor (again, the most severe condition) so that fragments strike the acceptor at their maximum velocity (V_o), i.e. there are no velocity losses which would increase with increasing distance from the donor. As shown in Figure 6, therefore, the ratio (V_o/V_{bmin}) is a criterion for predicting the gross mass-detonability characteristics of explosive systems.

Development of relationships for calculation of safe distances in terms of probability of high order detonation occurrence or risk of propagation of detonation by fragment impact at these distances will now be discussed. For the sake of simplicity and convenience a graphical representation of these relationships is shown schematically in the next series of figures.

The plot presented on Figure 7 is based on equation (4). It relates fragment striking velocity (V_s) with fragment mass (m) at any distance from the detonation source (d) (constant distance lines - d_m being limiting distance at which detonation will occur). Each plot is made for a single value of initial velocity of donor fragments (V_o). A series of plots like the one presented on Figure 7 can be prepared for different values of (V_o). The constant (k) is a function of the presented area to fragment mass ratio, density of air, and air drag coefficient. (References 7 and 9). Figure 8 is a schematic representation of equation (3) which defines the minimum velocity a fragment must have in order to detonate a given acceptor. This plot relates the boundary velocity (minimum striking velocity at which a high order detonation will occur) with fragment mass (m) and acceptor casing thickness (t_a) and/or thickness of shielding in front of acceptor charge. The graph is plotted for a single explosive sensitivity (expressed in terms of the sensitivity constant (K_f), discussed previously).

When the plots from Figures 7 and 8 are combined as shown on Figure 9 useful relationships are obtained. Figure 9 relates striking velocity (or boundary velocity) of a fragment with fragment mass at various distances (d) and acceptor casing thickness (t_a). If boundary velocity of a fragment is now equated to its striking velocity, it becomes possible to find the minimum effective mass of a fragment produced by the donor explosive that will cause a high order detonation in the acceptor charge at any distance from the donor (d) and/or shielding of the acceptor (t). The number of such effective fragments produced at any distance from the donor charge can then be calculated from equation (2).

It is of interest to note the limiting case which is shown by equation (4a) on Figure 9. This indicates the maximum distance (d_m) at which propagation by fragment impact can occur for a given donor - acceptor situation. This is the distance at which the largest fragment (m_{max}) produced by the donor strikes the acceptor at the minimum velocity ($V_{b_{min}}$) required for detonation. It should be noted further that in terms of probability of acceptor detonation this is a boundary situation representing minimum probability of acceptor detonation occurrence, i.e. maximum distance, minimum boundary velocity, and minimum number of effective fragments. (the single largest donor fragment). At greater distances and/or lower velocities, the probability of acceptor detonation is, therefore, presumed to be zero.

The general case of reducing design distances from the limiting distance value (as expressed by equation (4a)) and/or shielding thickness by accepting a certain risk or probability of the possibility of high order detonation occurrence will now be considered. The probable number of effective hits (i.e. hits which upon striking the acceptor charge will cause high order detonation) by impacting fragments is expressed by equations (5) and (5a), Figure 10 (Reference 7). As can be seen from this equation, the probability per unit area is proportional to the number of effective fragments (N_x) (obtained from equation (2) previously discussed) and inversely proportional to the distance between the donor and acceptor charges. Included in the equation is a constant (g) governing the distribution of fragments, which depends on the spacial angular distribution of fragments. The plot shown on Figure 10 relates the distance between the donor and acceptor charges (d), shielding (t_a), and probability of high order detonation occurrence (E). The zero probability curve (P_o) indicates a relationship between the distance (d) and shielding (t) beyond which no high order detonation is possible. This line represents the limiting case mentioned earlier.

The higher the probability level that can be tolerated, the lower the distance-shielding combination necessary. This relationship permits gross prediction of the necessary separation and/or shielding between two explosive systems at any degree of probability of high order detonation occurrence. To compose such a relationship for a specific situation all that would be necessary is knowledge of the geometry of the system and the previously discussed explosive properties relating to sensitivity and output.

Phase III - Design of Protective Structures

The design or capacity of a protective wall or combination of walls (a manufacturing bay or storage cubicle) must be determined when considering any explosive manufacturing and/or storage situation. Although current regulations give guide lines for establishing barricades and substantial dividing walls which have been effective for many years, a quantitative procedure for assessing the degree of protection which may be expected from existing protective walls, or designing new walls is not available.

Developing protective wall design criteria (based on existing data and theoretical consideration) has been primarily concerned with relatively distant effects of explosions where a plane wave approach may be employed. Although situations of this sort are of occasional interest in Ordnance, the majority of cases are concerned with close-in effects where explosives are in relatively close proximity to the protective wall. Application of plane wave theory is not valid in such cases because of non-uniformity of wall loading (Reference 4).

A typical situation for which structural design criteria must be considered consists of three separate but related systems as presented on Figure 11, i.e. the

donor (explosive material) which produces the damaging output, the acceptor (explosives, equipment, personnel) which will regulate the allowable tolerances of the overall system, and the intervening protective barricades, walls and/or distances which reduce the donor output to a tolerable level with respect to the acceptor.

Donor Effects

The damaging output of the donor is in the form of blast pressures and/or primary fragments, depending upon whether the explosive is cased or uncased. Based upon maintaining the overall stability of a protective wall, the blast pressures and impulse loads resulting from the detonation will be of prime importance (References 10 and 11). The physical properties of the donor system will determine the magnitude of the blast loads and the distribution of the pressure pattern on the wall, as well as the mass-velocity characteristics of primary fragments. These properties consist of (1) explosive characteristics, namely, type of explosive material and energy output, weight of explosive, and type and thickness of casing, (2) location of the explosive relative to the barrier and/or acceptor, (3) magnification and reinforcement of the initial blast wave by the presence of adjacent obstructions and/or structures.

Three basic donor charge locations are of interest as shown on Figure 12. First, the donor may be in free air with the blast wave propagating out from the center of the explosion and striking the wall (Figure 12a). Secondly, the donor may be at such a location relative to the wall that a Mach stem will be formed which only partly envelopes the wall, while the remainder of the wall is subjected to free air pressures (Figure 12b). Third, the charge location may be such that the pressure in the Mach front will be felt over the entire wall surface. The wall is then subjected to a uniform blast load or plane wave (Figure 12c). Further details are given in Appendix A.

In considering any particular wall of a cubicle type structure the blast enhancement effects due to reflections from the ground and adjacent walls must be considered. This is done by determining applicable reflection coefficients, which in turn are used to determine the equivalent weight of the charge acting on the wall.

Figure 13 indicates graphically the method for determining reflection factors as a function of various parameters. These reflection factors are utilized as multiplying factors to be applied to the actual charge weight, thus obtaining an equivalent charge weight (see Appendix B).

Wall Responses

The response of the protective structure to donor output will depend on the properties of the donor system as described above and the physical characteristics (material, strength, and configuration) of the structure itself. The donor output

will establish the loading on the wall while the wall characteristics will govern its restraining capabilities to the applied load. When a protective wall is subjected to the detonation effects of an explosion, the wall will either remain intact (elastic response) undergo plastic action (permanent deformation) or fail, depending on magnitude of the load, load distribution, and the wall response. (Reference 12). For close-in detonations, design for elastic response of a wall will be practical only for small charges and generally is only of concern in the design for protection of personnel and/or valuable equipment. For those systems where the integrity of the wall is not essential, the wall response may be expressed in terms of various modes of failure. A schematic representation of these failure modes is shown in Figure 14. The wall can be affected either by primary fragments or by blast. Primary fragments can either perforate the wall and come out on the acceptor side with some residual velocity, be embedded in the wall resulting in spalling, or be embedded in the wall without causing any damage on the acceptor side (indicated by "no action" on the chart). Spalling caused by primary fragments produces secondary (concrete) fragments of extremely low velocity (several feet/sec.). In most cases (except where personnel protection is involved) these effects can be neglected. On the other hand perforation of the protective wall by primary fragments may cause propagation in the acceptor charge if their mass and residual velocity are sufficiently high. A quantitative method has been developed for estimating residual velocity of primary fragments as a function of wall thickness, fragment size and material, and initial fragment velocity. (See Appendix C).

Response of the wall to blast effects of close-in detonation may be expressed in terms of several modes of wall failure (shown on the chart). Under the action of a blast load, these modes consist of (1) the formation of concrete fragments, (secondary fragments) by scabbing (spalling) action of the rear surface of the wall (2) local failure of the wall resulting from development of excessive local shear stresses (punching failure), (3) flexural failure of the wall due to the overall bending action of the structure (including chearing at the base), and (4) total destruction resulting in collapse of the wall due to the combined action of several of the previously mentioned failure modes. Figure 15 is a plot relating mass, velocity and kinetic energy with charge weight and distance from the wall for the spalling mode of wall failure. Figure 16 is a similar plot indicating the mass, velocity and kinetic energy of the punched out section of the wall as a function of donor charge weight and distance from the wall. When total protection is required, such as for personnel or very specialized equipment, neither punching nor spalling can be tolerated. Figure 17 relating charge weight with scaled distance indicates threshold conditions of non-occurrence of spalling for various wall thicknesses. For a given charge, spalling failure will generally occur at threshold scaled distances greater than that required to produce punching. This chart, therefore, also serves as a conservative criterion for determining the occurrence or non-occurrence of punching.

The flexural mode of failure involves failure due to overall bending action and/or shearing of the wall at its base produced by the blast load impinging on the wall surface. The wall bends and deflects until such time as the entire

system comes to rest at some permanent distorted position or collapse occurs at an overstressed section of the wall. The occurrence of the final permanent distorted position or failure will depend upon the magnitude of the applied load and the load carrying properties of the wall such as its moment and shear capacities. Figure 18 represents incipient conditions of flexural failure for a cantilever wall. The charge weight is correlated with the wall height for various wall resistance requirements expressed in terms of moment capacities (determined by concrete strength, reinforcement and wall thickness). For any point on the line of constant pressure leakage (blast leakage over and around the wall) relating minimum wall height with donor charge weight, the intersection with a constant resistance line indicates the flexural failure threshold condition for the wall. For total protection the wall capacity must be greater than that for incipient failure conditions indicated on the chart. On the other hand, when protection against explosion propagation is the only requirement, wall collapse is tolerable as long as the secondary fragments do not become a new source of propagation of the acceptor charge.

The total destruction mode of failure will now be considered. Figure 19 is a plot for determining velocity and kinetic energy which will be produced by the failure of a wall due to punching, flexural failure, or a combination of both as a function of donor charge weight, for various secondary fragment masses. Each chart is for a particular wall thickness and scaled distance. The mass distribution of these fragments will depend upon such factors as charge size and location, wall configuration (height thickness, reinforcement, support conditions) and the properties of the concrete, while the fragment velocity will be governed by the fragment mass and the magnitude of the impulse load acting on this mass after wall break-up. The properties of reinforced concrete cannot be completely defined due to its non-homogeneous nature, and therefore the velocity of the various fragments cannot be precisely predicted for a given condition. However, an estimate can be made of the average value of the maximum velocity of any particular size fragment formed upon collapse of the wall. The chart presented in Figure 19 is based on such estimates.

This paper, thus far, has dealt with standard reinforced concrete cantilever walls. Charts similar to those shown have been developed for walls with two adjacent fixed edges and two free edges, walls with three fixed edges and a free top edge, walls fixed on all four edges and one way spanning walls restrained on both edges. Also, in addition to the standard reinforced concrete wall, two other types of wall construction have been considered, namely, a standard reinforced concrete wall with stirrups added primarily to increase resistance to punching, and a sandwich wall (two concrete walls with sand fill between them). Further details on the sandwich-type construction are given in Appendix D.

Acceptor Response

The acceptor regulates the tolerances for which an overall system is designed. Here the yield and location of the donor along with the capacity of the protective structure must be selected to produce a balanced system with respect to acceptor sensitivity. The acceptor may consist of either another explosive charge, personnel and/or valuable equipment. In case of personnel and equipment, full protection will usually be required. For explosive acceptors the degree of protection required for prevention of propagation will usually be less than that required for total protection, and will generally, be governed by the detonability of the acceptor when subjected to (1) blast effects developed by detonation of the donor explosive, (2) primary fragment impact, and (3) secondary fragment impact resulting from break-up of the wall. Based on limited data available from initial tests conducted under one phase of the confirmatory test program mentioned early in this paper, impact of secondary fragments appears to be the most probable cause for detonation of the acceptor charge. No conclusive experimental data are available thus far for complete quantitative evaluation of secondary fragment parameters (mass, velocity, shape etc.) and their relation to occurrence of detonation in the acceptor charge. As the test program progresses, these relationships will be established.

In conclusion, it is expected that the Safety Design Criteria program will result in far reaching and continuing benefits to defense agencies as well as private industry engaged in manufacture of explosives and high energy propellants with respect to permitting most effective use of existing explosives storage and manufacturing facilities, and optimization of construction of new facilities.

APPENDIX A

Blast Loads on Walls Subjected to Combined Free Air and Reflected Pressures and Walls Subjected to Plane Wave

When an explosion occurs near a dividing wall such that a Mach stem is formed, partly enveloping the wall, the structure is subjected to both free air and reflected pressures.

As the incident shock wave expands radially from the center of the detonation, the shock front will come in contact with one or more reflecting surfaces. These surfaces are the wall in question and adjacent members of the structure (walls, floor, etc.) If a portion of the wall in question is subjected to the shock wave front before the frontal pressures have been magnified by the wave impinging on adjacent members, this section of the wall is considered to be subjected to free air pressure only. On the other hand, if the pressures acting on a portion of the wall have been intensified by the presence of one or more adjacent members, then this section of the wall experiences reflected pressures. The demarcation between the two loading conditions is defined by height of the triple point (point at which incident shock, reflected shock, and Mach fronts meet), ground zero distance (measured along the reflecting surface from a point normal to the explosion to the point in question) and the height of explosion above the reflecting surface. (See Figure A1).

When a wall is subjected to a plane shock front traveling normal to the wall, every point on the front surface of the wall may be assumed to be subjected to the same shock overpressure at any particular time after the arrival of the blast wave at the wall. Therefore the reflected (face-on) pressures, resulting from the shock front impinging on the wall, will be uniform over the entire wall surface.

Whether a wall is subjected to a plane shock front may be determined by the path of the triple point. If the height of the triple point is greater than the height of the wall, when the shock wave arrives at the wall, the wall is subjected to uniform pressures or a plane shock wave (Figure A2).

APPENDIX B

Calculation of Blast Loads Acting On Protective Walls of Cubicle Type Structures

To analyze the effects of close-in detonation within a cubicle type structure, the actual loading conditions can be approximated by determining the reflection factor (R_I) based on the positive free air impulse loading. The reflection factor, is defined as the ratio of the yield of an explosion in free air to the yield of an explosion near a reflecting surface, each of which produce equal total impulse loads and therefore relates the magnified value of the free air positive pressure impulse acting on a wall, due to the surrounding structure, to the total impulse of the blast loading (positive phase of both free air and reflected pressures) acting on a wall. For the utilization of the reflection factor, the type of wall (boundary conditions) and the location of the charge in relation to the wall and the surrounding structure must be known. For cubicle type structures where the walls are generally supported on two and/or three sides (Figure 11)(one side and top open to the atmosphere), the reflection factors are related to the normal scaled distance (Z_A) between the charge and the wall being investigated, the scaled distances between the centerline of the wall in question and the adjacent wall (Z_B), the ratio of the distance between the charge and the nearest adjacent wall, to the length of the wall in question (l/L) and the ratio of the height of charge above the floor slab to the height of the wall (h/H). Figure 13 is a typical chart which indicates graphically a method for determining reflection factors as a function of these parameters. In calculating the reflection factors for the side walls, the effects of the reflection of the blast loads off the wall opposite to the one being investigated, have been neglected. After corrections for reflection effects have been made, an equivalent scaled distance of the charge from the wall in question is established. Pressure and impulse loads are then determined from Figure B1 (Reference 10).

APPENDIX C

Primary Fragment Penetration Through Concrete Wall

Some previous data pertaining to a problem (effects of bombs and projectiles striking concrete structures) similar to primary fragment penetration have been obtained (Reference 13). The results of the study covered by this paper, which is based upon empirical and theoretical relationships correlates fairly well with these data.

Figures C1 and C2 are based on these relationships. Figure C1 relates the striking velocity of primary fragments (V_1) with maximum penetration (X_m) for various fragment sizes (m). Once the maximum penetration of a given size fragment is known the fragment residual velocity can be obtained using Figure C2. This plot correlates two ratios, namely, the ratio of the residual velocity to striking velocity (V_2/V_1) and the ratio of wall thickness to maximum penetration (T/X_m). Residual velocity is obtained by multiplying the striking velocity, by the V_2/V_1 ratio.

In order for a fragment to have a residual velocity after penetration through the wall, maximum penetration (X_m) indicated on the previous figure must be greater than the wall thickness (T). The particular charts shown are for a fragment of armor-piercing steel having a general hemispherical shape. For other than armor-piercing fragments a correction factor must be applied (e.g. correction factor for mild steel is 0.70).

In order to provide total protection for personnel and valuable equipment neither spalling nor primary fragment penetration can be tolerated. Figure C3, is a total protection chart for fragments. It relates maximum allowable striking velocity for prevention of spalling and/or penetration, and thickness of the concrete wall for various primary fragment masses.

APPENDIX D

Sandwich-Type Wall Construction

A sandwich type wall is two reinforced concrete walls separated by a compacted sand fill (Figure D1). To evaluate the ultimate capacity of a sandwich type reinforced concrete wall for spalling, punching and flexural capacity, the wall may be reduced to anequivalent standard-type wall by obtaining the attenuated stress wave parameters acting on the front surface of the outside concrete portion. A portion of this reduction is due to the stress and impulse attenuation as the wave passes through the inside concrete wall and sand fill sections of the wall (reduction due to distance). Further stress reduction is due to the change in the magnitude of the stress wave as it passes from one medium to another medium of different density.

Figure D2 is a chart for determination of attenuation of peak pressure in sand and concrete as a function of scaled concrete and sand thicknesses. The solid family of lines refer to concrete, while the broken lines refer to sand. Starting at a point corresponding to the front face of the inside concrete wall a point is located on a solid line corresponding to a given value of pressure (P_r) and scaled thickness of concrete ($T/W^{1/3}$). A vertical downward reading from this point to the point on a broken line corresponding to a known value of scaled thickness of sand ($T_e/W^{1/3}$) is then made. From this point a horizontal reading is made to determine the attenuated peak pressure at the front face of the outside concrete wall. It should be noted that this chart accounts for coupling effects between the sand and concrete.

A similar chart has been developed for the determination of attenuation of scaled impulse per unit area in sand and concrete.

REFERENCES

1. Rindmer, R.M. Establishment of Safety Design Criteria for Use in Engineering of Explosives Facilities and Operations. Report No. 1: Sympathetic Detonation Picatinny Arsenal Technical Report DB-TR: 1-59, January 1959 (Classified)

2. Rindner, R.M. Establishment of Safety Design Criteria for Use in Engineering of Explosive Facilities and Operations. Report No. 2: Detonation by Fragment Impact. Picatinny Arsenal Technical Report DB-TR: 6-59, May 1959 (Classified)

3. Rindner, R.M. and Wachtell, S. Establishment of Safety Design Criteria for Use in Engineering of Explosive Facilities and Operations. Report No. 3: Safe Distances and Shielding for Prevention of Propagation of Detonation by Fragment Impact. Picatinny Arsenal Technical Report DB-TR: 6-60, December 1960 (Classified)

4. Ammann & Whitney, Consulting Engineers Industrial Engineering Study to Establish Safety Design Criteria for Use in Engineering of Explosive Facilities and Operations. Wall Responses. Prepared for Picatinny Arsenal under Contract No. DA-28-017-ORD-3889, April 1963

5. Explosion Effects Data Sheets U.S. Naval Ordnance Laboratory, NAVORD Report No. 2986, October 1955 (Classified)

6. Sperazza, T. et. al Comparison of the Blast from Explosive Charges of Different Shapes. Ballistic Research Laboratory Report No. 681, January 1949 (Classified)

7. Mott, R.I. A Theory of Fragmentation. Army Operational Research Group Memo No. 113 AC 4627, Great Britain, 1943 (Classified)

8. Feist, A.V. The Sensitivity of High Explosives to Attack by Steel Fragments ADE Technical Note T/2/L9/AVF, Great Britain, (Classified)

9. Thomas, L.H. Computing the Effects of Distance on Damage by Fragments Ballistic Research Laboratory Report No. 468, May 1946

10. Granstrom, S.A. Loading Characteristics of Air Blasts from Detonating Charges Transactions of the Royal Institute of Technology, Stockholm, Sweden, 1956

11. Brode, H. A Calculation of the Blast Wave from a Spherical Charge of TNT The Rand Corporation RM-1965, August 1957

12. Whitney, C.S. and Cohen, E. Guide for Ultimate Strength Design of Reinforced Concrete Journal of the American Concrete Institute, Proceedings, Vol. 53, November 1956

13. Effects of Impact and Explosion Vol. 1, National Defense Research Committee, Office of Scientific Research and Development, 1946

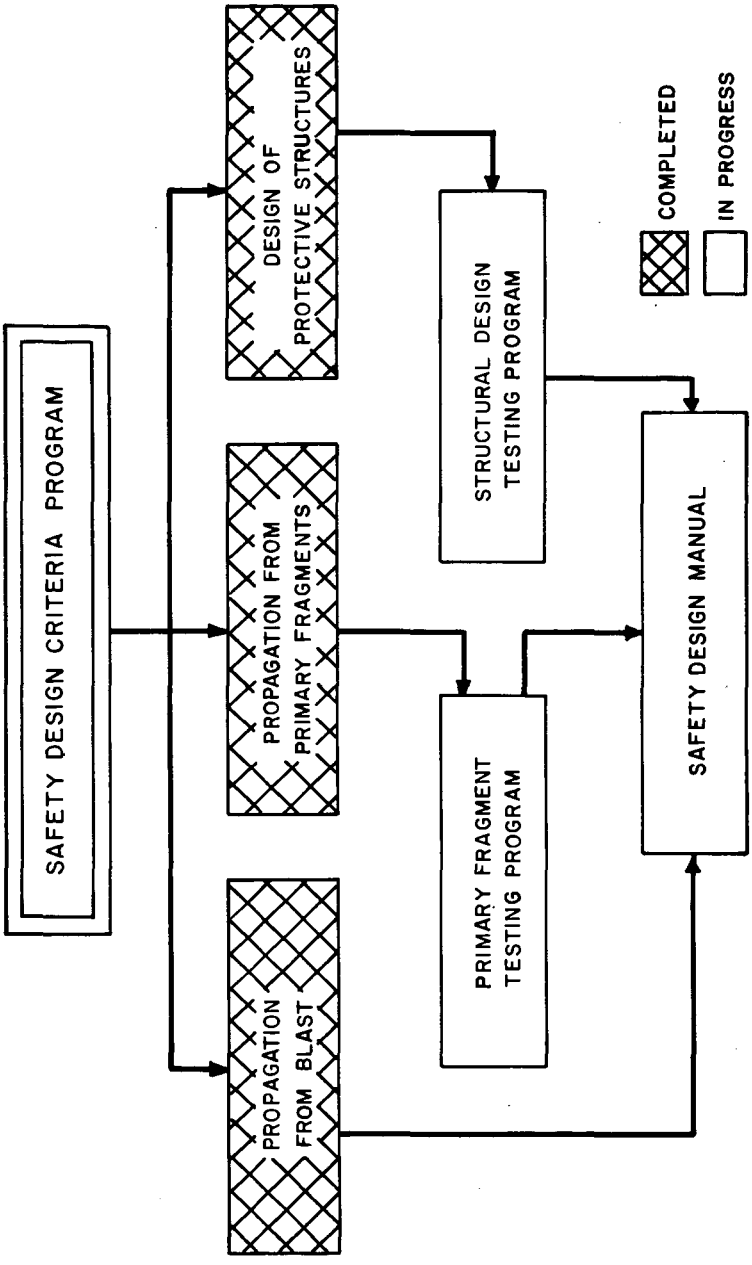
SAFETY DESIGN CRITERIA PROGRAM
PROPAGATION FROM BLAST
PROPAGATION FROM PRIMARY FRAGMENTS
DESIGN OF PROTECTIVE STRUCTURES
PRIMARY FRAGMENT TESTING PROGRAM
STRUCTURAL DESIGN TESTING PROGRAM
SAFETY DESIGN MANUAL
COMPLETED
IN PROGRESS

Figure 1

QUANTITY DISTANCE RELATIONSHIP FOR SYMPATHETIC DETONATION

$$d_m = KW_e^{1/3}, \text{ where } W = F_c\ F_r\ F_e\ F_s\ W$$

d_m = Maximum distance between donor and acceptor charges, at which sympathetic detonation occurs (ft.)

W_e = Weight of a bare, spherical, TNT charge, detonated in free air, which would produce a peak pressure blast output equivalent to that of the actual donor charge (lbs.)

W = Weight of donor explosive charge (lbs.)

K = Blast sensitivity constant (corresponding to minimum peak pressure required at acceptor charge to cause sympathetic detonation)

F_c = Confinement coefficient-Ratio of equivalent bare explosive weight to actual weight of confined explosive (equivalent bare explosive weight is that weight of bare charge which would produce the same peak pressure blast output as the confined donor charge)

F_r = Reflection coefficient-Ratio of equivalent free-air detonated bare explosive weight to equivalent bare explosive weight of the actual donor charges (equivalent free-air detonated bare explosive weight is that weight of bare explosive which, when detonated in free-air, would produce the same peak pressure blast output as a given donor charge)

F_e = Composition coefficient-Ratio of equivalent free-air detonated bare TNT weight to equivalent free-air detonated bare explosive weight of actual donor charge (equivalent free-air detonated bare TNT weight is that weight of bare TNT which, when detonated in free-air, would produce the same blast output as a given donor charge)

F_s = Shape coefficient-Ratio of peak pressure which would be produced by detonation of equivalent weight $F_c\ F_r\ F_e\ W$ of actual donor shape to peak pressure which would be produced by detonation of same equivalent weight having spherical shape.

Figure 2

DETERMINATION OF EXPLOSIVE COMPOSITION COEFFICIENT, F_e

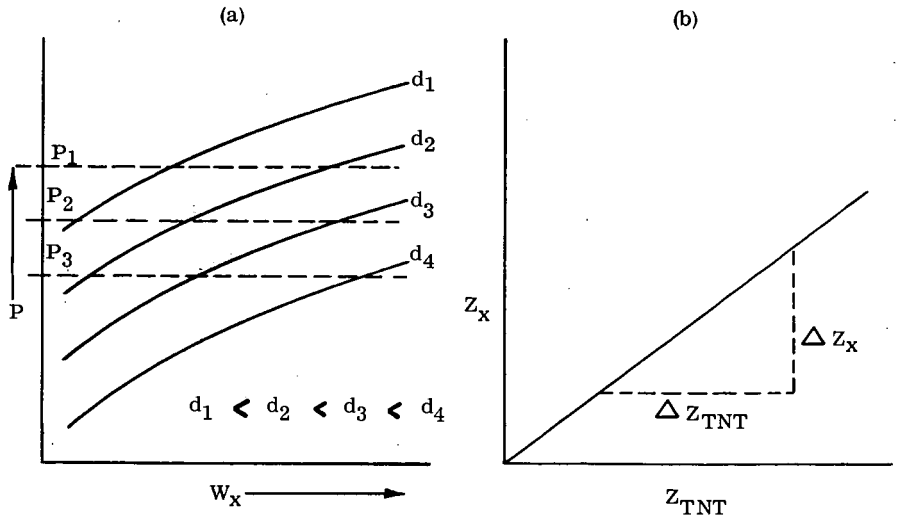

1. Conduct a series of small scale tests in which different weights (W_X) of bare spherical charges of propellant X are detonated high enough from the ground so that ground reflections are negligible (i.e. F_c, F_s, and F_r each equal 1) and peak pressure (P) measurements are taken at various distances (d) from the detonation source. Plot the data as indicated in Fig. (a).

2. For lines of constant peak pressure obtain the corresponding values of d and W from Fig. (a). Calculate the reduced distance ($d/W_X{}^{1/3}$) for each point. This should be a constant value for each pressure.

3. For each of the above pressures, obtain the corresponding reduced distance from the Kirkwood-Brinkley relationship for bare, spherical TNT charges detonated in free air (Ref 5).

4. Plot propellant X reduced distance (Z_X) against TNT reduced distance (Z_{TNT}) for each pressure as shown in Fig. (b). These points should fall along a straight line passing through the origin. The slope of this line equals $F_e{}^{1/3}$, or

$$F_e = \left[\frac{\Delta Z_X}{\Delta Z_{TNT}}\right]^3 \equiv \left[\frac{d/W_X{}^{1/3}}{d/W_{TNT}{}^{1/3}}\right]^3 = \frac{W_{TNT}}{W_X}$$

Figure 3

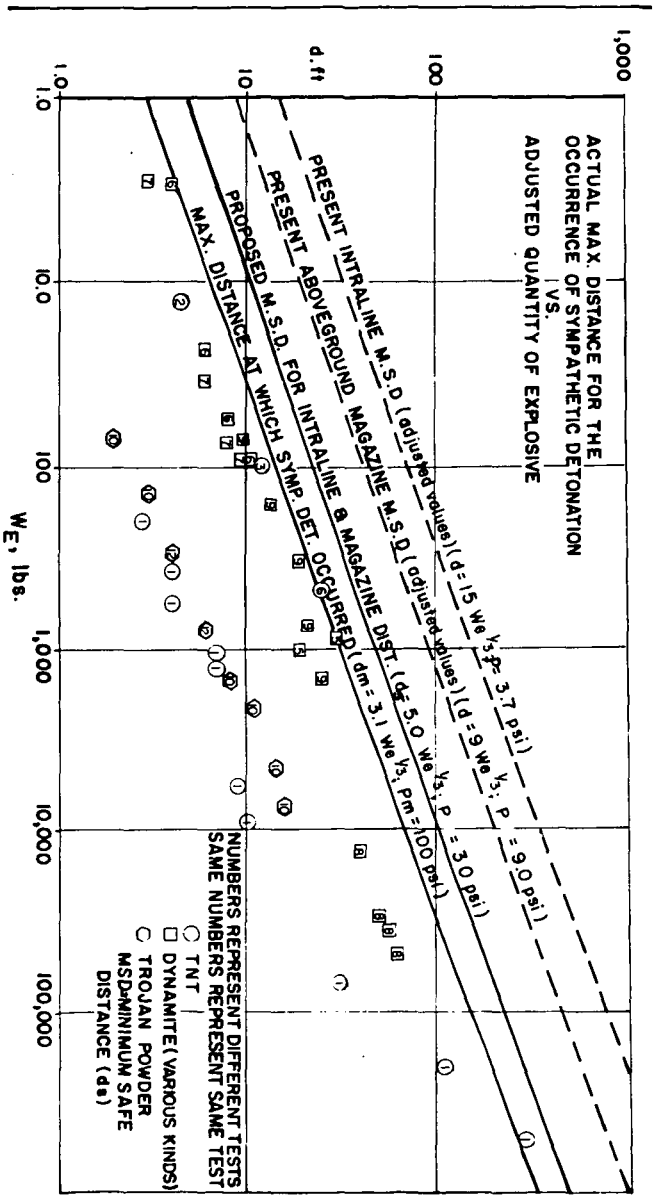
ACTUAL MAX. DISTANCE FOR THE OCCURRENCE OF SYMPATHETIC DETONATION
VS.
ADJUSTED QUANTITY OF EXPLOSIVE
PRESENT INTRALINE M.S.D (adjusted values) (d = 15 We 1/3; P = 3.7 psi)
PRESENT ABOVEGROUND MAGAZINE M.S.D (adjusted values) (d = 9 We 1/3; P = 9.0 psi)
PROPOSED M.S.D. FOR INTRALINE & MAGAZINE DIST. (ds = 5.0 We 1/3; P = 30 psi)
MAX. DISTANCE AT WHICH SYMP. DET. OCCURRED (dm = 3.1 We 1/3; Pm = 100 psi)
NUMBERS REPRESENT DIFFERENT TESTS
SAME NUMBERS REPRESENT SAME TEST
TNT
DYNAMITE (VARIOUS KINDS)
TROJAN POWDER
MSD-MINIMUM SAFE DISTANCE (ds)
d, ft
We, lbs.
1.0
10.0
100
1,000
10,000
100,000

Figure 4

Effect of Various Explosive Weight Correction Factors on Minimum Safe Distance

Assume 10,000 lbs of donor explosive of cylindrical over all shape (F_s=1.25)

Explosive	Reflection Factor Explosive/ Total wt. ratio, C.		(Assumed F_r=1.5) C=0.9 F_c=1.17	C=0.7 F_c=1.04	C=0.5 F_c=0.6	(Assumed F_r=1.8) C=0.9 F_c=1.17	C=0.7 F_c=1.04	C=0.5 F_c=0.6	(Assumed F_r=2.0) C=0.9 F_c=1.17	C=0.7 F_c=1.04	C=0.5 F_c=0.6
TNT		W_e	24,000	21,500	12,500	29,000	25,500	15,000	32,000	28,500	16,300
(F_e=1.0)		d_s	144.0	139.0	116.0	153.0	146.0	122.0	158.0	153.0	127.0
Explosive X		W_e	27,000	24,000	14,000	32,200	28,500	17,000	36,000	31,800	18,500
(F_e=1.13)		d_s	150.0	144.0	120.0	158.0	153.0	129.0	165.0	158.0	132.0
Explosive Y		W_e	28,800	25,600	14,900	34,600	30,500	17,800	37,100	34,000	19,500
(F_e=1.19)		d_s	153.0	147.0	123.0	163.0	157.0	131.0	169.0	162.0	134.0
Explosive Z		W_e	30,500	27,500	16,000	37,000	32,500	19,100	40,600	36,200	20,800
(F_e=1.27)		d_s	157.0	151.0	126.0	169.0	159.0	133.0	172.0	165.0	138.0

NOTE: According to present quantity-distance regulations, d_s for the assumed 10,000 pound donor explosive charge would be 400 feet, regardless of the widely varying conditions indicated above.

Figure 5

SCHEMATIC REPRESENTATION OF DONOR–ACCEPTOR RELATIONSHIPS GOVERNING PROPAGATION BY FRAGMENT IMPACT

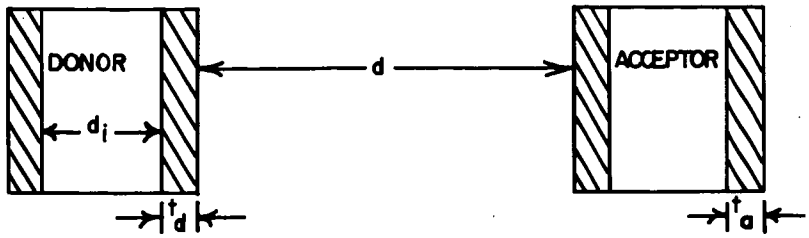

$$V_o = f(E')(E)/C) \quad \text{----------(1)}$$

V_o = initial fragment velocity

E' = explosive output constant

E/C = explosives / casing weight ratio

$$N_x = f(B)(C)(t_d)(d_i)(m) \quad \text{-------(2)}$$

N_x = number of fragments greater than mass (m)

m = mass of fragment produced by donor detonation

B = constant depending on donor explosive and casing material

C = donor casing weight

t_d = donor casing thickness

d_i = inside diameter of donor casing

$$m_{max} = f(B)(C)(t_d)(d_i) \quad \text{-----------(2a)}$$

m_{max} = mass of largest fragment produced by donor detonation.

$$V_b = f(K_f)(t_a)(m) \quad \text{----------(3)}$$

V_b = boundary velocity or fragment striking velocity of mass, m, below which high order detonation of the acceptor will not occur.

K_f = explosive sensitivty constant

t_a = acceptor casing thickness

$$V_{b_{min}} = f(K_f)(t_a)(m_{max}) \quad \text{---------(3a)}$$

$V_{b_{min}}$ = minimum boundary velocity required for detonation of given acceptor by fragment from given donor.

IF $\frac{V_o}{V_{b\ min}} < 1$: detonation by fragment impact will not occur.

IF $\frac{V_o}{V_{b\ min}} \geq 1$: possibility of detonation by fragment impact exists.

Figure 6

STRIKING VELOCITY OF A FRAGMENT AS A FUNCTION OF FRAGMENT MASS AND DISTANCE

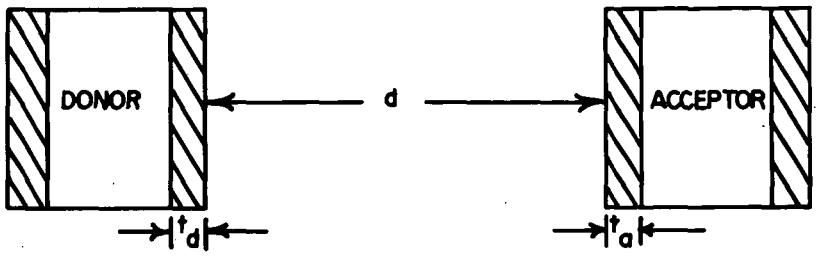

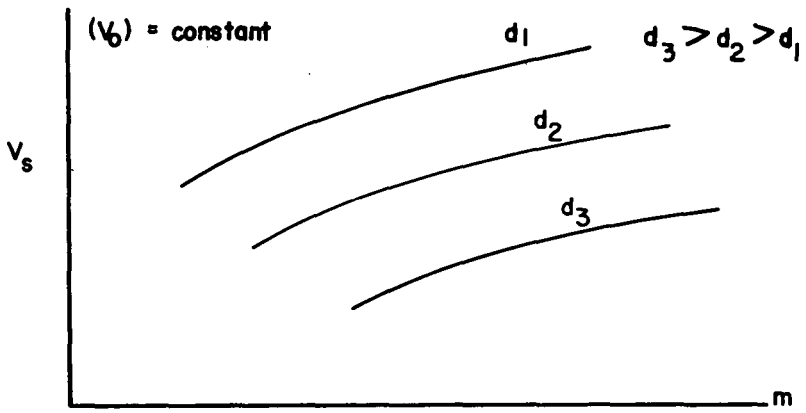

$$d = f(k)(V_0/V_s)(m) \quad \text{----------} \quad (4)$$

d = distance from the donor charge.

k = constant depending on fragment size, shape, air density and drag coefficient.

V_s = striking velocity of fragment at a distance. d

Figure 7

BOUNDARY VELOCITY OF A FRAGMENT AS A FUNCTION OF FRAGMENT MASS AND ACCEPTOR SHIELDING

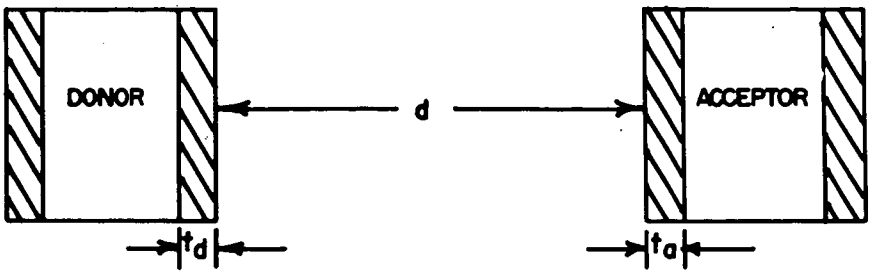

(K_f) = constant

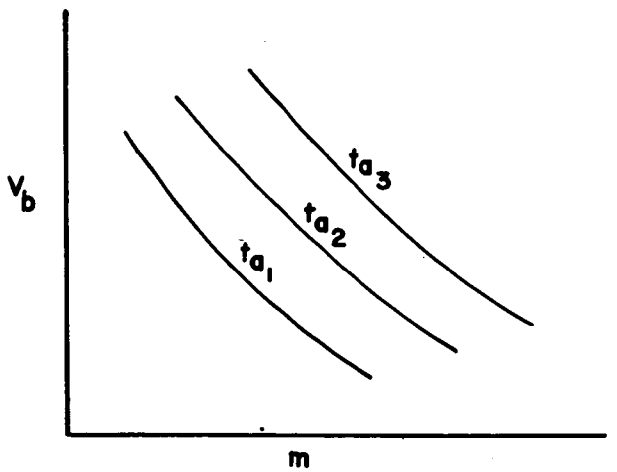

$t_{a3} > t_{a2} > t_{a1}$

$$V_b = f(K_f)(t_a)(m) \quad \text{.....(3)}$$

Figure 8

MINIMUM EFFECTIVE FRAGMENT MASS AND CORRESPONDING VELOCITY AS A FUNCTION OF DISTANCE AND SHIELDING

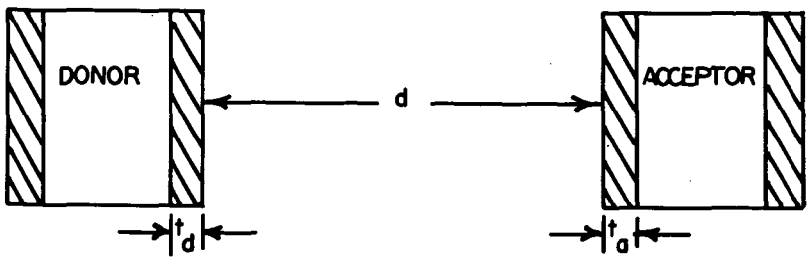

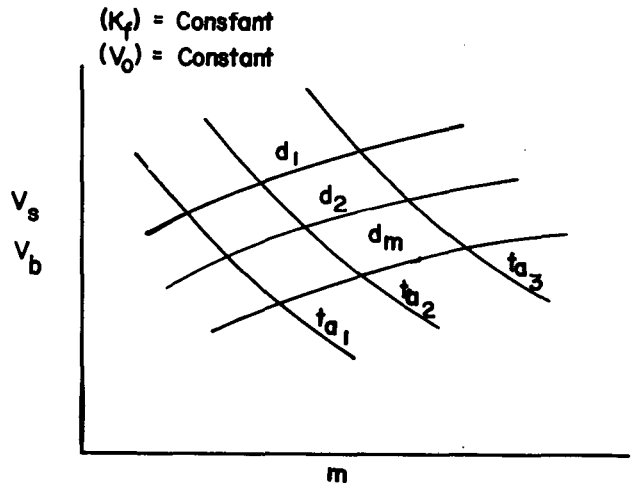

$$d_m = f(k)\,(V_o/V_b)_{min}\,|M_{max}) \quad \text{----------} \quad (4a)$$

WHERE d_m = maximum distance from given donor charge at which detonation of given acceptor is possible.

Figure 9

PROBABILITY OF DETONATION OCCURRENCE AS A FUNCTION OF DISTANCE AND SHIELDING

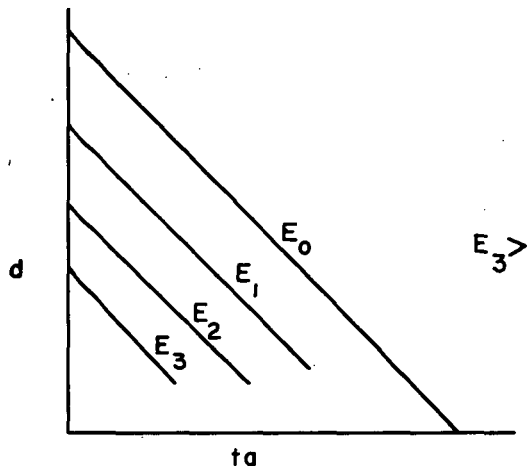

$E_3 > E_2 > E_1$

E_0 – Zero probability curve

$$P/A = f(N_x)(d)(g) \text{ - - - - - - - - - (5)}$$

$$E = f(P) \text{ - - - - - - - - - - - - - (5a)}$$

P/A = Probable number of effective hits per unit area.
(N_x) = Total number of effective fragments.
(g) = Factor governing the distribution of fragments.
(D) = Distance between donor and acceptor charge.
(E) = Probability of high order detonation occurrence in the acceptor.
(A) = Presented area of the acceptor

Figure 10

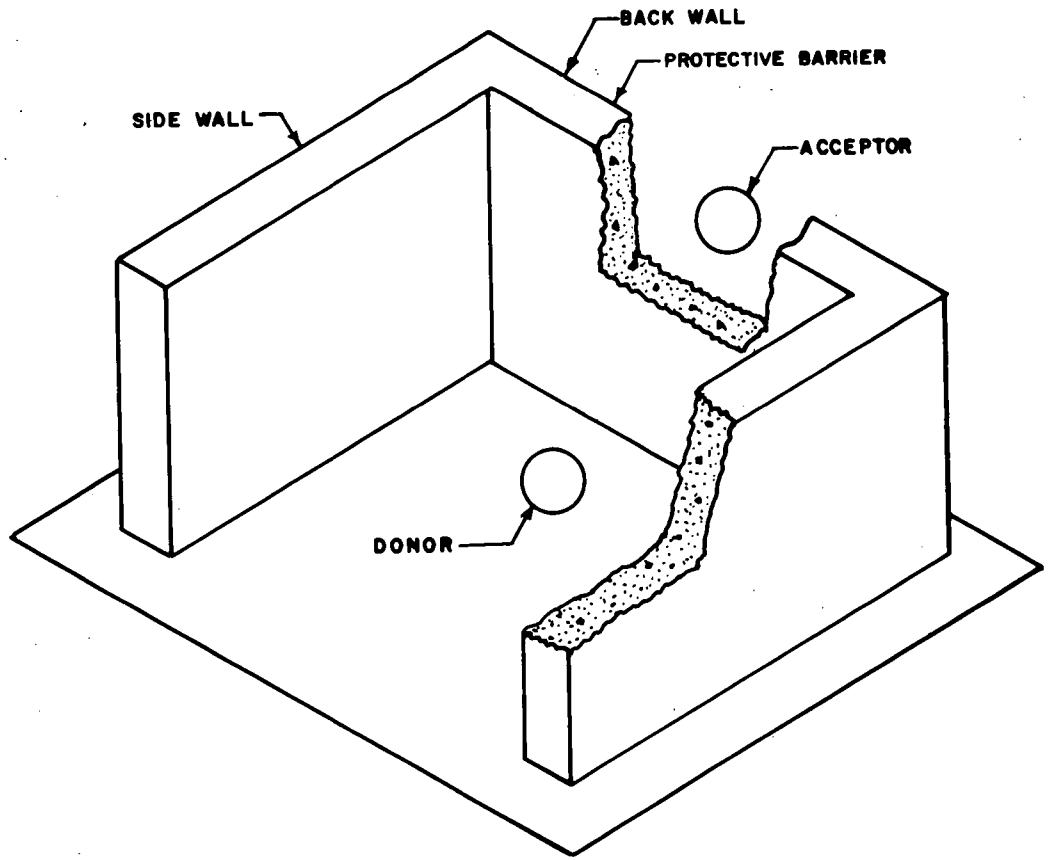

ISOMETRIC OF WALL CUBICLE

Figure II

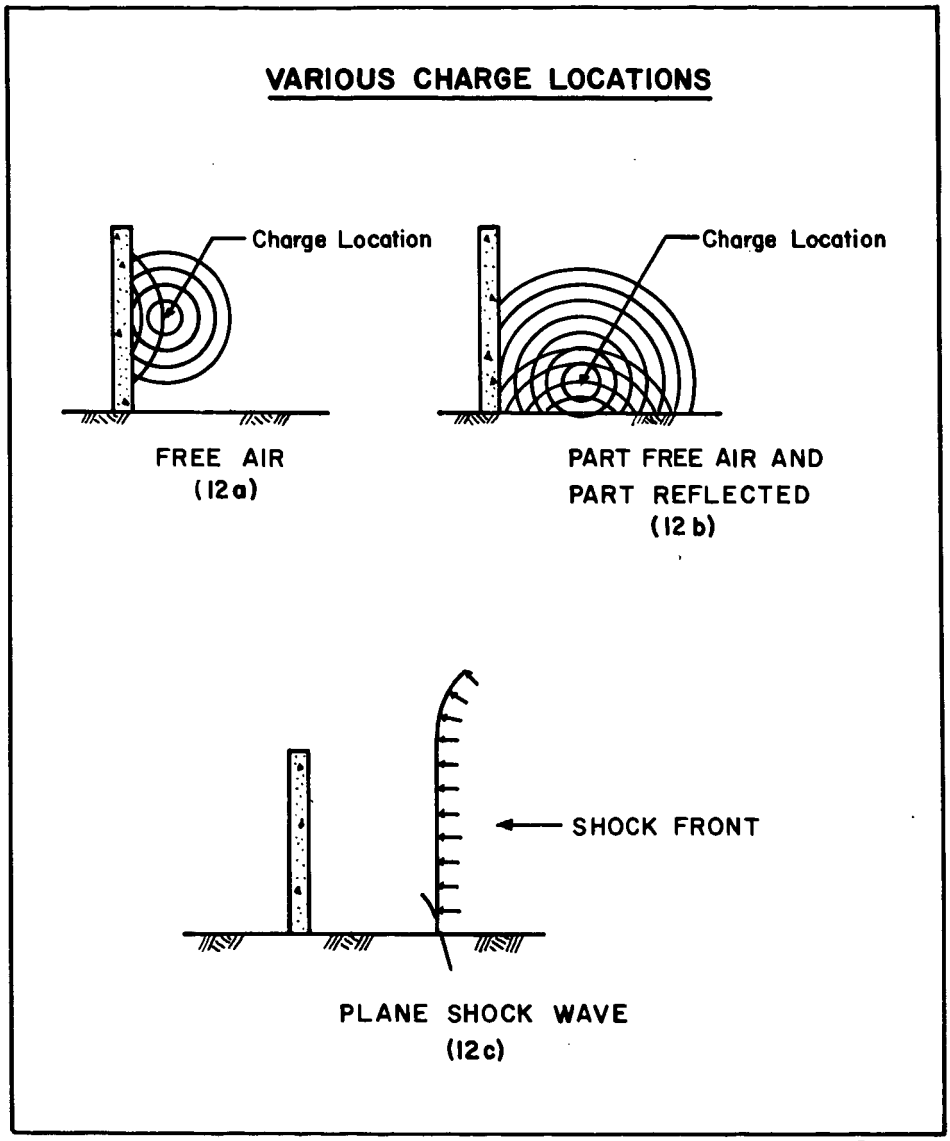
VARIOUS CHARGE LOCATIONS
Charge Location
FREE AIR
(12a)
Charge Location
PART FREE AIR AND
PART REFLECTED
(12b)
SHOCK FRONT
PLANE SHOCK WAVE
(12c)
Ref. 4

Figure 12

REFLECTION FACTORS IN A CUBICLE TYPE STRUCTURE FOR WALL FIXED AT THE BASE AND TWO SIDES

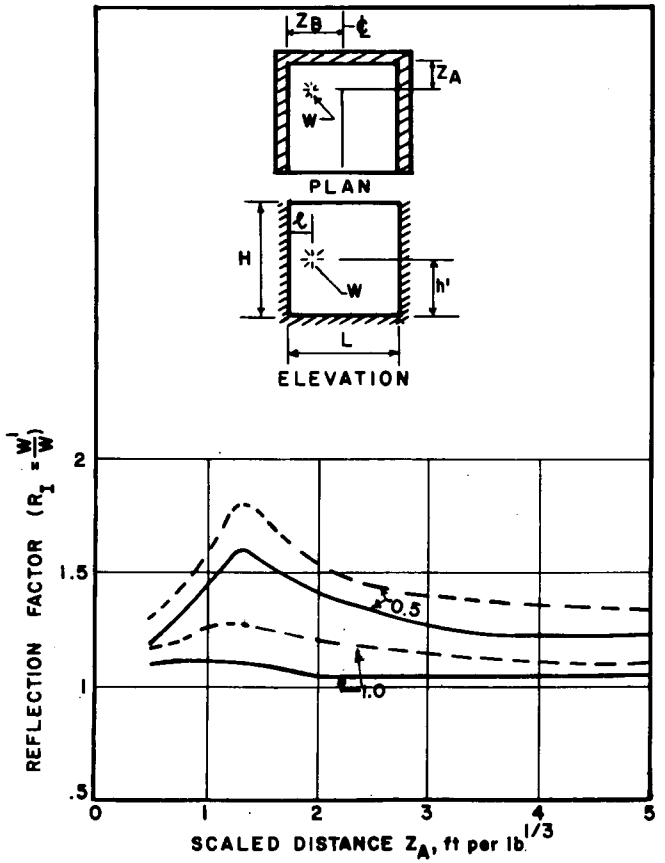

LOCATION OF CHARGE
——— 0.5 x H = h'
– – – 0.25 x H = h'

NOTE: NUMBERS ADJACENT TO CURVES INDICATE VALUES OF Z_B/Z_A

Ref. 4

Figure 13

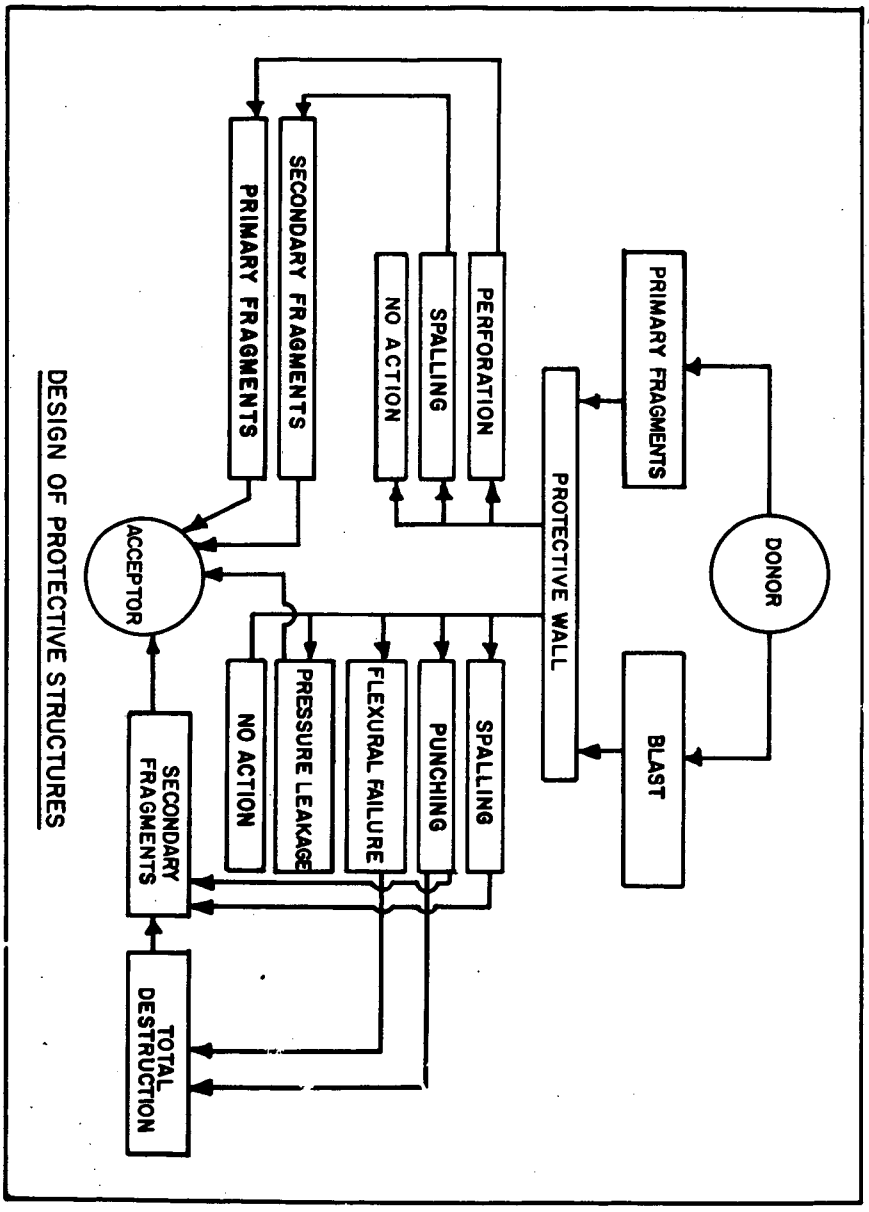
DESIGN OF PROTECTIVE STRUCTURES
DONOR
PRIMARY FRAGMENTS
BLAST
PROTECTIVE WALL
PERFORATION
SPALLING
NO ACTION
SECONDARY FRAGMENTS
PRIMARY FRAGMENTS
ACCEPTOR
SPALLING
PUNCHING
FLEXURAL FAILURE
PRESSURE LEAKAGE
NO ACTION
SECONDARY FRAGMENTS
TOTAL DESTRUCTION

Figure 14

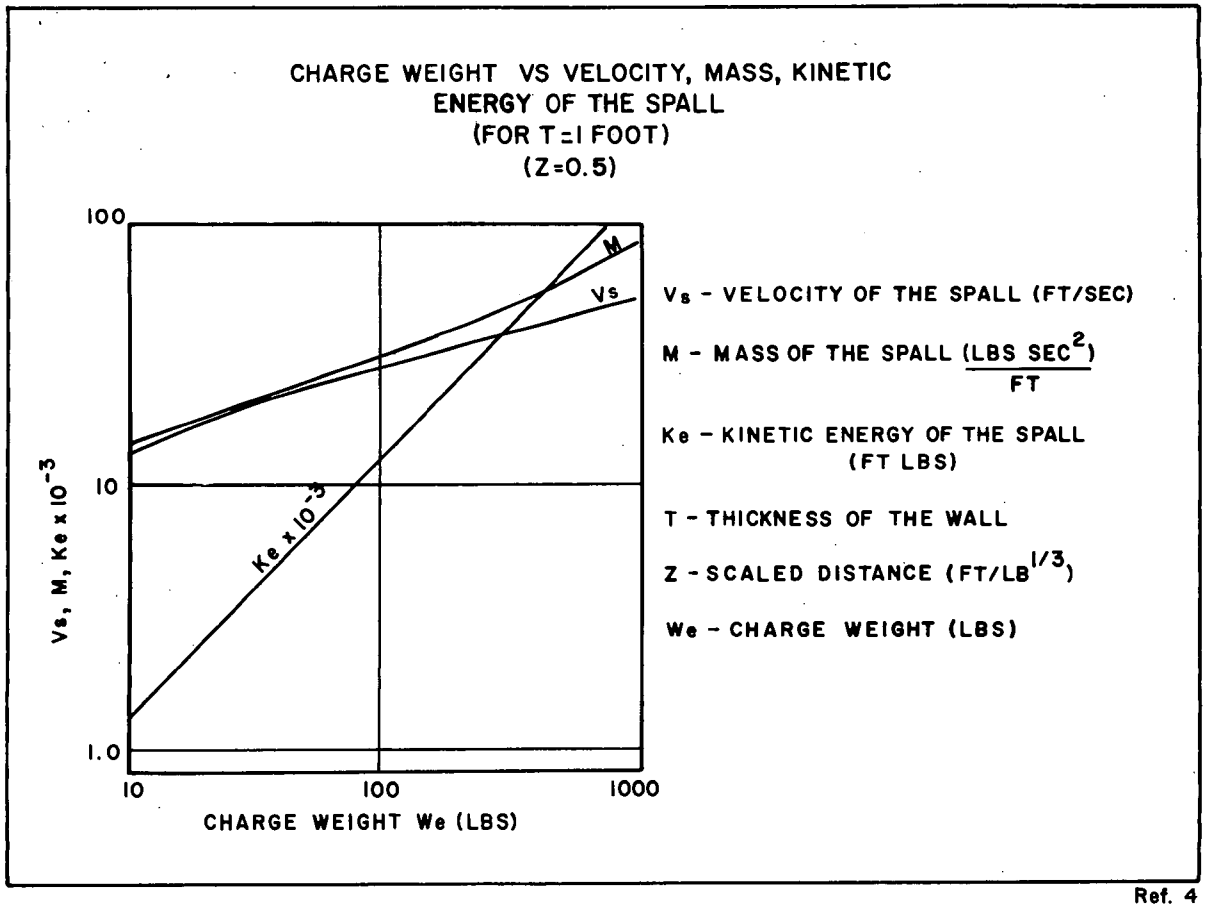

Ref. 4

Figure 15

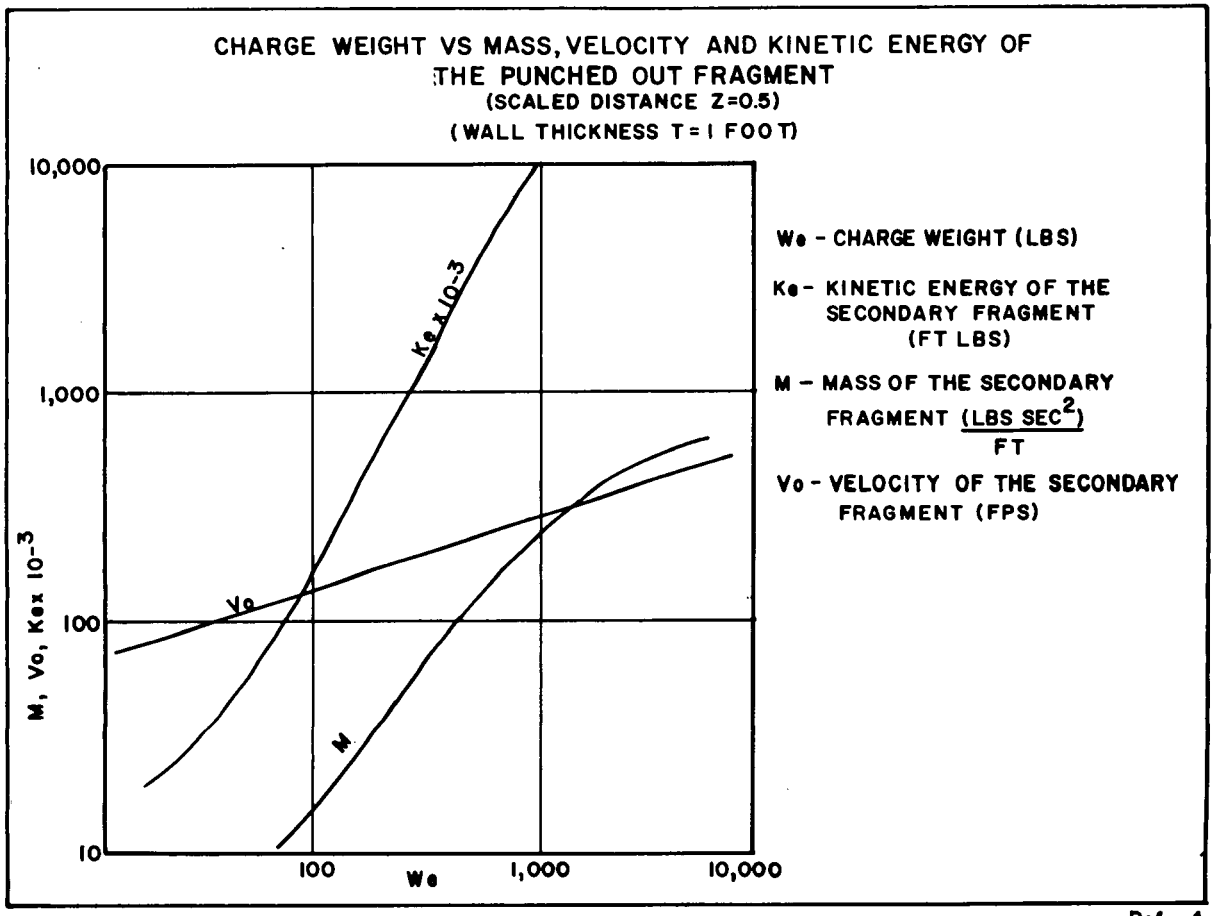

Ref. 4

Figure 16

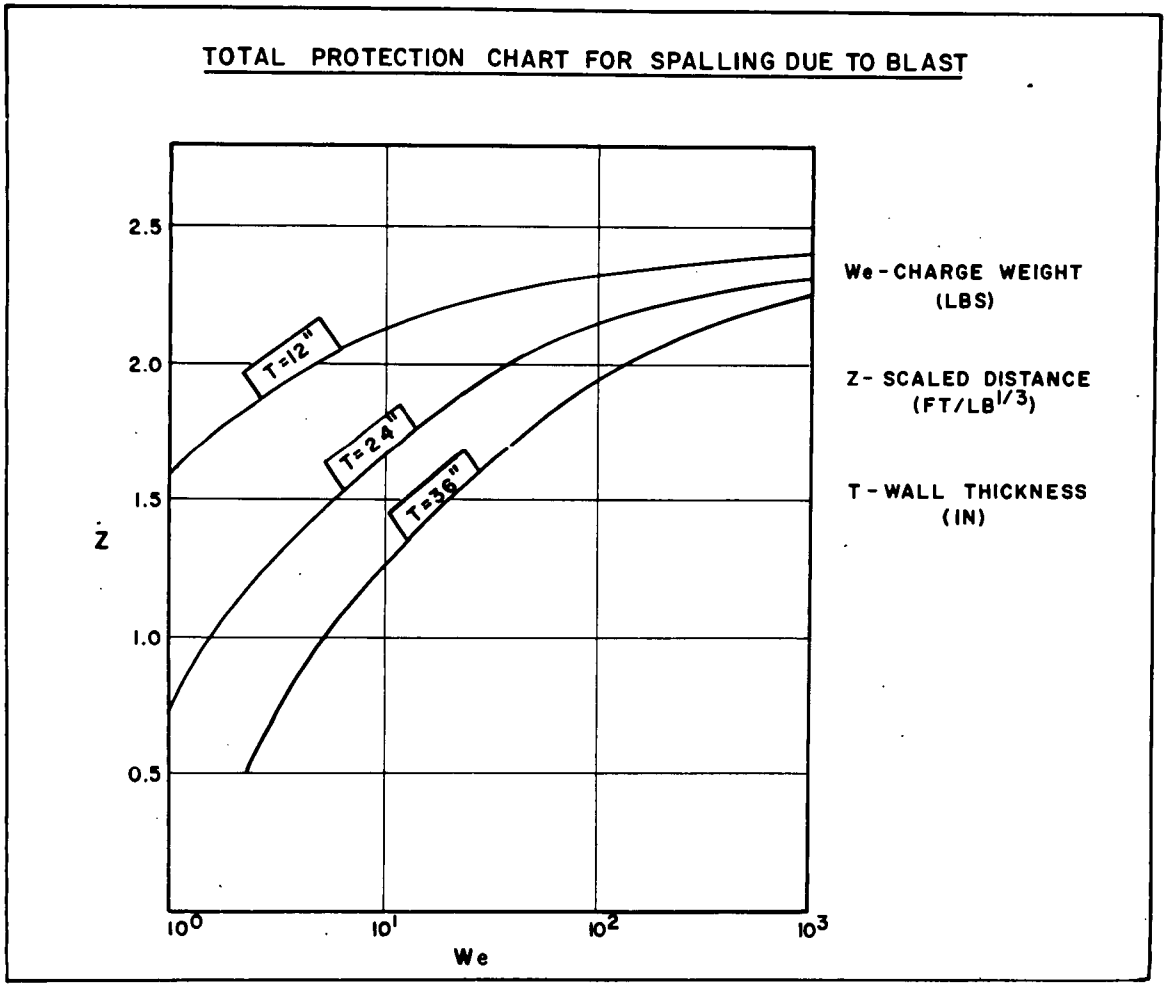

Ref. 4

Figure 17

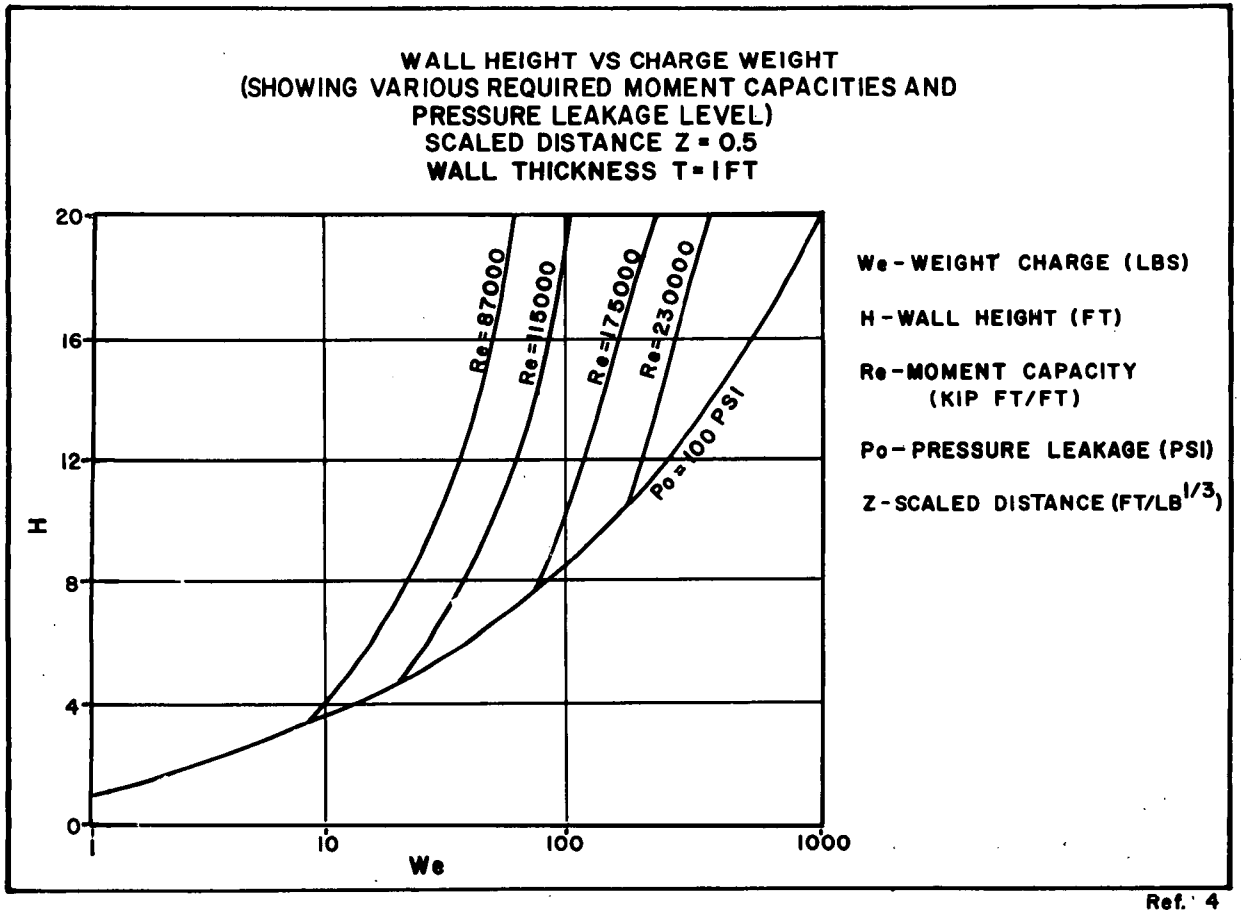
WALL HEIGHT VS CHARGE WEIGHT
(SHOWING VARIOUS REQUIRED MOMENT CAPACITIES AND
PRESSURE LEAKAGE LEVEL)
SCALED DISTANCE Z = 0.5
WALL THICKNESS T = 1 FT
H
We
0
4
8
12
16
20
1
10
100
1000
Re=87000
Re=118000
Re=175000
Re=230000
Po=100 PSI
We - WEIGHT CHARGE (LBS)
H - WALL HEIGHT (FT)
Re - MOMENT CAPACITY (KIP FT/FT)
Po - PRESSURE LEAKAGE (PSI)
Z - SCALED DISTANCE (FT/LB^1/3)
Ref. 4

Figure 18

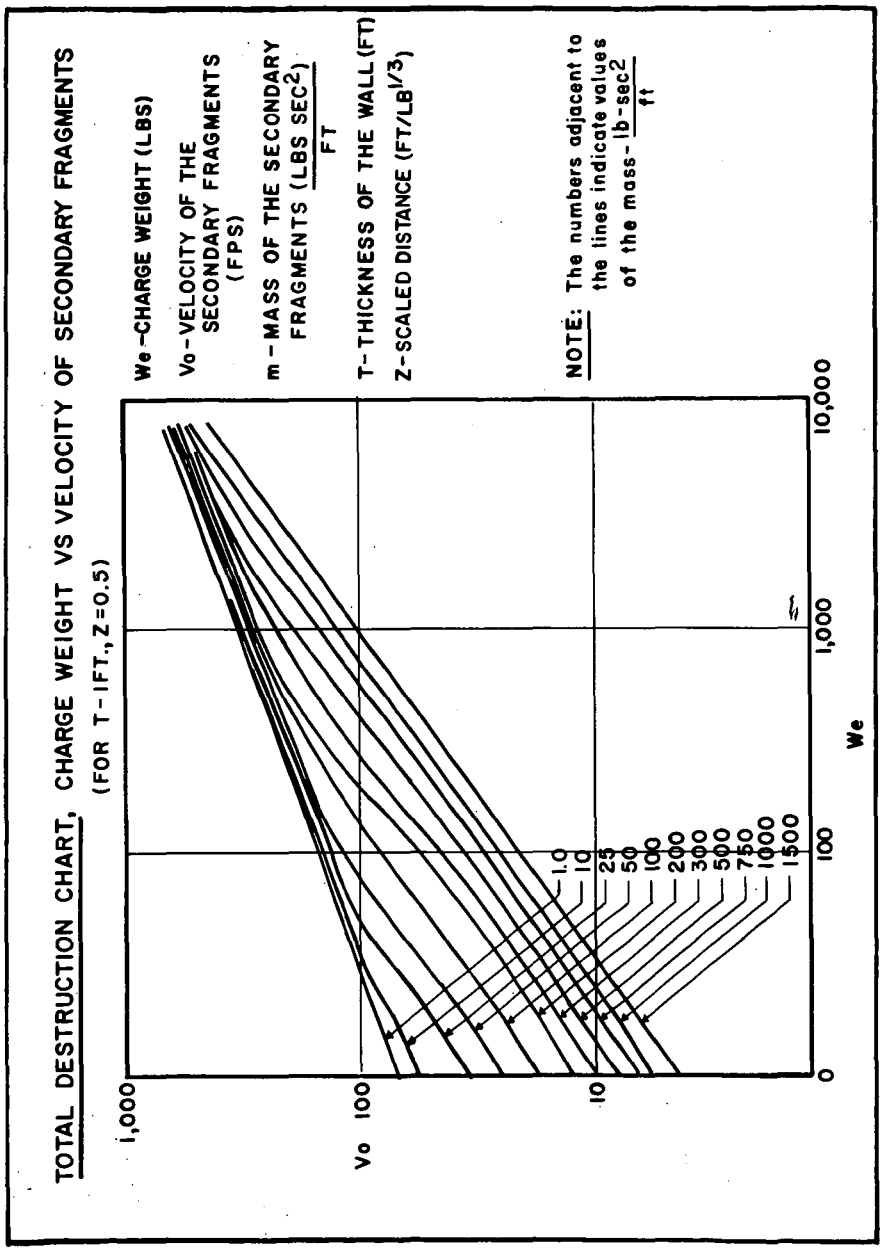
TOTAL DESTRUCTION CHART, CHARGE WEIGHT VS VELOCITY OF SECONDARY FRAGMENTS
(FOR T-1FT., Z=0.5)
We-CHARGE WEIGHT (LBS)
Vo-VELOCITY OF THE SECONDARY FRAGMENTS (FPS)
m-MASS OF THE SECONDARY FRAGMENTS (LBS SEC²/FT)
T-THICKNESS OF THE WALL (FT)
Z-SCALED DISTANCE (FT/LB^1/3)
NOTE: The numbers adjacent to the lines indicate values of the mass-lb-sec²/ft
Vo
1,000
100
10
0
100
1,000
10,000
We
1.0
10
25
50
100
200
300
500
750
1000
1500
Ref. 4

Figure 19

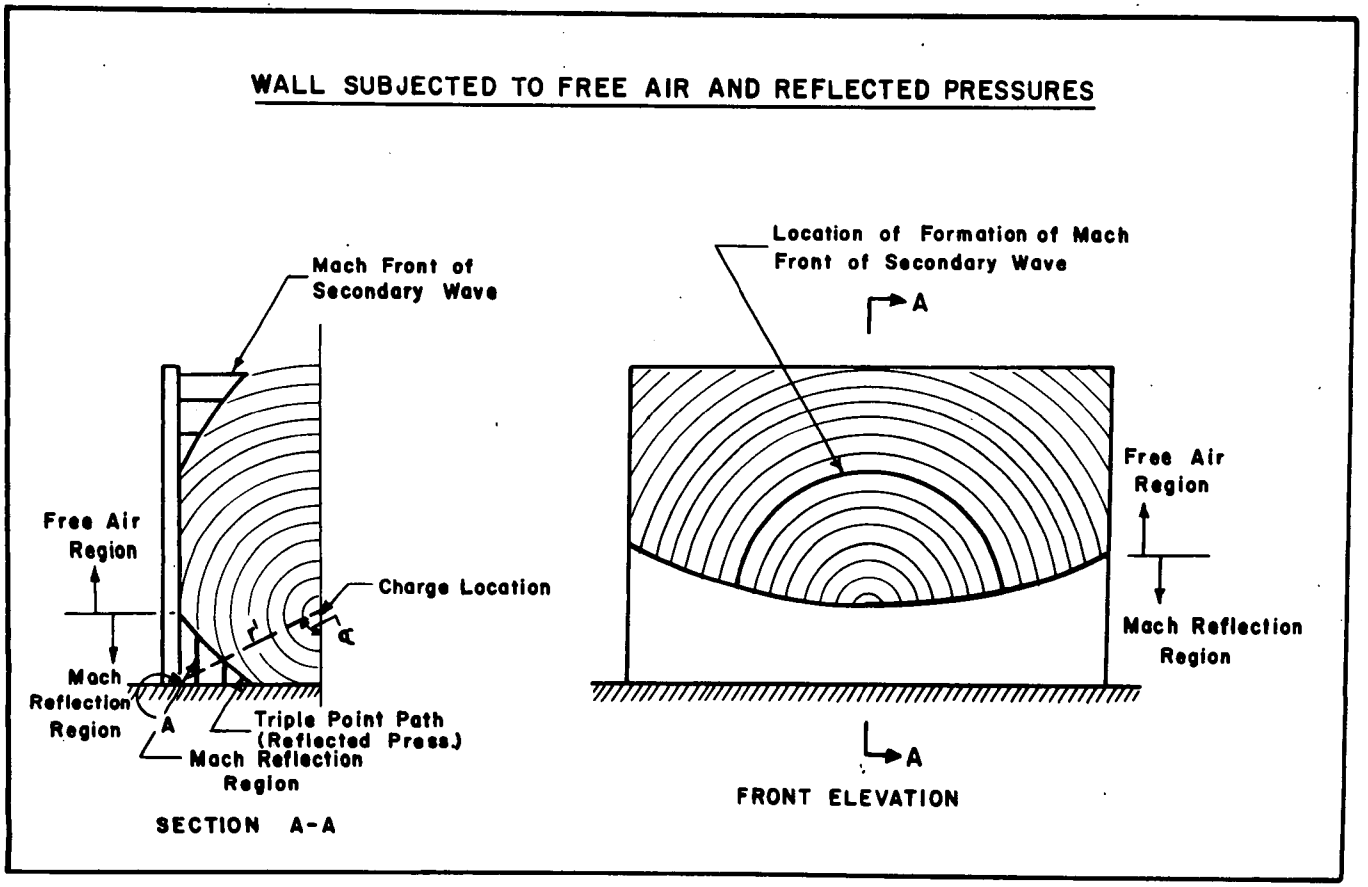
WALL SUBJECTED TO FREE AIR AND REFLECTED PRESSURES
Mach Front of Secondary Wave
Free Air Region
Charge Location
Mach Reflection Region
A
Triple Point Path (Reflected Press.)
Mach Reflection Region
SECTION A-A
Location of Formation of Mach Front of Secondary Wave
A
Free Air Region
Mach Reflection Region
A
FRONT ELEVATION
Ref. 4

Figure A1

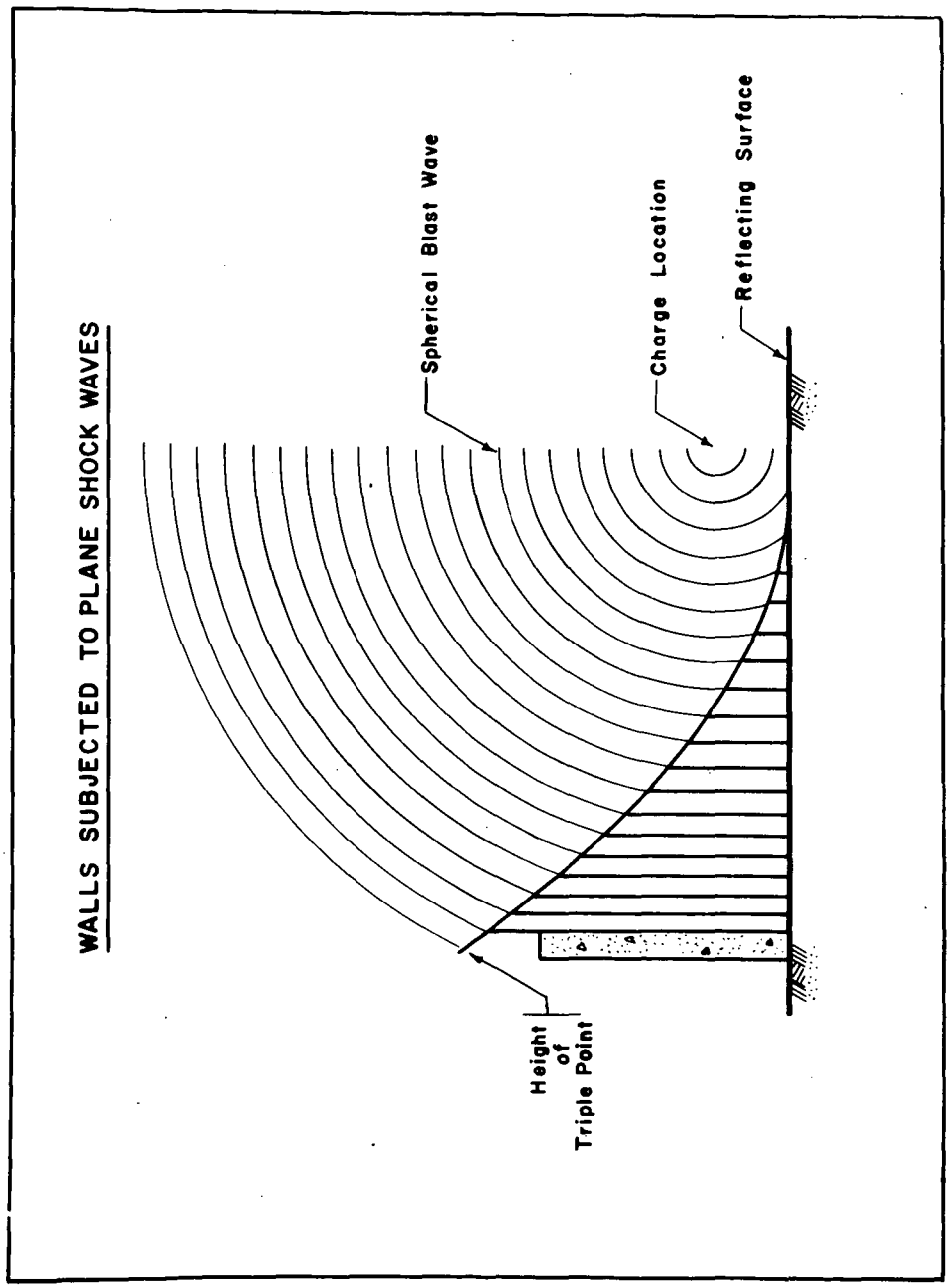
WALLS SUBJECTED TO PLANE SHOCK WAVES
Spherical Blast Wave
Charge Location
Reflecting Surface
Height of Triple Point
Ref. 4

Figure A2

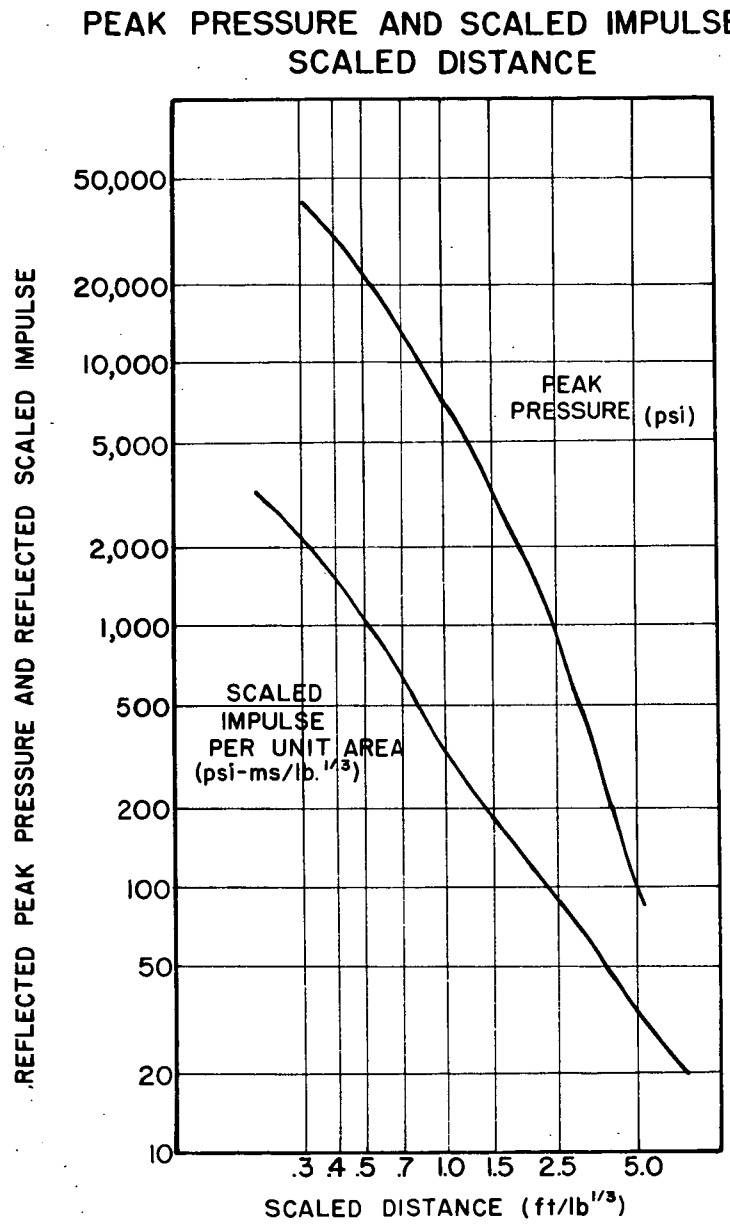

Figure B1

Ref. 4

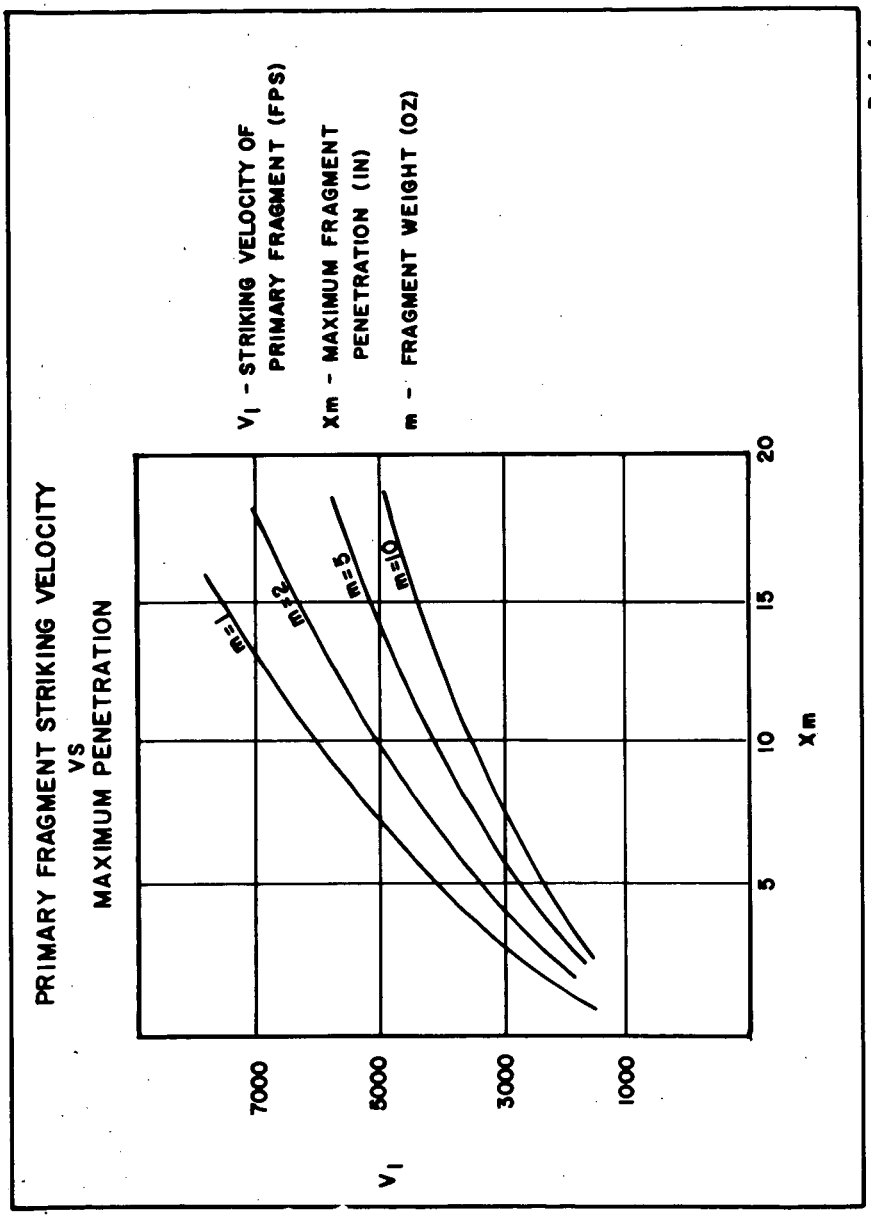
PRIMARY FRAGMENT STRIKING VELOCITY
VS
MAXIMUM PENETRATION
V_1 - STRIKING VELOCITY OF PRIMARY FRAGMENT (FPS)
Xm - MAXIMUM FRAGMENT PENETRATION (IN)
m - FRAGMENT WEIGHT (OZ)
m=1
m=2
m=5
m=10
7000
8000
3000
1000
V_1
5
10
15
20
Xm
Ref. 4

Figure C1

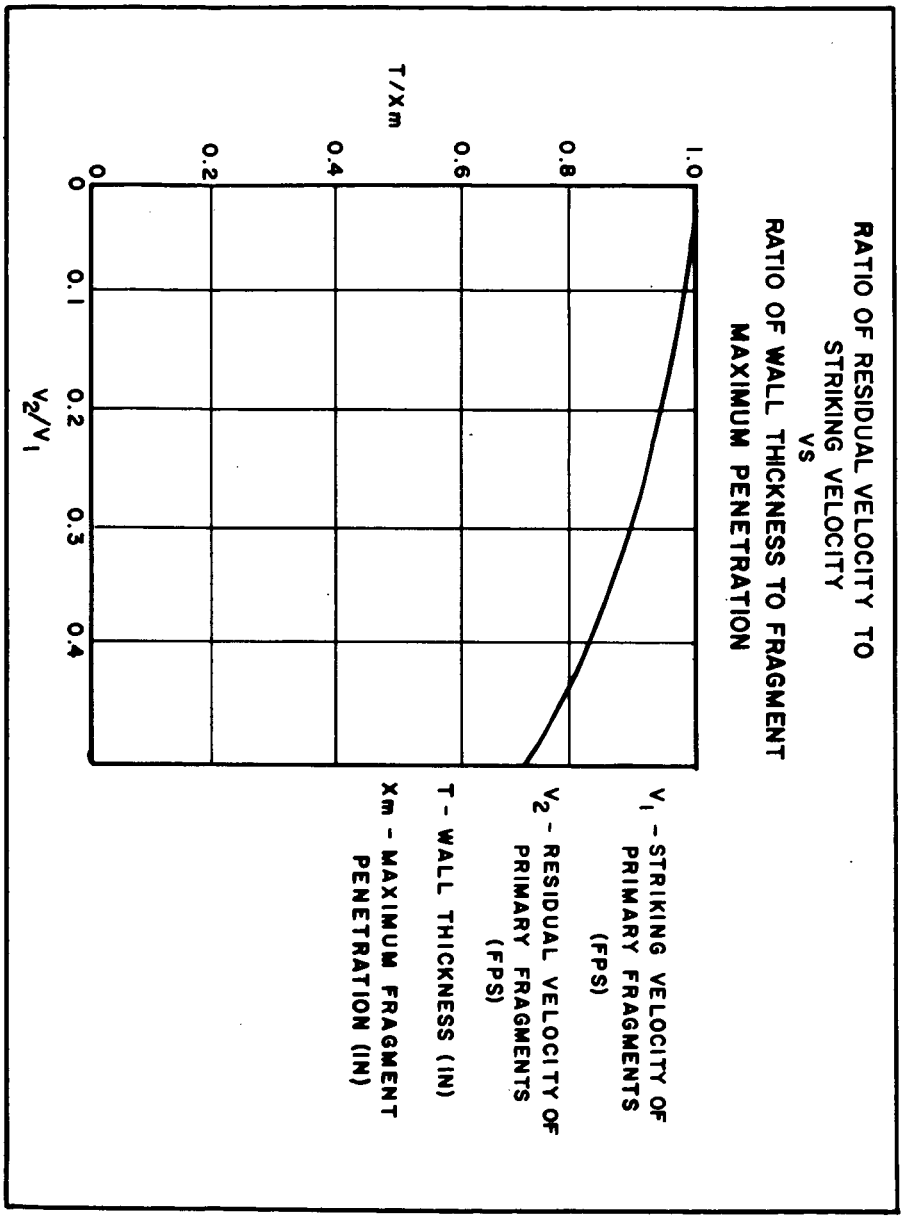
RATIO OF RESIDUAL VELOCITY TO
STRIKING VELOCITY
VS
RATIO OF WALL THICKNESS TO FRAGMENT
MAXIMUM PENETRATION
T/Xm
0
0.2
0.4
0.6
0.8
1.0
V2/V1
0
0.1
0.2
0.3
0.4
V1 - STRIKING VELOCITY OF PRIMARY FRAGMENTS (FPS)
V2 - RESIDUAL VELOCITY OF PRIMARY FRAGMENTS (FPS)
T - WALL THICKNESS (IN)
Xm - MAXIMUM FRAGMENT PENETRATION (IN)
Ref. 4

Figure C2

VELOCITY OF PRIMARY FRAGMENTS
VS
THICKNESS OF THE WALL

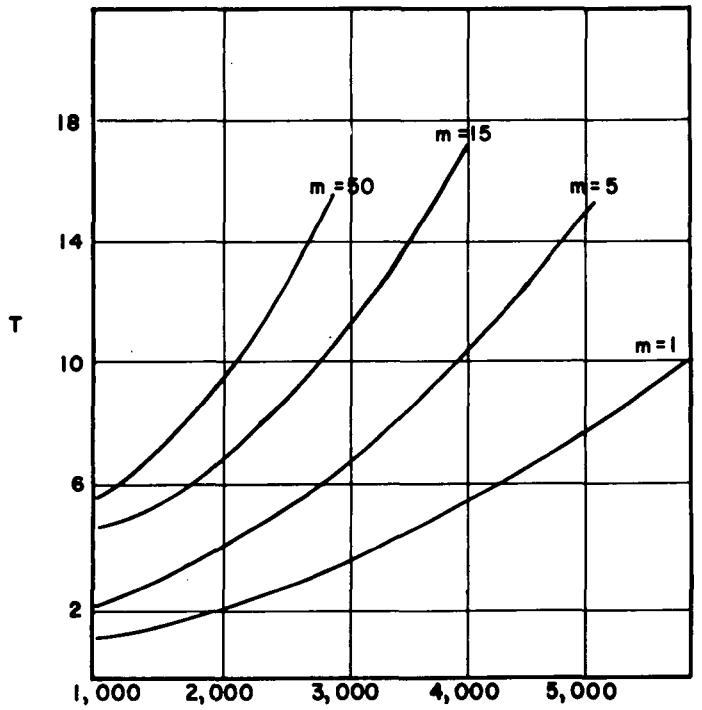

V_1 - VELOCITY OF PRIMARY FRAGMENTS (FPS)

T - WALL THICKNESS (IN)

m - WEIGHT OF PRIMARY FRAGMENTS (OZ)

Figure C3

Ref. 4

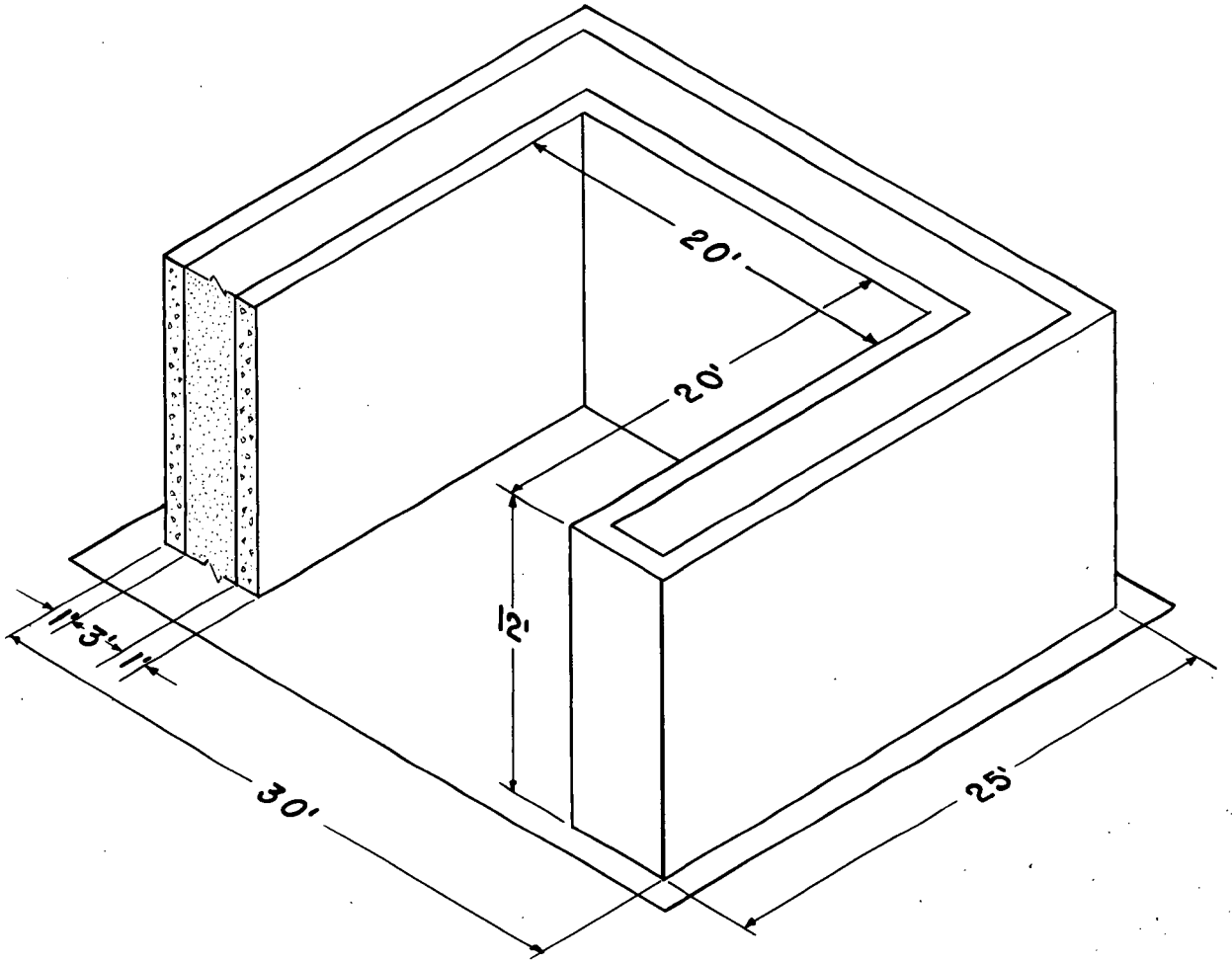

ISOMETRIC OF SANDWICH WALL CUBICLE

Figure DI

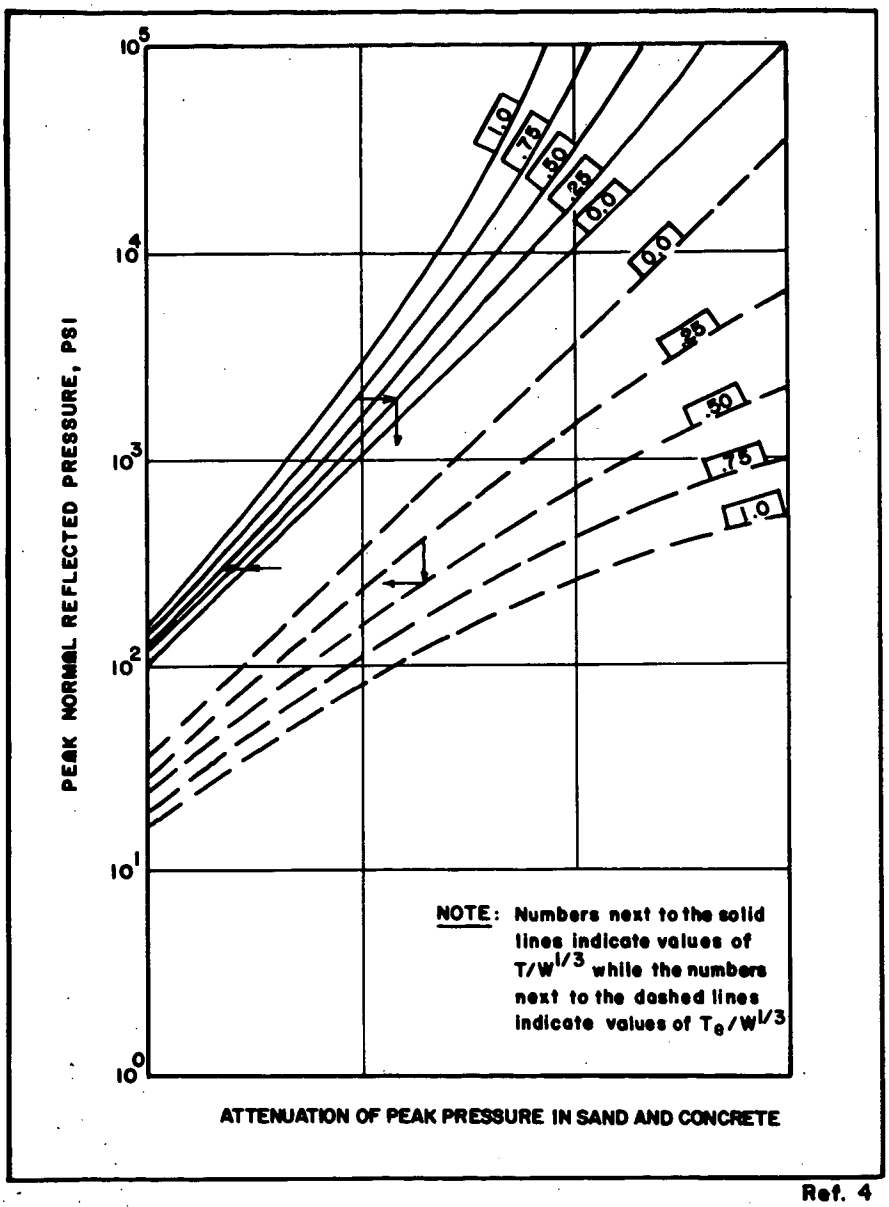
PEAK NORMAL REFLECTED PRESSURE, PSI
10^5
10^4
10^3
10^2
10^1
10^0
1.0
.75
.50
.25
0.0
0.0
.25
.50
.75
1.0
NOTE: Numbers next to the solid lines indicate values of $T/W^{1/3}$ while the numbers next to the dashed lines indicate values of $T_e/W^{1/3}$
ATTENUATION OF PEAK PRESSURE IN SAND AND CONCRETE
Ref. 4

Figure D2

TEST EQUIPMENT AND TECHNIQUES FOR EVALUATING COMPOSITE PROPELLANT PROCESSING AND HANDLING HAZARDS

by

V. T. Dinsdale[1]

THIOKOL CHEMICAL CORPORATION
Wasatch Division
Brigham City, Utah

ABSTRACT

An essential aspect of rocket propellant manufacturing is the accurate evaluation of processing and handling hazards. To determine the hazards of propellant constituents, intermediate compositions, and final compositions present in composite solid propellant, adequate test equipment and techniques were required. The program initiated by Thiokol Chemical Corporation's Wasatch Division to develop the specialized test equipment and techniques necessary will be the subject of this paper.

Hazards were evaluated for normal process conditions and for hazardous conditions which could result from equipment failure or operator error. The primary objective of the program was to develop equipment and techniques with procedures requiring minimum manpower and equipment expenditures.

Equipment was developed to obtain hazard data for friction, impact, thermal, and electrostatic sensitivity. Preliminary work was also conducted to determine the detonation properties of propellants using small laboratory samples.

INTRODUCTION

With rapid advances being made in the development of higher energy propellants, the demand for hazard test data for new propellant constituents, intermediate, and final compositions has also increased. These data are often required prior to making laboratory samples larger than 10 grams because of personnel exposure during some handling and manufacturing operations. Lack of a means to rapidly determine this information with small laboratory samples reduces operating efficiency due to delays incurred while waiting for the test data and the excessive time required to make the number of test samples.

---

[1]Supervisor, Explosive Development Laboratory

Most of the effort expended during recent years on hazard test equipment improvement programs was on the development of precise hazard measuring equipment. The major portion of this equipment was unsatisfactory for production-type testing, because the equipment is not capable of testing minimum size test samples in a short period of time.

The purpose of the program, as summarized in this paper, was to improve existing hazard test equipment designs and test techniques to permit more efficient hazard determination using minimum sample sizes.

INVESTIGATION

A survey was made of Thiokol Chemical Corporation Wasatch Division propellant processing facilities to determine the type and extent of hazardous environments that exist during normal operations or that could exist as a result of minor equipment failure or operator error. This information was classified into types of hazardous environments and the physical state of materials that would be present in these processing environments, i e, powders, liquids, or solids. Hazardous environments given major consideration were friction, impact, thermal, electrostatic, and detonation. Materials currently being processed were thoroughly evaluated; and with existing facility design and safety practices, these materials do not pose unnecessary hazards to processing equipment or to personnel. However, during normal operations a certain amount of hazardous environments exist. New compositions which may be more sensitive and create a hazardous condition during processing must be evaluated. All combustible materials, including fuel and oxidizer powders, premixes, intermediate propellant compositions, and uncured and cured propellants, are evaluated with this equipment to simulate the various process conditions.

Estimated energy levels for friction, impact, and heat were obtained primarily by duplicating operating and minor incident conditions. A study of types of equipment necessary to duplicate these environments was then made to ascertain the most severe operating hazards present during normal operations and minor failures and also to establish a hazard limit.[1]

A survey was then made of several propellant and explosive manufacturing facilities in the United States to determine availability of equipment that could be used to obtain the required hazard data. This equipment also was to comply with the program objectives of being able to obtain this information with procedures requiring small test samples and minimum manpower and equipment expenditures. A summary of the information obtained from this survey and the resultant equipment designed during this program is as follows.

---

[1] Hazard limit is the environment that will barely cause the test material to react.

Friction Testing

A review of the friction equipment used throughout the propellant and explosive industry showed that there was only one satisfactory friction tester design available. This piece of equipment was a strip friction tester designed by Allegany Ballistics Laboratory. However, this tester would meet only part of the test requirements. The design was more than adequate, but Thiokol ordnance designers felt that the same data could be obtained with a tester less expensive to fabricate and operate. Available friction testers of designs that were used for a number of years were not considered satisfactory because of unrealistic friction values and difficulty of operation.

Three basic friction testers were subsequently designed. The first was a slurry friction tester, which with minor changes, was converted into three separate testers to duplicate all friction environments and permit testing of the various types of materials. One of the testers uses a one inch diameter piston and cup arrangement similar to that shown in Figure 1. The applied forces are shown in Figure 2-C. The piston is lowered on top of the sample and into the cup prior to starting the motor. The force is varied by adding weights to the piston carriage, and the rotating speed is adjusted by changing pulley ratios. This type of tester was not considered an accurate friction measuring device; however, the tester does provide an evaluation of the friction sensitivity of materials that might be subjected to confined friction environments, such as combustible materials in a mixer packing gland.

The second slurry friction tester utilized a twelve inch bowl with a spring-loaded friction head that impinges against the side of the bowl. The tester and the forces involved are shown in Figures 2-A and 3. The applied force and rotation speed are set by changing the spring tension on the friction-head assembly and changing the pulley ratios. The test material is distributed in front of the friction head by two Teflon directional scoops. Medium-viscosity materials such as intermediate and uncured propellant compositions are the only materials tested with this device because the tester scrapes on a vertical plane. This tester simulates friction environments experienced in mixing and cleanup operations. Various types of friction head and bowl materials can be used to achieve the desired friction environment. The vertical tester was considered in addition to the horizontal scraper because of the constant test radius eliminating the changing force variable.

The third type of slurry friction tester also utilized a twelve inch bowl, but the friction head applies force against a bottom portion of the bowl that is grooved to contain low viscosity liquids. The friction tester and the application of forces are shown in Figures 2-B and 4. The force on the friction head is controlled by adding or removing weights from the top of the assembly. Friction conditions are simulated for mixing and cleanup processes involving low-viscosity premixes and intermediate and uncured propellant compositions. Friction heads and bowl materials are changed to achieve the desired friction environment.

A strip friction tester was designed for testing fine powders and propellant samples. Two thin strips of metal similar to those shown in Figure 5 are used for each test. The strip surfaces are machine cut to eliminate surface variables. The tester and the application of forces are shown in Figures 6 and 7. Obtaining the desired force to the roller compressing the strips together is accomplished by removal or addition of weights on a lever. A falling weight provides the energy to pull the strips apart. The falling weight impinges upon a lever attached to a wheel, which in turn pulls one of the strips. The other strip is secured to the stand. The applied force and the mass of the falling weight are varied to obtain the desired friction environment. The direct impact tester was modified to incorporate this device as an attachment. The strip tester also used the same framework and drop weight as the direct impact tester.

This particular test not only provides a means of determining friction sensitivity of powder materials and propellant samples that is difficult to obtain on other types of friction testers, but also duplicates friction environments occurring in processes such as scraping of a drum on a floor contaminated with oxidizer and propellant scraps.

A third type of friction tester called, a rotary friction tester, was designed (Figure 8). A rotating wheel impinges upon a shoe of known surface area to produce the friction environment. This tester is primarily used to determine friction sensitivity of viscous materials (premix and uncured propellants). Tests are conducted on cured propellants, but the setup time is excessive. The applied force is varied by adding or removing weights on the end of a lever attached to the friction shoe (Figure 9). The wheel speed is varied by a variable-speed gear box and pulley system. Shoe and wheel materials are changed to obtain any desired combination.

Impact Testing

Prior to initiation of this program, Thiokol's Wasatch Division ordnance engineers designed an impact tester based upon test and design data obtained from the Naval Ordnance Laboratories at Silver Spring, Maryland. Throughout the missile industry there are numerous impact-tester designs, very few of which are directly comparable. Even when designs are the same, sample preparation and test techniques are different. The Thiokol tester was designed to reduce as many of the test variables as possible and improve on test efficiency. The design consisted of a piston and cup arrangement, with the piston guided into the cup as shown in Figures 10 and 11. Propellant samples are prepared by cutting thin slices using a microtome cutter (uncured samples are frozen with CO_2 prior to slicing). Powdered samples are weighed out or measured volumetrically. A disc of sandpaper is placed face down into the sample to increase sensitivity. To avoid excessive galling of the striker surface, a thin shim of steel, 0.005 inch thick, is used between the striker surface and the sandpaper disc.

The second impact tester is called a direct impact tester (Figure 12) because the striker impacts directly on the sample as shown in Figure 13. A small sample of controlled size is placed on the anvil (Figure 14), and the anvil is inserted into the anvil holder and impacted by the falling weight. The drop height and weights are changed to obtain the desired impact environments.

Autoignition Testing

Autoignition tests are conducted in a convective-type oven because most autoignition data are required on samples too large for a Woods metal bath arrangement. Depending upon whether the samples are liquid or solid the samples are suspended in the oven as shown in Figures 15 and 16. A thermocouple is suspended adjacent to the sample to record the sample temperature during test and to indicate when the sample fires. The oven is designed to withstand the firing of up to ten gram propellant samples and contains a blowout plug and exhaust ducting to prevent contamination of the surrounding areas.

Electrostatic Testing

Most of the electrostatic test devices used by the various facilities were not permanent and lacked unity of design. Several of the designs used common devices for energy application, such as the use of a phonograph needle for one electrode, but the devices still varied in sample size, and sample preparation. It was decided to design an electrostatic tester that would incorporate many of the better features of existing designs to meet program objectives. The electrostatic tester and the major subassemblies are shown in Figures 17, 18, and 19. A sketch of the sample test fixture is shown in Figure 20. Samples are inserted into a plastic holder of a given hole size and then placed on a steel blank attached to one electrode. The other electrode is attached to a steel ball placed on top of the hole in the plastic holder. The ball is four times the diameter of the sample hole.

The capacitors are charged with a NJE high voltage power supply capable of generating 60,000 volts. Switching is accomplished with a solenoid operated knife switch to eliminate switch bounce experienced with vacuum switches. Arrangement of the capacitors in a circle with the contacts in the center permits rapid selection of the desired capacitance value.

Detonation Testing

The most important detonation characteristic in propellant processing facilities is the critical diameter.[1] If a critical diameter exists within the maximum diameter of material being processed, then other detonation characteristics such as minimum

[1] Critical diameter is the minimum charge diameter that will sustain a detonation when initiated by a booster charge greater than the minimum booster or equal in diameter to the test charge.

booster, deflagration-to-detonation, and projectile impact sensitivity will be determined.

After reviewing other facilities, it was found that very few improvements were made in the method of determining critical diameters, and that all attempts to determine critical diameters of compositions with subcritical diameter samples were unsuccessful.

Two approaches to determine critical diameters with subcritical diameter charges are being investigated. The first is the development of a relationship between the critical diameter of a material and grain reaction determinations extrapolated to a theoretical detonation temperature and other chemical and physical parameters such as density, temperature, and confinement. The second method is a study of the detonation reactivity of subcritical diameter propellant samples when subjected to large booster charges.

INTERPRETATION

The following is a summary of the test techniques and data interpretation for each of the testing devices described.

Friction Analysis

One Inch Diameter Piston-to-Cup Slurry Tester--The most uniform results were obtained using a sample size of approximately 0.4 gram so the material would not be extruded out of the cup. A vertical force and rotational speed were obtained for which a reference uncured propellant sample would fire in approximately one minute. A fire is evidenced by an audible or visual reaction. If the cup or piston temperature rises above 10 degrees Fahrenheit during a test, cooling is provided to maintain a temperature within 10 degrees of room temperature prior to the next test. Ten tests were run on each sample to obtain the minimum, maximum, and average fire times.

A sensitivity index is established by dividing the average fire time of the test material by the average fire time of the reference material and multiplying by ten. Hazard limits are established based on the index values.

Twelve Inch Diameter Vertical Slurry Friction Tester--A thin film of propellant is spread around the periphery of the bowl the same width as the friction head. The sample sizes vary between 0.5 and 2 grams. On some tests it is desirable to put the test sample in front of the friction head instead of spreading it around the side of the bowl. The speed and force are varied to obtain a fire point for a reference material of approximately 15 seconds. A fire is evidenced by an audible or visual reaction. The temperature of the bowl and friction head is maintained to within 10 degrees of ambient temperature prior to each test. One test replaceable metal strips are used on the friction head when conducting standard tests to determine the friction index.

The number of tests conducted and the evaluation of the test data for establishment of a friction index are the same as on the piston-and-cup tests.

Twelve Inch Diameter Horizontal Slurry Friction Tester--The horizontal friction tester uses a sample size of approximately 5 grams. The rotational speed and force settings, number of tests, and data evaluation are similar to the vertical tester.

Strip Friction Tester--The most uniform test results were achieved by placing the sample between the strips in front of the roller pressure point. The preparation of the sample and uniformity of the strips must be carefully monitored to produce accurate test results.

A standard is tested with either beta-HMX (Cyclotetramethylenetetranitramine) explosives or a propellant composition, depending upon the type of test material. The most useful information is obtained by determining a drop height and weight to provide satisfactory results with the standard. Then all similar materials are tested using the drop weight and height, with the applied force being varied.

A Bruceton-type analysis is followed to obtain a 50 percent fire point. The 50 percent fire point is used to establish a friction index, as compared to a reference material. A fire is evidenced by an audible or visual reaction.

Rotary Friction Tester--The rotary friction tester is used for two types of tests. One test is to establish a rotary friction sensitivity index using a stainless steel shoe and wheel. The other is a comparative test using varying shoe and wheel combinations similar to that shown in Figure 21.

The average time-to-fire is used on the standard test to compute a rotary friction index, which is the average time-to-fire of the test material divided by the average time-to-fire of the standard material multiplied by ten.

On the tests using varying wheel and shoe combinations, the data are evaluated by plotting the average time-to-fire in seconds versus the radial wheel velocity in feet per second times the applied force in pounds per square inch (Figure 22). By this method, varying wheel and shoe sizes are used and still compared with other tests using different size wheels and shoes.

Impact Analysis

Indirect Impact Tester--Preparation of propellant samples for the indirect impact tester is accomplished by slicing the propellant into 0.021 inch thick strips using a microtome cutter. Dried materials are sampled volumetrically. The Bruceton test technique is used to obtain the 0, 50, and 100 percent fire points, with the 50 percent fire point being used for determining the impact index. Beta-HMX is

used as a standard; and the reference material, an uncured propellant composition, is used to compute the impact index. The impact index is computed similarly to the rotary friction index, or the 50 percent fire point of the unknown material is divided by the 50 percent fire point of the reference uncured propellant multiplied by ten. A typical test data sheet is shown in Figure 23.

Direct Impact Tester--Because of the difficulty or time consuming efforts in raising or lowering the weights on the direct impact tester, a Probst analysis is used rather than the Bruceton analysis. The Probst analysis involves conducting 20 tests at each height within the range of the 0 and 100 percent fire points. Small (0.009 gram) samples are used. Propellants are sliced with a microtome cutter and punched out with a circular punch. An audible sound is used to determine whether or not the material fired.

Autoignition Analysis

Autoignition tests are conducted with the oven set at a constant temperature. A thermocouple placed adjacent to the sample records the temperature and the time-to-fire. The temperature is increased or decreased until the autoignition characteristics for approximately one hour are obtained, similar to the data shown in Figure 24. If a material to be tested has an unknown autoignition temperature range, a dynamic temperature environment test is performed on the material with the oven temperature increased over a given period of time until the fire point is reached. These data are then evaluated to determine the temperature range to be used.

Electrostatic Analysis

Electrostatic tests are conducted between the ranges of 100 pf to 0.1 μf capacitance and 100 to 60,000 volts. A 50 percent fire point is estimated using a Bruceton-type analysis by increasing or decreasing the voltage. A chart for which voltages, capacitance, and energy levels are displayed is shown in Figure 25. The sensitivity of materials is compared by taking a constant energy line in joules which is tangent to the test data curve. This energy value is then used to compute an electrostatic sensitivity index, the same as for the friction and impact test data.

Use of the one test replaceable plastic holders enables rapid testing and uniformity of sample preparation with a minimum material required.

Detonation Analysis

At the present time, sufficient tests had not been conducted to prove the validity of determining critical diameters either by reaction rates or reactivity measurements with laboratory samples.

Tests are still being conducted using a standard pipe detonation test setup similar to that shown in Figure 26. A booster having the same diameter as the test charge is used to ensure adequate boostering, and a charge of sufficient length is used to evidence the reaction. Pin gages are used to record the shock velocities, and the signals from the gages are recorded with a coded pin mixer system to ensure more reliable data pickup.

CONCLUSION

The friction, impact, autoignition, and electrostatic test equipment and techniques developed during this program enable rapid and inexpensive determination of the hazardous characteristics for propellant constituents and compositions present in propellant manufacturing and storage facilities.

This equipment and these techniques are providing better utilization of propellant development facilities and manpower because hazard test data are being obtained with less test delays than was possible with previous designs and techniques.

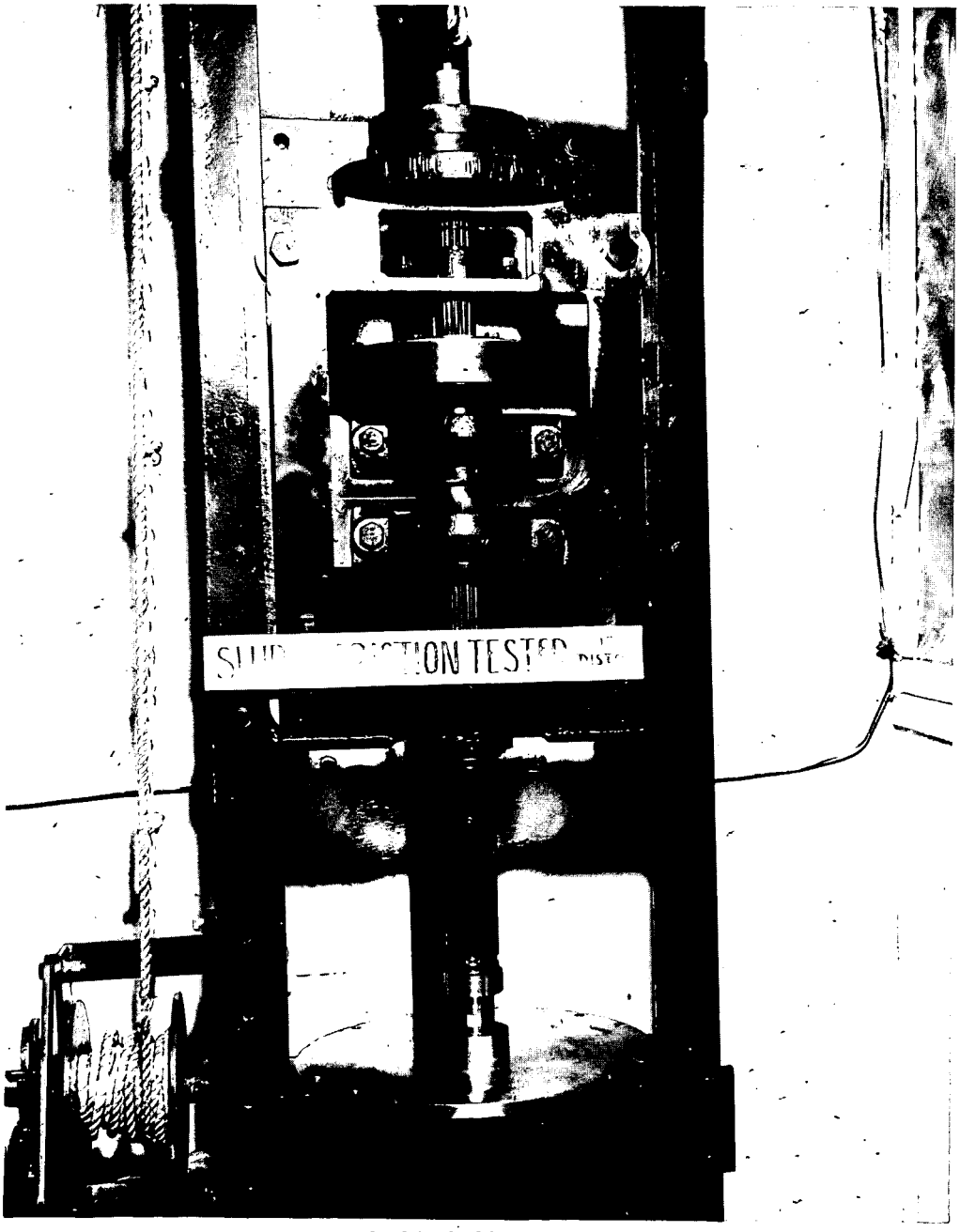

Thiokol CHEMICAL CORPORATION
WASATCH DIVISION • BRIGHAM CITY, UTAH

Figure 1. One Inch Piston and Cup Slurry Friction Tester

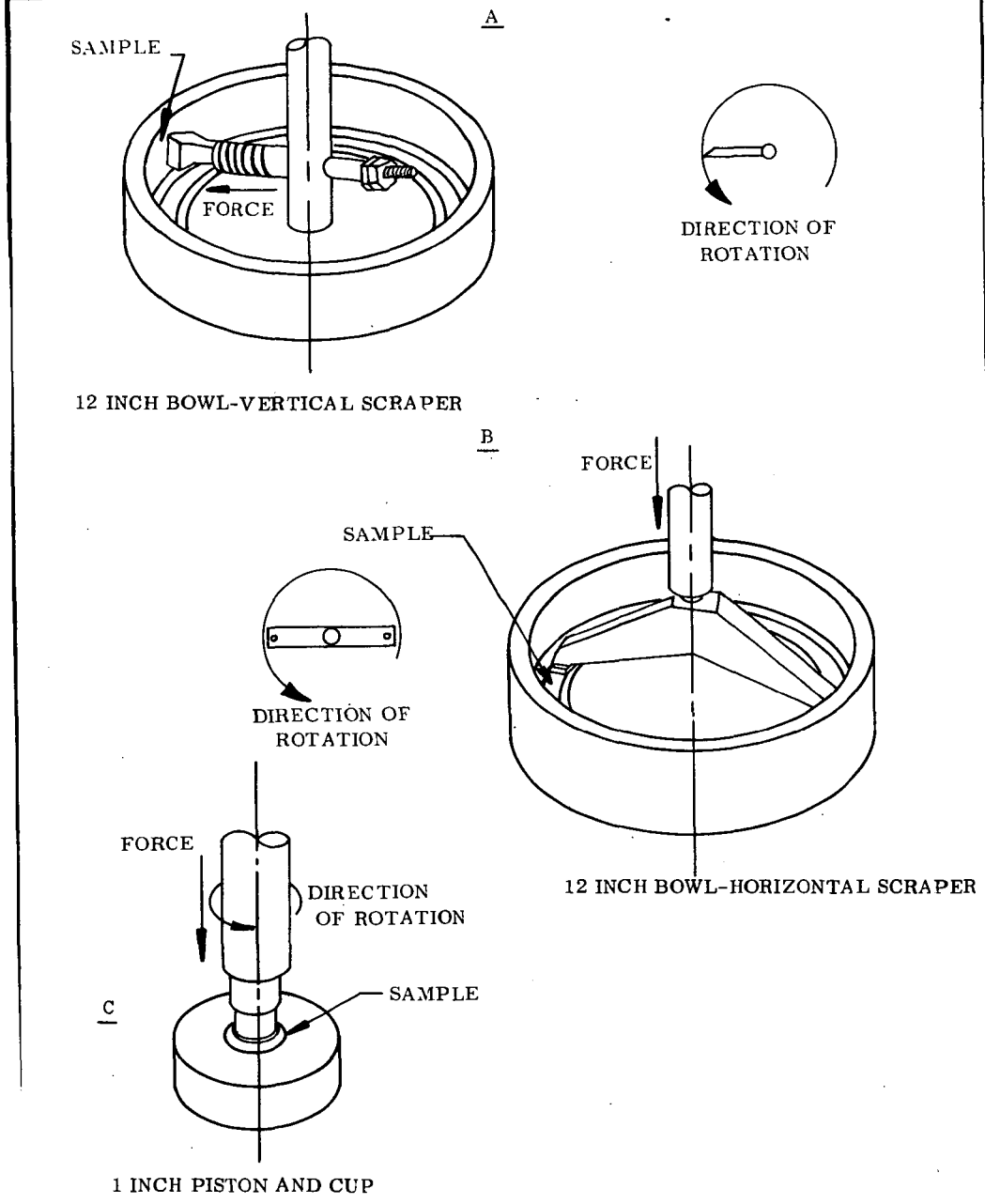

Figure 2

Application of Forces in Slurry Friction Testers

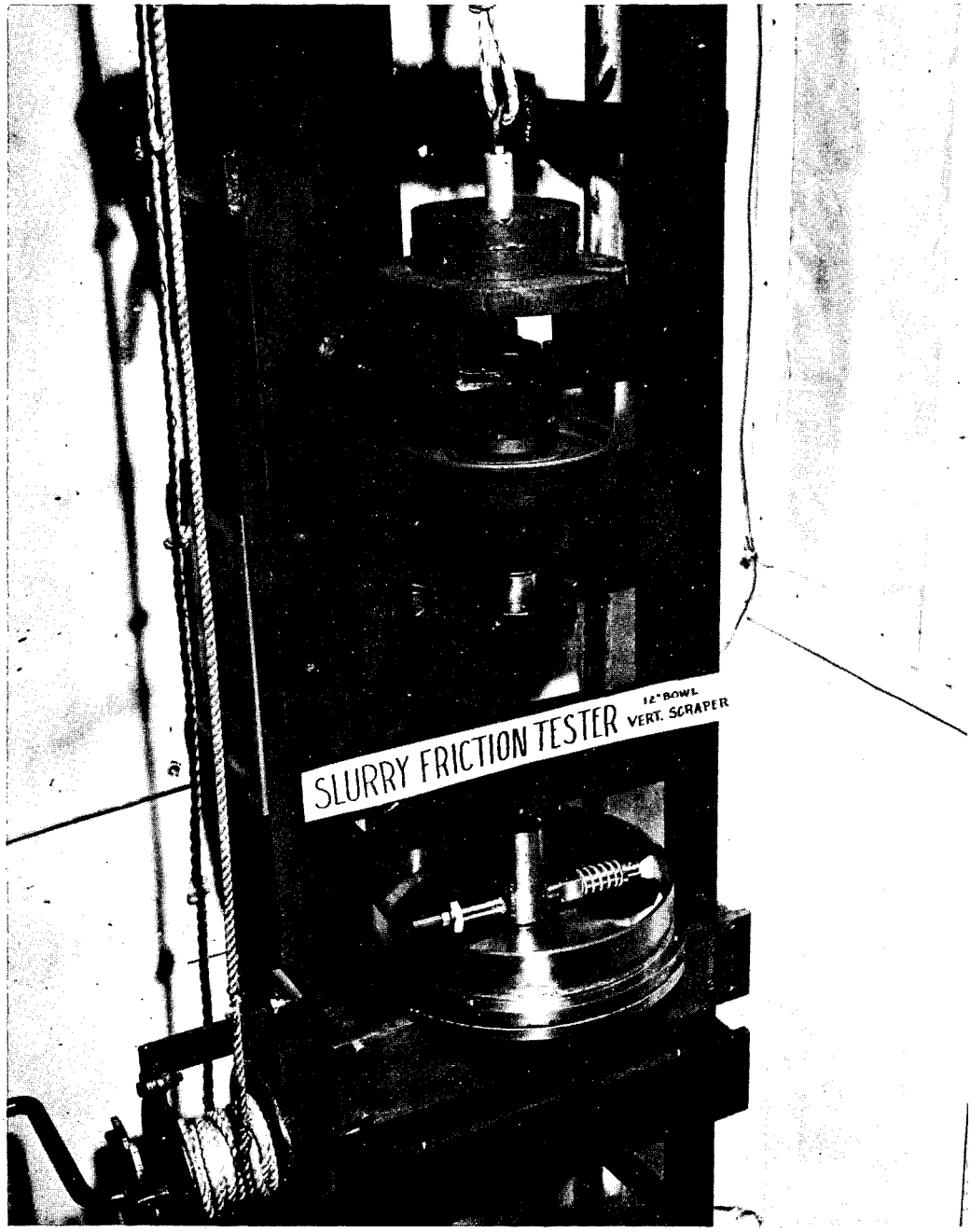

Figure 3. Twelve Inch Bowl Vertical Slurry Friction Tester

Figure 4. Twelve Inch Bowl Horizontal Slurry Friction Tester

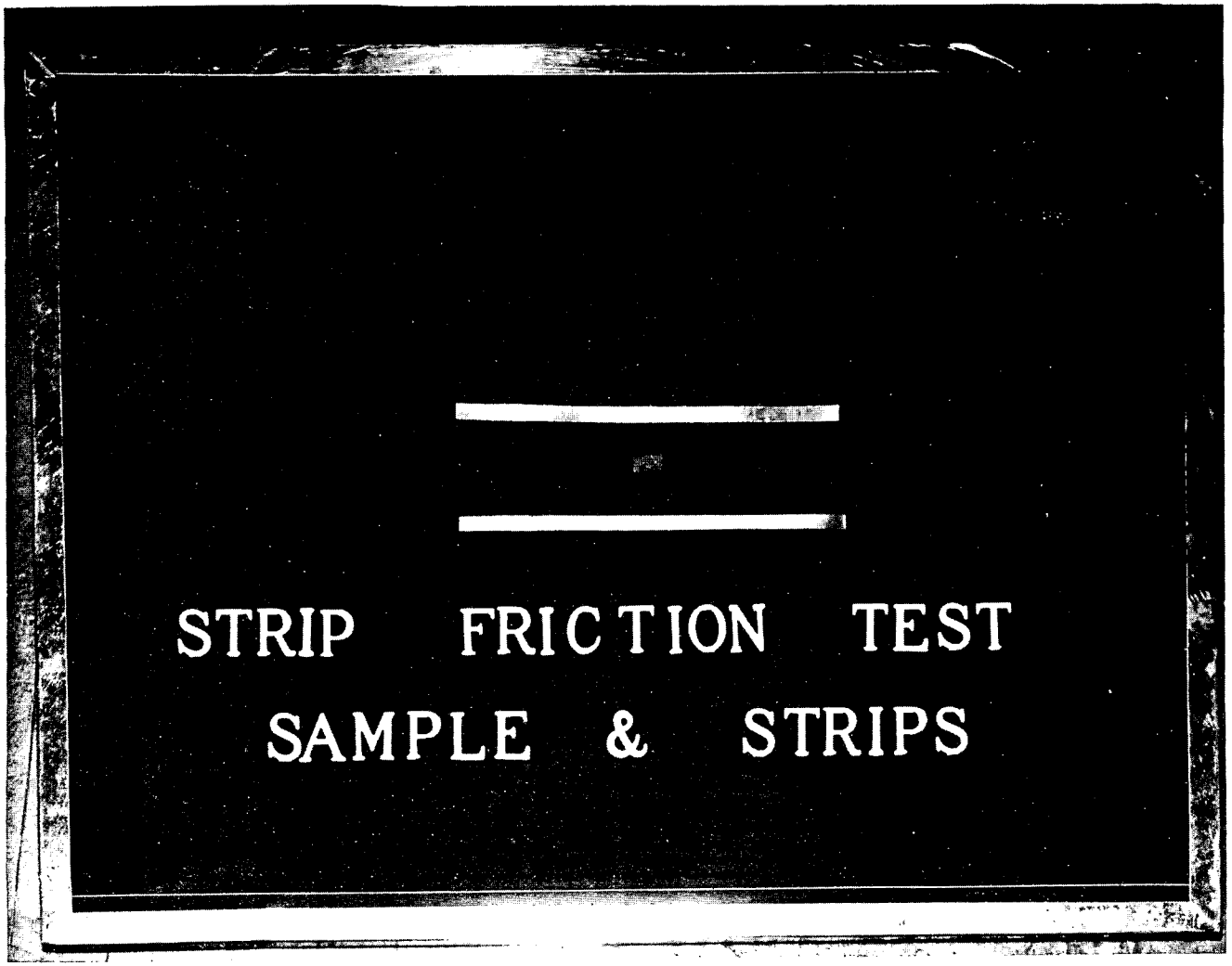

Thiokol CHE WASATCH Figure 5. Strips and Propellant Sample Used on Strip Friction Tester

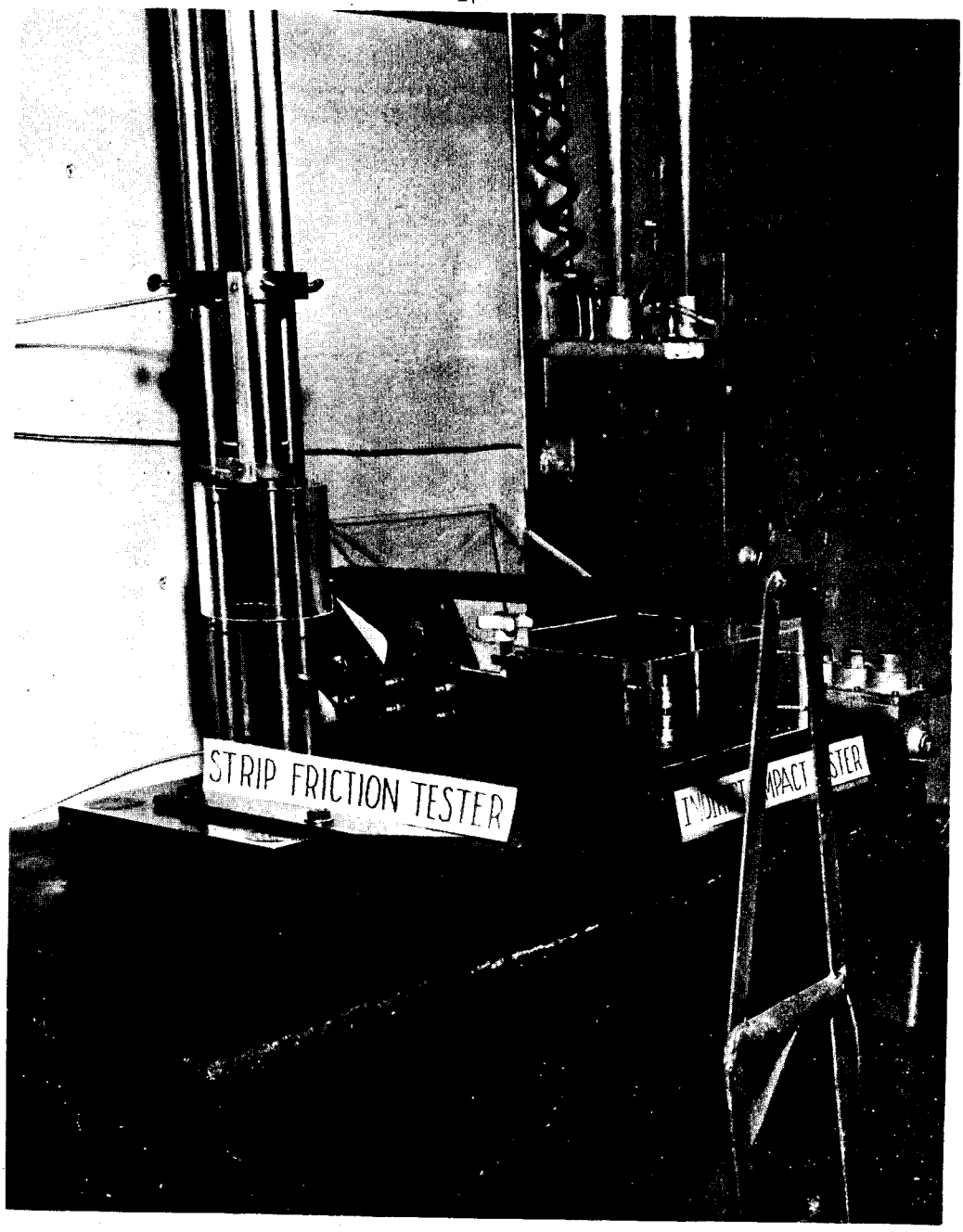

Thiokol CHEMICAL CORPORATION
WASATCH DIVISION • BRIGHAM CITY, UTAH

Figure 6. Strip Friction Tester

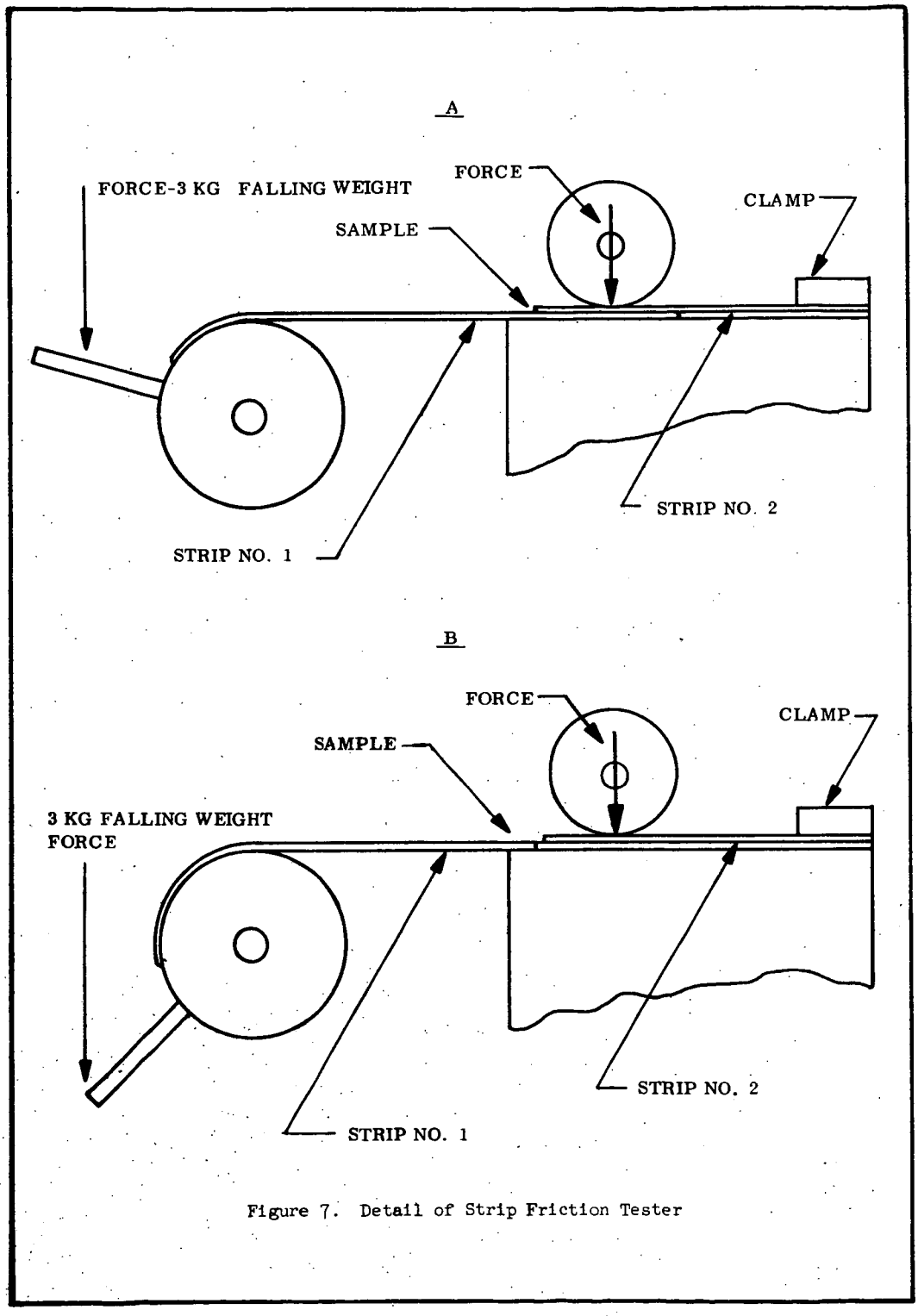

Figure 7. Detail of Strip Friction Tester

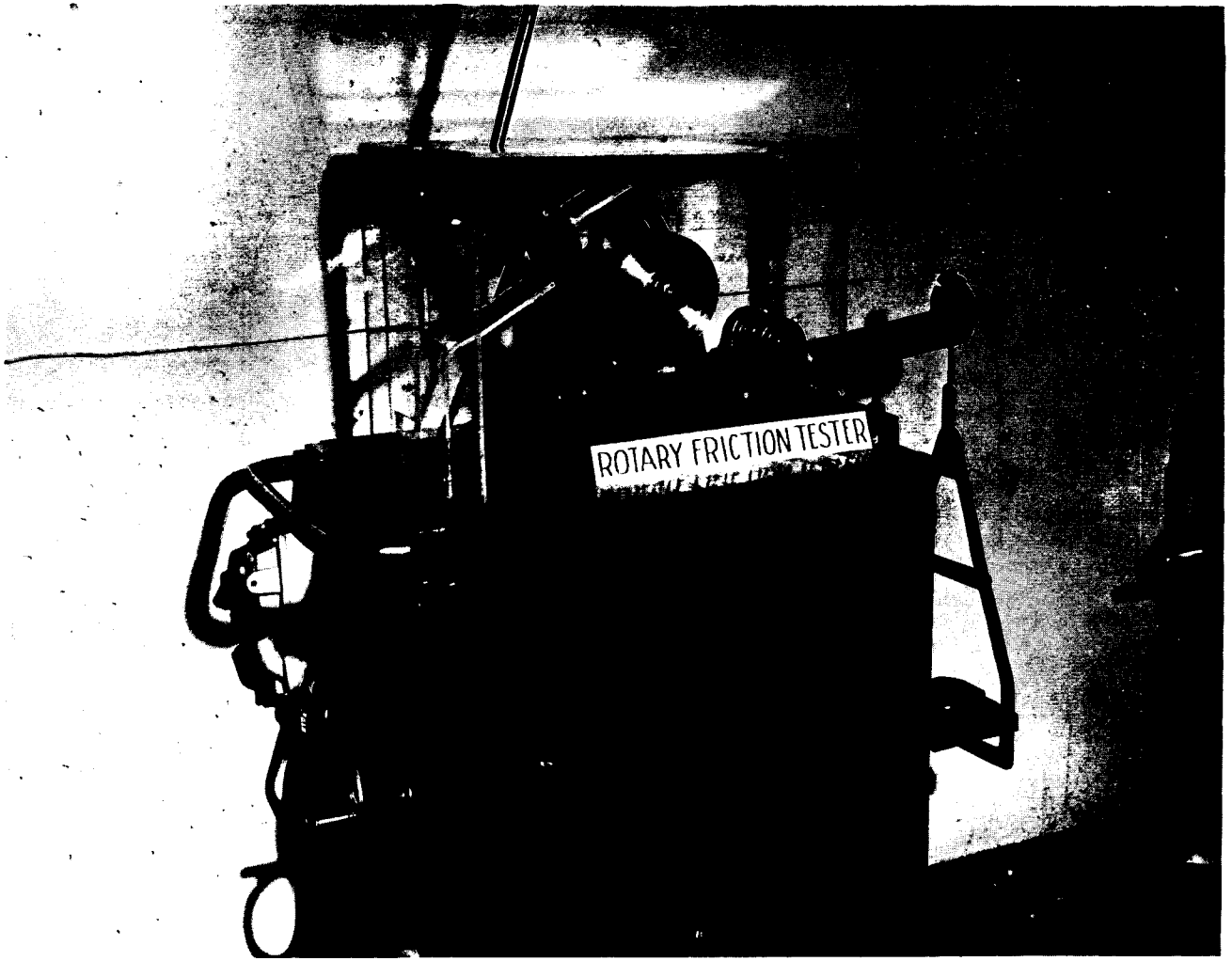

Figure 8. Rotary Friction Tester

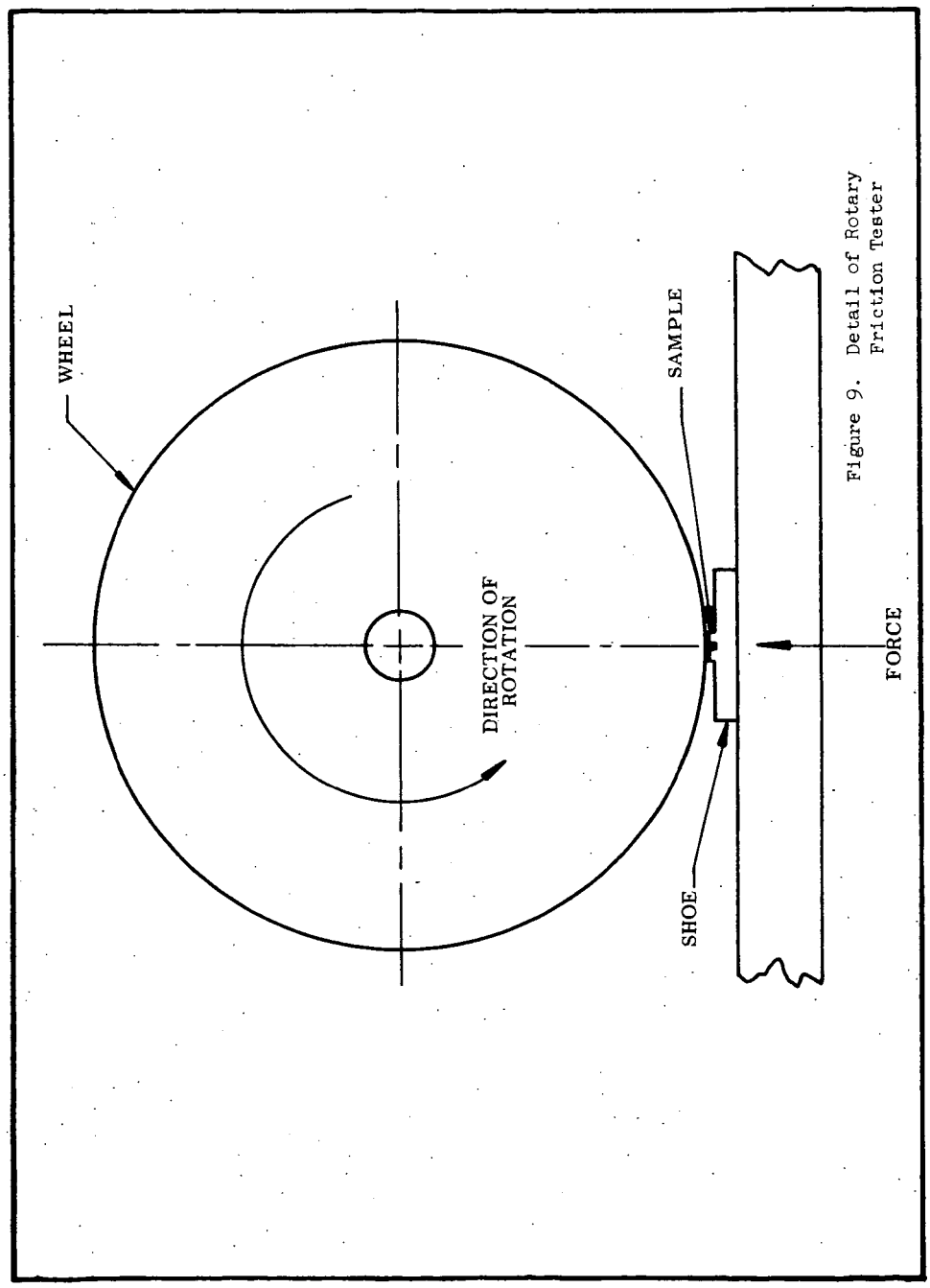

Figure 9. Detail of Rotary Friction Tester

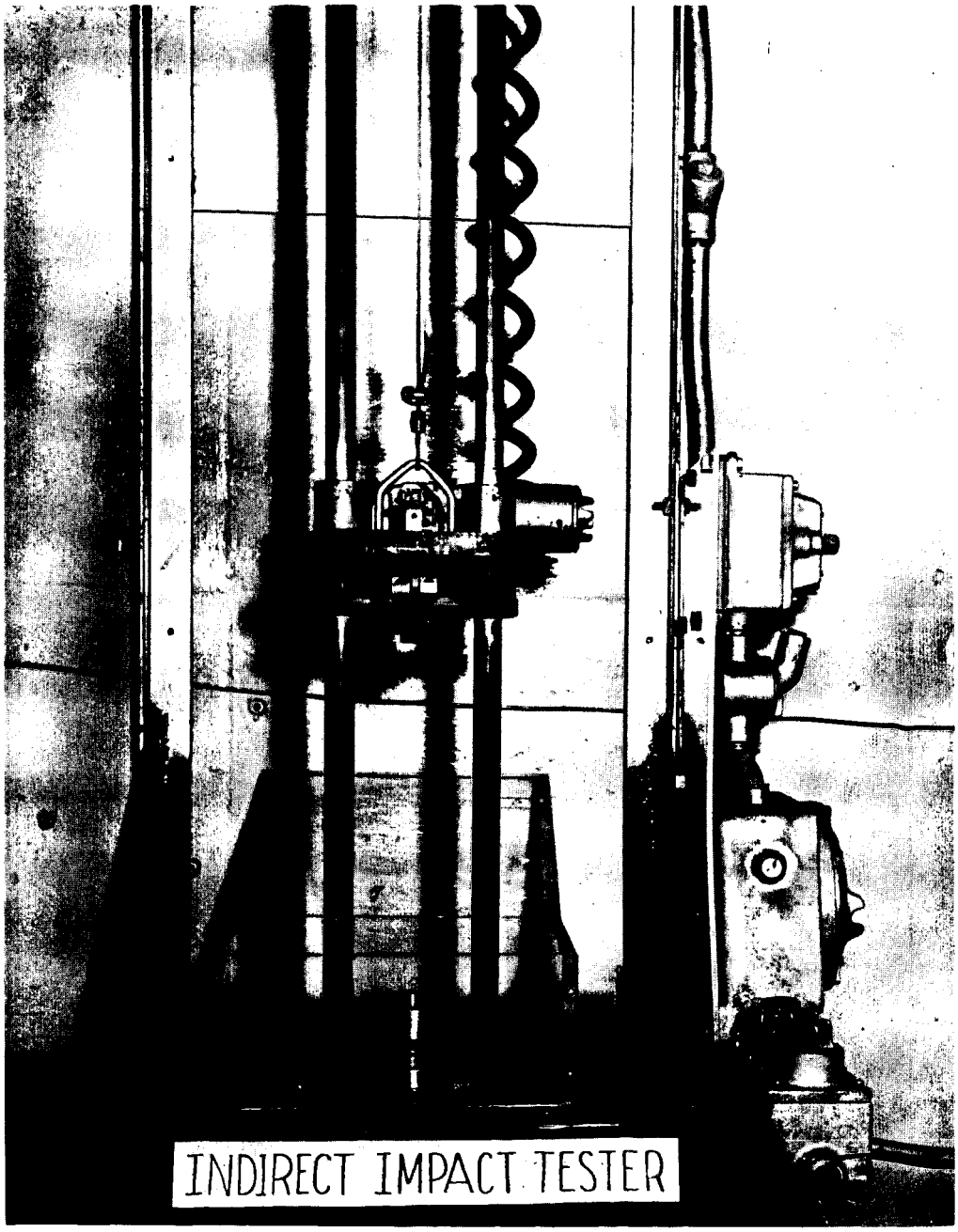

Thiokol WASATCH DIVISION • BRIGHAM CITY, UTAH

Figure 10. Indirect Impact Tester

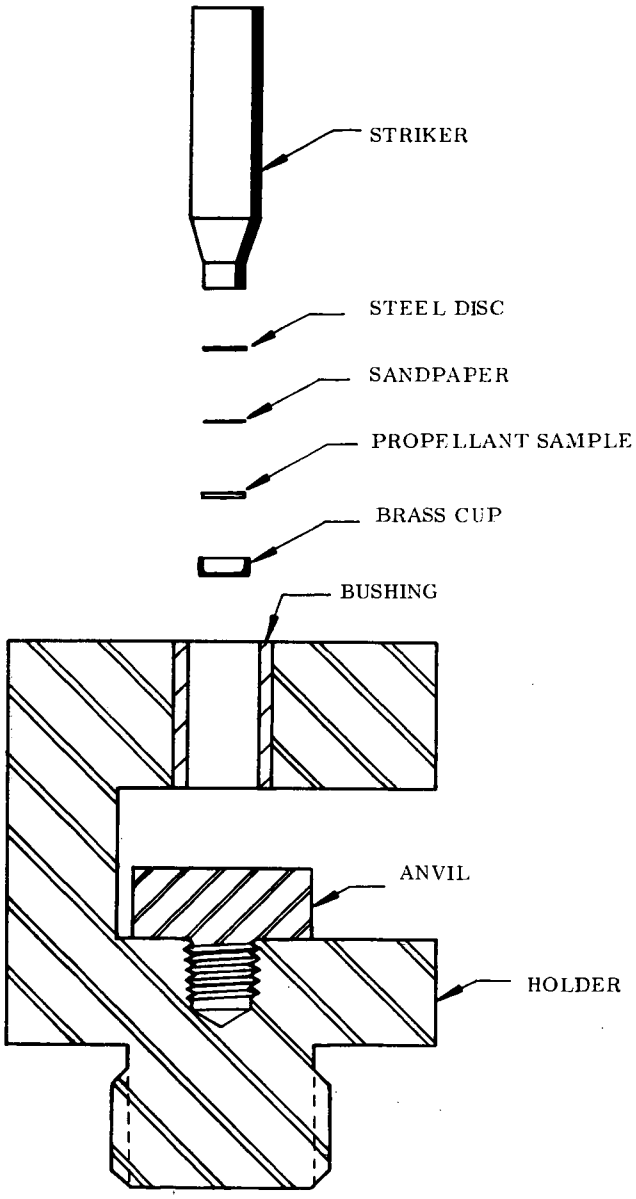

Figure 1

Details of Indirect Impact Tester % Assembly

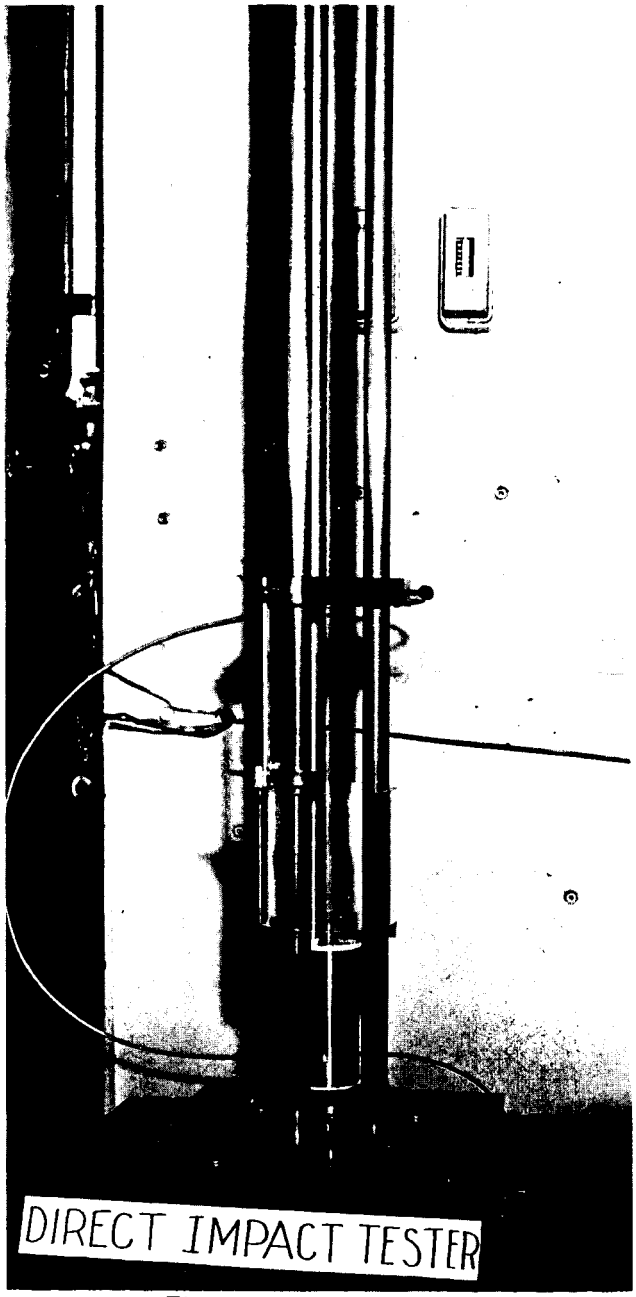

Figure 12. Direct Impact Tester

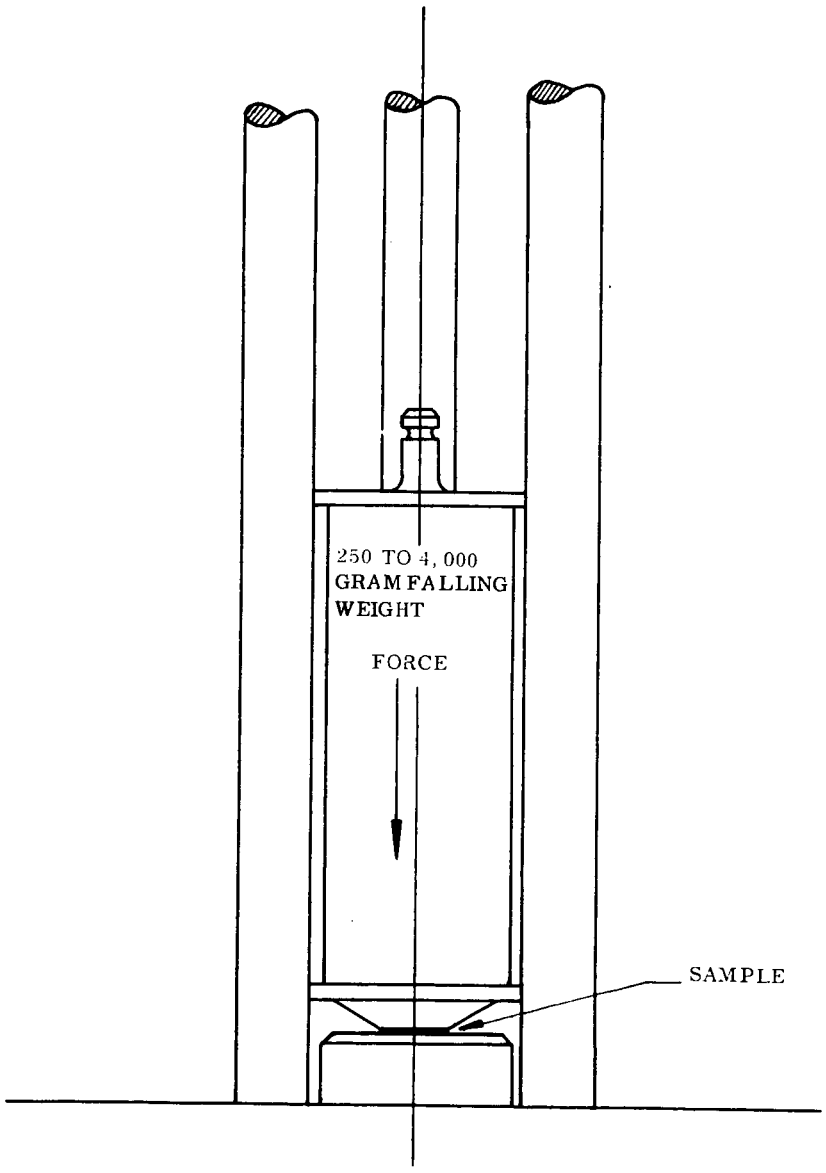

Figure 13

Striker Impacting on Sample
in Direct Impact Test

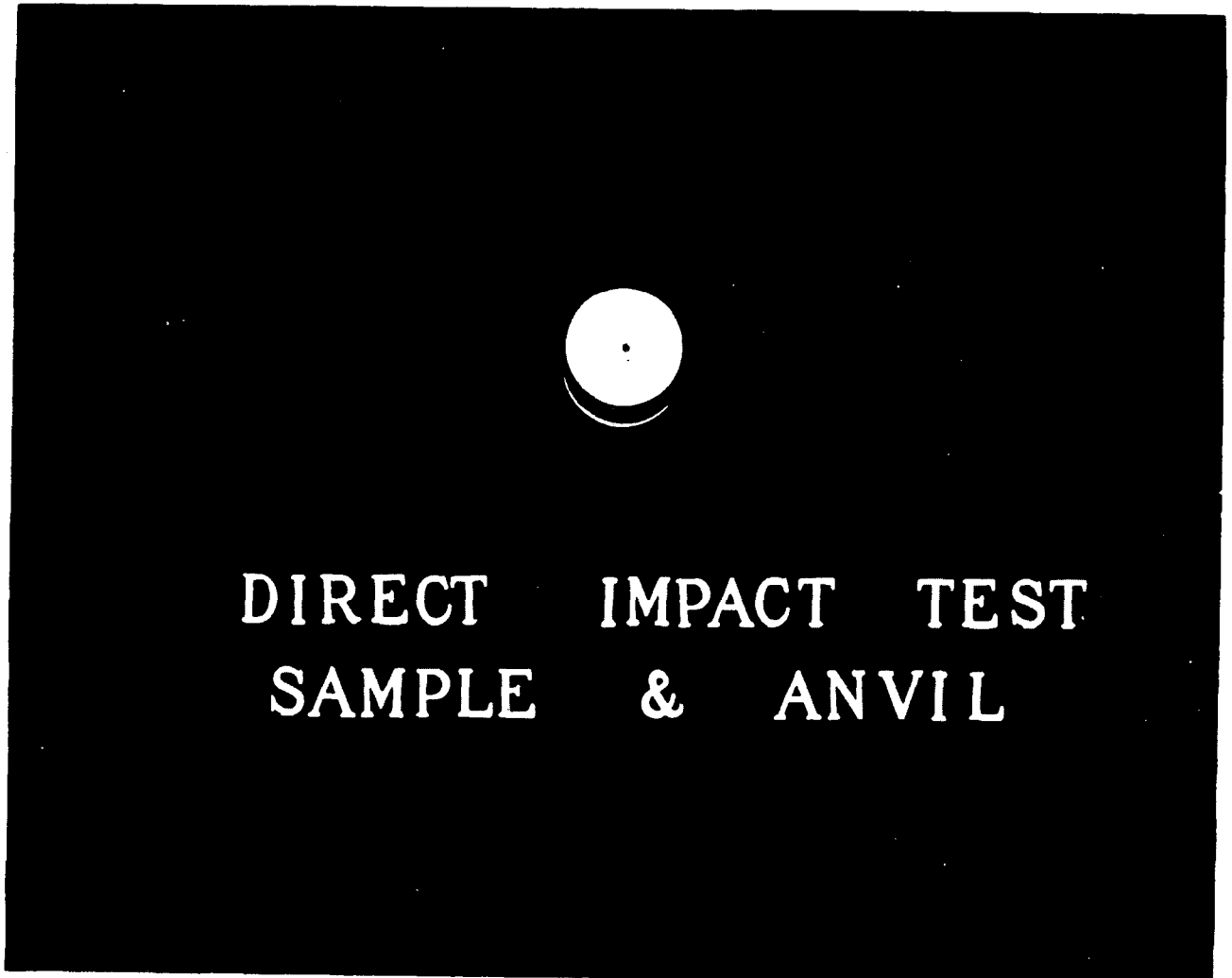

Figure 14. Anvil and Propellant Sample Used on Indirect Impact Tester

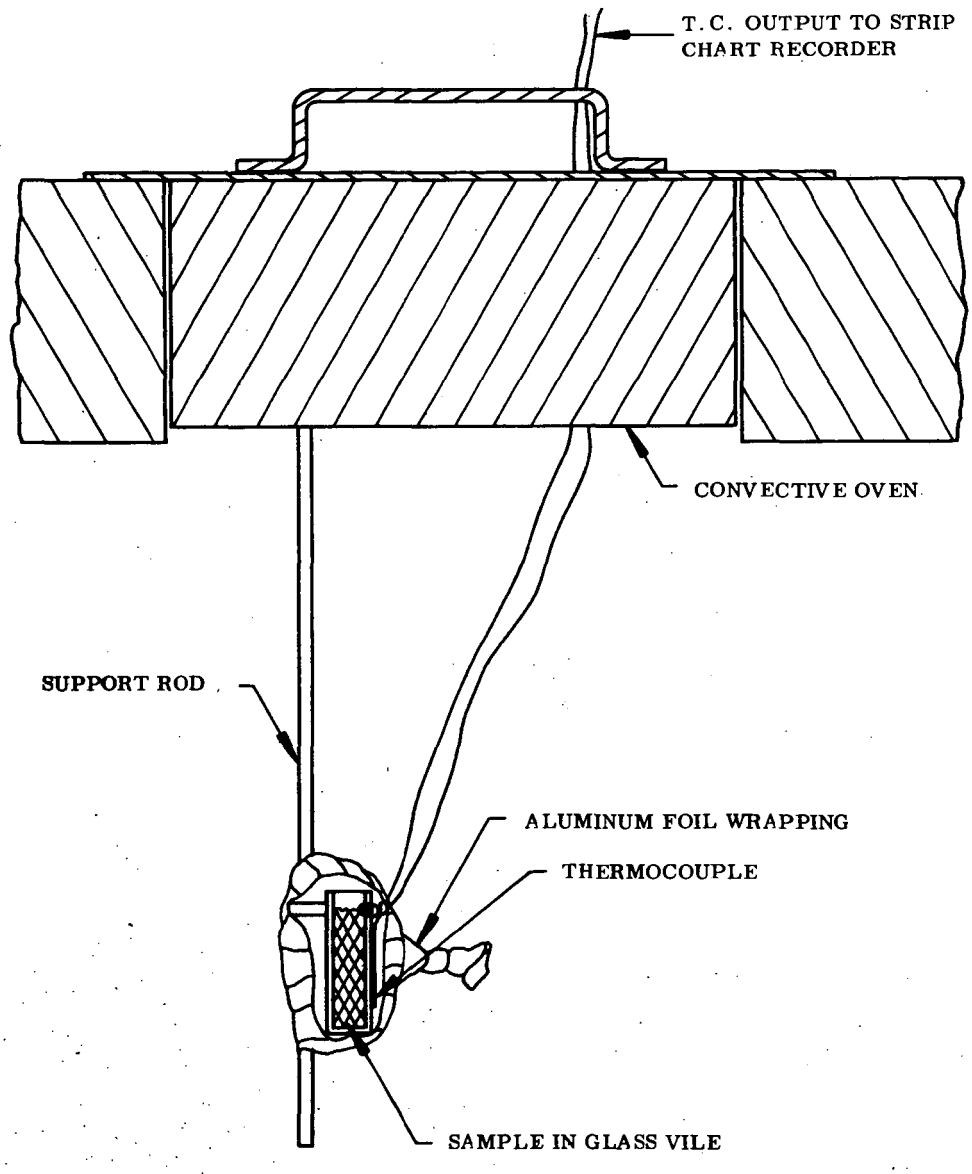

Figure 15

Autoignition Test for Liquid Samples

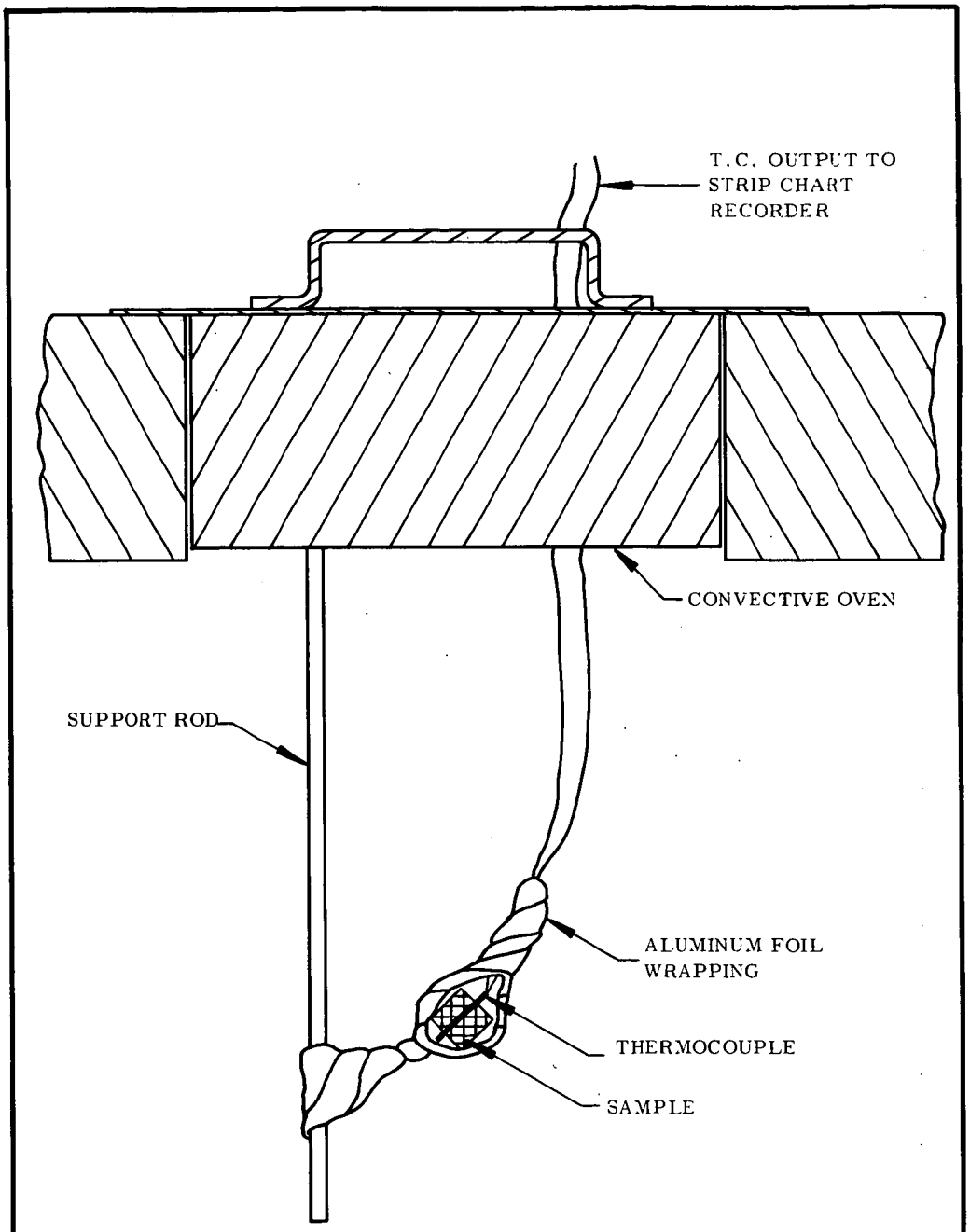

Figure 16

Autoignition Test for Solid Samples

Figure 17. Electrostatic Test Equipment

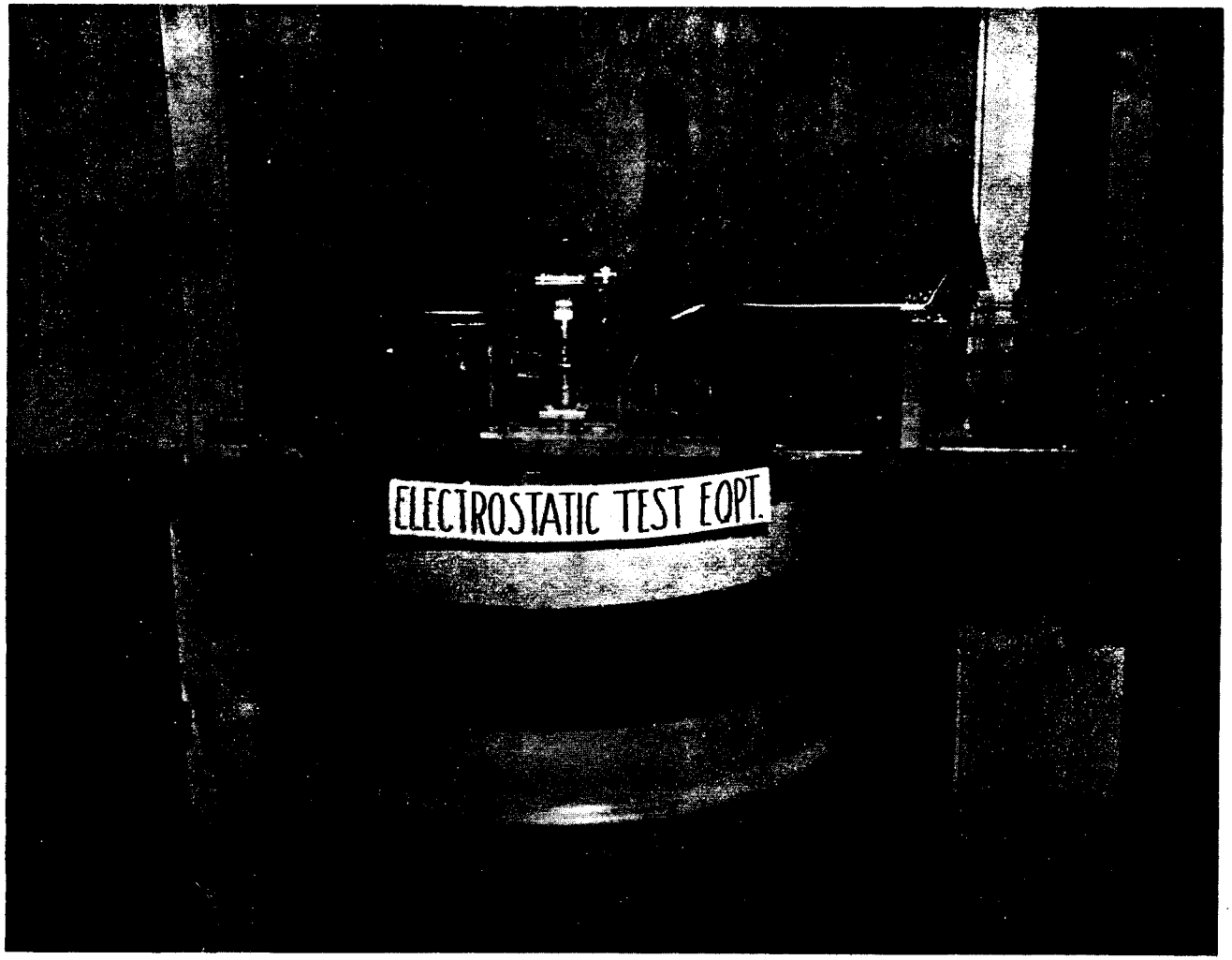

Figure 18. Sample Holder and Switch of Electrostatic Test Equipment

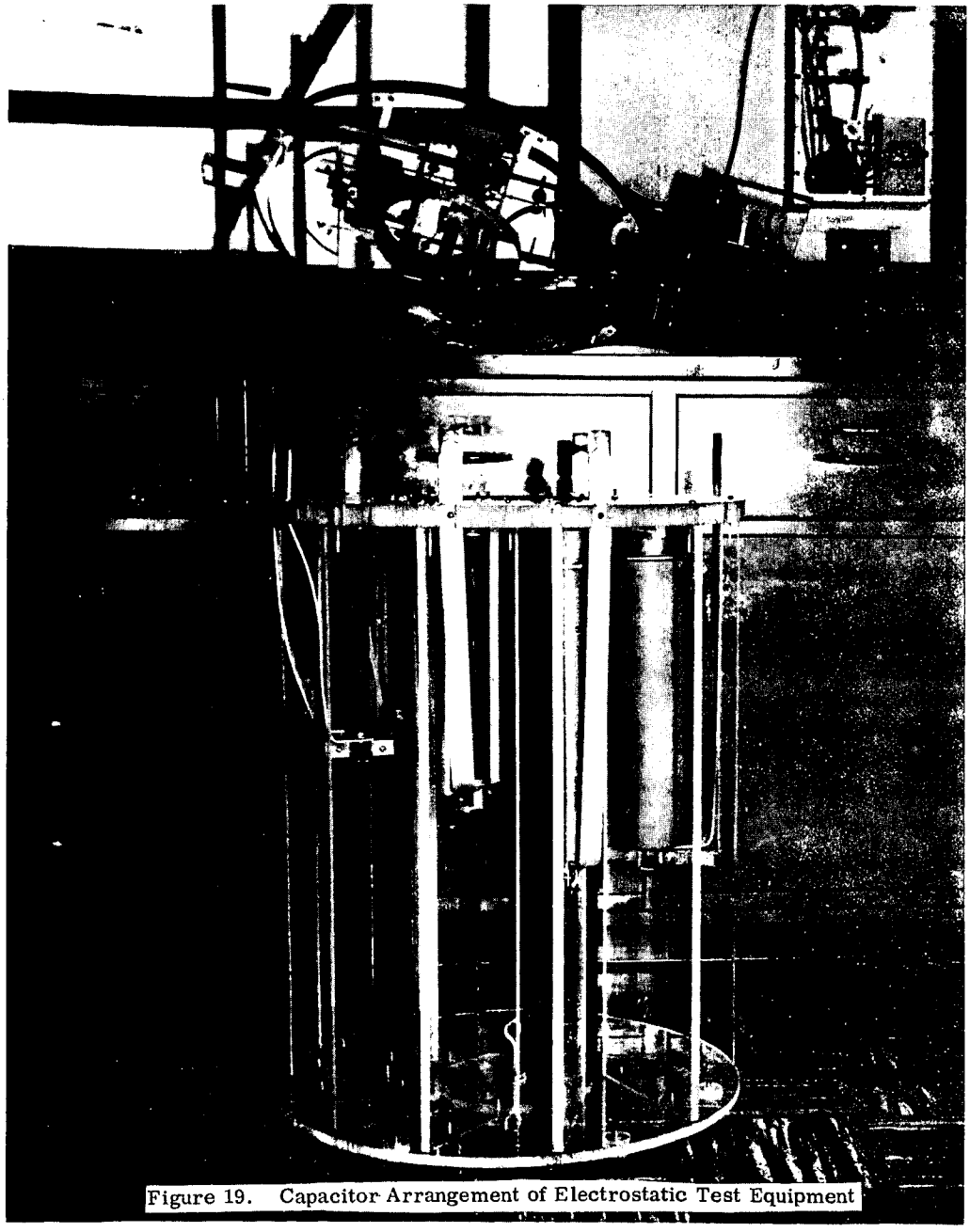

Figure 19. Capacitor Arrangement of Electrostatic Test Equipment

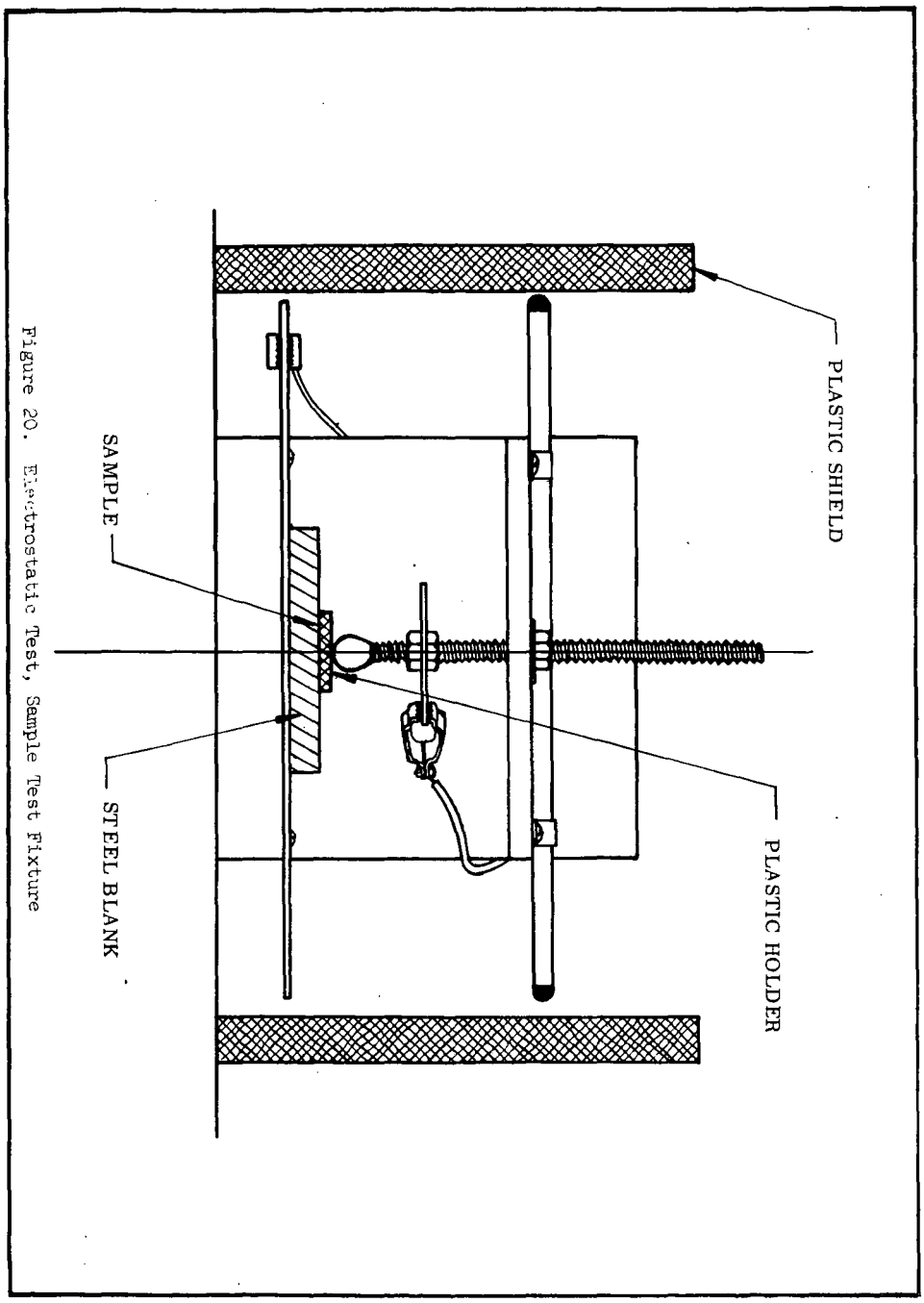

Figure 20. Electrostatic Test, Sample Test Fixture

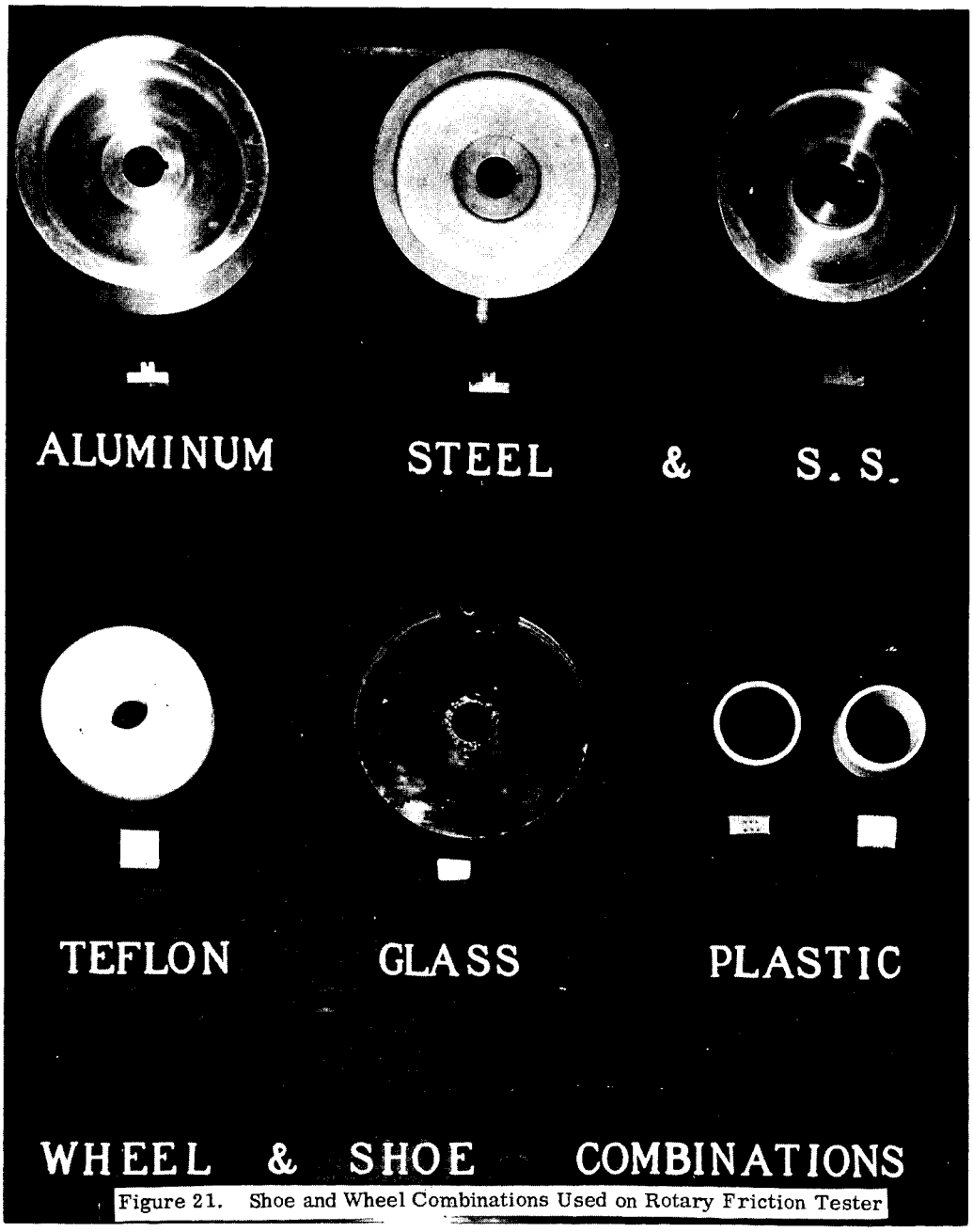

Figure 21. Shoe and Wheel Combinations Used on Rotary Friction Tester

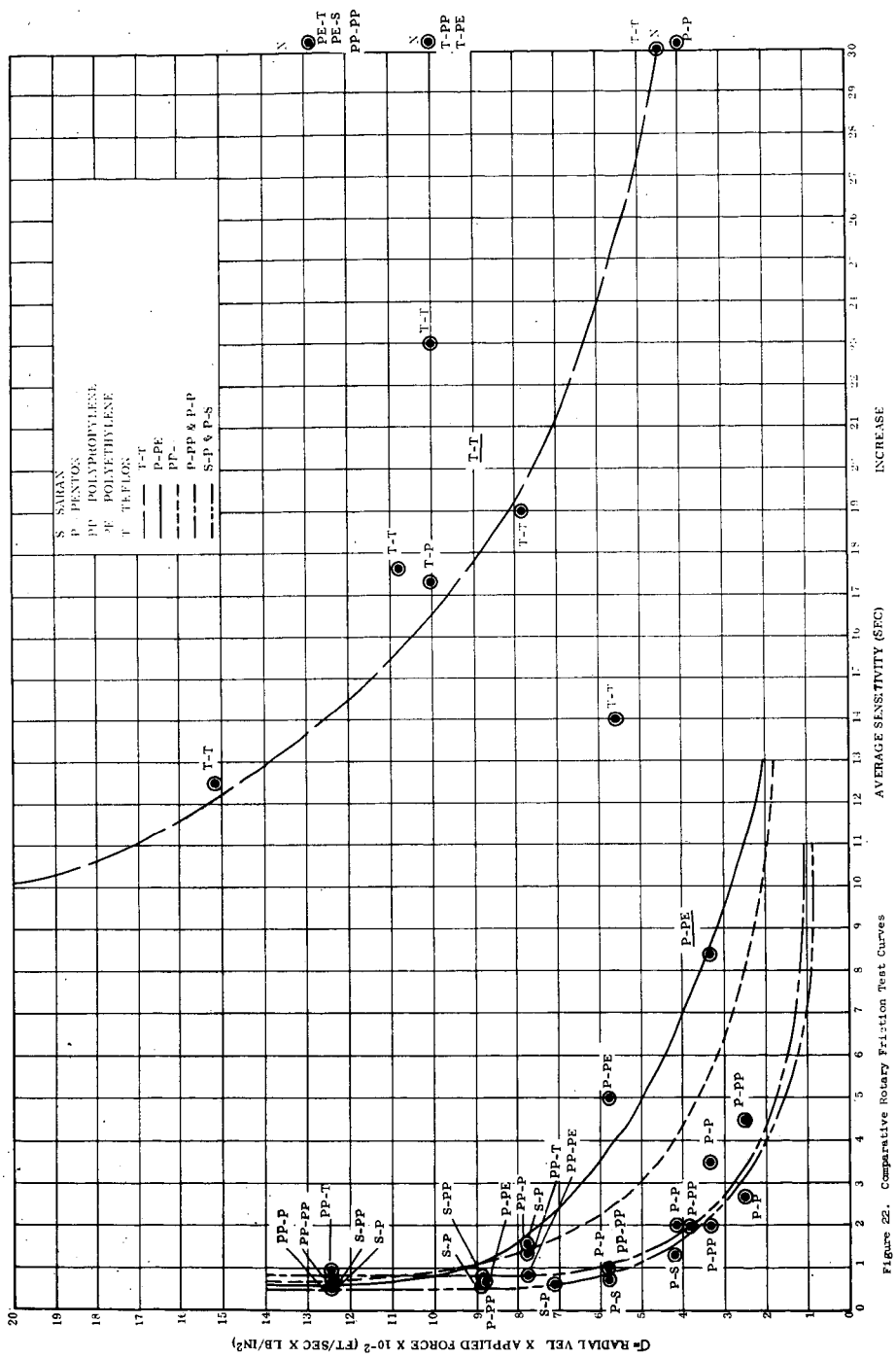

Figure 22. Comparative Rotary Friction Test Curves

Figure 23. Typical Test Data Sheet

PROPELLANT SAFETY TESTS

PST NO.

DATE | WORK ORDER NO. | OPERATOR

THE FOLLOWING INDICATED SAFETY TESTS WERE CONDUCTED ON:

SAMPLE: 001 | EXPERIMENTAL: Y Propellant

CONTAINING

IMPACT SENSITIVITY ESOP NO. 63-2 REV 3 | 50% EXPLOSION CORRECTED INCHES: 12.8 | IMPACT INDEX: 9.4

DROP HEIGHT	1	2	3	4	5	6	7	8	9	10	11	12	13	14	15	16	17	18	19	20	RATIO	PERCENT
16	E	e		e	e			e			E	e		e	e		e				10/10	100
14		E		E	e			E		N		E		E	e		e			N	8/10	80
12			N		E		N		N	n			N		E		E		N	n	3/10	30
10			n			N	n		n	n			n			N		N	n	n	0/10	0

COMMENTS

RESULT CODE

E = EXPLOSIONS
e = ASSUMED EXPLOSIONS
N = NO EXPLOSIONS
n = ASSUMED NO EXPLOSIONS

DETONABILITY
ESOP NO. 63-7 REV 1 THE SAMPLE ~~DID~~ (DID NOT) DETONATE IN A 2 INCH CHARGE DIAMETER.

AUTOIGINITION
ESOP NO. 63-8 REV 1

°F	200	250	300	350	400	450	475	500	525
MIN				No fire 24 hr	64	25	18	15	6

NOTE: 1. A FIVE POUND DROP WEIGHT IS USED IN IMPACT TESTING. THE HMX STANDARD 50% EXPLOSION WAS 30 INCHES.

2. SENSITIVITY COMPARED WITH STANDARD PROPELLANT WITH AN ASSIGNED IMPACT INDEX OF 10. ANY SAMPLE WITH AN IMPACT INDEX LOWER THAN 5 IS IN THE CRITICAL RANGE AND EXTREME CARE SHOULD BE EXERCISED IN MANUFACTURE AND HANDLING.

FORM TC NO. 1444

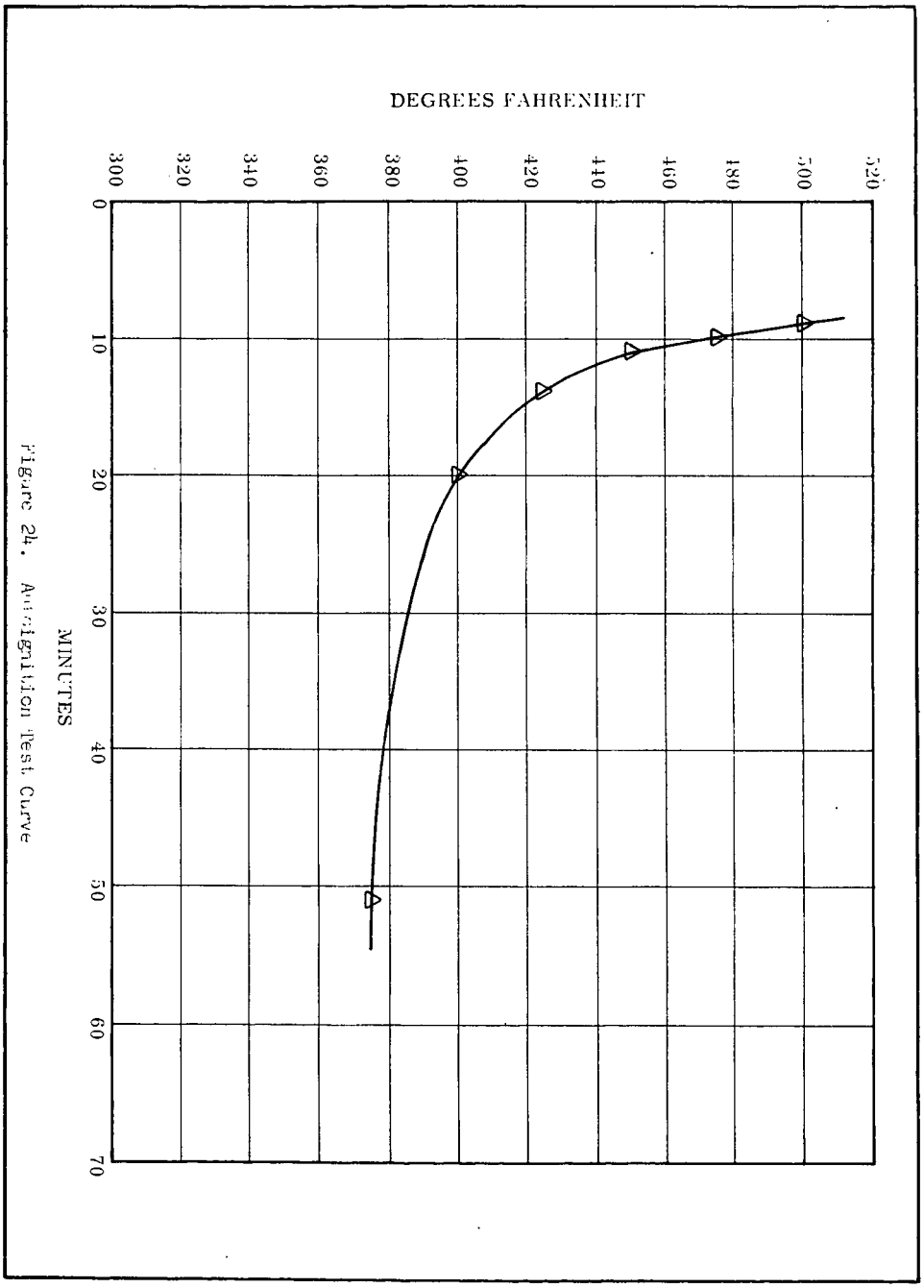

Figure 24. Autoignition Test Curve

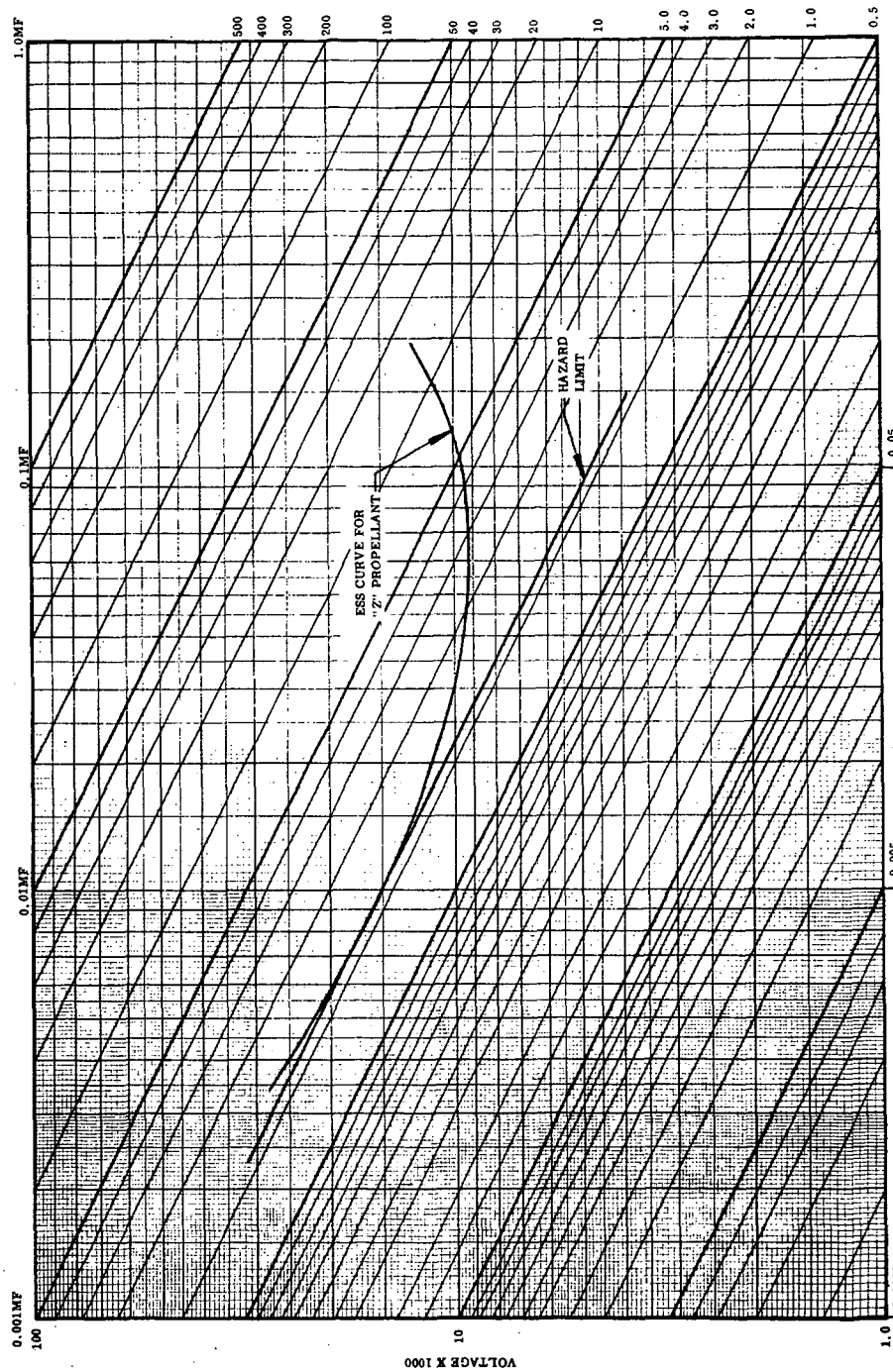

Figure 25. Chart of Voltages, Capacitance and Energy Levels

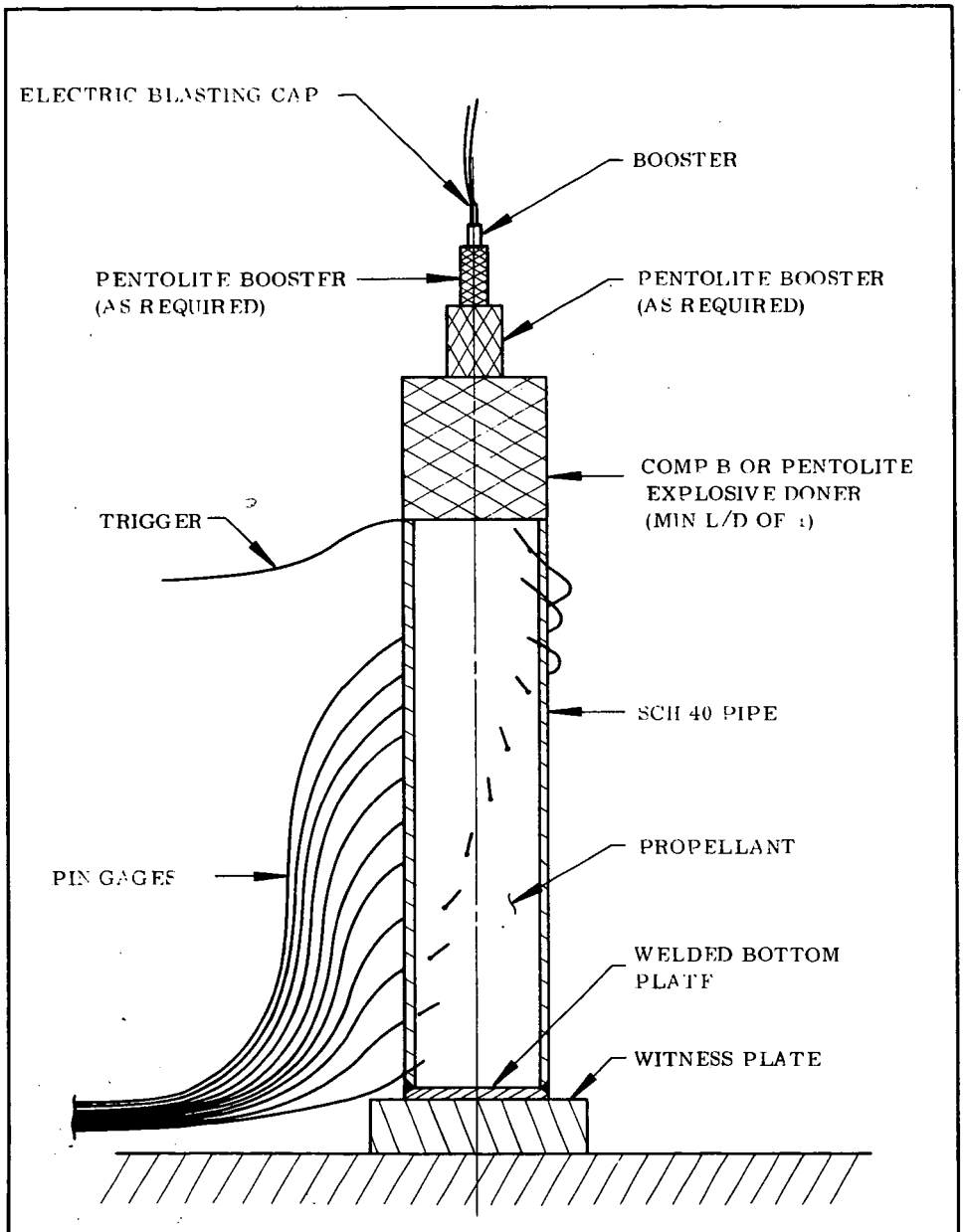

Figure 26. Standard Pipe Detonation Test Setup

SHOCK COUPLING, LOADING DENSITY AND THE EFFICIENCY OF EXPLOSIVES IN COMMERCIAL BLASTING

Robert B. Clay, Melvin A. Cook, & Vernon O. Cook
Intermountain Research and Engineering Company, Inc.
Salt Lake City 4, Utah

Factors considered most important in the blasting of rock are:

1. The maximum available energy A - determined by the heat of explosion Q and the mechanical efficiency, a factor intimately associated with the mode of application, ($A \sim Q$ at highest gas concentrations).

2. The "borehole pressure" p_b which is the maximum pressure attained in the borehole after passage of the detonation wave and before the burden has had time to move or become compressed appreciably. (Owing to the short duration of the detonation wave at any particular point in the borehole, the fact that the explosive may not always fill the borehole completely and the further fact that the burden may not actually "see" the detonation pressure, the borehole pressure is considered more significant than the detonation pressure p_2 in borehole blasting) The borehole pressure is determined by the explosion or adiabatic pressure p_3 and the loading density Δ, or the fraction of the borehole filled by explosive.

3. The physical conditions important in the application of the explosive:

a. The "powder factor" (W_e/W_r), or the ratio of the weight of the explosive to that of the rock being blasted expressed as pounds per ton (more generally in pounds/cubic yard).

b. The relative impedance R, or the ratio of the (effective) impedance of the explosive $(\rho V)_e$ to that of the rock $(\rho V)_r$.

c. The "burden" or "line of least resistance", the spacing between boreholes and the geometry of the borehole pattern.

d. The physical and chemical properties of the rock, most significant of which are possible heterogeneities, such as faulting, prefracture, and greater than micro-scale chemical heterogeneities.

All of these factors need to be carefully considered in the most economical engineering of a blast. It is possible today to give a relatively satisfactory scientific outline of the mechanism of blasting even though much remains to be learned regarding the detailed mechanism. Here is considered firstly an outline of the present status of rock mechanics as it pertains to blasting. The factors pertaining to the most efficient application of blasting agents are then considered followed by a discussion of methods of application to achieve optimum explosives performance.

Rock Mechanics

Rock mechanics is currently a rapidly developing science contributing greatly to a better understanding and consequently the more effective

application of explosives in blasting of rock[1-14]. Basic to the development of the science of rock mechanics were the advances of Goransen[15] and the Los Alamos and NOL groups[16-20] concerning shock wave phenomena and the transmission and reflection characteristics of shocks at interfaces between different media. Basing considerations on this new knowledge as well as new experimental methods of study (ultra-high speed streak and framing cameras and electronic timers) the theory of fracture and failure of solids under impulsive loading by shock waves developed rapidly[6,8,10,19-21]. Also the recent development of accurate methods for measuring the pressures in high intensity shock and detonation waves has made possible more quantitative work in this field[22,23].

Fragmentation of hard rock by explosives occurs predominantly in stress relief and in tension waves created in yet incompletely defined ways by a blast. Tensile fragmentation may really be the only means of breaking the hardest rocks although fragmentation directly by the compression wave may be important in the softer and lower density rocks. Tension waves develop prominently by reflection of compression waves at free surfaces. The shock wave theory of blasting[1-6] therefore has emphasized, perhaps too strongly, the phenomenon of successive "scabbing" by shock wave reflections at free surfaces as described by Rinehart and Pearson[14,19]. Some investigators considered the scabbing process to be practically the only means by which hard rocks are fragmented in blasting, although others[7,8,11-13] described other mechanisms of fragmentation by tensile forces some of which may prove to be of much greater importance than fragmentation by means of release waves reflected from free surfaces. Shock waves from a high explosive separate into the P-waves (longitudinal) and the lower velocity S-waves (shear). The latter is considered to cause appreciable radial fracture[7a,11,12] and possibly close-in shattering of the rock. The predicted "shatter zone" near the borehole does not actually occur in the hardest rocks as seen by the presence of semi-boreholes on a new free face in certain good blasts, namely those that produce good fragmentation and no "back break", i.e., no gross fracture of the rock on the inward side of the borehole.

Kovazhenkov[7b] described an energy theory of rock fragmentation similar to the model wherein rock breakage is a "release of load" or stress relief effect following the temporary transfer of the energy of the blast from the explosive gases into potential energy by powerful compression under the sustained pressure of the products of detonation and the great inertia of the burden. This is the concept described as the "rock bursting" mechanism of fragmentation[13]. The initial shock wave from a detonation carries into the rock generally less than 0.1 (sometimes less than 0.05) of the blast energy, whereas the total energy transferred to the burden by the initial compression of the rock may be a much larger fraction of the available energy of the explosive at some critical early stage of the blast, e.g., the instant the initial shock wave reaches the free surface. Kovazhenkov postulated that there will be numerous means of creating the necessary tensile forces for fragmentation once the rock

has first been excessively compressed. Even a relatively long duration stress relief may be the source of most of the fragmentation. The period of the main over-all relief actually involved in a blast is between 5 and 10 times the period between detonation and the emergence of the shock wave at the free surface. The rise time of the stress wave turns out to be appreciably greater in general than the time required for detonation of the charge, and the fall of the stress wave is even longer. The total time the main rock mass is under compression is several times greater than the stress wave rise time. Moreover, a long-time stress relief fracturing of rock seems to have been amply verified by recent studies by Obert[1a] who found that stressed rock fractures in proportion to the magnitude of the stress by simply cutting it away from the source of stress. One may demonstrate this effect by pressing fine powder at very high pressures; upon stress relief the specimen often fractures into layers perpendicular to the axis of the die. The number of such fractures is proportional to the magnitude of the initial stress. Additional evidence for long time stress relief fragmentation is the "step" (and perhaps sometimes continuous) increase in the velocity of fragments ejected from the free surface of the blast in release wave fragmentation discussed below.

In the shock wave theory of fragmentation three zones of a blast are described: 1) the fragmentation zone beginning at the free surface and extending inward to, 2) an unfragmented zone which in turn is sandwiched between the fragmentation zone and, 3) a shatter zone adjacent to the borehole. The unfragmented zone is, of course, absent when the burden/charge ratio is sufficiently small. (It could not be tolerated in commercial blasting.) The energy theory of fragmentation does not deny the release wave fragmentation zone and the shock wave shatter zone (occurring in porous and soft rocks) but replaces the unfragmented zone by a release of load type fragmentation zone. An unfragmented zone will, of course, occur in blasts with excessive burden/charge ratios, but, when it does, release wave fracturing is usually also absent. Kovazhenkov added (to the predicted conical-shaped crater of a spherical charge, or wedge-shaped crater of a cylindrical charge running parallel to a free face, which he called the ejection zone) a fracture zone associated exclusively with shear type release-of-load or stress-relief fragmentation. Whereas the shock wave theory predicts the conical or wedge type craters, ellyptical craters actually occur due, according to Kovazhenkov, to the fracture zone inside the ejection zone.

A serious difficulty in the shock wave theory is seen in the frontal fragment velocity measurements of Petkof, et. al.[1e] taken from the free surfaces of quarry blasts. By focusing a high speed camera on a given spot on the free surface, they were able to follow the distance-time behavior of particular fragments during the blast. They observed "step" velocity curves for these fragments in which the initial velocity was sometimes only a fraction of the ultimate velocity, velocity apparently increasing discontinuously or in steps due to collision from behind by faster moving fragments. The significance of stepwise

(sometimes fairly continuous) acceleration of frontal rock fragments in a blast may be better appreciated by a brief consideration of the simplified multiple scabbing model of fragmentation by release waves at free surfaces.

A shock wave generally is considered to have a pressure-distance characteristic in which the pressure falls exponentially with distance behind the shock front following an equation of the form

$$p = p_m e^{-t/\tau} \tag{1}$$

where p_m is the pressure at the shock front, τ is the relaxation time and t the time for a given characteristic in the wave to pass a fixed point. (The stress waves observed in blasting are not actually of this type: they exhibit a relatively long rise time of the order of 0.1 to 0.2 m sec or more.) If desired, t/τ may be replaced by αx where α is also a relaxation constant and x the distance behind the wave front at a given instant. The velocity of a fragment ejected from the free surface by reflection of a shock was as a release wave of intensity greater than the tensile strength S_t of the rock is given by the equation

$$V_{ti} = 2p_i/(\rho V)_i \tag{2}$$

where V_{ti} is the free surface velocity of the i^{th} fragment and $(\rho V)_i$ is the impedance of the rock (ρ = density; V = velocity). If a shock wave enters a free face from within the condensed medium with a peak pressure p_m, it has the potential of generating N fracture planes by successive tensile scabbing as the release wave moves back into the solid, N being given simply by

$$N \leq p_m/S_t \tag{3}$$

The upper limit condition corresponds to no losses in the wave due to friction, viscosity and heating of the solid during scabbing. Owing to the exponential decay form of the incident shock wave, which is simply mirrored into the tension region during reflection, a tensile failure should occur in the solid for each increment of decay in the net pressure in the amount $\Delta p = S_t$. The velocity of the first fragment must be the highest because p_i is greatest for this fragment. On the basis of these considerations the only apparent way to account for the step (or continuous) acceleration of a rock fragment scabbed off the free surface in the shock wave theory of fragmentation is for the pressure to rise discontinuously following a decay by at least the amount $\Delta p = S_t$. This would require, in effect, multiple shock waves

of progressively increasing intensity, a condition which seems unlikely, and in fact, is not apparent in the strain wave measurements described by Bureau of Mines investigators. As a matter of fact, the strain waves observed by Atchison, Duvall, et. al.[1] showed relatively long rise time and even longer, more gradual decay. Therefore, the scabs should be much thicker than the observed fragments unless there were to exist much higher frequency wave components with pressure fluctuating in magnitude by at least S_t.

From the magnitude of the pressure at the free face, the observed initial velocity V_t of the fragments at the free surface and the known tensile strength of rock also one may show the relative unimportance of free surface fracturing. The observed initial fragment velocities are in the range 3 to 7 m/sec for the shots studied by Petkof, et. al. Equation (2) thus gives about 0.2 to 0.4 kb for the peak pressure in the shock wave upon striking the free surface. From equation (6) and reasonable values of S_t ($\geq$0.05 kb) one can account for only 4 to 8 successive scabs which is much too small a value to account for the fragmentation observed in normal blasts.

Massive acceleration of the burden provides an explanation for the acceleration of fragments at the free surface following their ejection by release wave scabbing. In the relatively much slower stress relief following a relatively long duration of sustained pressure in the borehole, the whole burden accelerates to reach an ultimate velocity around 30 m/sec, appreciably greater than the free surface velocity of fragments, ejected from the free surface. Calculations were made applying Newton's equation

$$Md^2r/dt^2 = \text{force} \qquad (4)$$

using a method of stepwise integration[20]. Upper limits were computed by assuming idealized perfect confinements, incompressible and suitably prefractured rock to permit uniform acceleration under a hypothetical hemi-cylindrical expansion of the products of detonation perfectly confined within the rock mass. Velocity-time V(t) curves for the burden were plotted along with pressure-time p(t) curves for the products of detonation and the maximum available energy-time A(t) curves for the energy transferred from the hot gases to the burden. Comparison of these velocity-time curves with those observed by Petkof et. al. shows an interesting correlation for times following detonation of the order of 20 to 50 m sec and greater. To account for this seemingly fortuitous order-of-magnitude agreement, let us consider more carefully the actual conditions that may exist in the rock and borehole at various stages of the blast beginning with the instant t_o the initial shock wave reaches the free surface. The $p_m(r)$ relationships that should exist at this instant and at various times thereafter are illustrated in Figure 1, based on an application to the case of hemicylindrical symmetry and a negligible detonation time along the depth interval under consideration. Even after taking into account the compressibility of the burden the

pressure in the expanding borehole should still be an appreciable fraction (evidently about a quarter) of the borehole pressure at the time t_o. One may therefore expect a pressure of about 25 kb (using the highest pressure explosives) for the gases in the borehole at this stage based on an upper limit borehole pressure p_b of about 100 kb. The assumption of an exponential decay in pressure with distance permits one to draw a straight line between the two points p_m^o and $p_m(r_o)$ in log p vs r plots.

Following the initial emergence of the shock wave the release wave moves back into the rock mass at a velocity comparable to that in the initial shock wave. Shocks and release waves thus have time to rebound enough times in say 20 m sec effectively to smooth out pressure and velocity gradients in the rock. Therefore, assuming that the energy associated with fragmentation is, for example, half of the total blast energy, at about 30 m sec after detonation the velocity of the whole burden would be about 0.7 of that computed by equation (4) for the idealized conditions there mentioned. Since half of the blast energy is probably a fair representation to that going ultimately into fragmentation and surface tension in the rock, one thus accounts approximately for the observed acceleration.

Explosives Performance

a. Shock Coupling

According to the theory of "impedance mismatch", the initial pressure p_m^o in the rock next to the borehole is related to the detonation pressure p_2 for a loading density Δ of unity by the relationship

$$p_m^o/p_2 = 2/(1+R) \tag{5}$$

where

$$R = (\rho V)_e/(\rho V)_r \tag{6}$$

Measurements of the strain energy-distance relationships in rock were shown[1b-d] to follow the relationship

$$\epsilon = (W^{1/3}K/r)\exp(-\alpha r/W^{1/3}) \tag{7}$$

where K is a constant considered to be approximately directly proportional to p_m^o and α is a constant independent of the explosive but dependent on the nature of the rock being blasted. Thus K should be a function of the

detonation pressure p_2 and the impedance ratio R. (It is also a function of the heat of explosion since the weight factor W alone does not account completely for the extensive property of the explosive. One must expect also that α is a function of the available energy A or heat of explosion Q because explosives differ sometimes appreciably in available energy. This difficulty may be avoided if W is taken to be the TNT-equivalent weight rather than the actual weight.) Theoretically, one may express these parameters by the functions

$$K = f(p_2, \Delta, R) \tag{8}$$

$$\alpha = g(W_e/W_r, A, R) \tag{9}$$

K and α are, of course, different for each type of rock. If on the other hand, one uses the concept of borehole pressure p_b instead of detonation pressure p_2 for cases in which the explosive does not completely fill the borehole, i.e., $\Delta < 1.0$, equation (8) may be written in the form

$$K = f(p_b, R) \tag{8a}$$

Atchison and Duvall[3] attempted to modify equation (5) based on results with four explosives using measured detonation velocities to compute R and p_2. They suggested the following modified impedance mismatch equation

$$p_m^g/p_2 = (1+N)/(1+NR) \tag{10}$$

They proposed the value N = 5 based on results with these four different explosives. Since two of these explosives were non-ideal their detonation velocities in the borehole should not be the same as the measure (unconfined) velocities. Therefore the basis for equation (10) seems questionable in addition to uncertainties in the meaning of $R(p_2)$. One is, in general, concerned with the application of cylindrical charges. In case the explosive does not completely fill the borehole, there is a serious ambiguity in the use of the detonation pressure p_2 as being truly representative of the pressure applied to the rock and conditions contributing to the impedance ratio R. Even when the explosive fills the borehole completely, there is no assurance that the detonation wave will extend all the way to the rock-explosive interface owing to an observed "edge effect" which does not always disappear even under strong confinement, especially in the most non-ideal explosives. Moreover, the detonation pressure p_2 is very short in duration or transient; the borehole pressure p_b exists unattenuated for a much longer time.

(This is based on an assumed negligible compressibility of the rock; when compressibility is taken into account, the borehole pressure is found also to be relatively transient in favor of a still lower, more sustained pressure.) The (ideal) borehole pressure is identically the adiabatic or explosion pressure p_3 at $\Delta = 1.0$, but at lower loading densities it is related to p_3 by a relation of the form

$$p_b = p_3 \Delta^n \tag{11}$$

where n is a constant between 2.0 and 3.0[20]. Detonation pressure is given (neglecting ambient pressure) by the relation

$$p_2 = \rho_1 DW \tag{12}$$

where D is the detonation velocity, W is the particle velocity and ρ_1 is the initial density of the explosive. Using the (good) approximations $p_2 = 2p_3$ and $W/D = 0.25$, the impedance of the explosive in terms of the explosion pressure for impulse transfer through the end of a detonating charge becomes approximately

$$(\rho_1 D) = (8\rho_1 p_3)^{1/2} \tag{13a}$$

The effective borehole impedance should more properly be related, not to p_2 or p_3, but to the actual pressure which the borehole experiences, namely p_b. Therefore, in the general case borehole impedance should be given by the relationship

$$(\rho V)_e = (4\Delta \cdot \rho_1 p_b)^{1/2} \tag{13}$$

The relative borehole impedance R_b should, therefore, be given approximately by the relation

$$R_b = (0.4\Delta \cdot \rho_1 p_b)^{1/2}/(\rho V)_r \tag{14}$$

for $(\rho V)_r$ in g/cc · km/sec, p_b in kb and ρ_1 in g/cc. The initial peak pressure p_m^o in the rock is then given by

$$p_m^o = 2p_b/(1+R) \tag{15}$$

The (shock) coupling should therefore be related to Δ, or the "decoupling" factor $\Delta^{1/2}$ defined by Atchison[5], by the relationship

$$p_m^o(\Delta) = p_m^o(1)\cdot\Delta^n \left[1+R(1)\right] / \left[1+R(1)\cdot\Delta^{(n+1)/2}\right] \qquad (16)$$

where R(1) and p_m^o are values of the relative impedance and initial peak pressure in the rock at $\Delta = 1.0$. Taking $n = 2.5$ one finds that for $R(1) \ll 1.0$ "decoupling" should vary as $\Delta^{2.5}$; for $R = 1.0$ it should vary as $2\Delta^{2.5}/(1+\Delta^{1.75})$ and for $R \gg 1.0$ it should be given approximately by $\Delta^{2.5}\, R(1)/\, 1+R(1)\Delta^{1.75} \approx \Delta^{0.75}$. Based on upper and lower limits of R, one thus expects p_m^o to vary within the limits $\Delta^{0.75}$ and $\Delta^{2.5}$ for values of Δ not too far below unity.

Studies of decoupling in limestone by Atchison[5] showed it to vary about as $\Delta^{0.75}$, and comparable results were obtained in granite by Atchison and Duvall[3]. On the other hand conditions employed in these investigations were such that results should have varied as $\Delta^{2.0+}$ because $R_b < 0.5$ in all cases considered by them.

b. Energy Coupling

In the theory of energy coupling the impedance mismatch equation is not applicable; if one neglects compressibility, the borehole pressure p_b will be the actual pressure applied on the inner (borehole) boundary at all stages prior to emergence of the shock wave into the free surface of a properly loaded blast. This will then be the initial pressure p_m^o in the rock. In the idealized case, therefore, the energy theory predicts that the (effective) decoupling should vary also approximately as $\Delta^{2.5}$. The observed decoupling factor $\Delta^{0.75}$ may, however, be accounted for in the energy theory by taking into account rock compressibility.

The strain energy density ϵ in the compression of rock is approximately $\bar{\beta}p^2/2$, where $\bar{\beta}$ is the average compressibility at pressure p. Let us assume a pressure distribution function for rock compression in cylindrical expansion of the compression wave in a long borehole to be given by the equation

$$p_m = p_m^o e^{-a(t)x} \qquad (17)$$

where $x = r/r_o$ and $r_o = V_r t_o$. The constant a is given by the equation

$$a = \ln p_m^o / p(r_o) \qquad (18)$$

The total energy of compression is then obtained by integrating over the whole volume of the rock under compression giving

$$E_T = p_m^{o2}\bar{\beta}\pi r_o^2 \cdot L/8a^2 \qquad (19)$$

The maximum available energy density of an explosive at its maximum density is approximately p_3[24]. Therefore, for a charge of $\Delta = 1.0$ and $\rho_1 = 1.5$ g/cc one obtains, using equation (18) and this approximation for A, the result

$$r_o/r_b = 4.6(E_t p_b/\rho_1 W_e A\beta p_m^{o2})^{1/2} \log p_m^o/p_m(r_o) \qquad (20)$$

for the ratio of the burden to the borehole radius.

At r_o it has been observed that $p_b/p_m(r_o) \sim 500$ for blasts employing an explosive of density around $\rho_1 = 1.5$ g/cc, and borehole pressure $p_b \doteq 100$ kb ($\Delta = 1.0$) corresponding to the best modern blasting agents. Since E_T may be known as a function of p_m^o from the theory of the maximum available work function A (cf. Figure 11.6, ref. 20) one may therefore use it to obtain, via equation (20), the ratio p_m^o/p_b. For $E_T/AW_e \sim 0.5$, for example, $p_m^o \sim 0.25\ p_b$ as seen in the above reference. Then equation (20) becomes roughly $r_o/r_b = 25 \log p_b/4p(r_o)$. Taking $p_b/4p_m(r_o) = 100$ one then finds $r_o/r_b = 50$. This agrees essentially with the observed distance to the free surface of a properly loaded blast. It thus justifies qualitatively the p(r) relations depicted in Figure 1 and shows that a large portion of the energy of the blast is, indeed, stored temporarily as compression energy in the rock at the instant that fragmentation begins at the free surface. Of course, half of this energy then is in the region back of the borehole, but in the subsequent stress relief this energy is partially, at least, transferred to the other half of the blast to assist in further stress relief fragmentation.

The above considerations apply in the case of an ideally loaded blast. Let us now consider conditions existing (a) in an underloaded blast (excessively low W_e/W_r) and (b) in an overloaded blast (excessively high W_e/W_r). In considering poorly loaded blasts, note that $a(t_o)$ will not be changed if all conditions are the same except that the burden has been increased (a) or decreased (b). However, p_m at the free surface will be different in each case.

Let us consider the case in which all conditions of a blast are the same as those depicted in Figure 1 except that the burden is 20 percent greater ($r_o' = 1.2\ r_o$). At the time t_o after the blast, therefore, the rock in the region between the borehole and the distance r_o will be under identically the same pressure as in the case in which the free surface is encountered at r_o (dotted line, Figure 2). Since no free surface is encountered at this stage there is no fragmentation except in the borehole fracture zone. Instead, the compression wave must continue on the additional time $t_o/5$ before fragmentation can commence. When it reaches the free surface there has been considerable attenuation of compression throughout the

burden. Moreover, the amplitude of the wave when it reaches r_o' may have dropped below that required to produce release wave fragmentation. Stress relief then occurs much more gradually so that fragmentation in the stress-relief zone becomes much less extensive. This type of shot produces excessive back break owing to stress relief then tending to become symmetrical around the borehole, and fragmentation is poor.

Conditions will be opposite in case (b). Figure 3 depicts conditions for the case in which again all conditions are identical with those in Figure 1 except that the burden is now 20 percent too small. Free surface fragmentation then begins at $t_o'' = 0.8\ t_o$ at which point the pressure $p_m(r_o'')$ is considerably higher. This results in greater release wave fracturing and in ejection of rock at much higher velocity; the burden experiences excessive "throw". The stress-relief zone fragmentation becomes excessive at $r_o'' = 0.8\ r_o$ owing to more sudden release from higher pressures.

Consider now the case of a blast in which all conditions are the same except that $\Delta = 0.75$ and, therefore, $p_b \sim 0.4\ p_3$. That is, the "powder factor" and the "burden" are the same as in Figure 1, but the borehole is a third greater in volume than in the blast depicted in Figure 1. The result of the blast is almost the same as that depicted in Figure 2. That is, decoupling to the extent $\Delta = 0.75$ has nearly the same effect on fragmentation as increasing the burden about 20 percent. This situation is depicted in Figure 4.

The above illustrates the theory qualitatively; in a quantitative application there are three unknowns in equation (20), namely $E_T(t)$, $p_m^o(t_o)$ and $p_m(r_o)$ which must be defined. They are interrelated through the theory of the maximum available energy A because in reversible expansion, A is a single-valued function of the specific volume v of the gaseous products of detonation. Any loss of energy from the gases to the burden is associated with an increase in the specific volume $\Delta v(t)$ of the gases in the borehole. By knowing $\Delta v(t)$ one may then compute A(t) by the method given in ref. 20, p. 267. (The ratio E_T/W_eA in equation (20) is identically A(t)/A, where A(t) is the work done on the burden per unit weight of explosive during the time t and A is the ultimate work per unit weight of explosive over the whole period that the gases are able to do work on the burden.) One is thus primarily interested in $\Delta v_b(t_o)$, the increase in specific volume of the borehole at t_o. This may be obtained from the equation

$$W_e \Delta v_b(t_o) = -W_r \bar{\Delta} v_r = \int_o^{r_b} \int_o^{p_m} 2\pi r \beta \, dp \, dr$$

giving

$$\Delta v(t_o) = 2\pi r_o^2 \, L \bar{\beta} p_m^o / W_e a^2 \qquad (21)$$

where minus the total increase in volume of the borehole at time t_o has

been equated to the total decrease in volume of the rock due to compression at this particular stage of the blast.

Since p_m^o may be derived from p_b and $v_b(t)$ once $A(t)$ is known the only remaining unknown in equation (20) is $p_m(r_o)$. For a properly loaded blast $p_m(r_o)$ must be large enough to permit fragmentation to begin at the free surface, i.e., it must be several times greater than S_t. From the Bureau of Mines studies $p_m(r_o)$ for a good blast is $N_i S_t$ where $N_i \sim 4$. For example, for granite $p_m(r_o) \sim 0.25$ kb and $S_t = 0.075$ kb. If a borehole in granite is loaded with an explosive of $p_b = 100$ kb one then finds, by an iterative simultaneous solution of equations (20) and (21), that $p_m^o \sim 25$ kb and $p_m^o/p(r_o) = e^a \sim 100$, giving $a \sim 4.6$. Therefore $\Delta v_b(t_o)/v_b \sim 3$; the borehole apparently has increased in diameter by approximately a factor of 2.0 (Figure 5) at the instant (t_o) that the shock wave reaches the free surface in a properly loaded shot in granite using an explosive with $p_b = 100$ kb.

In applying the stress-relief theory here outlined to various types of rock to be blasted with different explosives one should first determine more accurately the ratio $p_m(r_o)/S_t$ for best results. Then p_m^o, the ratios $p_m^o/p(r_o) = e^a$ and $A(t_o)/A$, and $\Delta v_b(t_o)$ may be obtained with good accuracy by an iterative procedure. This should permit one to predict optimum loading ratios W_e/W_r for the various combinations of rock and explosive. It will thus be necessary in the further development of the theory to provide more reliable data on $p(r_o)/S_t$ and $\bar{\beta}$ for various rocks and on p_b, A and p_m^o for various explosives.

c. Explosives

The parameters of equation (17) have a complex dependency; they depend ultimately not only on the burden, spacing, borehole diameter and depth and the properties of the rock, but also on loading density Δ and the explosive density ρ_1 (or pressure) and A. To emphasize the part played by the explosive let us express $p_m^o(t)$ and $a(t)$ in the form

$$p_m^o(t) = (\Delta \cdot \rho_1)^n \, f(\phi_r, X) \tag{23}$$

$$a(t) = g(\phi_r, X)/A^m \tag{24}$$

where $n \sim 2.5$, $m \sim 1/3$, f and g are functions of the physical and chemical properties of the rock ϕ_r, and on the geometrical factors X (burden, spacing and borehole diameter and depth). Thus, maintaining f and g constant p_m^o is found to vary essentially as $(\rho_1 \cdot \Delta)^n$ and $\underline{a}$ as $A^{-1/3}$, which are the important factors pertaining to the explosive irrespective of whether one accepts the shock wave theory, the energy theory or both.

Prior to the advent in 1955 of "prills and oil" (the 94/6 prilled ammonium nitrate/fuel oil[13]) commercial explosives comprised principally dynamites (based on nitroglycerin) and the NCN ("nitro-carbo-nitrate") explosives comprising essentially fuel-sensitized ammonium nitrate. The average density in these products ranged from 0.6 to 1.4 g/cc, but owing to their application in cartridge form Δ was generally appreciably below 1.0. Thus seldom was their $\Delta \cdot \rho_1$ product much above that for prills and oil in which ρ_1 is only 0.85 g/cc, but Δ is generally 1.0; it is generally used in bulk form such that it always fills the borehole completely. A/A_o for prills and oil is close to unity and therefore also about the same as for an average commercial explosive, A_o being the maximum available energy of TNT or the "TNT equivalent". In retrospect it is thus understandable that prills and oil, generally previously regarded by explosives technologists as an inferior blasting agent, has actually performed far above expectations. Owing to its low cost, roughly only a quarter that of an equal (weight) strength dynamite, and the great importance of Δ on performance, prills and oil has replaced well over half of the dynamites and NCN explosives previously comprising the commercial market in America.

Shortly after the discovery of prills and oil the "slurry" explosives were discovered by Cook and Farnam[13,25,26]. Slurries are based on thickened or gelatinized aqueous ammonium nitrate solutions; they differ in type depending on the sensitizer employed in them, types being:

a) Coarse TNT and TNT-aluminum slurries

b) Smokeless powder slurries

c) The NCN slurries in which the sensitizer is a non-explosive "fuel", e.g., aluminum, emulsified fuel oil, etc.

Slurries are characterized by their high density and fluidity which makes it relatively easy for them to attain $\Delta = 1.0$ in the borehole. The $\Delta \cdot \rho_1$ product is thus generally 1.5 to 2.5 times greater for slurry than for prills and oil. The A/A_o ratios of slurries range from 0.85 to 1.5, those with the highest aluminum contents developing borehole pressures about five times greater and A/A_o values up to 1.5 times greater than for prills and oil.

On an equal strength basis the cost of slurries averages about half to two-thirds that of the older commercial explosives and about twice to three times that of prills and oil.

By virtue of the much higher $\rho_1 \cdot \Delta$ of slurry compared with prills and oil and the older commercial explosives, and excellent new methods for

economic, rapid and safe loading of them at $\Delta = 1.0$ they represent a major advance in the commercial explosives field and should not only replace dynamites and other explosives in wet hole and underwater blasting where prills and oil is inapplicable, but may even replace much of the prills and oil in dry hole blasting. Already slurries are being produced in quantities exceeding 10^8 pounds per year in the U.S.A., Canada and foreign countries.

Novel Loading Method

Until recently the importance of $\Delta \cdot \rho_1$ was not fully appreciated, operators frequently using larger and larger boreholes to obtain their necessary high powder factors rather than taking full advantage of best methods for maximizing $\Delta \cdot \rho_1$. With the current much better appreciation of coupling and high borehole pressures many are turning to the slurry explosives to achieve high powder factors in blasts of high burdens without having to increase borehole diameters. In fact, some are even now contemplating reduction in borehole diameters. The savings resulting from this more scientific application of explosives are not only reduced explosives and drilling costs, but also reduced shovel, crushing and grinding costs, and sometimes also large increases in the rates of production.

Successful bulk loading units and field mixing methods for prills and oil developed rapidly after its introduction[13,27]. On the other hand, considerable research was required for the development of bulk handling methods for slurries; field mixing and loading proved much more difficult with slurries because 1) slurries with suitable properties (water resistance, plasticity and high density) require much more accurate control in their formulation, and 2) they are usually applied under more difficult conditions, e.g., in water-filled holes. After several years of research an excellent new principle of handling slurries was recently introduced by IRECO having great potential for rapid development and extensive application especially in the large operations. This is a unique on-site mixing and loading method called the "pump truck" method. Pump truck units were introduced early in 1963 simultaneously at the Kaiser Steel Corporation's Eagle Mountain Mine in California, at the Iron Ore Company of Canada's Nob Lake and Carrol Lake Mines in Northern Quebec and on the Northern Minnesota and upper Michigan iron ranges.

A photograph of a unit now in routine operation is shown in Figure 6. The pump truck method utilizes a hot, preconditioned, aqueous solution of ammonium and sodium nitrate with other additives, e.g., one for prevention of the aluminum-water reaction, and another for promoting rapid slurry gelatinization. Solid ingredients are fed by vibrators from one, two or three storage bins depending on the particular slurry desired. The hot solution is fed into the slurry stream by an especially designed pump. All ingredients come together in a second specially designed pump which quickly mixes them and forces them rapidly through a long nose

into the borehole. The rate of mixing and loading averages more than 400 lbs/min. The truck may be loaded at a nearby storage facility, e.g., with about 25,000 lbs of ingredients, in about 15 minutes, or it may be loaded continuously during loading of boreholes depending on the method desired. It is thus possible to mix and load with a single such unit up to about 50 tons of slurry per eight-hour shift.

The products produced by the pump truck method are generally superior to corresponding plant-manufactured products because they are generally higher in density, they are more water resistant and require less of the explosively ineffective ingredients required for products that need to be stored, transported and handled. A valuable feature of the pump truck method is that it can load more than one type of slurry into the same borehole by merely switching vibrators and adjusting their speeds. For example, the most powerful, high density aluminized slurry may be loaded at the bottom or "toe" of the hole where it is most needed, and the much less costly, less powerful NCN type slurry may be used in the upper part of the borehole where less power is required. In this combination both slurries are of the NCN type, i.e., they are properly called slurry blasting agents[13] for which no storage or transportation of actual explosive is required. Thus safety is maximized; when only NCN type slurries are used, the blasting agent made by the pump truck method may be formulated to become a detonatable explosive only when it is actually in place in the borehole. Such NCN-slurries, moreover, may be formulated for use in water-filled boreholes by the same mixing procedures used in dry boreholes, except that the product is then extruded from the loading hose into the bottom instead of the top of the borehole. This procedure does not reduce the loading rate appreciably, but prevents the finished slurry from mixing with water as it would do if it were required to fall through water. One may provide additional water resistance for the slurry by extruding it into a large diameter, polyethylene tube that may be quickly and easily raveled over the end of the hose, pushed to the bottom of the borehole, then pushed off the end of the loading hose by the extruded slurry to line the borehole as the slurry fills it.

Possibly the future of NCN-slurry blasting agents may be judged by the fact that one such type (designated DBA-KS) made available for use only by the ideal conditions made available only by the use of pump truck mixing and loading, actually costs less than prills and oil when both explosive and loading costs are considered. Despite its low cost this slurry is considerably better than prills and oil, e.g., its properties are $\rho_1 \cdot \Delta \sim 1.4$ g/cc, $p_b \sim 50$ kb and A/A_o about 0.9. Reduction in the costs of explosive, drilling, shovel, crushing, and grinding are all phenomenal with this product especially when used in conjunction with the powerful aluminized slurry (DBA-10) in bottom loads.

TNT slurries are sometimes preferred to the NCN type because they are more reliable under difficult conditions, e.g., running water and in very cold boreholes. The TNT most suitable for pump truck handling is the coarse, largely +10 mesh "pelletol" TNT manufactured by the duPont Company or the

"Nitropel" TNT made by CIL in Canada. This coarse TNT product is not cap sensitive and has a critical diameter of 2". Since it is therefore no more sensitive than some of the field-mixed and bulk loaded prills and oil products, particularly those used in small diameter, underground blasting, and since the handling of this product comprises simply the periodic reloading of the bulk TNT bin on the pump truck from which it is fed into the slurry stream via a safe vibrator feed, the TNT slurry made and loaded by the pump truck presents no hazard greater than the use of corresponding plant-manufactured products. The pump truck method of mixing and loading slurry explosives and blasting agents should thus prove to be a major advance in commercial blasting that will result in increased safety, improved performance, reduced costs and greater rates of production.

REFERENCES

1. Bureau of Mines Reports of Investigations:
   a. "Effects of Stress Relief...on...Rock", L. Obert, 6053 (1962)
   b. "Comparative Studies of Explosives in Salt", H. R. Nichols and V. F. Hooker, 6041 (1962).
   c. "Comparative Studies of Explosives in Marble", T. C. Atchison and J. Roth, 5797 (1961).
   d. "Comparative Studies of Explosives in Granite", T. C. Atchison and W. G. Tourney, 5509 (1959).
   e. "Photographic Observations of Quarry Blasts", B. Petkof, T. C. Atchison and W. I. Duvall, 5849, (1961).
   f. "Strain Energy in Explosion-Generated Strain Pulses", D. E. Fogelson, W. I. Duvall and T. C. Atchison, 5514 (1959).
   g. "Spherical Propagation of Explosion-Generated Strain Pulses in Rock", W. I. Duvall and B. Petkof.
   h. "Rock Breakage by Explosives", W. I. Duvall and T. C. Atchison, 5356, (1957).
   i. "...Strain Waves in Rock", L. Obert and W. I. Duvall, 4683, (1950).

2. Duvall, W. I., Geophysics 18, 310 (1953).

3. Atchison, T. C. and Duvall, W. I., "Effect of Characteristic Impedance on....Strain Pulses in Rock", Rock Mechanics, Pergamon Press, p 331, 1963.

4. Nichols, H. R., and Duvall, W. I., ibid, p331, 1963.

5. Atchison, T. C., "Effects of Coupling on Explosive Performance", Drilling and Blasting Symposium, Colorado School of Mines, Quarterly, Jan. 1961.

6. Hino, K., "Theory and Practice of Blasting", Nippon, Kayaku Co., Ltd., 1959.

7. Twentieth Congress, Acad. Sci. USSR Min. Inst., "Problems of the Theory of Destruction of Rocks by Explosives", Publishing House of the Academy of Sci., USSR, Moscow, 1958
   a. A. N. Khanukayev, "Physical Nature of Rock Breakage", pp 6-56.
   b. A. V. Kovazhenkov, "Investigation of Rock Breakage", pp 99-130.

8. Poncelet, E. F., "Theoretical Aspects of Rock Behavior Under Stresses", Fourth Symp. on Rock Mechanics, Science Press, Inc., Ephrata, Pa, 1961; Inst. Min. Met. Engrs. Techn. Publ. No. 1684 (1944).

9. Bauer, A., "Blasting Characteristics of Frozen Ore and Overburden", Canadian Industries Ltd, Montreal, 1961

10. Livingston, C. W., "Theory of Fragmentation in Blasting", Ann. Drilling and Blasting Symp., University of Minn., Oct., 1956.

11. Johansson, C. H., and Langefors, U., Mine and Quarry Engg 17, 287 (1951).

12. Selberg, H., "Transient Compression Waves from Spherical and Cylindrical Cavities", Kangl. Svenska Vetenskopsakal. Arkiv for fysik (Stockholm) 4, (1951); 5(1952).

13. Cook, M. A., Science 132, 1105 (1960).

14. Rinehart, J. S., Quarterly of the Colorado School of Mines, Vol. 55, No. 4, October 1960.

15. Duff, R. E., and Houston, E. E., "Measurement of the C-J Pressure", Second ONR Symp. on Detonation, Washington D.C., Feb. 1955, p. 225.

16. Mallory, H. D., and Jacobs, S. J., "The Detonation Reaction Zone in Condensed Explosives", ibid., p. 240.

17. Walsh, J. M., and Christian, R. H., Phys. Rev. 97, 1544 (1955).

18. Rice, M. H., and Walsh, J. M., J. Chem. Phys. 26, 824 (1957).

19. Rinehart, J. S., and Pearson, J., "Behavior of Metals under Impulsive Loading", Am. Soc. Met., Cleveland, 1954.

20. Cook, M. A., "The Science of High Explosives", Reinhold Publishing Corp., New York, 1958.

21. Kolsky, H., Stress Waves in Solids, Claredon Press, Oxford (1953).

22. Cook, M. A., Keyes, R. T., and Ursenbach, W. O., J. Appl. Phys. 33, 3413 (1962).

23. Bauer, A., and Cook, M. A., Trans. Cana. Inst. Min. and Met. 61, 62(1961).

24. Vance, R. W., Cryogenic Technology, Chapter 13, (M. A. Cook), John Wiley and Sons, Inc., New York, 1963.

25. Cook, M. A., Farnam, H. E., USP 2,930,685, Mar. 29, 1960; Canadian Patents 619,653, May 9, 1961, 605,314, Sept. 20, 1960, 597,177, May 3, 1960, (Other countries).

26. Cook, M. A., "Water Compatible Ammonium Nitrate Explosives for Commercial Blasting", Univ. of Missouri School of Mines and Metallurgy Bulletin, Technical Series No. 97, 1958.

27. Farnam, H. E., Jr., J. Am. Min. Congr., Mar. 1958; Ann. Drilling and Blasting Symp., Univ. of Minn., 1958.

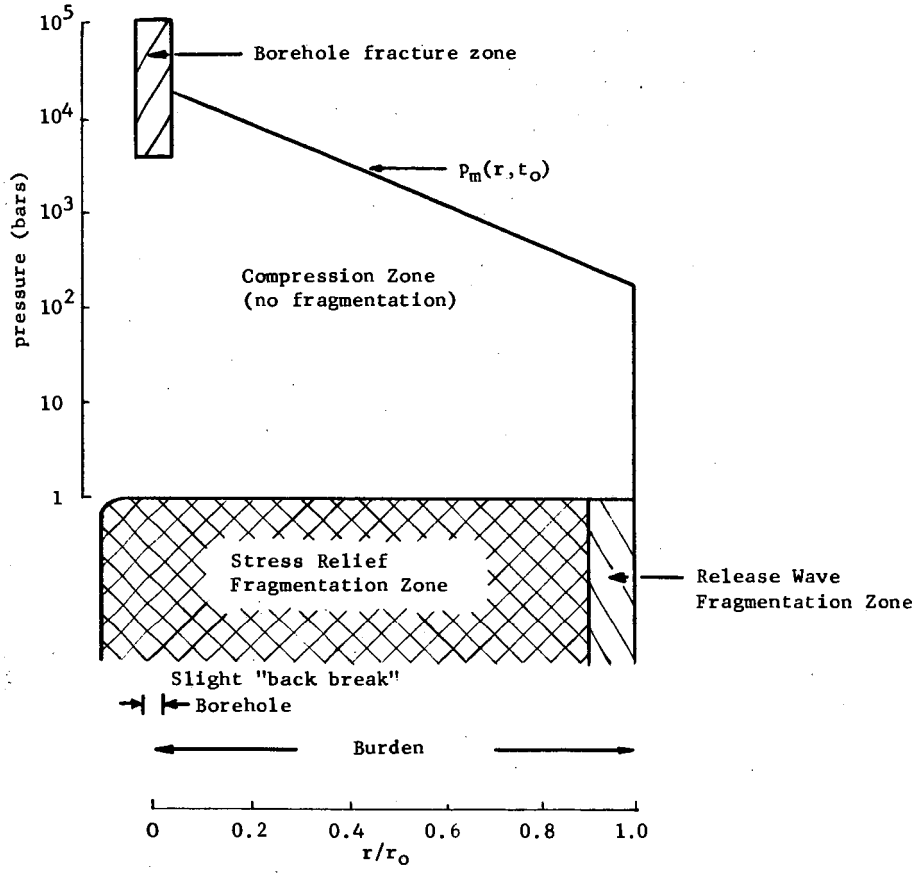

Figure 1. The $p_m(t_o)$ curve and fragmentation zones.
(p_b = 100 kb, Δ = 1.0, ρ_1 = 1.5 g/cc, W_e/W_r - ideal)

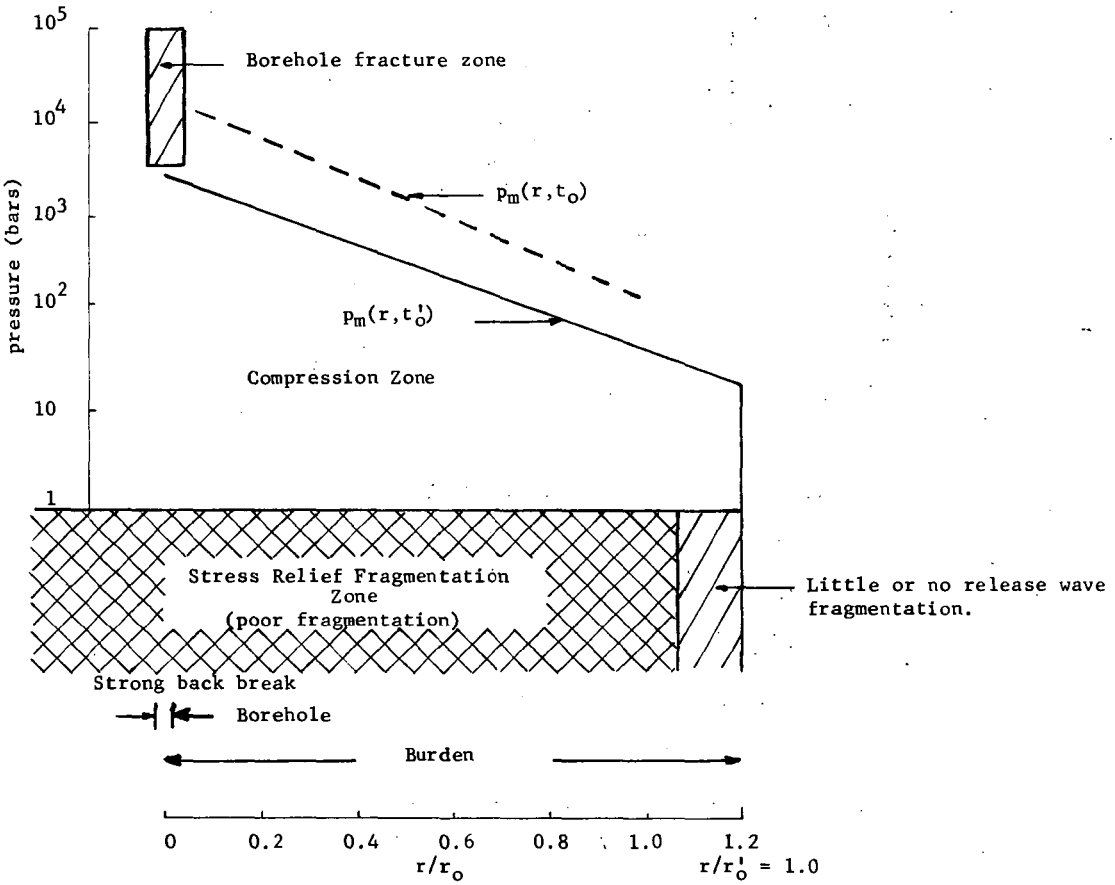

Figure 2. The $p_m(t_o')$ and $p_m(t_o)$ curves and fragmentation zones. (p_b = 100 kb, ρ_1 = 1.5 g/cc, Δ = 1.0, W_e/W_r too low)

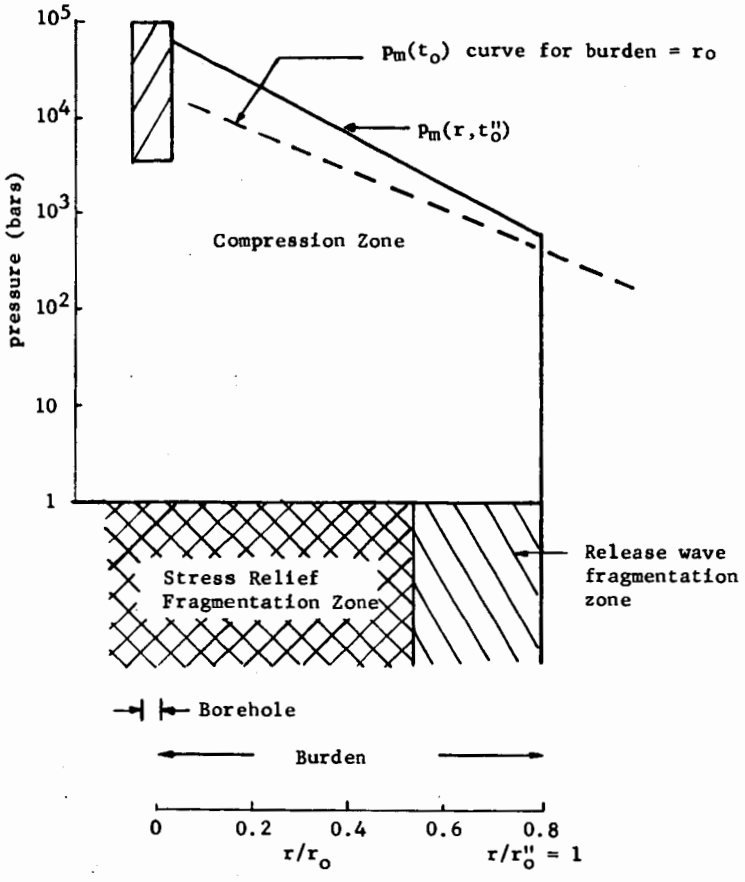

Figure 3. The $p_m(t_o'')$ curve and fragmentation zones for $t_o'' = 0.8\ t_o$ (p_b = 100 kb, ρ_l = 1.5 g/cc, Δ = 1.0, W_e/W_r too large)

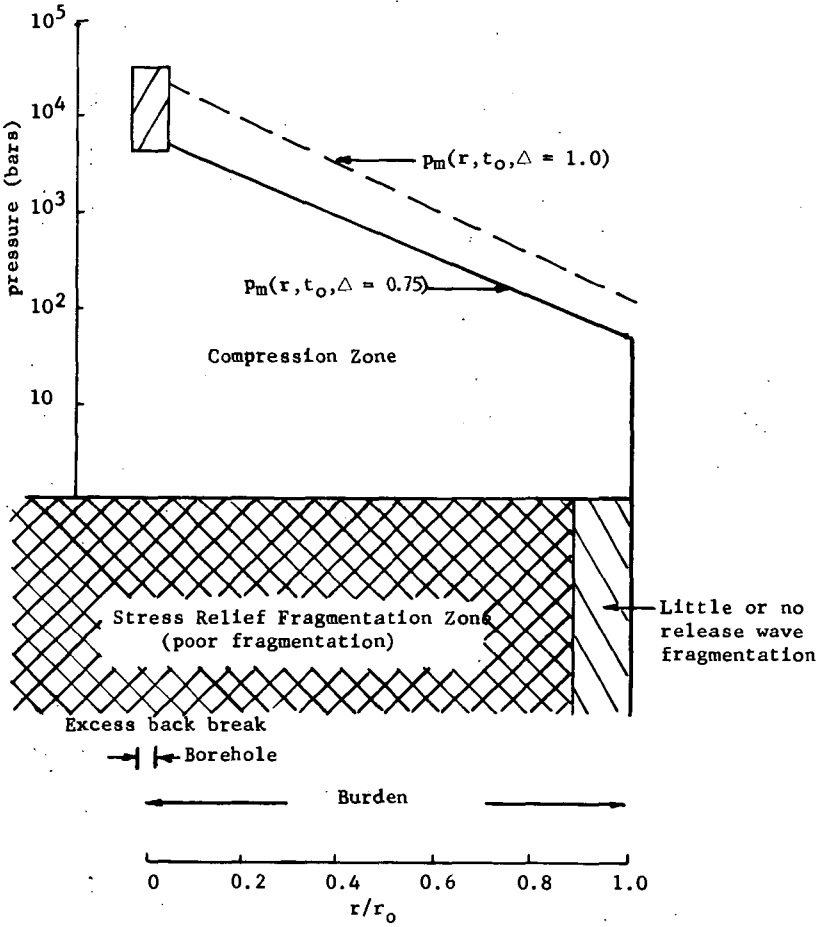

Figure 4. The $p(t_o)$ curve and fragmentation zone. (P_b = 40 kb, ρ_1 = 1.5 g/cc, Δ = 0.75, W_e/W_r - same as in Figure 1)

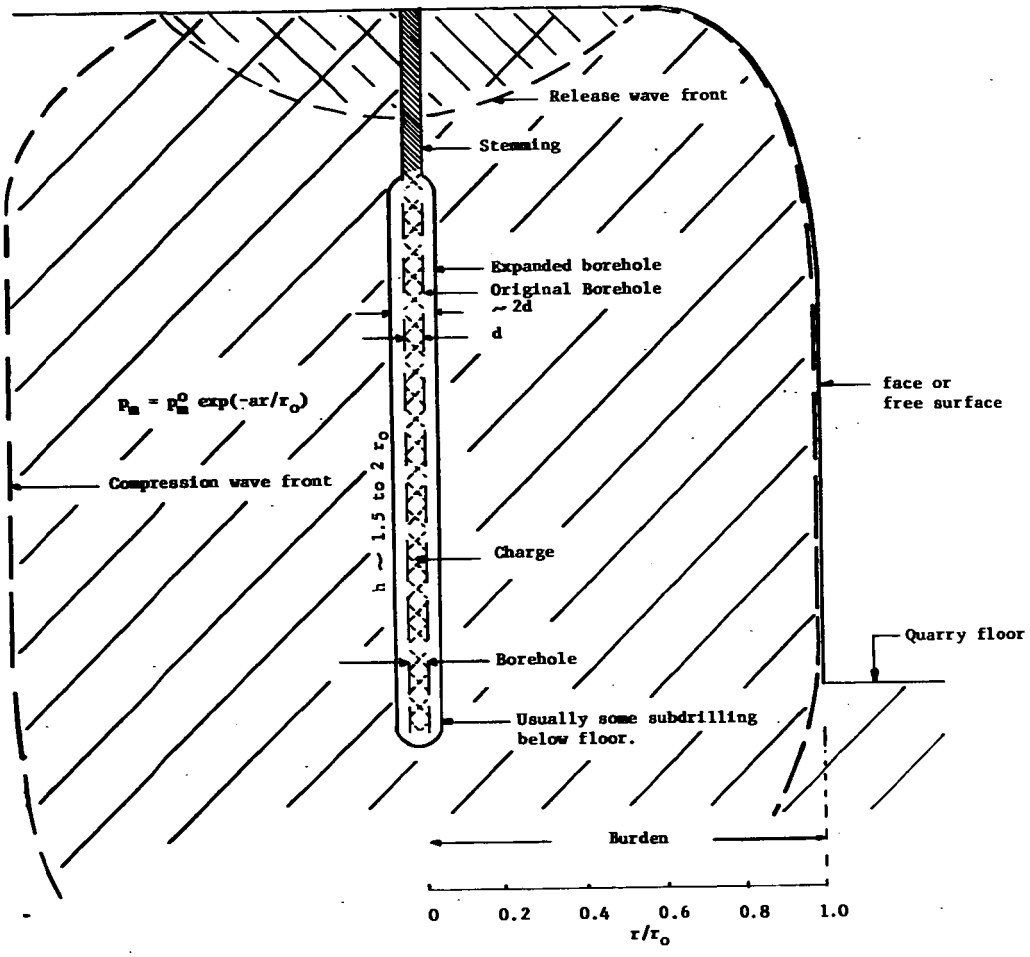

Figure 5. Diagram of borehole and compressed burden at t_o for 9" borehole filled with "slurry".

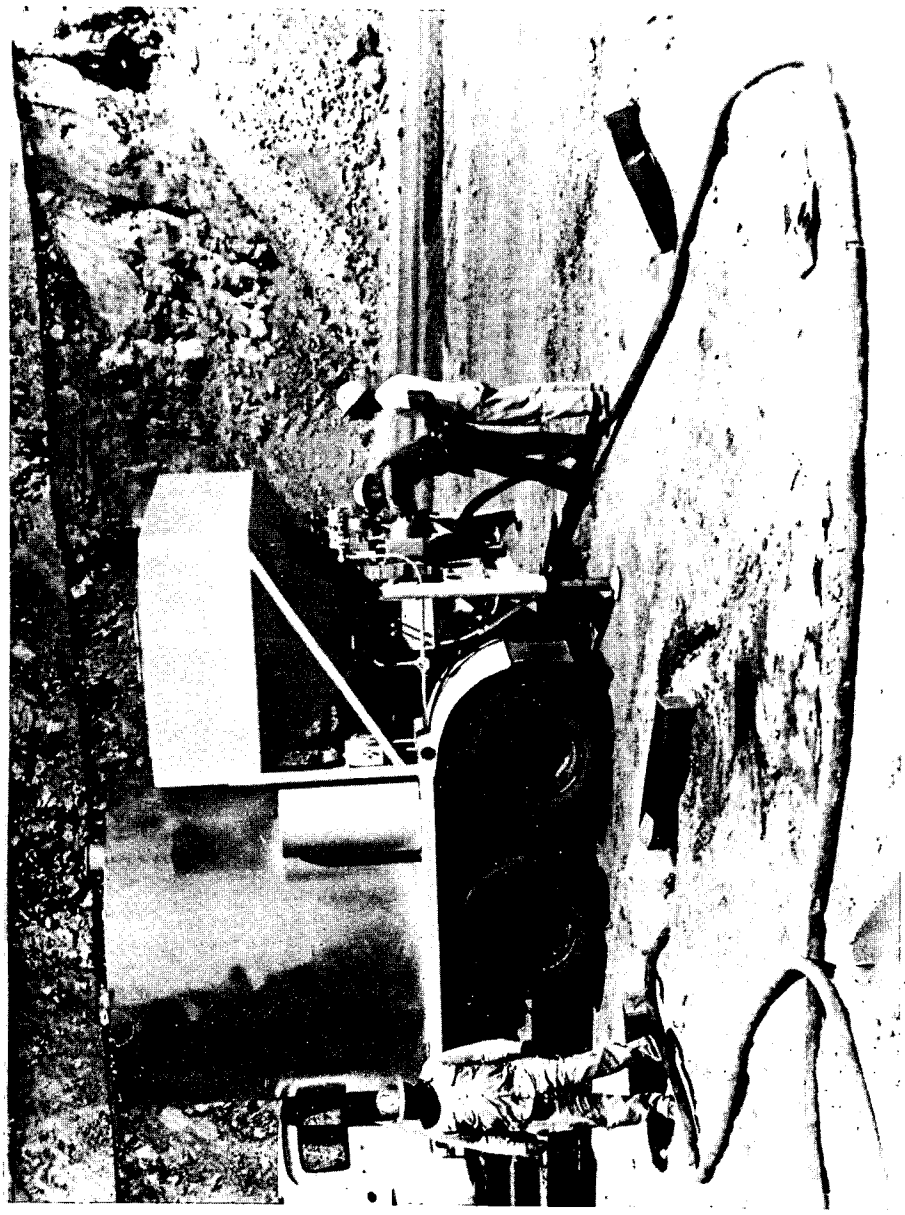

LOW DETONATION PRESSURE EXPLOSIVES

M. T. Abegg *
H. J. Fisher **
H. C. Lawton **
W. T. Weatherill **

* Sandia Corporation, Albuquerque, New Mexico
** Aerojet-General Corporation, Downey, California

Most explosive materials in wide use today may be characterized by detonation pressures ranging from approximately 150 to 350 kilobars. Propellant materials, on the other hand, exhibit comparatively low pressures typical of deflagration reactions. The difference in pressures exhibited by these two classes of materials leaves an interesting gap, the exploration of which may yield valuable information on the chemical and kinetic limitations of detonating materials.

The reliable generation of detonation pressures under 100 kilobars should offer advantages from an engineering standpoint in applications where higher pressures are neither needed nor desired. Certain plastic/explosive formulations described below offer these advantages in addition to others, such as the capability of being extruded or injection molded into difficult configurations and then polymerized in place.

Over the past two years the Aerojet-General Corporation and the Sandia Corporation have collaborated in a preliminary investigation of this interesting low detonation pressure regime. The results recorded below describe some of the courses pursued and techniques developed in this study to date.

EXPERIMENTAL TECHNIQUES

a. Material Specifications

All chemical ingredients utilized in the formulation of the plastic-explosive compositions described herein were purchased to meet pertinent military specifications. Because of the importance of the particle size distribution of the primary and secondary explosives used, tests were run to measure this by microscopic techniques using a Filar eyepiece. The particle size distributions of pentaerythritol tetranitrate (PETN), superfine grade; cyclotrimethylenetrinitramine (RDX), acetone fine; eight hour ball-milled dextrinated lead azide (PbN_6); coarse dextrinated PbN_6; and thallous azide (TlN_3) are presented in Figs. 1 through 4, respectively.

b. Formulating Techniques

Of primary consideration in working with new explosive formulations are the compatibility of the various ingredients and general safety precautions. Initially, in all cases, small quantities (about 1/10 gram) were used. and if no adverse reaction resulted the quantities were increased to one gram, 10 gram, and 100 gram lots. Analyses were made to determine the compatibility and stability of the compositions at the 10-gram level. Among the tests used were vacuum stability, impact sensitivity, differential thermal analysis (DTA), and. in some cases, explosion temperatures. The results of such tests are shown in Table 1.

Safety precautions common to the explosive industry were rigorously observed along with many laboratory precautions used in the chemical industry. In all cases while working with small quantities of materials (under 10 grams) work was conducted behind adequate safety shields. When working with larger quantities, the mixing procedures were carried out with remote control methods, viewing the processes through mirrors, periscopes or closed circuit television. Explosives were handled and stored in conducting rubber containers. The quantity of explosive materials was limited to 50 grams in the laboratory. In the mixing buildings, the materials were limited to the actual quantities needed.

c. Rheological Characteristics

During the formulation of high-solids-content compositions extremely viscous, putty-like systems were encountered. It was found that the addition of small quantities (0.1 to 1.0 percent) of special surfactants caused a significant increase in the fluidity.

Changes in the rheological characteristics were determined by the use of a parallel plate plastometer technique. A small cylindrical sample of the paste-like test sample was placed upon a glass plate and loaded with another glass plate of known weight. The radius to which the sample spread after 30 seconds' duration was taken as an indication of the apparent fluidity of the test system. The greater the radius, the greater the effectiveness of the surfactant.

d. Testing Procedures

Detonation Velocity Measurements - Detonation velocity measurements were carried out using two well-known methods, the streak camera and pin switch techniques. A Beckman-Whitley Model 194 streak camera was utilized. Ionization pin switches in conjunction with a mixer circuit and Moran Model 101A raster oscilloscope were also used to measure detonation velocities of both confined and unconfined charges. The ionization pin switches were mounted in special holding devices and distances were measured with a Gaertner Scientific Corporation microcomparator capable of measurement to ±0.002 millimeters. All velocity measurements were started at least four diameters from the point of initiation.

Detonation Pressure Measurements - The detonation pressure measurements were carried out using a modified plate dent test. Attempts were also made to use the aquarium technique.

The modified plate dent test consisted of 20 grams of explosive material in a copper tube (3/4 in. x 5 in. x 1/16 in. wall). The detonation was initiated by an Engineer's Special blasting cap with a five-gram booster of Composition C-4. An aluminum witness plate (1 3/4 in. x 5 in. x 5 in. of 6061-T6 alloy) was used. This technique was used to determine the approximate detonation pressure range of the various formulations.

A series of calibration tests using standard explosives of varying densities was conducted to determine detonation pressure as a function of depth of indentation in the witness

plates. Detonation velocities as a function of density for each explosive were obtained from W. R. Tomlinson[1] and O. E. Sheffield[2]. Detonation pressures were calculated from the detonation velocities at known densities of the explosives by the approximate equation[3]

$$p \doteq 0.010 \rho \frac{D^2}{4} \qquad (1)$$

where:

p = detonation pressure in bars
ρ = density in grams per cubic centimeter
D = detonation velocity in meters per second

A review of other possible methods of measuring detonation pressures of large samples (2 in. diameter x 8 in. length) indicated that the "aquarium" technique originally developed by Holton[4] and later described by Cook, Keyes and Ursenbach[5] appeared to offer good possibilities for application in this test program. In this method a streak camera is used to measure the detonation velocity of the plastic explosive and also the velocity of the resultant shock wave through water. From the measured velocity of the shock wave together with the equation of state of water, it is possible to calculate the shock pressure in water. However, a considerable number of problems were encountered in attempts to measure pressures by this technique. The principal objection lay in the ambiguity of the slope of the shock at the explosive/water interface. This ambiguity seemed to be more pronounced at lower shock pressures. Accordingly, this technique was abandoned and all of the pressure data reported here are based on plate dent and $1/4 \rho D^2$ approximations.

e. Sensitivity Tests - Sensitivities and compatibilities of the various explosive formulations were determined by impact, vacuum stability and differential thermal analysis. These methods are discussed in Ref. 2. The impact tests were run on a modified Bureau of Mines machine using a two-kilogram weight and flat anvil and striker. It was found that nitropolyurethane (NPU)/PETN and NPU/RDX formulations, containing concentrations of 20 percent by weight of explosive or larger quantities, were cap sensitive to Number 8 blasting caps. Compositions containing smaller quantities of these explosives required the use of a booster to insure initiation. However, in most of the firing tests a five-gram booster charge of Composition C-4 together with an Engineer's Special detonator were employed to insure initiation.

EXPERIMENTAL RESULTS

a. Compositions - The compositions of the plastic explosive formulations studied consisted of polyurethane, nitropolyurethane, and dinitropropyl acrylate matrices (continuous phase) to which various explosives (discrete phase) were added. The polyurethanes were composed of diols/triols or other cross-linking agents/diisocyanate, in 70/30/107 mole percents, together with 20 percent plasticizer. The nitropolyurethanes were composed of diols/triols or other crosslinkers/nitrodiisocyanate together with up to 50 percent by weight of nitro plasticizer. In the NPU formulation, the diol/triol/isocyanate ratio was 80/20/107 mole percents.

b. Chemical and Physical Properties - The chemical and physical properties were determined for each of the compositions and are given in Table I. The vacuum stabilities and DTA's were determined to ascertain the stability of several compositions to thermal decomposition. The vacuum stability data showed that in all cases the mixtures had satisfactory stability.

The DTA's for NPU and NPU/PETN formulations are given in Figs. 5, 6 and 7 and similar information for PU/PbN_6 mixtures is given in Figs. 8, 9 and 10. The data indicate that

the final compositions in both cases are as thermally stable as that of the least stable component. The compatibility of the individual ingredients and combinations thereof was determined for each of the formulations. It was found that both PETN and RDX are compatible with the ingredients of the PU and NPU plastic formulations. Similar studies using NPU and PU systems with lead and other azides showed that the nitro substituted plasticizing agents and nitro substituted diisocyanates were incompatible with azides: however, it was found that the components of the PU system were compatible with the azides

The densities of the various formulations varied from that of the pure plastic binder system up to that of the pure discrete phase. In the case of the NPU/PETN systems, the densities were found to vary from 1.2 g/cm^3 up to about 1.35 g/cm^3 depending upon the concentration of the discrete phase. In the plastic/PbN_6 systems, the densities varied between that of the binder system up to 2.1 g/cm^3 depending upon the concentration of PbN_6.

In high-solids-content plastic explosive compositions, the rheological characteristics are important. In one system composed of 30 percent DNPA (dinitropropylacrylate) binder system and 70 percent RDX, it was found necessary to add 10 percent calcium stearate, impalpable grade, by weight to prevent dilatancy while extruding the plastic composition under pressure. The large amount of calcium stearate (CS) acts as a phlegmatizing agent making it more difficult to propagate a detonation. It was advisable to find methods for reducing the required amount of CS and at the same time to increase the fluidity of the plastic/explosive mixture.

Earlier studies with propellant formulations had shown that pretreatment with small amounts of surface active agents caused a large increase in fluidity. In preliminary studies with RDX and PETN, the desired amount of surface agent was dissolved in methyl alcohol or chloroform and the explosive treated with the solution. The solvent was evaporated and the explosive was dried in vacuo, leaving a film of surfactant on the surface of the explosive.

Tests showed that SPAN 60 (Atlas Chemical Company) and calcium stearate, impalpable grade, were the most effective fluidizing agents tested. Using the above pretreatment technique, the maximum increase in fluidity occurred when using calcium stearate at a concentration of 0.5 percent by weight, and the fluidity decreased with further increase in concentration. Similarly, the maximum advantage of SPAN 60 alone was found to be at 0.25 percent by weight. In some systems a synergistic effect was observed with calcium stearate and SPAN 60 at similar concentrations. The DNPA/RDX mixtures showed a marked increase in fluidity after standing for three hours. Similar results were obtained with other highly loaded plastic explosive systems.

The reduction in the amount of calcium stearate in the explosive composition from 10 percent to 0.5 percent resulted in increased fluidity and ease of extrusion together with a significant increase in detonation velocity.

c. Explosive Properties - Tests were conducted to determine the effect of solids concentration, confinement and diameter on the explosive characteristics (detonation velocity and pressure) of the plastic explosive compositions. The compositions, diameter and confinement of samples tested are shown in Table II. Detonation velocity measurements were carried out on at least five charges for each diameter except with 3.58-inch diameter charges, where only three were tested. The effects of explosive concentration and charge diameter on detonation velocity are shown in Figs. 11 and 12. The data in Fig. 11 show that the detonation velocity increases in the usual fashion with an increase in diameter. It is of interest to note that 1/16 inch copper confinement had no apparent effect on detonation velocities in the charge diameter range from 1.0 inch to 1.875 inch. The 20 percent PETN - 80 percent NPU formulation reaches ideal detonation velocity at a diameter of 3.4 inches, compared with 3 inches for the 25 percent PETN - 75 percent NPU formulation. The data in Fig. 12 show that the detonation velocity

increases as expected with increase in explosive content. The data in Table III show the approximate minimum diameters at which detonation is sustained for the various compositions either unconfined or confined in 1/16-inch wall copper tubing.

d. Detonation Pressure - In preliminary experiments the calibarated plate dent method for determining detonation pressure was used to estimate the approximate detonation pressure for the various compositions. In those experiments where detonation velocities were determined, it was considered adequate for present purposes to calculate the approximate detonation pressure from the $1/4\ \rho D^2$ relationship. Detonation pressures calculated in this fashion are shown as a function of explosive composition in Fig. 13. These data show that the detonation pressures range from 25 to approximately 160 kilobars for the compositions tested.

Preliminary studies with PU/PbN_6 systems indicated that a system containing 40 percent PU/60 percent PbN_6 by weight will just sustain detonation. Plate dent tests indicated that the detonation pressure would be under 10 kilobars. A 30 percent PU/70 percent PbN_6 composition had a detonation pressure of approximately 22 kilobars as determined by the plate dent test. A typical witness plate from a plate dent test is shown in Fig. 14. It thus appears that detonation pressures in the very low pressure range may be obtained with PU/PbN_6 systems.

e. Impact Sensitivity - Impact sensitivities for the various explosives were measured as shown in Table I. It was found that the addition of secondary and sensitive primary explosives to the PU or NPU binder systems resulted in compositions much less sensitive to impact.

DISCUSSION OF RESULTS

The formulation of explosives composed of a high-energy discrete phase in a continuous matrix of combustible organic material necessarily involves an excursion into a number of physical and chemical problems. In general, this investigation was built around the incorporation of relatively sensitive explosives into a plastic such that inter-particle distances were relatively large. The composition of the plastic explosives ranged from 10 to 70 percent discrete phase by weight with corresponding amounts of poly and nitro polyurethanes, and other plastics.

The physical and chemical properties of this type of explosive imply a versatility not normally encountered with explosive materials. Prior to polymerization, the compositions are extrudable under pressure and readily assume the shape of the container. They bond readily to clean metal surfaces. They are capable of being introduced into irregularly shaped volumes and polymerized in place. Once the materials are polymerized they exhibit properties related to those of the plastics involved.

An interesting effect of average particle size on the ability of certain formulations to be initiated was observed. When the concentration of PbN_6 in polyurethane was held at 60 weight percent, initiation was not achieved at an average particle size of one micron, but was achieved at average particle sizes ranging from five to ten microns, using the same initiating charge. The region above this range has not yet been explored.

A marked effect on the extrudability of the non-polymerized compositions was achieved by the use of surfactants at concentrations of the order of 1/10 to one percent. The effect of surface active materials on the rheological characteristics of explosive compositions was pronounced and served to extend the useful range of these materials.

The incorporation of sensitive primary explosives into an inert plastic matrix introduces another family of explosive compositions. Their ability to inter-initiate from particle to particle through the continuous phase of the composition opens up other areas of low pressure explosive technology.

ACKNOWLEDGMENTS

This work was performed under the auspices of the United States Atomic Energy Commission. The cooperation of the Bureau of Explosives in the classification of new formulations is gratefully acknowledged. The technical assistance of Messrs. R. F. Van Cleve and B. R. Wenfer in the formulation of the explosive compositions, and Mrs. J. T. Knight in data reduction and preparation of the manuscript is greatly appreciated.

(1) W. R. Tomlinson, Jr., Properties of Explosives of Military Interest, Picatinny Arsenal, Technical Report No. 1740, 20 June 1949.

(2) W. R. Tomlinson, Jr., revised by O. E. Sheffield, Properties of Explosives of Military Interest, Picatinny Arsenal, Technical Report No. 1740, Revision No. 1, April, 1958.

(3) M. A. Cook, The Science of High Explosives, Reinhold Publishing Corporation, New York, 1958, p. 35.

(4) W. C. Holton, The Detonation Pressures in Explosives as Measured by Transmitted Shocks in Water, NAVORD Report 3968, 1 December 1954.

(5) M. A. Cook, R. T. Keyes and W. O. Ursenbach, Measurements of Detonation, Shock and Impact Pressures, Third Symposium on Detonation, ONR ACR-52, Vol. 2, p. 357, ASTIA No. 242 585.

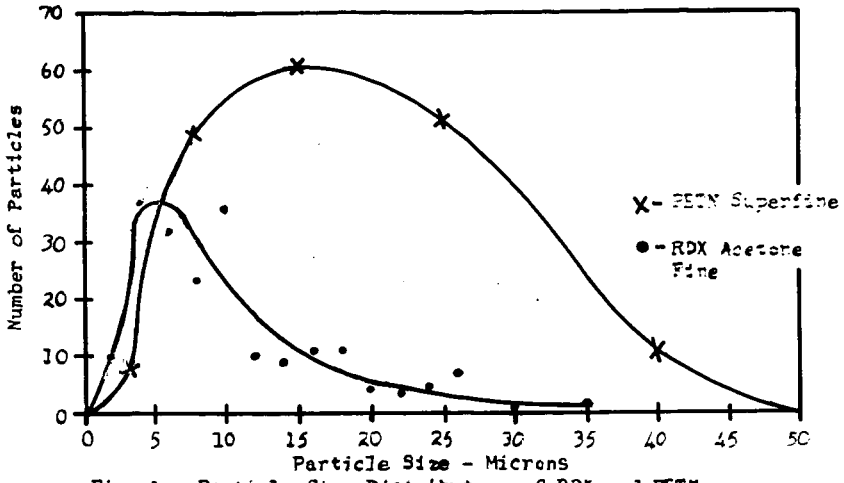

Fig. 1.—Particle Size Distribution of RDX and PETN (200 particles counted)

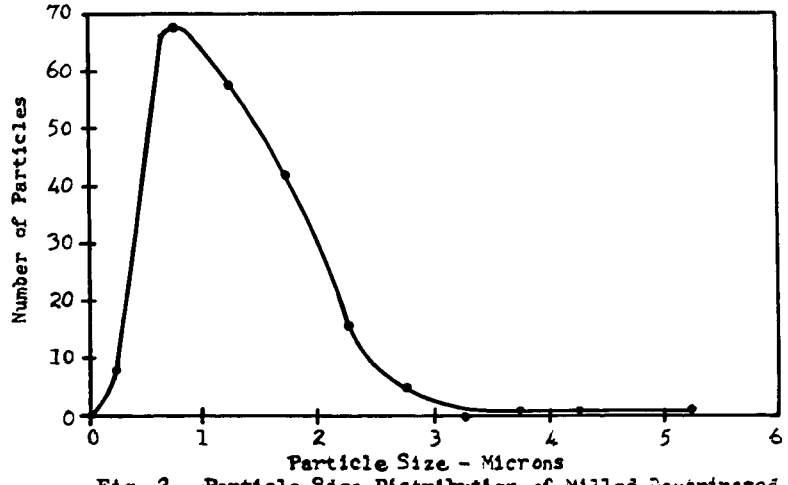

Fig. 2.—Particle Size Distribution of Milled Dextrinated PBX (200 particles measured)

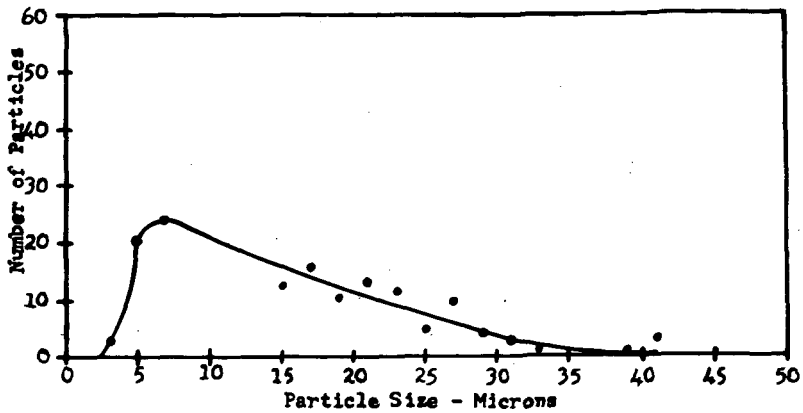

Fig. 3.—Particle Size Distribution of Coarse PbN_6
(200 particles measured)

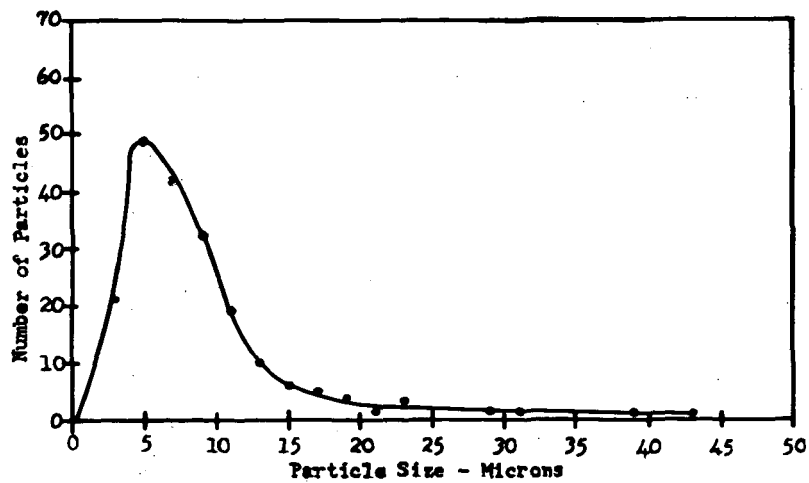

Fig. 4.—Particle Size Distribution of TlN_3
(200 particles counted)

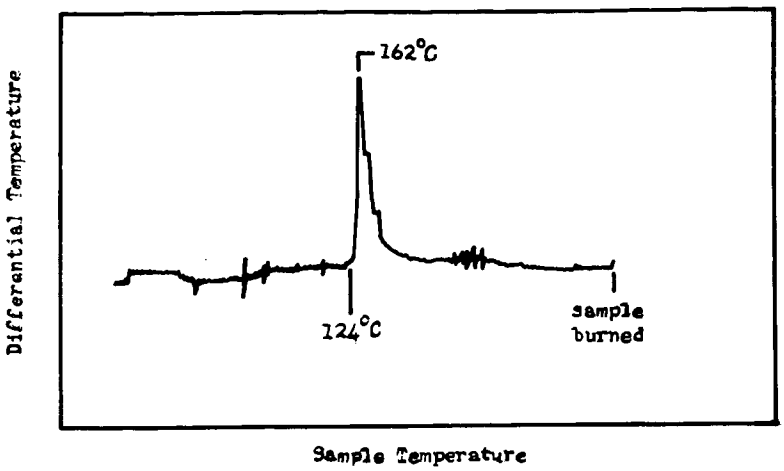

Fig. 5.—DTA – NPU

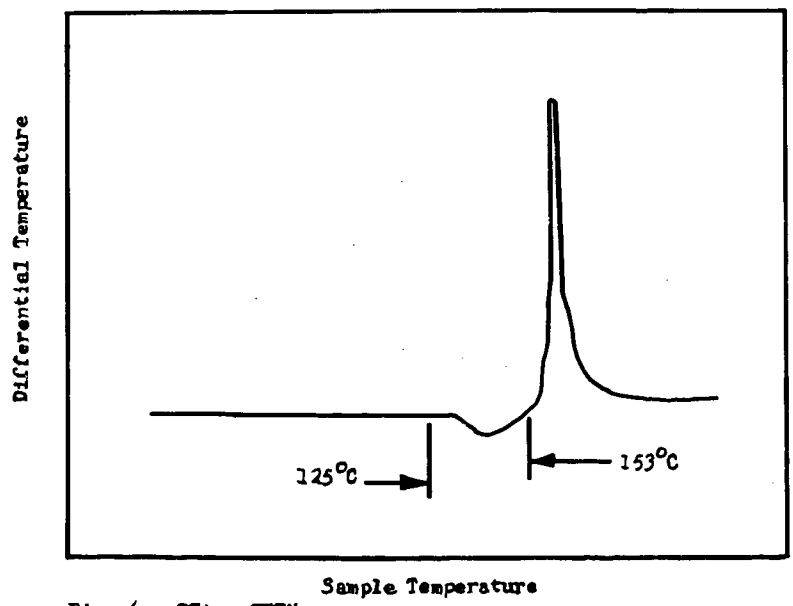

Fig. 6.—DTA – PETN

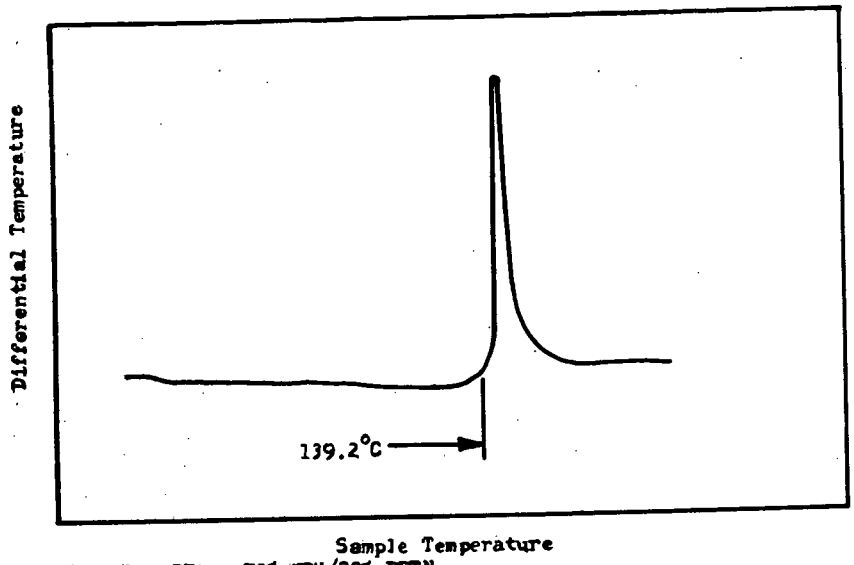

Fig. 7.—DTA - 70% NPU/30% PETN

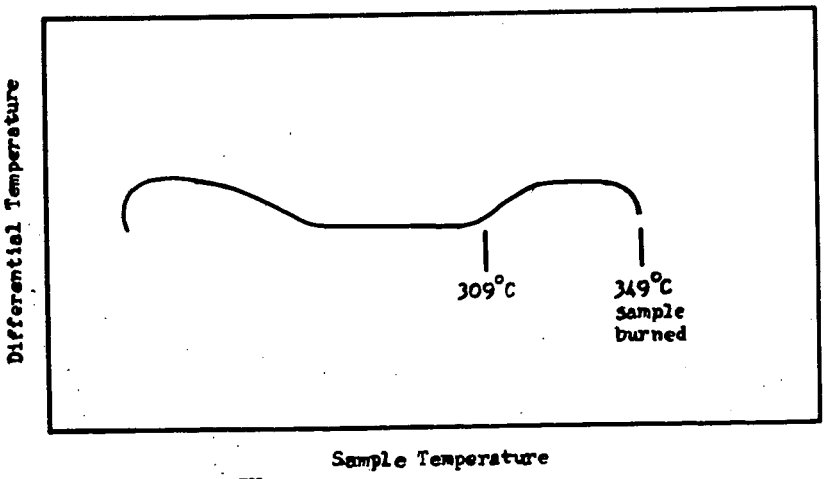

Fig. 8.—DTA - PU

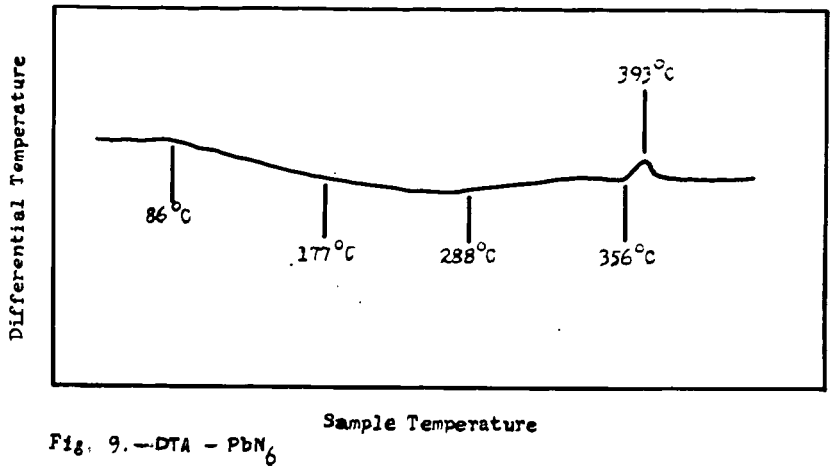

Fig. 9.—DTA - PbN_6

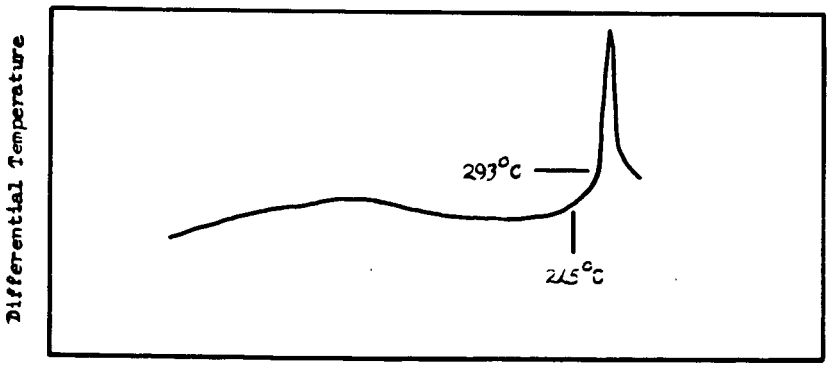

Fig. 10.—DTA - 40% PU/60% PbN_6

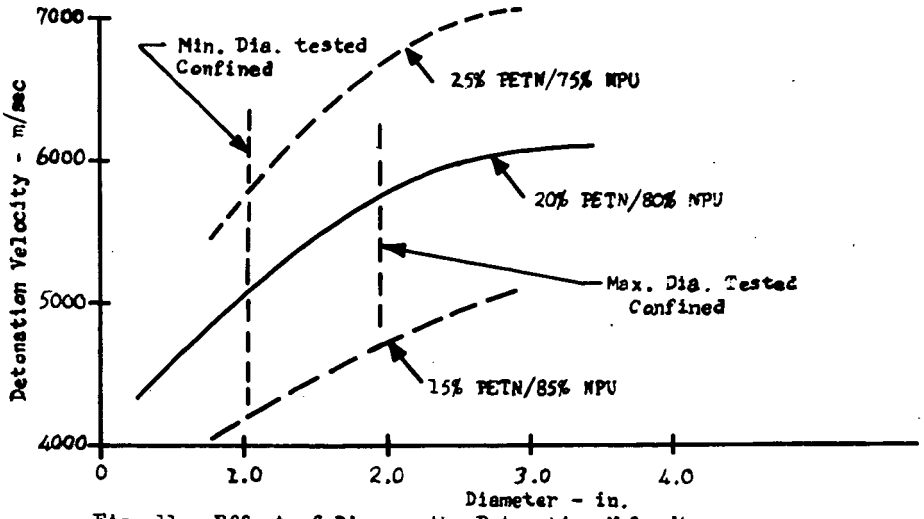

Fig. 11.—Effect of Dia. on the Detonation Velocity

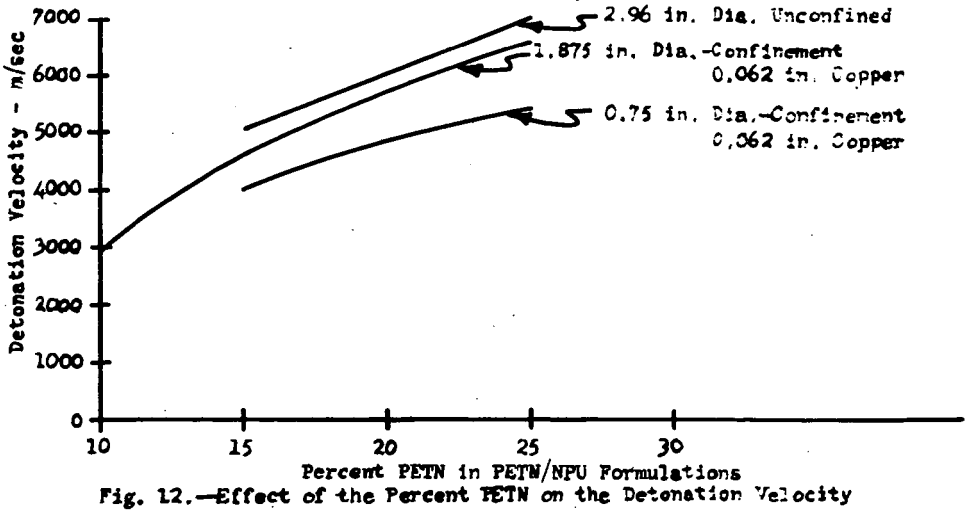

Fig. 12.—Effect of the Percent PETN on the Detonation Velocity

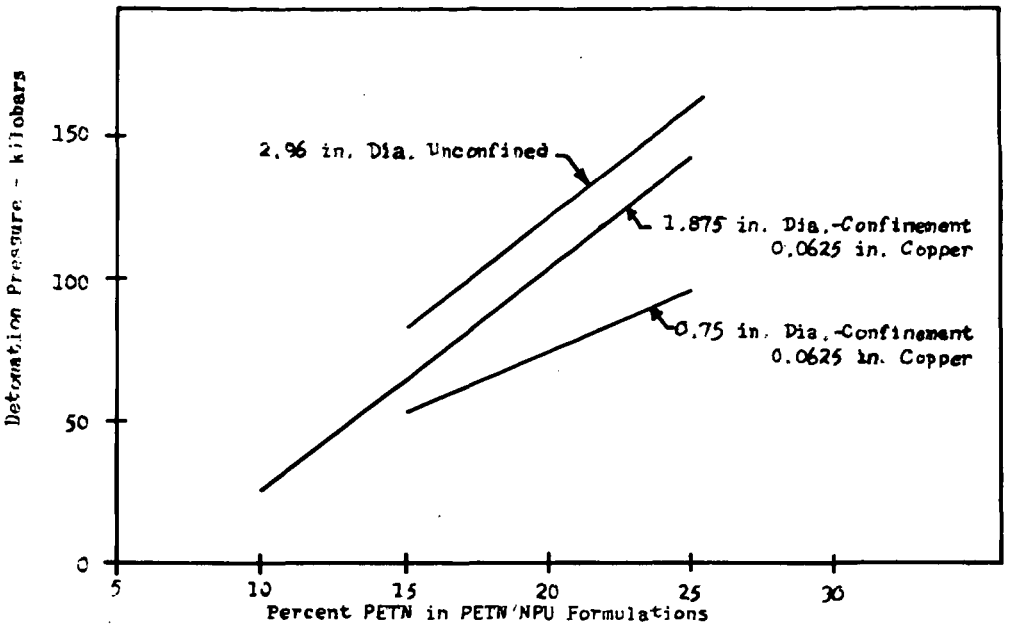

Fig. 13.—Effect of the Percent PETN on the Detonation Pressure

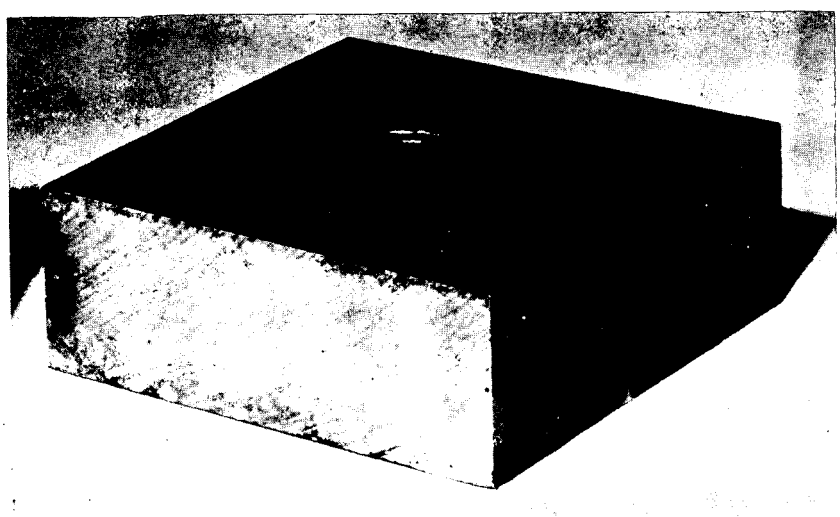

Fig. 14.—Test No. 194

Chg. Dia. 3/4 in.
Chg. Lgth. 4-3/8 in.
Chg. Density 2.06 g/cc
Depth of Dent .145 in.

Confinement 1/16 in. thick Aluminum
Witness Plate 5 in. X 5 in. X 1-3/4 in.
6061-T6 Aluminum
Approx. Detonation Pressure - 22 Kb

TABLE I

PHYSICAL AND CHEMICAL CHARACTERISTICS
OF PLASTIC EXPLOSIVE FORMULATIONS

Property	30% PETN 70% NPU	30% RDX 70% NPU	60% PbN_6 40% PU	60% TIN_3 40% PU	PbN_6 milled	TIN_3	RDX	PETN	NPU
Density at 25°C (g/cc)	1.345	1.385	-	-	4.38	3.68	1.82	1.77	1.21
Vacuum Stability at 100°C (cc's of gas/g/40 hr)	* 0.015	* 0.064	0.60	0.16	0.1	-	0.7	0.5	0.32
DTA Exotherm at °C	139.2	161.5	293	317	356	-	161.5	139.2	124
Impact Sensitivity (cm/2kg)									
100%	60	65	100	140	1	3	27	14	>200
50%	51	58	82	172	1	1/2	22	11	>200
0%	43	50	70	190	1	1/2	19	8	>200

* Vacuum stability at 180°F

TABLE II

TEST SAMPLES FOR DETONATION VELOCITY

Composition (%)		Charge Diameter (in.)											
		Confined*						Unconfined					
PETN	NPU	0.25	0.50	0.75	1.125	1.375	1.875	1.0	1.45	1.81	2.56	2.96	3.58
10	90			X			X					X	
15	85			X			X					X	
20	80	X	X	X	X	X	X	X	X	X	X	X	X
25	75			X			X					X	

* Confinement in all cases was copper tubing with 1/16-in. wall thickness

TABLE III

APPROXIMATE CRITICAL DIAMETERS OF SEVERAL NPU-PETN FORMULATIONS

FORMULATION (% PETN/% NPU)	CONFINEMENT	CRITICAL DIAMETER (in.)
10/90	CONFINED*	1.87
10/90	NONE	Greater than 2.96
15/85	CONFINED*	0.5
15/35	NONE	Greater than 1.0
20/80	CONFINED*	0.25
20/80	NONE	
25/75	CONFINED*	Less than 0.25
25/75	NONE	Less than 1.0

* All confined charges were confined in 1/16 in. wall copper tubing.

EXPLOSIVE EVALUATION OF COORDINATION COMPOUNDS

M. T. Abegg *
J. W. Fronabarger **
C. W. Hoppesch **
W. J. Meikle *
C. T. Rittenhouse **

*Sandia Corporation, Albuquerque, New Mexico
**Universal Match Corporation, Marion, Illinois

INTRODUCTION

An investigation of "low power" explosives was undertaken as a cooperative effort between the Sandia Corporation and the Universal Match Corporation. The primary objective of this program was the investigation of homogeneous chemical compounds expected to yield detonation pressures of less than 100 kilobars. Secondary objectives included the attainment of adequate thermal stability, suitable impact sensitivity and high density. The wide range of properties found in coordination compounds caused efforts to be concentrated in this area.

In general, a limited number of tests were performed in order to screen out unsuitable compounds. Those compounds which appeared promising were then subjected to further testing. The initial evaluation of explosive output was obtained from the standard sand bomb test. This test was abandoned when it became apparent that the consolidation density of the explosive was an important factor. Later testing utilized the plate dent test and a limited amount of streak camera data.

The explosive properties of the coordination compounds tested varied over a wide range, and depended on several factors. The consolidation density was important. The oxygen balance (to carbon monoxide) was also significant. The insertion of a heavy ion into the explosive (for example, iodate or thallous) lowered the detonation velocity but the increased density of the total molecule tended to keep the detonation pressure high.

EXPERIMENTAL

Detonation pressures were estimated by the plate dent technique. Figure 1 shows the plot of detonation pressure versus depth of dent in the steel plate (hardness in Rockwell, 88-90, B scale). Detonation pressures for those cases where the streak camera technique was utilized were calculated from the approximation:

$$p \doteq 0.010\rho\frac{D^2}{4}$$

where:

p = detonation pressure in bars
ρ = density in grams per cubic centimeter
D = detonation velocity in meters per second

The other tests conducted were 40-hour vacuum stability at 100°C, impact sensitivity by the Bureau of Mines two-kilogram drop test apparatus, density, melting point, and autoignition temperature. Not all tests were conducted on each compound, and unsuitable compounds were eliminated.

All compounds were prepared and purified by standard methods to be found in the literature, and analyzed by conventional techniques.

Table I summarizes the data collected during this investigation.

DISCUSSION

Cobalt - The oxygen balance of the cobalt complexes was varied by varying both the ligands and the oxidizing anion. The iodate anion was chosen for most of the compounds because of its high density, ability to cause propagation in small diameters, and low oxygen equivalent as compared to IO_4^- and ClO_4^-. The data collected on two cobalt compounds are shown in Figure 2.

Several interesting facts should be pointed out. (1) The compounds containing Cl^-, such as $Co(NH_3)_5Cl(IO_3)_2$, even though having a favorable oxygen balance, failed to sustain detonation. (2) The outputs of the compounds are variable over a wide range, for instance: $Co(NH_3)_6(IO_3)_3 \cdot \frac{1}{2}H_2O$ gave a pressure of 15 kilobars at a density of 1.51 g/cc (49.5 percent crystal density) and 215 kilobars at 2.70 g/cc (88.8 percent crystal density). Another example is $Co(en)_2(IO_3)_3$: 55 kilobars at 1.9 g/cc (69.1 percent crystal density) and 165 kilobars at 2.48 g/cc (90.1 percent crystal density) (See Figure 2).

Copper, Zn and Other Metal Complexes - The coordination compounds of copper, platinum, zinc, nickel, mercury, and cadmium were similar to those of cobalt in explosive properties. The metal ion does not appear to effect the output. The nickel ion, with its valence of two and possible coordination number of six, was interesting because of the low oxygen balances which could be obtained. None of the nickel compounds sustained detonation in a 0.5 inch diameter column. With $Cu(en)_2(IO_3)_2$ and $Zn(en)_2(IO_3)_2$, we see the production of low detonation pressure at high densities. Data on these two compounds are given in Table II and Figure 2.

Table II

Compound	Density (g/cc)	Percent Crystal Density	Estimated Detonation Pressure (kilobars)
$Cu(en)_2(IO_3)_2$	1.89	69.1	40
	2.38	87.2	155
$Zn(en)_2(IO_3)_2$	1.73	69.8	27
	2.43	97.8	145

It is to be pointed out that the explosive outputs of the two compounds are similar at equal actual densities rather than equal percent crystal densities. This phenomenon was shown by several other explosive complex salts.

Another interesting situation is the different behavior of two isomers $Cu(tmen)_2(IO_3)_2$ and $Cu(pn)_2(IO_3)_2$. In a 1/2 inch diameter by 1.37 inches long configuration, the tmen complex sustained detonation (See Figure 3) while the pn complex did not. The tmen complex gave 125 kilobars at a density of 2.30 g/cc (89.7 percent crystal density).

However, in a 1 1/4 inch diameter by 5.1 inches long configuration, the pn salt did sustain giving an estimated detonation pressure of 105 kilobars at a density of 2.13 g/cc.

SUMMARY

It appears that oxygen balances of 20-30 percent (to carbon monoxide) are necessary to obtain low pressures at densities approaching crystal density. This requirement probably necessitates the use of larger column diameters or more sensitive classes of compounds such as chlorates to obtain steady detonation.

One of the properties of these coordination compounds is the apparent low detonation pressure produced at relatively high densities. Figure 4 shows the relationship of detonation pressure to density for hexammine cobalt iodate hemihydrate and TNT. The coordination compound yields the same detonation pressure at a density of 2.7 g/cc that TNT exhibits at 1.6 g/cc. The coordination compounds, regardless of oxygen balance, ligand, or central ion, all appear to possess a similar relationship between output and density.

ACKNOWLEDGMENT

This work was performed under the auspices of the United States Atomic Energy Commission. Special appreciation is extended Dr. Herbert Ellern for his technical guidance and assistance.

TABLE I

Compound	Oxygen Balance (%)	Impact Value (cm)	Crystal Density (g/cc)	Sand Crush (g)	Detonation Velocity (m/sec) at density	Detonation Pressure (kilobars) at density
$Co(NH_3)_6(IO_4)_3$	115	22	- - -	23	- - -	230 (2.34)
$[Co(NH_3)_5(NO_3)](NO_3)_2$	100	47	1.846	37.6	- - -	- - -
$Co(NH_3)_6(IO_3)_3 \cdot \frac{1}{2}H_2O$	86	17	3.04	18	3750 (2.0)	15 (1.51) 90 (2.06) 210 (2.70)
$Co(NH_3)_3(NO_2)_3$	100	12	2.024	35.1	6400 (1.8)	- - -
$[Co(en)_2Cl_2]IO_3 \cdot HIO_3$ (trans)	50	35	2.658	12	- - -	- - -
$Co(NH_3)_6(NO_3)_3$	86	40	1.804	32.3	- - -	- - -
$Co(en)_3(IO_3)_3$	46	34	2.760	16.1	4610 (2.21)	54 (1.91) 96 (2.19) 170 (2.40)
$[Co(NH_3)_5NCS](ClO_4)_2$	73	26	1.906	44.5	6500 (1.70)	- - -
$[Co(NH_3)_5Cl](IO_3)_2$	71	>104	- - -	0	- - -	- - -
$[Co(en)_2Cl_2]IO_4$ (trans)	32	34	- - -	12.2	- - -	- - -
$[Co(en)_2Cl_2]-ClO_4$ (cis)	33	57	1.873	0	- - -	- - -
$[Co(en)_2Cl_2]-ClO_4$ (trans)	33	81	1.844	0	- - -	- - -
$[Co(NH_3)_4(NCS)_2]-ClO_4$	31	49	1.65	0	- - -	- - -
$Cu(en)_2(IO_3)_2$	46	37	2.709	17.6	- - -	40 (1.89) 160 (2.38)
$Cu(pn)_2(IO_3)_2$	35	19	- - -	13.1	- - -	- - -
$Cu(tmen)_2(IO_3)_2$	35	54	2.594	- - -	- - -	11 (1.52) 25 (1.72) 125 (2.30)

TABLE I (continued)

Compound	Oxygen Balance (%)	Impact Value (cm)	Crystal Density (g/cc)	Sand Crush (g)	Detonation Velocity (m/sec) at density	Detonation Pressure (kilobars) at density
$Pt(NH_3)_4(IO_3)_2$	100	- - -	- - -	17.0	- - -	- - -
$Zn(pn)_2(IO_3)_2$	35	- - -	- - -	6.8	- - -	- - -
$Zn(en)_2(IO_3)_2 \cdot 1\frac{1}{2} H_2O$	46	34	2.48	12.4	- - -	25 (1.73) 60 (2.00) 145 (2.43)
$Ni(en)_3(IO_3)_2$	32	51	- - -	0	- - -	- - -
$Ni(pn)_3(IO_3)_2$	24	24	- - -	0	- - -	- - -
$Hg(en)(IO_3)_2 \cdot H_2O$	100	>100	- - -	17.0	- - -	- - -
$Cd(en)_2(IO_3)_2$	46	31	- - -	16.2	- - -	- - -

NOTES: en = ethylenediamine

pn = propylenediamine

tmen = trimethylenediamine

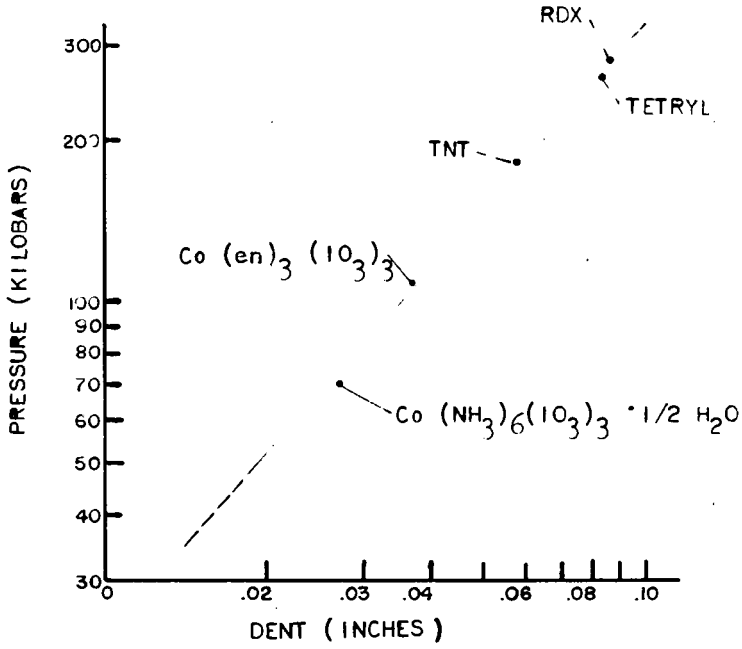

FIGURE 1

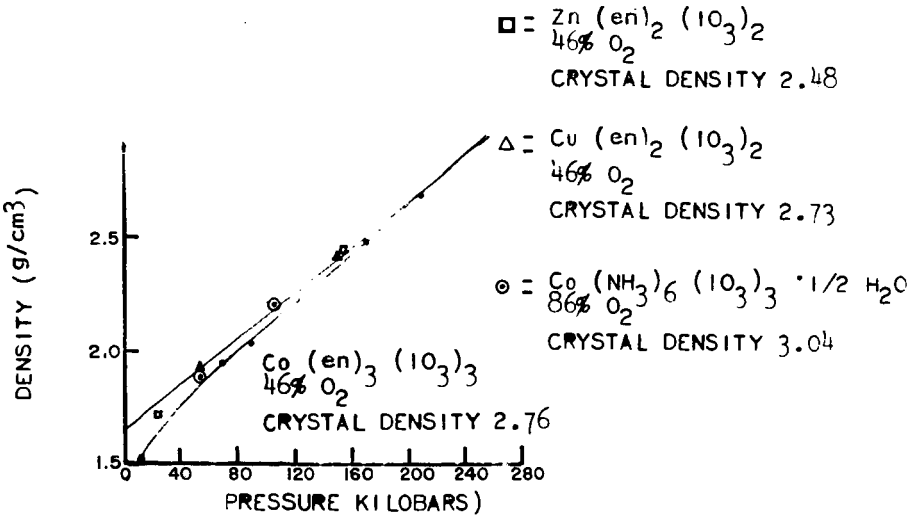

FIGURE 2

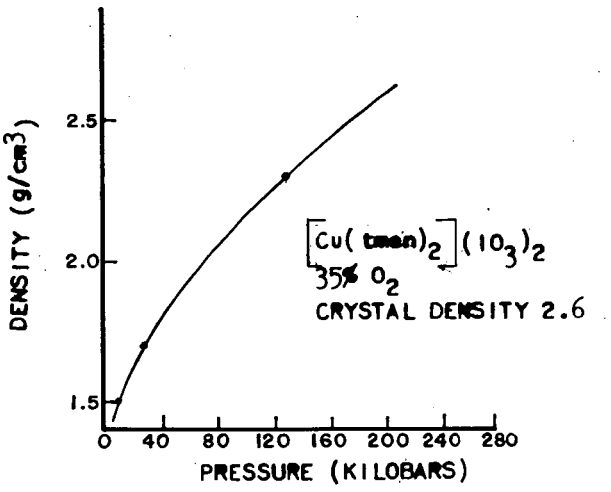

FIGURE 3

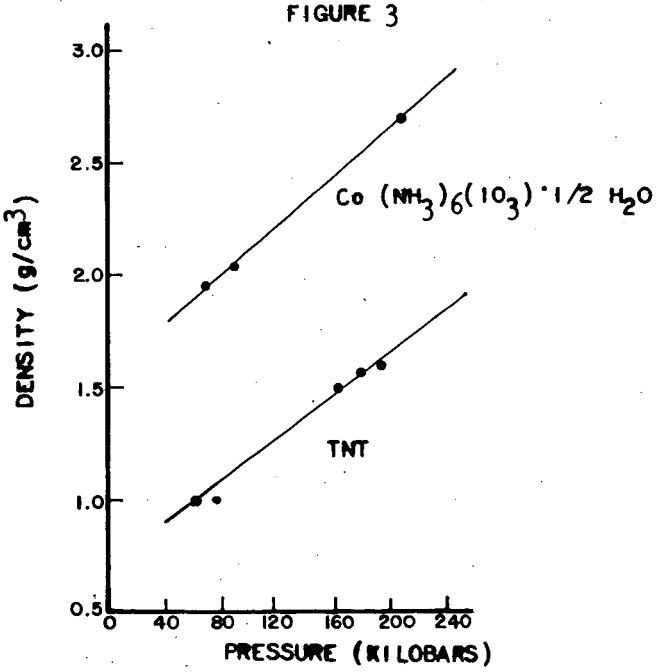

FIGURE 4